Development and Application of Single Beam Acoustics and Underwater Videography in Marine Benthic Habitat Assessment and Mapping

by

Miles Macmillan Lawler BSc (Hons)

Submitted in fulfilment of the requirements for the Degree of Doctor of Philosophy

University of Tasmania July 2011

Declaration

Statement of originality

This thesis contains no material which has been accepted for a degree or diploma by the University or any other institution, except by way of background information and duly acknowledged in the thesis, and to the best of the candidate's knowledge and belief no material previously published or written by another person except where due acknowledgement is made in the text of the thesis, nor does the thesis contain any material that infringes copyright.

Signed  Date 22/07/2011

Miles Macmillan-Lawler

Statement of authority of access

This thesis may be made available for loan and limited copying in accordance with the Copyright Act 1968.

Signed  Date 22/07/2011

Miles Macmillan-Lawler

Abstract

In marine habitat mapping, single beam echo sounders are widely used to derive information about the geophysical properties of the seabed, while underwater video can provide supplementary information about the physical structure of the seabed and associated marine biological communities.

In this thesis, data from both systems are integrated and used to classify seabed habitats. The habitat classification is based on categories within a hierarchical system that is conducive to information from different instruments or collected at different spatial scales.

The classification of single beam echo sounder data at different levels of the hierarchical classification is the focus of the first half of the thesis. The first data chapter examines the effect of depth, bottom slope, prevailing weather conditions, and vessel speed on measured acoustic return from the seabed, and the subsequent capacity to classify this data at the substrate level. The following three chapters are case studies that progressively develop techniques for classification of single beam acoustic data at lower levels of the hierarchical classification including identification of soft sediment habitats in commercial scallop fishing grounds; mapping the distribution of urchin barrens on rocky reefs; and detection and mapping of sub-surface giant string kelp, *Macrocystis pyrifera*. Each of the case studies develops analysis and classification techniques that are applicable for mapping at levels below substrate in the hierarchical classification.

At lower levels of the hierarchical classification, biological communities and species distributions are commonly used as habitat descriptors. The second half of this thesis focuses on extracting information from video for the classification of biological communities. In the first of these chapters, methods are compared for extracting estimates of algal cover on temperate rocky reef substrates from towed underwater video. The algal cover data is then used to examine the capacity of a towed video to detect changes in algal community structure at two spatial scales. The following chapter describes the design, construction and evaluation of a stereo video system developed to measure sponge morphological metrics. These metrics are then used to establish a quantitative classification of sponge functional morphology. Differences in sponge functional morphology are examined between sponge communities in two different regions with differences detected in both the composition of functional groups and the size of those functional groups.

The thesis presents a framework and methodologies for extracting both physical and biological information from single beam echo sounder and underwater video systems. These methods can easily be incorporated into existing seabed mapping programs, and provide information that will improve our understanding of the spatial distribution of subtidal habitats. This information is directly beneficial to marine resource management, including marine protected area planning and fisheries management, and will allow baseline documentation of habitats for future climate change research.

Acknowledgement

This thesis was made possible through the support for the SeaMap Tasmania program of Professor Colin Buxton, Director of the Tasmanian Aquaculture and Fisheries Institute. The establishment and ongoing support for this program provided the framework for much of the research conducted as part of this thesis. Dr Alan Jordan, Dr Neville Barrett, Dr Christine Crawford and Dr Vanessa Lucieer were instrumental in establishment of this program, and in ensuring the ongoing funding for this research.

Dr Jon Osborn (School of Geography, UTAS), primary supervisor, provided continuous support and valuable feedback. Our discussions on the philosophy of finishing a PhD and life in general helped keep me on track and provide me with the tools and direction to finish my thesis. Dr Alan Jordan (formerly UTAS, now NSW DEH), research supervisor, provided me with the opportunity to undertake these studies, for which I am truly grateful. His ongoing advice and knowledge of ecology and biology have been invaluable to me over the last few years. Dr Rudy Kloser (CSIRO), research supervisor, provided expert feedback on all things acoustic and seabed mapping, I am thankful for the time you have been able to dedicate to this project.

Chapter 3 was supported by Associate Professor Malcolm Haddon through the FRDC funded project 'Juvenile scallop trashing rates and bed dynamics: testing the management rules for scallops'. The side scan sonar data used in this chapter was processed by Fugro Spatial. Julian Harrington assisted with the field surveys, and both he and Malcolm provided useful review of this chapter. Rob Musk also provided useful review of this chapter.

A big thanks to all those who helped with laboratory processing and field work especially the crew of FRV Challenger, Tobias Probst, Cameron Veal, Dr Richard Mount, Dr Hugh Pederson, Tim Alexander and Andrew Pender. The many hours spent on small vessels in remote locations would not have been half the fun without you guys, especially developing new games to pass the mapping time.

To my colleague Ness, thanks for all the support over the last decade working together on the SeaMap Tasmania program. It was the greatest job in the world and we have been part of something to be proud of.

My parents have supported me throughout my education, and always believing in my abilities. This is reward for all the investment you have put in to me.

Finally my wife Lena, and two children Charlotte and Maximilian, thankyou for putting up with my never ending timelines and weekends locked away working. I am now all yours again. Lena your support and drive has been especially valuable to me, I could not have achieved this without you. I dedicate this thesis to the three of you as reward for the sacrifices you have all made in getting me to the end.

For Lena, Charlotte and Maximilian

Table of Contents

List of Figures

List of Tables

Chapter 1. General Introduction

Habitat can be defined as the place where an organism lives, and is characterised by its physical features, or by dominant biota (Oxford Dictionary of Science). Habitat mapping studies seek to characterise the seabed using a suite of tools, and classify similar seabed types into distinct categories based on the outputs of these tools. Mapping the spatial distribution of marine habitats is important for the conservation and management of marine resources. Habitat mapping has been utilised in marine protected area planning (Jordan *et al.* 2005b), fisheries management (Smith and Greenhawk 1998, Kloser *et al.* 2001b, Kostylev *et al.* 2003), baseline assessment of vulnerable habitat (Norris *et al.* 1997, Kendrick *et al.* 2001), and change detection (Kendrick *et al.* 1999, Kendrick *et al.* 2000).

There are a large number of tools that have application in habitat mapping studies, including airborne remote sensing (Mumby *et al.* 1997, Heege *et al.* 2007), underwater acoustics including single beam echo sounders (SBES), multi beam echo sounders (MBES) and side scan sonar (SSS) (Bates and Moore 2002, Anderson *et al.* 2008), underwater video (Norris *et al.* 1997, Holmes *et al.* 2008, Carbines and Cole 2009), diver sampling, and sediment sampling. This thesis focuses on the extraction of habitat information from two of these tools: Acoustic systems and underwater video.

Acoustic seabed classification methods were initially developed based on single beam echo sounders (SBES), operating on a normal incident angle to provide information on the acoustic reflectivity of the seafloor directly below the vessel (Chivers 1990, Anderson *et al.* 2008), and more recently the development of oblique angle systems including side scan sonar (SSS) and multibeam echo sounders (MBES) (Kostylev *et al.* 2001, Brown *et al.* 2005a). Acoustic systems for seabed mapping have been extensively reviewed in the literature (Basu and Saxena 1999, Anderson *et al.* 2008). Generally SBES have been used for the characterisation of physical substrates (Kloser *et al.* 2001a, Freitas *et al.* 2005b), with some application to the characterisation of biota (BioSonics 2001). While MBES and SSS are increasingly used to provide complete coverage maps of the physical seascape, including bathymetry for MBES and some types of SSS (Bates and Byham 2001, Kostylev *et al.* 2001).

The classification techniques for SBES are generally well developed, with several commercial systems available including RoxAnn, QTCView, EchoPlus and BioSonics (Bates and Whitehead 2001, BioSonics 2001, Ellingsen *et al.* 2002, Wilding *et al.* 2003, Freitas *et al.* 2005b). Well developed calibration techniques have also been developed for these systems based on fisheries acoustic work (Foote *et al.* 1987). However SBES only provide information

on the substrate directly below the vessel and as such interpolation of the data is needed to create a complete coverage map (Guan *et al.* 1999, Valley *et al.* 2005). Conversely classification techniques for both MBES and SSS have been a more recent development with many of these using image analysis techniques (Chakraborty *et al.* 2003, Cutter-Jr. *et al.* 2003, Blondel and Gómez Sichi 2008, Marsh and Brown 2008, Preston 2008, Simons and Snellen 2008). Processing the backscatter of both MBES and SSS needs to account for the angular response of the seabed at different grazing angles (Preston 2008). SBES systems that operate at a normal angle of incidence do not have this issue, thus they present a simple tool for development of classification methods that may ultimately be applicable to the swath systems.

However, SBES systems operating at normal incidence measure the acoustic response of the seabed across a relatively small acoustic footprint defined by the beam geometry and water depth. These systems can not resolve the seabed angular response and have poor spatial resolution when compared to MBES. Seabed scattering at normal incidence has reduced discrimination when compared to instruments that measure seabed reflectivity off normal axis such as MBES and SSS. For this reason measurement of the single beam data are typically made off axis to increase the discrimination ability (Chivers 1990, Kloser *et. al.* 2001b). Further detail on the methods for SBES classification is covered in Chapter 2 Sections 2.1 and 2.2.3.

This thesis primarily focuses on SBES for mapping of inshore temperate substrates, as these systems are generally readily accessible and easily deployed of small vessels commonly used to undertake this type of work.

SBES generally operate by emitting a short duration sound pulse at a set frequency from a transducer. The pulse propagates through the water column, where it undergoes spherical spreading and absorption (MacLennan 1986), with absorption frequency dependent (Blondel and Murton 1997). Where an impedance miss-match is encountered between objects or layers with different densities, such as the seafloor, scattering occurs. Echoes that are scattered back to the transducer are known as backscatter, with intensity and time from transmission recorded as they are encountered at the transducer face. Time varied gain (TVG) is applied to compensate for spherical spreading of the beam with range and absorption of the signal in water, and the resulting echoes envelope detected based on a set pulse length. The resulting echogram display is a representation of the returning echo energy based on the time taken to return to the transducer (see Chapter 2 Figure 2.2).

The classification of SBES data is based on the shape and intensity of the returning echoes

(Kloser *et al.* 2001a, Jordan *et al.* 2005b). Due to sperical spreading the shape of the transmitted pulse is similar to a shallow dish, with the diameter of the dish increasing with distance travelled, and the thickness of the dish related to the pulse length. At a normal incident angle (90^{o} from horizontal) the centre of the pulse is the first part to encounter the seafloor, through the progression of time parts of the pulse further off axis encounter the seafloor. Due to its shorter travel time the central part of the pulse returns to the transducer first and providing the seafloor is flat and horizontal will be the most intense part of the echo return. The parts of the pulse further off axis will not only take longer to reach the transducer, but as they are off the normal incident angle a greater proportion of these will be reflected away from the transducer, resulting in a weaker signal. This part of the echo return is often referred to as the tail of the echo. The tail of the first echo will generally be stronger on rougher surfaces, where there is an increased change of the pulse being directly reflected back to the transducer face. On harder substrates a second echo is commonly observed, this represents the returning sound energy that has been reflected off the surface of the water and back down to the seafloor a second time. Common methods for the classification of seabed habitats are based on integration of the acoustic energy contained within the tail of the first echo return, and the entire second echo return (Chivers 1990, Heald and Pace 1996, Kloser *et al.* 2001a), or alternatively the characterisation of the first echo return (Collins 1996).

The methods for analysis of SBES and underwater video that are described in this thesis are related to a pre-defined classification system (Table 1.1). The classification system is hierarchical in structure, and allows habitats to be classified at a number of levels, depending on the tools used and the scale of measurement (Bax *et al.* 1999, Greene *et al.* 1999, Jordan *et al.* 2005a). A number of classification systems for seabed habitats are used throughout the world (Bax *et al.* 1999, Greene *et al.* 1999, Allee *et al.* 2000, Davies *et al.* 2004), the one employed in this thesis is based on that of Allee (2000). It is hierarchical in nature and has been modified to include all the common habitat types found in Tasmanian coastal waters. A comparison of classification systems is beyond the scope of this thesis. The upper levels of the classification hierarchy are used to describe habitats at a broad level, often across broad geographic regions, while the lower levels of the classification system, especially the modifier level, are used to describe fine scale habitat structure. Within this thesis, SBES is examined at the bio-geomorphic, substratum/ecotype levels, with specific case studies at the modifier level, while the underwater video is examined at the modifier level of classification.

Table 1.1. SeaMap Tasmania hierarchical classification table, modified from Jordan *et al.* 2005.

Geomorphic Type					
Consolidated Substrate		Unconsolidated Substrate			
Bio-geomorphic Type					
Rocky Reef		Unvegetated Unconsolidated Substrate		Vegetated Unconsolidated Substrate	
Substratum/ Ecotype					
High Profile Reef Medium Profile Reef Low Profile Reef		Cobble Gravel Sand Silt		Seagrasses Algal Beds Aquatic Macrophytes	
Modifiers					
Modifier	**Eco-Unit**	**Modifier**	**Eco-Unit**	**Modifier**	**Eco-Unit**
Structure	Continuous Patchy Guttered Bommies	Attached Epifaunal Groups	Sponges Bryozoans Tunicates Etc.	Structure	Continuous Patchy Sparse
Substratum Texture	Solid Boulder	Relief	Hills Ripples Flat	Sediment Type	Cobble Sand Silt
Rock Type	Dolerite Granite Sandstone Limestone Basalt	Substratum Texture	Shell Burrows Smooth	Biota	*Heterozostera tasmanica* Caulerpa sp.
Vegetation/ Epifauna	Algae Barren Sponges				
Biota	Dominant algae e.g. *Ecklonia radiata* Dominant epifauna e.g. sponges				

Video and physical grab samples are commonly used to collect information on the dominant biota within an area, with the composition of dominant biota often used to define habitats below the geophysical level (Babcock *et al.* 1999, Shears *et al.* 2004). For instance, on temperate reef habitats the distribution and community composition of macroalgae are often used as habitat descriptors (Shears *et al.* 2004). Monitoring the changes in habitat at this level provides valuable information for climate change research, marine protected area planning and assessment, and to understand the ecological benefits or ramification of management decisions (Stevens and Connolly 2005). Detailed maps of habitats at this level can also supplement the experimental data from ecological studies and advance understanding of ecological processes (Parsons *et al.* 2004). Both single video systems (Norris *et al.* 1997, Carbines and Cole 2009) and stereo video systems (Chong and Stratford 2002, Negahdaripour *et al.* 2002) can be used to characterise the distribution of organisms and characterise community structure. These methods are especially relevant at the Modifier level of the hierarchical classification system (Table 1.1).

Within Tasmania there has been an ongoing marine habitat mapping program since 2000, known as SeaMap Tasmania. This project has systematically mapped seabed habitats within Tasmanian state coastal waters (Barrett *et al.* 2001, Jordan *et al.* 2005a, Lucieer *et al.* 2009). Whilst the SeaMap Tasmania project has been predominantly focussed on substrate level mapping, there has been a growing need to develop techniques to map the spatial distribution of habitats below this level to advance the management of marine habitats and ecosystems. In Tasmania this includes the spatial management of fisheries (Jordan *et al.* 2005a, Haddon *et al.* 2006), and to monitor the response of communities and individual species to human induced impacts and climate change (Edyvane 2003, Johnson *et al.* 2004). These types of ecological questions are relevant around the globe (Pickrill and Todd 2003, Ladah and Zertuche-González 2004, Lauzon-Guay and Scheibling 2007).

Early in the SeaMap Tasmania program it became apparent that there were limitations in the tools and methods employed for the classification of marine benthic habitats (Barrett *et al.* 2001). While the detection of habitats using established acoustic methods based hard/soft and rough/smooth characteristics allowed the differentiation of reef from unconsolidated substrates (Heald and Pace 1996, Kloser *et al.* 2001a), information on the spatial distribution of ecologically important habitat forming species and communities was not available. Within Tasmania reef habitat supports a wide range of species, and is the basis for several important commercial fisheries. However not all reef is ecologically the same, with differences in exposure and depth leading to different algal and faunal communities (Edgar 1984, Barrett *et al.* 2001). The capacity to map the spatial distribution of key habitat defining algae and communities including algal beds, urchin barrens (Johnson *et al.* 2004, Jordan *et al.* 2005a), and *Macrocystis pyrifera* beds (Edyvane 2003, Jordan *et al.* 2005a) was identified as an important component for the ongoing development of the SeaMap Tasmania program. Further, on soft sediment habitats there was the need to identify areas of ecological importance including sponge gardens and scallop habitat (Jordan *et al.* 2005b, Haddon *et al.* 2006).

This thesis aims to develop methods for processing single beam acoustic and underwater video data that will allow habitats at lower levels of the classification hierarchy (Table 1.1) to be spatially defined and/or quantitatively defined (Figure 1.1). The thesis structure is outlined below:

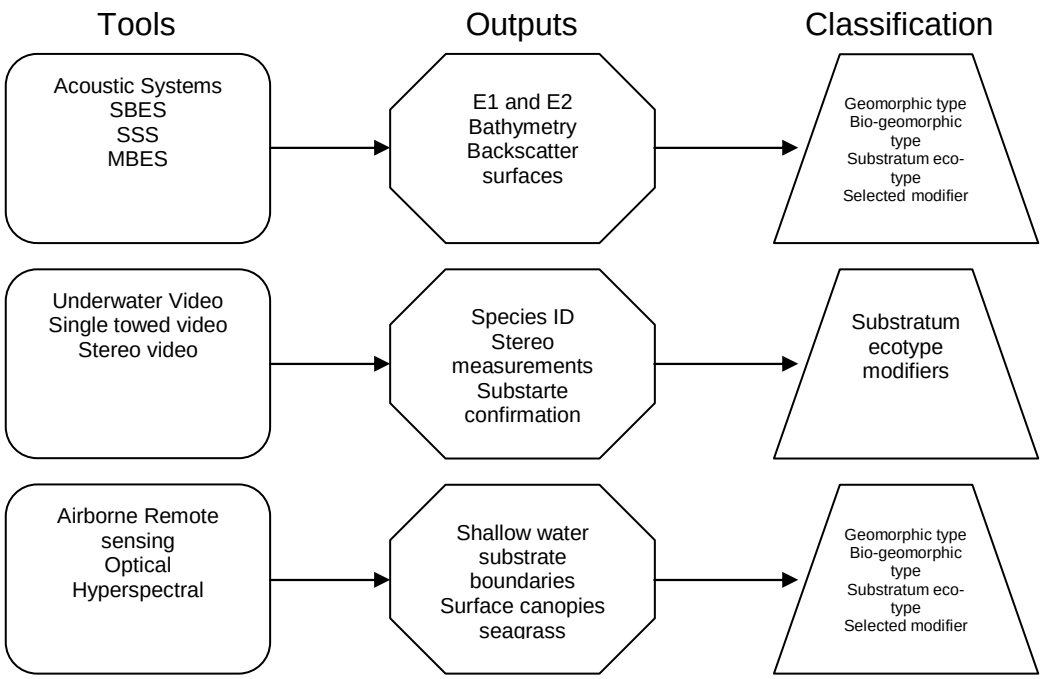

Figure 1.1. Schematic of the tools available for shallow water habitat mapping, their outputs, and relevant levels in the classification hierarchy.

Chapter 2 examines factors affecting the classification of SBES data. Simple acoustic indices are used as a tool to examine the effect of vessel speed, seabed slope, depth, and environmental conditions on the measured acoustic response from typical temperate seabed habitats at the bio-geomorphic and substratum/ecotype level of the classification hierarchy (Table 1.1). Indices of acoustic roughness (E1) and acoustic hardness (E2) of the seabed based on those of Kloser *et al.* (2001) are compared in a range of operational conditions to examine the magnitude of effect for each of the tested factors. Changes in vessel speed have previously been shown to affect the consistency of classification of SBES data (Greenstreet *et al.* 1997, von Szalay and McConnaughey 2002), with the acoustic hardness parameter E2 particularly affected by changes in vessel speed (Hamilton *et al.* 1999). Similarly, seabed slope also affects the consistency of classification, with increased error in rough or steep seabeds (Hamilton *et al.* 1999, von Szalay and McConnaughey 2002). Depth dependent bias in SBES data occur due to spherical spreading and pulse length effects (Kloser *et al.* 2001b, Pouliquen 2004, Dommisse *et al.* 2005). Environmental conditions can affect the quality of the acoustic signal leading to reduced capacity to classify SBES data (MacLennan and Simmonds 1992, Kloser *et al.* 2001b). Within this chapter the magnitude of these effects is investigated in relation to typical operating conditions encountered on small vessels.

Chapter 3 focuses on the classification of SBES acoustic data in relation to soft sediment substrates, at the substratum/ecotype and modifier/eco-unit levels of the classification hierarchy (Table 1.1). Within soft sediment habitats, modifiers such as particle size, surficial shell, and biota are all used to define different habitats (Ellingsen *et al.* 2002, Jordan *et al.* 2005b). Several of these modifiers have previously been shown to affect the acoustic response of the seabed, including enhanced backscatter due to the presence of surficial shell (Fenstermacher *et al.* 2001), and increased acoustic roughness due to the presence of sponge (Jordan *et al.* 2005b).

Habitat mapping studies have previously been used to characterise the distribution of critical fisheries habitat, and improve the management of many fisheries worldwide. The distribution of geophysical habitat within traditional scallop fishing grounds in Canada has lead to increased efficiency in the fishery, and thus a reduction on the impact of non-target habitat by the fishing gear (Kostylev *et al.* 2003, Pickrill and Todd 2003). Mapping of the distribution of rockfish habitat has also benefited the assessment of stocks and the management of these fish (McRea *et al.* 1999, Cochrane and Lafferty 2002). Generally, studies linking habitat mapping and fisheries have provided spatial maps of habitat at a geophysical level, with supplementary data on habitat forming biota provided by video or physical grab samples (Bax *et al.* 1999, Kostylev *et al.* 2001, Jordan *et al.* 2005a).

Within this chapter the particle size, percentage surficial shell, and percentage sponge cover are linked to changes in acoustic roughness (E1) and acoustic hardness (E2) indices from an area of seabed within the Tasmanian scallop fishery. Cluster analysis and interpolation techniques are used to define the spatial distribution of several habitat classes based on the above factors. Data from side scan sonar (SSS) is used to examine the veracity of the spatial patterns identified from the SBES. Finally, fishing activity derived from vessel monitoring system (VMS) data is compared with the acoustic data to determine whether scallop fishing grounds can be identified based on a unique acoustic signature.

Chapter 4 and Chapter 5 focus on classification of SBES data at the lowest level of the hierarchical classification system, the modifier/Eco-Unit level (Table 1.1). Chapter 4 investigates the acoustic detection of urchin barrens on temperate reefs in the 0 to 30 m depth range. Urchin barrens are an alternate state to algal communities, and are caused by over grazing of the canopy algae by sea urchins (Mann 1977, Levitan 1992, Andrew 1993). This alternate habitat state leads to reductions in primary productivity, and a changed suite of associated species (Gagnon *et al.* 2004). Tasmanian rocky reefs support extensive macroalgae

communities, which support a wide range of different species (Edgar *et al.* 2004). However, there has been a rapid range expansion of the barren forming urchin *Centrostephanus rodgersii* along the Tasmanian east coast over the past few decades (Johnson *et al.* 2004, Valentine and Johnson 2005).

Algae and urchin barren distribution have previously been studied by diver surveys (Andrew 1993, Valentine and Johnson 2005), towed video (Johnson *et al.* 2004), and remote sensing (Simms and Dubois 2001). Diver surveys and airborne optical remote sensing are restricted to shallow depths, while diver surveys and towed underwater video surveys have limited coverage. Acoustic systems are not limited within the depth range commonly occupied by urchin barrens (typically less than 30 m depth), and provide increased coverage when compared to diver and towed video surveys. The processing of SBES data is usually focussed on detection of benthic substrate types (Hamilton *et al.* 1999, Kloser *et al.* 2001b, Freitas *et al.* 2003a), however the capacity of these systems to detect algae growing on reef substrate has been documented (Anderson *et al.* 2002). SBES have also been used to map and assess other submerged aquatic vegetation, with systems like BioSonics EcoSAV designed for the rapid assessment of submerged aquatic vegetation (BioSonics 2001). Segmentation of algal dominated reef from barren reef using SBES data is the focus of Chapter 4. Methods are developed to analyse the echo return above the sounder detected bottom.

Chapter 5 examines the identification of *Macrocystis pyrifera,* a key habitat forming algae with a distinct growth habit. *Macrocystis pyrifera* is found on temperate rocky reefs of Southern Australia, New Zealand, North America and South America (Lewis and Neushul 1994). This species has large inter-annual variations in growth related to changes in temperature and nutrient availability (Brown *et al.* 1997). Large diebacks of this species have been documented in California and along the east coast of Tasmania (North *et al.* 1993, Edyvane 2003, Ladah and Zertuche-González 2004). For this reason mapping the distribution of this species is needed to assist in management plans for its conservation.

Macrocystis distribution is usually identified using airborne remote sensing including optical, infrared and satellite based methods (Deysher 1993, Simms and Dubois 2001). These techniques are suited to detection of the surface canopy of the *Macrocystis*, which can lead to an underestimation of the total *Macrocystis* cover where significant sub-surface canopies exist. Deep *Macrocystis* beds with no surface canopy have been shown to be an important refuge for this species during periods of unsuitable environmental conditions (Ladah and Zertuche-González 2004). SBES present a possible tool for the mapping sub-surface *Macrocystis*.

Previous work using paper traces from SBES was able to identify individual and clusters of plants in the echo trace trough visual means (Zabloudil *et al.* 1991). SBES technology and acoustic processing software have greatly advanced since this work was conducted and as such now is an ideal time to revisit this subject.

The detection of sub-surface *Macrocystis* is tested using a combination of tools, including aerial photography, SBES, and surface mounted underwater video. In particular SBES data analysis techniques for the segmentation of sub-surface *Macrocystis* are developed. For each of these tools, derived maps of basal *Macrocystis* covered are compared, highlighting the strength of SBES for detection and mapping of sub-surface *Macrocystis* canopy.

Chapter 6 investigates methods for classification of algal community structure at two spatial scales. Temperate reefs support a wide array of algal species, which form distinct communities based on exposure, temperature, nutrient availability, light availability, and depth (Edgar 1983, Reed and Foster 1984, Schiel and Foster 1986). These communities are often dominated by a small number of large canopy species and a larger number of understorey species, with the canopy species a useful indicator for the understorey species (Irving and Connell 2006). As different algal communities can support a wide range of different fish and invertebrate species, it is important to be able to characterise the spatial distribution of algal communities for biodiversity management and conservation, to gain a better understanding of biogeographical patterns, and to improve our understanding of species interactions (Edgar 1984).

Algal communities are commonly studied using diver based surveys (Valentine and Johnson 2003, Johnson *et al.* 2004), although video based surveys are becoming more common (Johnson *et al.* 2004, Parsons *et al.* 2004). Video offers several advantages over diver surveys including increased coverage due to time and depth limits associated with diving, and they also provide a permanent record for future comparison and re-analysis. However, video generally leads to a loss of taxonomic resolution compared with diver surveys (Kenyon *et al.* 2006).

Within Chapter 6, methods for extracting quantitative information from underwater video are investigated. Time based and frame based methods, including point intercept counts, percentage rankings, and presence/absence methods used to analyse the video data (Valentine *et al.* 2004, Jordan *et al.* 2005a, Kenyon *et al.* 2006, Kohler and Gill 2006). These methods are compared for correlation, processing time, and misclassification. The sensitivity of these methods to detect changes in algal communities is then examined at two broad spatial scales.

Chapter 7 examines the extraction of quantitative measurements from underwater video using sponge communities as a test habitat. Sponges play an important role in the function of the marine environment including physical, chemical and ecological functions (Bell 2008). There is a need for tools to rapidly assess the composition and structure of sponge communities for management and conservation planning. However, sponge taxonomy is inherently difficult, with colour, shape and size often having a high degree of variation within a single species, making visual identification difficult (Bell and Barnes 2000c, Bell and Barnes 2001). Fortunately, the diversity in sponge functional morphology has been shown to be a good surrogate for species diversity, both in temperate and tropical systems (Bell and Barnes 2001, Bell and Barnes 2002).

This chapter develops techniques for the measurement of gross sponge morphology from a stereo video system. Classification methods are then applied to the morphological data components to develop an objective classification system for sponge functional morphology. Based on functional morphology, sponge communities are compared between two locations, one located on soft sediment and the other rocky reef.

Chapter 8 provides a general discussion on the application of the methods developed within this thesis to habitat mapping and ecological research.

Chapter 2. Evaluation of factors affecting the acoustic response of the seafloor as measured by a single beam echo sounder

2.1. Introduction

Single beam echo sounders represent a relatively low cost and readily accessible tool for broad scale baseline seabed mapping (Foster-Smith *et al.* 2001, Foster-Smith and Sotheran 2003). Single beam echo sounders generally operate by emitting a short duration sound pulse at a set frequency from a transducer. This pulse propagates through the water column and reflects off objects and layers with different densities to seawater, including the seafloor. The returning echoes from these objects are detected by the transducer, time varied gain (TVG) is applied to compensate for spherical spreading of the beam with range and absorption of the signal in water (MacLennan 1986), and the resulting echoes envelope detected based on a set pulse length. The resulting echogram display is a representation of the returning echo energy based on the time taken to return to the transducer.

The acoustic reflectance of the substrate will depend upon its composition, including its roughness, hardness, and the angle of acoustic incidence, which is affected by the slope of the seafloor. Seabed echoes from single beam echo sounders can be classified into bottom types based on visual discrimination of the echograms (Bax *et al.* 1999) or by quantitative description of various components of the returning echoes. The length and intensity of the tail of the first echo (E1), and the intensity of the second echo (E2) can often be used to differentiate soft, hard and rough habitats (Orlowski 1984, Chivers 1990, Bax *et al.* 1999). Simple acoustic indices, the most basic of which are the E1 and E2 indices (Orlowski 1984, Chivers 1990, Kloser *et al.* 2001b), are commonly used in seabed classification. These indices have often been related to seabed roughness and seabed hardness respectively (Orlowski 1984, Chivers 1990, Heald and Pace 1996, Cholwek *et al.* 2000, Kloser *et al.* 2001b).

Several classification systems used in commercial software are based on these E1 and E2 acoustic measures. These include the *RoxAnn* system (Greenstreet *et al.* 1997, Pinn and Robertson 1998, Cholwek *et al.* 2000, Pinn and Robertson 2003, Wilding *et al.* 2003, Humborstad *et al.* 2004b, Brown *et al.* 2005a), Echo plus (Bates and Whitehead 2001) and part of the BioSonics Visual Bottom Typing (VBT) classification software (Acker *et al.* 1999, Burczynski 2001, Dommisse *et al.* 2005). An alternative approach is used by the *QTC View* seabed classification (Collins *et al.* 1996, Galloway and Collins 1998, Morrison *et al.* 2001b, Freitas *et al.* 2003b). This system analyses data parameters from the first echo return only.

QTC View applies a series of algorithms to the shape and energy of the first returning echo, translating it into an array of 166 elements (Collins *et al.* 1996, Freitas *et al.* 2003b). These 166 elements are reduced to three Q-values using principal component analysis (PCA) (Anderson *et al.* 2002, Freitas *et al.* 2003b).

Classification of acoustic data from single beam echo sounders generally relies on some form of clustering to assign like acoustic signatures to substrate classes. This may be as simple as fitting a "box pattern" to E1 vs. E2 scatter plots, with separate boxes representing the acoustic responses from different habitats (Chivers 1990, Greenstreet *et al.* 1997, Caddell 1998, Cholwek *et al.* 2000, Burczynski 2001), through to statistical methods including PCA coupled with cluster analysis to define confidence intervals around acoustic clusters (Siwabessy *et al.* 1999, Cholwek *et al.* 2000, Siwabessy *et al.* 2000, Siwabessy *et al.* 2004). Alternative methods for the classification of E1 and E2 data have been suggested by a number of studies, including the use of image classification techniques on a false colour composite image derived from interpolated surfaces of E1, E2 and depth information (Foster-Smith *et al.* 2001, Brown *et al.* 2003, Foster-Smith and Sotheran 2003, Pinn and Robertson 2003, Brown *et al.* 2005a).

Regardless of the classification technique used, the classification of single beam data is based on an assumption that the acoustic response from a given substrate is consistent, and different from that of other substrates. There are however many factors that affect the measured acoustic response from a given substrate. The stability of the acoustic system, both within and between surveys, is the first consideration. A level of noise is present in all acoustic systems, which results in the measured acoustic response varying from the expected acoustic response (Collins and Voulgaris 1993). Changes in vessel, power supply and system components can all affect the system stability. Standard calibration protocols (Foote *et al.* 1987) have been developed for single beam echo sounders used in fisheries acoustics to account for system variation. However for seabed mapping, information on the beam pattern, pulse length and shape are also needed.

A second group of factors that affect the measured response from the seabed are environmental and operational factors. Classification efficiency of single beam echo sounder data can be affected by vessel speed (Hamilton *et al.* 1999, von Szalay and McConnaughey 2002, Wilding *et al.* 2003), water depth (Siwabessy *et al.* 1999, Kloser *et al.* 2001b, Humborstad *et al.* 2004b, Dommisse *et al.* 2005), weather conditions (Siwabessy *et al.* 1999, Siwabessy *et al.* 2000, Kloser *et al.* 2001b) and bottom slope (von Szalay and McConnaughey

2002). Vessel speed has been shown to affect the performance of the acoustic systems due to associated changes in vessel noise (Schiagintweit 1993, Hamilton *et al.* 1999, Wilding *et al.* 2003). Classification from the *RoxAnn* system was found to be consistent only at constant speed (Schiagintweit 1993), with the E2 parameter being inversely related to speed (Hamilton *et al.* 1999). The *QTC View* classification system has been shown to be less affected by vessel speed (Hamilton *et al.* 1999, von Szalay and McConnaughey 2002).

Depth has a strong effect on the performance of acoustic classification systems. Due to spherical spreading, the beam footprint size and absorption increase with range (Kloser *et al.* 2001b). Whilst these are generally accounted for by the TVG function, depth bias has been noted in acoustic data in numerous studies (Orlowski 1984, Greenstreet *et al.* 1997, Bax *et al.* 1999, Hamilton *et al.* 1999, Siwabessy *et al.* 1999, Kloser *et al.* 2001b, Dommisse *et al.* 2005). Increased footprint size with depth may result in a different acoustic response from the same physical substrate type as the scale of the physical characteristics, such as rugosity, will differ in relation to the footprint size. For example in shallow depths the footprint size may be smaller than the size of boulders on a reef, while at depth the footprint may incorporate many boulders in a single ping. The acoustic footprint size will also vary depending on which part of the echo return being integrated. Within this thesis the E1 index integrates the echo energy from 15 to 30 degrees which results in an annulus of area that is sampled and due to spherical spreading of the beam increases with range from the transducer. The footprint of the E1 index represents the beam spreading which occurs between the surface to the seafloor, while the E2 index represents the beam spreading which occurs between the surface to the seafloor, back to the surface and then back to the seafloor again.

The depth dependence is influenced by the beam width and frequency of the echo sounder (Kloser *et al.* 2001b). Depth bias in single beam acoustic data may be reduced or removed through normalising the data for depth (Siwabessy *et al.* 1999, Dommisse *et al.* 2005), or by using constant angular algorithms when calculating acoustic indices (Kloser *et al.* 2001b). However as commercial echo sounders all have a fixed pulse length, there will always be a depth bias (Pouliquen 2004). Depth biases have been shown to be a particular problem in shallow water (< 50 m) (Orlowski 1984).

The weather conditions at the time of survey also have an affect on the measured acoustic response from the seabed. Swell can increase the pitch and roll of the vessel, which will result in variable seabed incident angles, affecting the acoustic response. If the pitch and roll is severe, it may also create cavitation around the hull and transducer and may entrain bubbles in

the water column. Wind also increases the amount and depth of entrained air bubbles in the upper layer of the water column. These small bubbles will act as acoustic targets, and will cause attenuation of the acoustic energy from the transducer, resulting in less energy reaching the seafloor (Siwabessy *et al.* 1999, Kloser *et al.* 2001b).

The slope of the seafloor also affects the acoustic return. Both the QTC and *RoxAnn* systems have been shown to misclassify seabed over steep rocky terrain (Hamilton *et al.* 1999, von Szalay and McConnaughey 2002). This is primarily due to a steep bottom reflecting more of the acoustic energy away from the transducer, resulting in a similar effect to the transducer being off normal incident.

This chapter focuses on classification of benthic habitats at the bio-geomorphic and substratum/ecotype levels of the classification hierarchy (Table 1.1). The studies reported in this chapter investigates the effects of vessel speed, water depth, prevailing weather conditions, and seabed slope on the consistency of measured E1 and E2 acoustic indices based on surveys from a small (6m) vessel. This contrasts with much of the current literature which is based on larger vessels as acoustic platforms. The magnitudes of these effects are discussed in relation to the classification of benthic habitats commonly encountered in shallow temperate waters of Tasmania.

2.2. Methods

The effects of vessel speed, depth, prevailing conditions, and seafloor slope were separately assessed. Different study sites and data collection methods were used for each investigation in order to optimise the data for each analysis. These four investigations are separately described below. Each of the four investigations used the same acoustic system also described below. The method used to calculate E1 and E2 indices was the same in all investigations and so it is also described here.

2.2.1. The Acoustic System

All surveys were conducted using a calibrated Simrad ES60 single beam echo sounder with a 120 kHz 10-degree beam width (-3 dB full angle) transducer. The transducer was pole mounted on the side of a 6.5 m aluminium planing hull vessel powered by twin 90 hp outboard motors (Figure 2.1). The transducer was fixed at a depth of 70 cm below the water surface. The system operated with standard settings for all the surveys reported within this chapter (Table 2.1). Positional information was acquired using an OmniLite132 differential GPS (Fugro Spatial, Perth), with a positional accuracy of ± 0.9 m (R.M.S.). Data was logged using the Simrad ES60 logging software version 1.5.2.76 (Kongsberg Simrad, Norway) as

Simrad Raw data files. The system volume backscatter strength (S_v dB re m^{-1}) was calibrated using a standard 38.1 mm tungsten carbide sphere according to standard methods and standard units (Foote *et al.* 1987, MacLennan *et al.* 2002).

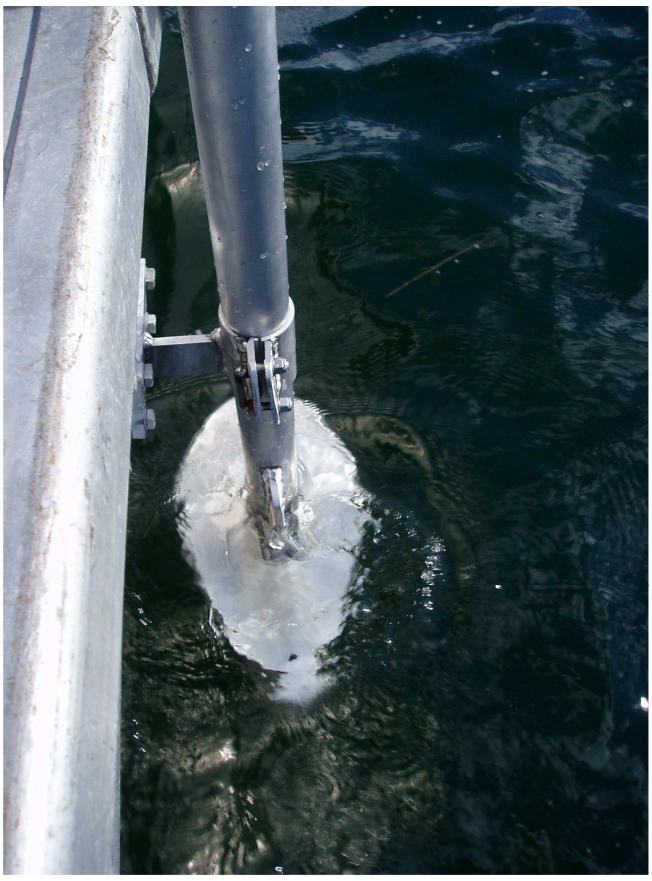

Figure 2.1. Pole mounted acoustic transducer of the Simrad ES60.

Table 2.1. Calibration settings required by Echoview for calculation of echo integration.

Setting	Unit	Value
Absorption coefficient (dB/m)	dB/m	0.0387
Sound speed (m/s)	m/s	1490.0
Transmitted Power	W	100.0
Two-way beam angle (dB re 1 Steradian)	dB re 1 Steradian	-17.50
Transducer Gain	dB	23.2
Sa correction	dB	-3.54
Transmitted pulse length	ms	0.256
Frequency	kHz	120

2.2.2. Acoustic Pre-processing

The ES60 single beam echo sounder has a systematic ping indexed variation (1 dB) in the digitised echogram data. This variation can be described by a triangle wave function, with 1 dB amplitude and a period of exactly 2721 pings (Ryan and Kloser 2004). Prior to calculating the acoustic indices in Echoview, the raw ES60 data was corrected for this error using a java application, es60adjust1.jar (CSIRO Marine, Hobart). This application integrates a portion of the ring down where the signal is constant, and then uses this to calculate where in the triangle

wave cycle this ping occurs. A correction factor is then applied to the raw data and this is saved as a new corrected file.

The corrected echo data were imported into Echoview. The calibration data were applied to the acoustic data within Echoview (Table 2.1). The absorption co-efficient and the speed of sound were calculated using the sonar calculator in Echoview (Mackenzie 1981, Francois and Garrison 1982), based on the water temperature, salinity, depth (half maximum bottom depth) and pH. Temperature and salinity were measured using a conductivity temperature depth probe (CTD), with pH assumed to be 8 (Byrne 2002).

2.2.3. Calculating E1 and E2 Indices

E1 and E2 are simple indices that can be used to describe the average acoustic energy returned from the seabed based on echo integration. The E1 value is an integration of the tail of the first echo and is reported to be sensitive to the roughness of the seabed. The E2 value is an integration of the entire second echo and is reported to be sensitive to the hardness of the seafloor (Figure 2.2). The method for calculating these indices is outlined below.

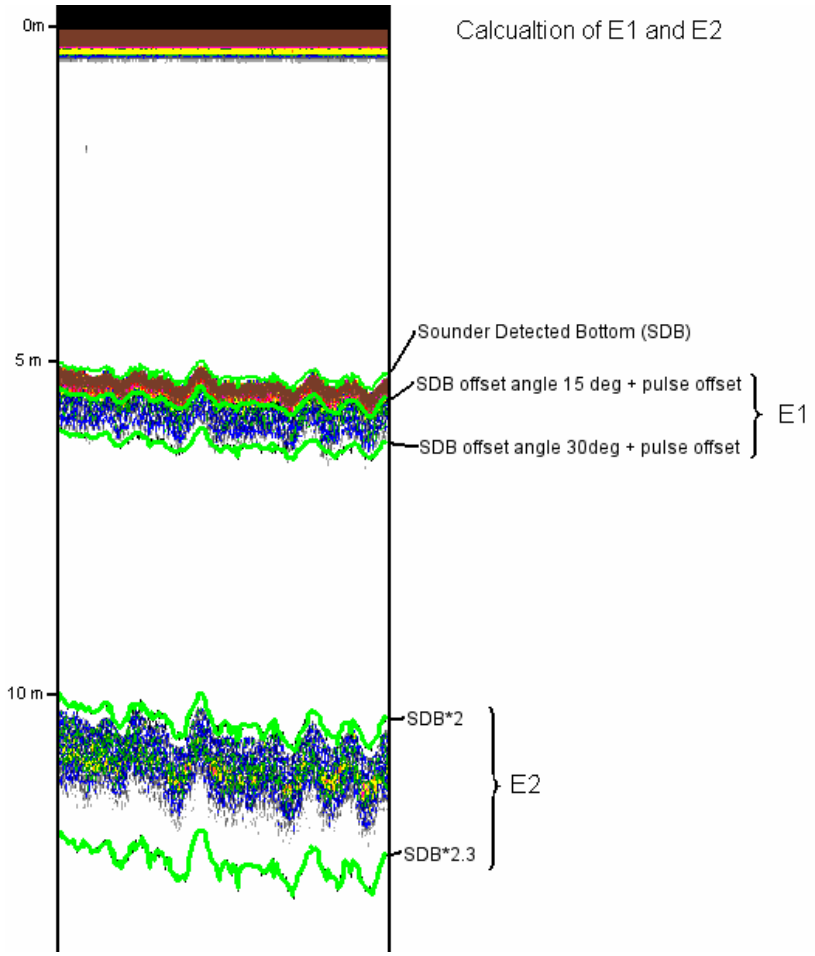

Figure 2.2. Echogram displayed in Echoview showing the lines used to calculate the E1 and E2 indices

The E1 and E2 values calculated in Echoview were based on those described in Kloser *et al.* (2001) with modifications to account for the shallow water as described below. All lines were based on the estimate of the echo sounder detected bottom. Due to problems with the Simrad ES60 algorithm in areas of dense algae, the line pick algorithm in Echoview was used to define a line related to the bottom. The Maximum Sv with backstep function was used (Table 2.2). The E1 index was defined as the integration of the tail of the first echo based on two lines defined by an offset angle plus one pulse offset. For the upper limit the offset angle was set at 15 degrees, while for the lower limit the offset was set at 30 degrees. Pulse offset was calculated as the speed of sound, c (m/s) multiplied by the pulse duration, τ (ms), (1489.97 m/s x 0.000256s = 0.38 m). The footprint of the E1 index is an annulus of seafloor, with the diameter of the inner and outer circles which define this annulus related to the offset angles. Due to beam spreading this annulus will increase in size with increasing range from the transducer.

Table 2.2. Settings used for Maximum Sv with backstep algorithm in Echoview, used to calculate position of sounder detected bottom.

Setting	Unit	Value
Maximum Sv for good pick	dB	-25.00
Discrimination level	dB	-15.00
Backstep range	m	-0.15
Start depth	m	2.00
Stop depth	m	20.00

The E2 index was calculated as the integration of the entire second echo between two defined lines. The upper line was defined as 2 times the bottom pick and the lower line as 1.3 times the upper line. The integration was calculated for single pings, with this data then averaged over a five ping moving window to account for ping to ping variability inherent in SBES data. This ping to ping variation is due to differences in the microstructure of the seabed and the echo statistics contained within this variability can be used to estimate bottom roughness, correlation lengths and bottom microstructure (Stanton 1985). Five pings were determined as the minimum number that was required to minimise the inherent variability in the data whilst still maintaining a small sampling unit. At an average vessel speed of 6 kts and a ping rate of 2 pings per second this equates to a distance of approximately 7.5 m.

The E1 and E2 values were output from Echoview as Nautical Area Scattering Coefficient (NASC) which is a measure of area scattering and designated by the symbol s_A. NASC is defined as:

$$s_A = 4\pi(1852)^2 s_a \qquad \text{(MacLennan } et\ al. \text{ 2002)}$$

where s_a is the area backscattering coefficient.

The NASC data was converted to Nautical Area Backscattering Strength (S_A) for analysis and display using the following formula:

$$S_A = 10\log_{10}(s_A) \qquad \text{(MacLennan } et\ al. \text{ 2002)}$$

2.2.4. Additional Sampling Equipment

Additional sampling equipment was used to sample the seafloor at each of the study sites in order to characterise the seabed properties and ensure as far as possible that similar seafloor types were being sampled by the acoustic system.

The video system used to sample the seafloor consisted of a single underwater digital video camera (SciElex, Tasmania) mounted in a heavily weighted tow fish (Figure 2.3). The system was deployed from a davit mounted above the transducer mount and its height in the water column was controlled by an electric winch. The camera system was flown approximately 0.5 to 1 meter above the seafloor, whilst the vessel was allowed to drift or slowly driven forward. This ensured that the camera system remained more or less directly below the vessel, especially in shallow water depths. Positional information from a differential GPS were overlayed on the video which was recorded in digital format, with the positional information also recorded in the vessel tracklog. Estimates of the positional accuracy of this video system are provided in Chapter 6, section 6.3.1. The video data were analysed by examining the video in four second blocks, with information on the substrate composition and texture recorded as well as any biota noted.

Sediments were sampled using a Van Veen grab (Figure 2.3). This grab worked effectively in sediments ranging from fine silts through to coarse sands. The grab used in this study had a maximum volume of approximately 27 litres. A small flap in the top of the grab allowed a sample to be removed for particle size analysis, while the rest of the sample was then examined for the presence of biota and large shell fragments. The process for analysing particle size is given in section 2.2.6.

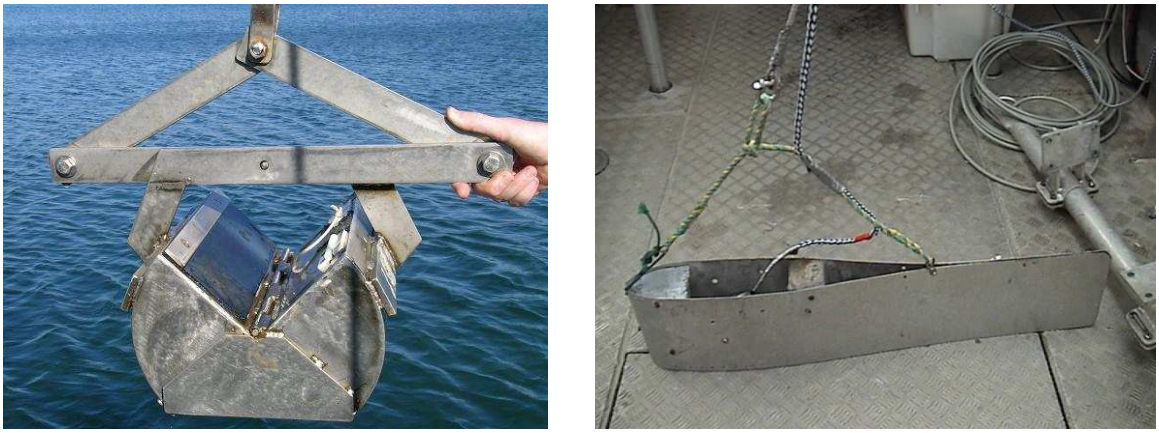

Figure 2.3. Van Veen grab (left) and underwater video system in weighted tow fish (right) used to sample the physical properties and biota of the seafloor.

2.2.5. Vessel Speed

The effect of vessel speed was examined by repeated surveys of an area of seafloor at a variety of speeds. An area of unconsolidated seafloor approximately 300 m by 250 m was chosen as the study site. The seafloor was composed of medium sands and ranged in depth from 8.5 – 10.5 m. It was located approximately 1 km southeast of Stanley on the northwest coast of Tasmania (Figure 2.4). This study site was chosen as it contained an area of uniform substrate with minimal structural complexity. The site also had little variation in depth across a large area which could otherwise confound such an analysis. Finally, the area was relatively sheltered making it an ideal area for survey in a small vessel.

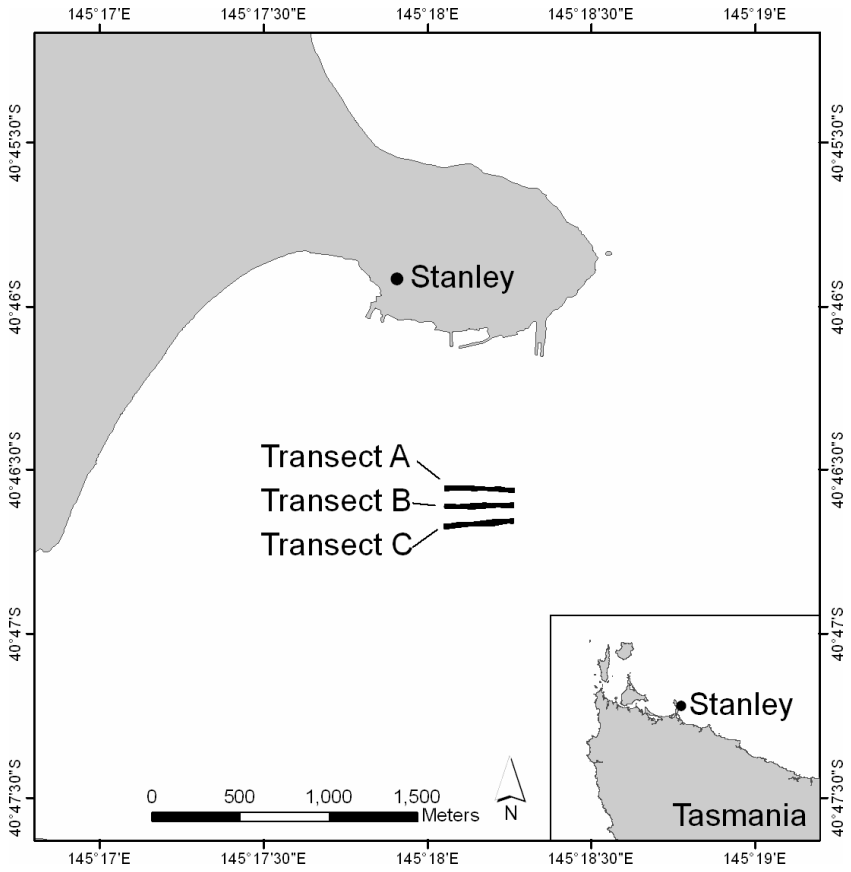

Figure 2.4. Location of study site for examining the effect of vessel speed on the measured acoustic response of the seabed showing the three transects sampled.

The study site was surveyed along three parallel 300 m transects running in an east-west direction at 2, 4, 6 and 8 kts. Each transect was surveyed in both directions at each of the four test speeds. The echo sounder was set to transmit at 100 W with a 0.256 ms pulse length. The ping rate was set to maximum. For each speed the vessel pitch was measured using an inclinometer, and acoustic noise was estimated based on integration of a region of the echogram below the echo return from the seafloor (De Robertis and Higginbottom 2007). The primary assumptions of the method are that background noise is independent of elapsed time during one transmit-and-receive cycle, and that at some point in the measured cycle, the measurement is dominated by contributions from background noise (i.e. $S_{v,noise} >> S_{v,signal}$). If these assumptions are met, a portion of the return observed from an active ping will give similar readings to those of an echo sounder in passive mode, which is a measurement of background noise. The signal received at the transducer face from long-range targets is attenuated by spherical spreading and absorption, and there is often little backscattering of the transmitted signal at ranges exceeding that of the seafloor. Often, the section between the first and second bottom echoes of an active ping is dominated by TVG-amplified background noise.

The weather conditions at the time of the survey were calm, with the wind 5 – 10 kts in an easterly direction, and an easterly swell of less than 0.5 m. Hence transects were run both with and against the light prevailing conditions, with the westerly transects running with the prevailing conditions and the easterly transects running against the prevailing conditions.

The E1 and E2 values were calculated as described previously (Section 2.2.2). Prior to analysis the E1 and E2 data were plotted to ensure that they were normally distributed. Analysis of variance (ANOVA) were used to separately examine the effects of transect, direction of travel and vessel speed on the acoustic response of the seabed. Firstly, an analysis was conducted on each of the three transects at a single speed (6 kts) to test the effect of direction of travel along the transects (either with or against the prevailing conditions). The speed of 6 kts was chosen as this represented a typical mapping vessel speed employed in the SeaMap Tasmania mapping program. Secondly, the difference between the three transects was tested again at a single speed (6 kts) and in a single direction (west). Finally, the effects of the four test speeds were analysed for each transect in a single direction (west) in order to discount the effect of prevailing conditions. Where significant effects were observed in the ANOVA, Tukey-Kramer HSD (honestly significant difference) tests were used to determine where these significant differences were occurring. The Tukey-Kramer HSD adjusts the alpha level where multiple test are run to decrease the chance of a false positive (type I error).

2.2.6. Depth

Acoustic data were sampled from three habitat types (reef, sand, and silt) at study sites in southern Tasmania for silt and eastern Tasmania for reef and sand substrates (Figure 2.5). These sites were chosen as they represented the spectrum of substrates typically found in coastal Tasmanian waters, and contained these substrates in across relatively large areas. Approximately 35 000 individual acoustic pings were collected in the 5 to 30 m depth range across these three habitats. The echo sounder settings were kept constant with the power output at 100 W and a pulse length of 0.256 ms. The acoustic system, vessel and vessel speed were kept constant for this data collection, and all data collection was conducted during similar weather conditions (wind < 5 kts, swell < 0.5 m). The raw acoustic data were corrected for the triangle wave error and processed for E1 and E2 values in Echoview 3.30. The E1 and E2 values were segmented into 5 metre depth strata for subsequent analysis.

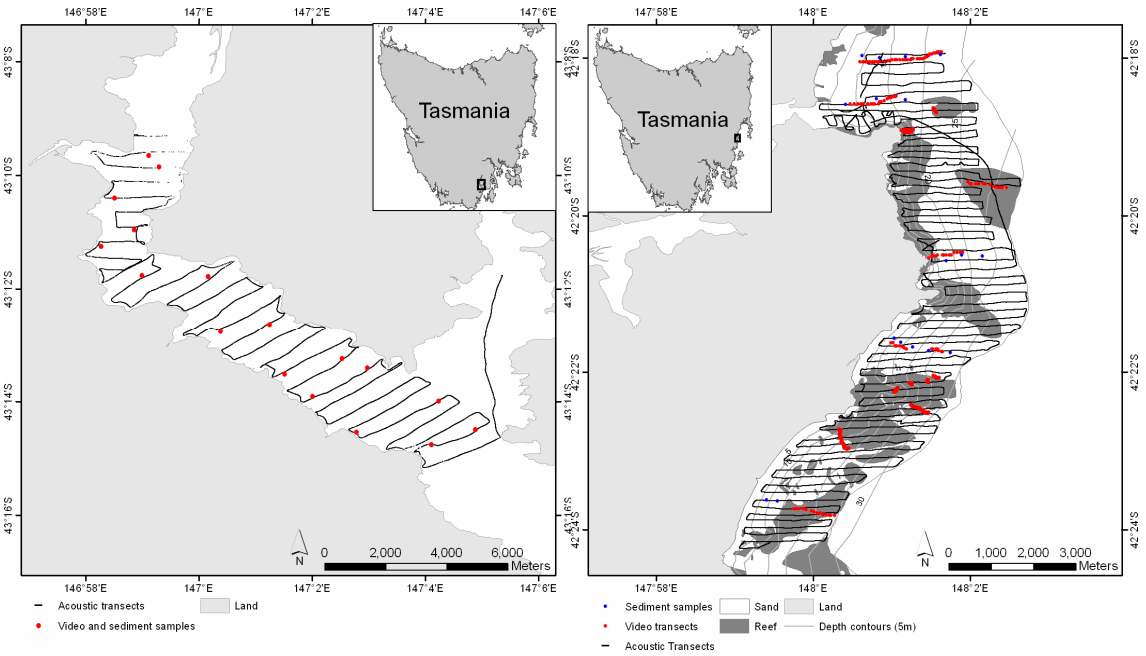

Figure 2.5. Location of study sites for silt (left) and reef and sand (right) showing location of acoustic transects and video and sediment sampling stations.

The habitats within each study site were surveyed with video and sediment grabs (for unconsolidated habitat) to ensure their uniformity in composition and structure. Sediment particle size information was used to compare the sediment structure for the sand and silt substrates.

Sediment samples collected from the Van-Veen grab were processed for particle size distribution (Wentworth 1922). Approximately 30 – 80 g from each sample was dried overnight at 80^{o} C. The dry samples were then weighed before being wet sieved through a series of stacked sieves (2 mm, 1 mm, 0.5 mm, 0.25 mm, 0.125 mm and 0.063 mm). The fraction in each sieve was then re-dried overnight at 80^{o} C before being weighed.

The final weights were used to calculate the percentage of each component. The proportion of sediment less than 0.063 mm that was washed through the finest sieve was then calculated as the difference between the sum of the weights of all the fractions and the original total sample weight. Particle size information was converted to the phi-scale, and used to calculate the phi 50% value for classification on the Wentworth scale (Wentworth 1922). Sediment particle information was used to confirm the grain size of the substrates being tested were similar across all depths. It should be noted that this process does not measure the consolidation of the substrate.

The underwater video was used to survey the surface structure of the reef and unconsolidated habitats, to ensure that the structure was similar across all depths surveyed. Only acoustic data

from unconsolidated substrate with little evidence of epifauna and/or structuring was included in the analysis. For reef substrate, only acoustic data from reef with a low profile and little structure was included in the analysis.

Whilst the use of sediment grabs and video can be broadly used to confirm similar substrates across different depth ranges, they can not be used to ensure complete conformity, especially in deeper water where due to the increase in footprint size with depth the acoustic system is likely to be sampling seafloor at a scale larger than these ground truthing systems provide data. To further ensure that homogenous substrate types were being used the acoustic data was also examined to ensure that there were no major shifts in the acoustic response of the seabed in the areas being surveyed which might indicate differences in the substrate type. The limitation of trying to select similar and homogenous substrate types across a range of depths are discussed in section 2.4.2.

Prior to analysis the E1 and E2 data were plotted ensure they were normally distributed. Analysis of variance was used to examine for differences in mean E1 and E2 between the depth ranges for the three substrate types. Where significant differences occurred, Tukey-Kramer HSD tests were used to examine which depth ranges had significant differences in the mean E1 and E2 indices.

2.2.7. Weather Conditions

To test the effect of the prevailing weather conditions a series of transects were run in both calm and rough conditions. Calm conditions were defined to be when the wind was less than 5 kts and swell less than 0.5 m, while rough conditions were defined to be when the wind was greater than 15 kts (as indicated by the presence of small whitecaps) and swell greater than 1 m. The transects were conducted at a study site situated at Bicheno on the east coast of Tasmania which contained a mix of reef and sand habitat between 5 and 20 m depth (Figure 2.6). This site represented an area of coastline that was safely accessible from a small vessel in both calm and rough conditions. While the identical transects were attempted to be run in both conditions, due to difficulties in navigating a small vessel, especially in rough conditions, the transects were generally within ± 10 m of each other, however were up to a maximum of 30 m apart. Only data from points within ± 5 m of each other were considered for the analysis. The acoustic system was the same as that used in the previous two experiments, with the same sounder settings used (Table 2.1). The raw acoustic data were corrected for the triangle wave error and imported into Echoview 3.30 with E1 and E2 values calculated as described in section 2.2.2. Due to potential depth bias, only data from 10 m ± 1 m were included in the

analysis. Prior to analysis the E1 and E2 data were plotted ensure they were normally distributed. T-tests were used to compare the data for each of the substrate types between the calm and rough conditions.

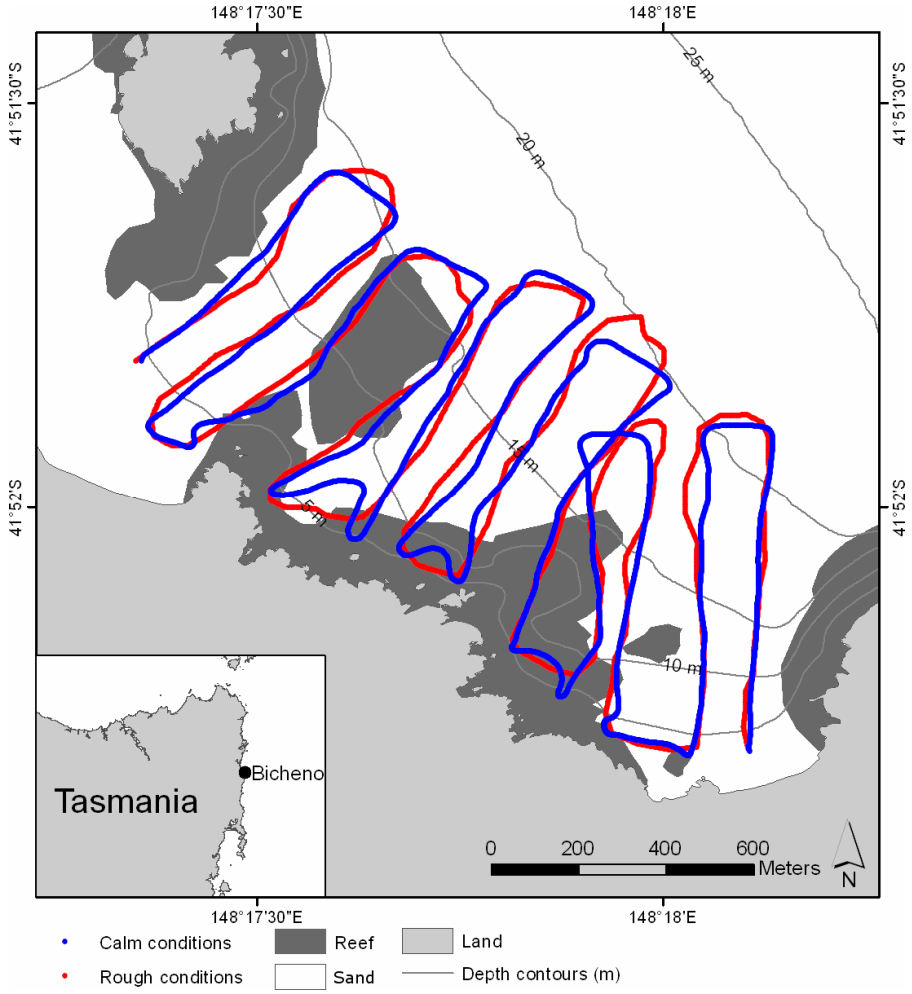

Figure 2.6. Map of the transects used to assess the effect of weather conditions on the classification of acoustic systems. Habitats and depth contours are from SeaMap Tasmania ((Lucieer *et al.* 2009)).

2.2.8. Slope

The effect of slope on the acoustic response of the seabed was examined through the comparison of acoustic data collected from a reef habitat of varying slopes around Bicheno on the east coast of Tasmania (Figure 2.7). Slope was only tested across reef habitat as this substrate was both the most variable and also had the largest magnitude of slopes. A total of approximately 50 acoustic transects were conducted. The reef within this region varied from relatively flat to steeply sloping undersea cliffs, and was predominantly comprised of large slabs of granite.

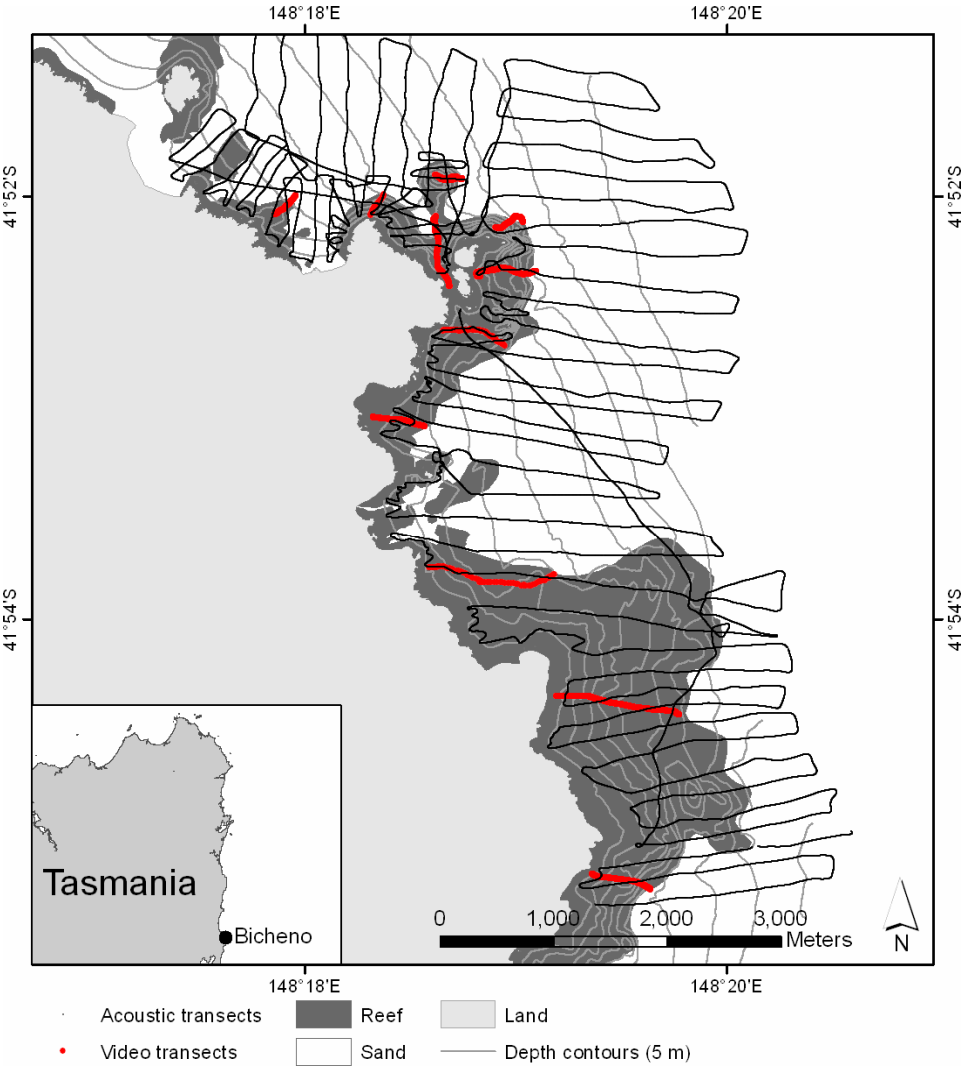

Figure 2.7. Location of the study site for examining the effect of slope on acoustic classification indicating the location of the acoustic transects and video ground truth sites in relation to bathymetry and habitats from the SeaMap Tasmania project ((Lucieer *et al.* 2007))

Slope was calculated for transects running perpendicular to the shore, across the depth gradient. The slope was calculated as the rise or fall of the seabed between adjacent echo sounding points, with the distance between points calculated from differential GPS positions. Slope was converted to angular degrees from the horizontal, with data only used where the slope stayed constant (± 2 degrees) for more than 10 consecutive acoustic pings. To account for potential depth bias only data between 10 and 15 m were analysed. Routine video tows were used to examine the structure of the seafloor. A series of 11 video transects were used to characterise the seafloor topography and biota to ensure the substrate was as similar as possible between the different slope categories examined (Figure 2.7). The video in the 10 to 15 m depth range was assessed for structure of the seafloor and dominant biota. Only areas of solid reef were used in this analysis; where extensive boulder fields were observed the data

was excluded from the analysis. In all video transects the biota in the 10 – 15m depth range was dominated by a mix of macroalgae (*Phyllospora comosa* and *Ecklonia radiata*) with consistent dense coverage across transects. Only the slope data from the acoustic transects that were covered by these video transects were analysed.

Prior to analysis the E1 and E2 data were plotted ensure they were normally distributed. Analysis of variance was used to examine for differences in mean E1 and E2 between the depth ranges for the three substrate types. Where significant differences occurred, Tukey-Kramer HSD tests were used to examine which depth ranges had significant differences in the mean E1 and E2 indices.

2.3. Results

2.3.1. Vessel Speed

The effect of the direction of travel was found to be significant based on analysis of variance for both the E1 and E2 indices for each of the three transects (Table 2.3). In all cases the E1 and E2 means were higher for the westerly direction of travel (with the prevailing conditions) than the easterly direction of travel (against the prevailing conditions).

Table 2.3. Results of ANOVA for effect of transect direction on the acoustic response (E1 and E2) for the three transects at 6 kts.

Transect	Mean E1 East (± S.E.) dB re1(m^2 nmi^{-2})	Mean E1 West (± S.E.) dB re1(m^2 nmi^{-2})	F-stat (df) probability	Mean E2 East (± S.E.) dB re1(m^2 nmi^{-2}	Mean E2 West (± S.E.) dB re1(m^2 nmi^{-2})	F-stat (df) probability
A	26.67 ± 0.09	26.96 ± 0.10	F = 5.48 (1, 2078) p = 0.02	31.51 ± 0.09	32.15 ± 0.08	F = 26.8 (1, 2078) p <0.01
B	26.04 ± 0.09	26.53 ± 0.08	F = 15.7 (1, 2012) p <0.01	30.27 ± 0.09	31.82 ± 0.08	F = 205.6 (1, 2012) p <0.01
C	25.89 ± 0.08	26.22 ± 0.07	F = 7.28 (1, 2006) p <0.01	30.36 ± 0.09	30.63 ± 0.07	F = 6.86 (1, 2006) p <0.01

The analysis of variance for the three transects at 6 kts in a westerly direction showed significant differences between all transects in both the E1 (F = 18.7, (2, 2853) p <0.01) and E2 indices (F = 113.1 (2, 2853), p <0.01). The average E1 and E2 values were highest on transect A, and lowest on transect C (Figure 2.8 and Table 2.3). Tukey-Kramer HSD showed that the means for all pairs of transects were significantly different for both E1 and E2.

Table 2.4. Comparison of E1 and E2 means for the three transects in a westerly direction at 6 kts based on Tukey-Kramer (HDS) test.

Transect	Transect	E1 p-value	E2 p-value
A	B	<0.001	<0.001
A	C	<0.001	<0.001
B	C	0.03	<0.001

From the above results the effect of speed on the E1 and E2 values was tested for each transect separately, and in only the westerly direction. The results of the ANOVA again showed a highly significant effect (F-stat probability < 0.001) for both indices on all transects. Tukeys-Kramer HSD tests between the different speeds showed all combinations to be significantly different at P = 0.05, with the majority of p-values less than 0.001, with the exception of E1 for transect B at speeds of 6 and 8 kts (P = 0.306), and E2 for transect A at speeds of 4 and 6 kts (P = 0.741) and transect B at speeds of 4 and 6 kts (P = 0.926). In all cases, increasing speed led to a decrease in the values of E1 and E2, with the exception of E2 for transect B (where values increased from 4 kts to 8 kts), E2 for transect A (where the value increased slightly between 4 and 6 kts before falling again at 8 kts), and E2 for transect C (where the value increased slightly from 6 to 8 kts) (Table 2.3). For the E2 index the greatest change was between 2 and 4 kts, while for the E1 index the change was more stable across all speeds tested.

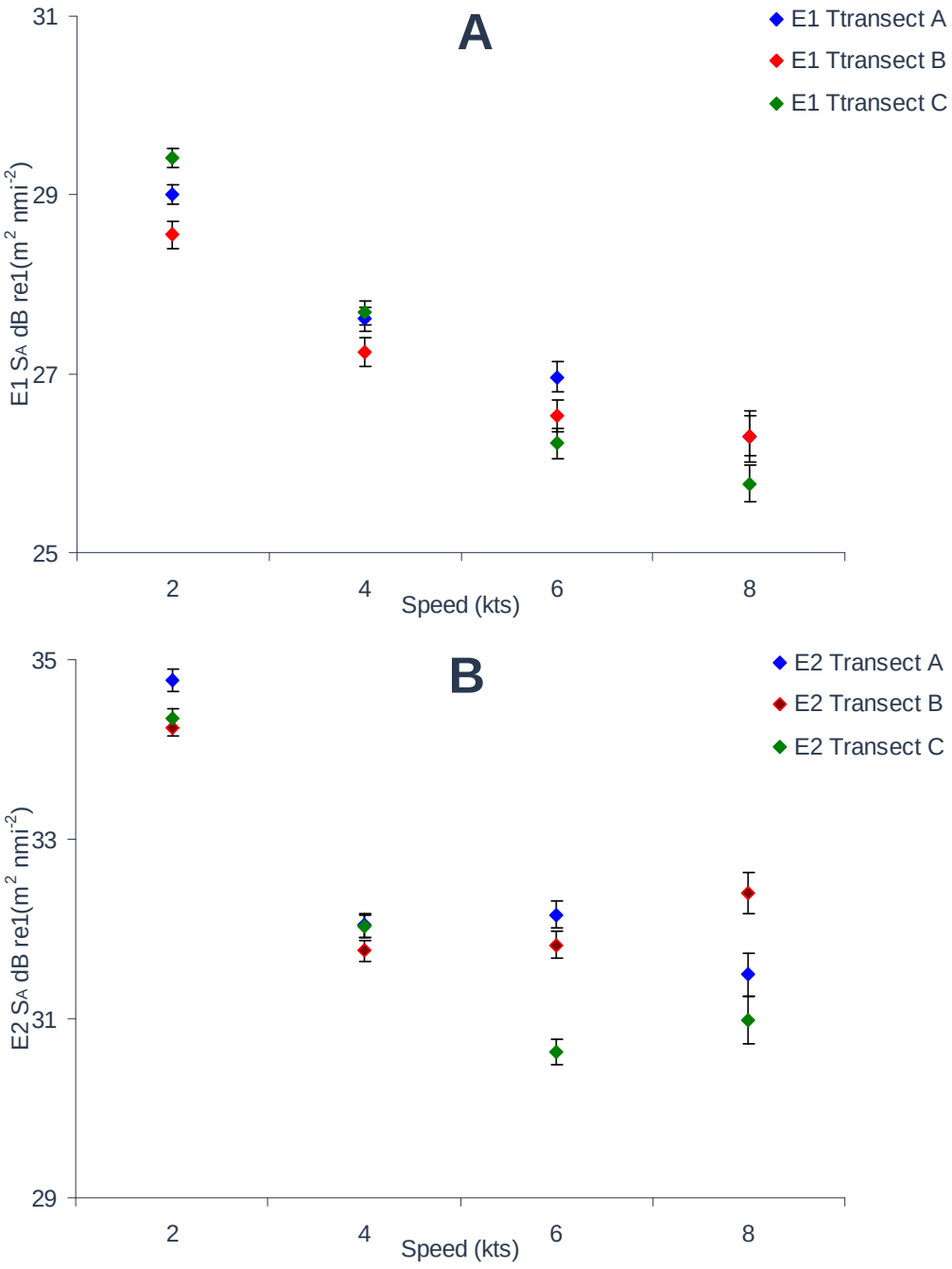

Figure 2.8. Mean E1 (A) and E2 (B) values for the three transects (A, B, and C) running in a westerly direction for speeds of 2, 4, 6 and 8 kts. Error bars give 95% confidence intervals.

Changes in vessel speed are coupled with changes in both engine revolutions per minute (rpm) and, for small planing hull vessels, also the pitch. The engine rpm increased with vessel speed, with a related increase in acoustic noise (Table 2.5). The estimates of noise were relatively constant for 2 and 4 kts but increased for 6 and 8 kts. The pitch of the vessel also changed with increasing speed, with the greatest increased between 6 and 8 kts (Table 2.5).

Table 2.5. Acoustic noise estimate (at 50 m) for vessel speeds and corresponding engine rpm between 2 kts and 8 kts.

Vessel Speed (kts)	Engine rpm	Noise estimate (volume reverberation noise @ 50m S_V dB re m^{-1}))	Vessel pitch (degrees)
2	6000	-88.0	0
4	10000	-87.5	0.8
6	16000	-84.8	1.2
8	20000	-75.5	3.7

2.3.2. Depth

Sampling equivalent habitats across a range of depths was difficult because of the patch size. Sediment particle size distribution from the two unconsolidated sediment classes, silt and sand, showed little variation with depth. Several of the samples of silt between 5 and 15 m depth showed slight increases in proportion of fine sands (Phi size 2 to 3), while in the deeper sediments a few of the samples exhibited small proportions of larger particle sizes which were predominantly made up of fine shell grit. The particles size for the sand substrate showed little or no larger particles (Phi size -2 to 1), with an average phi size of between 2 and 3.

Depth 5 – 10 m

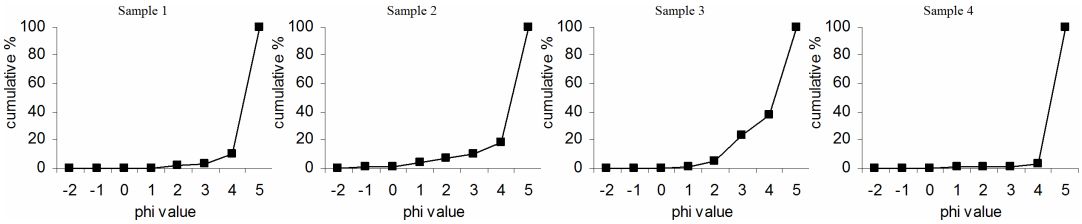

Depth 10 – 15 m

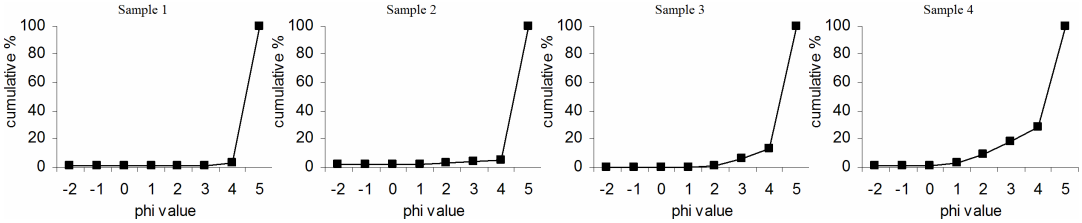

Depth 15 – 20 m

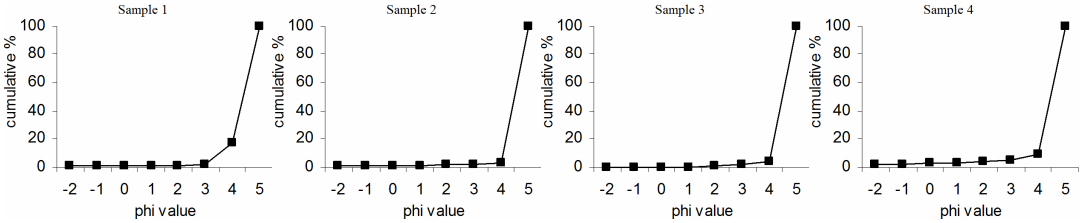

Depth 20 – 25 m

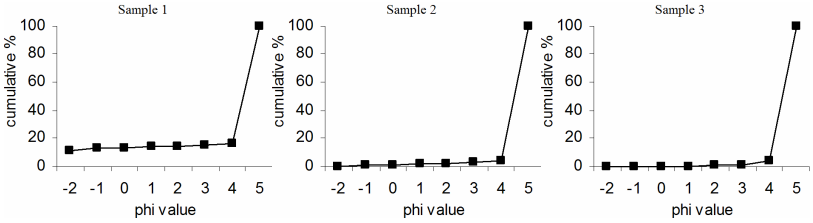

Depth 25 – 30 m

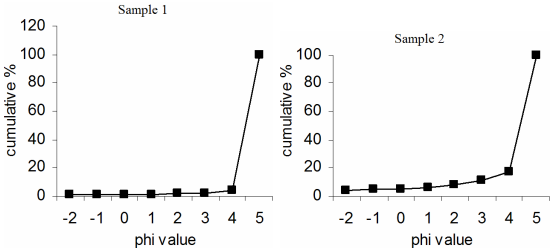

Figure 2.9. Sediment particle size graphs for silt substrate across the depth range 5 - 30 m.

Depth 5 – 10 m

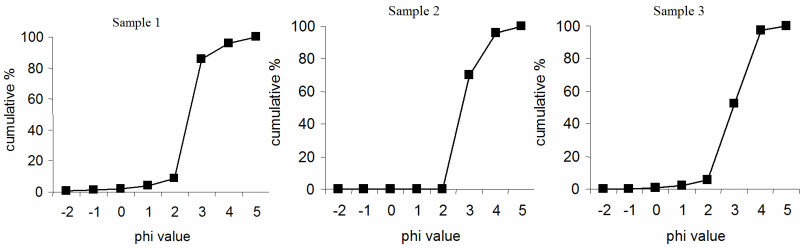

Depth 10 – 15 m

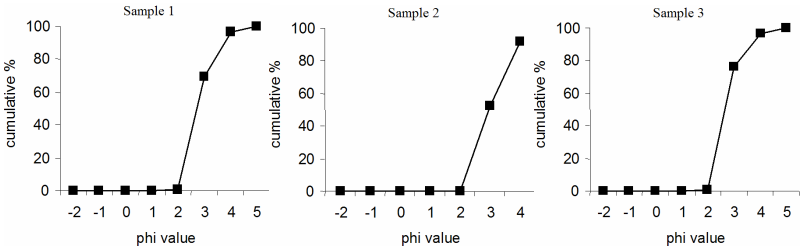

Depth 15 – 20 m

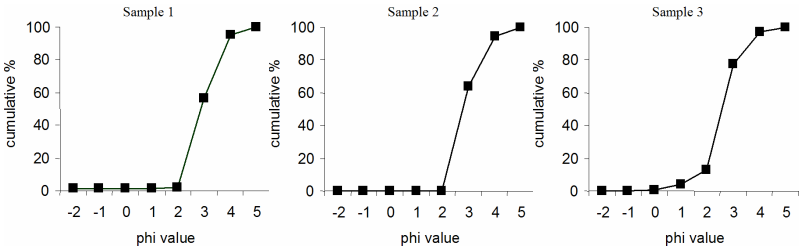

Depth 20 – 25 m

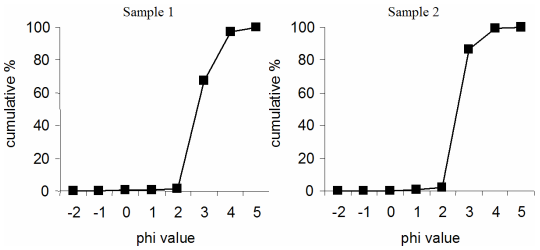

Depth 25 – 30 m

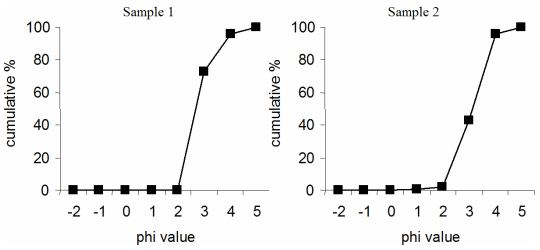

Figure 2.10. Sediment particle size graphs for sand substrate across the depth range 5 - 30 m.

The video description of the three substrate classes by depth showed, overall, that they remained relatively constant with depth (Table 2.6). The reef structure was similar across depth, generally low profile (rise and fall less than 1 m) with occasional cracks and small boulders. The algal distribution on the reef showed a strong structuring with depth (Table 2.6).

The silt remained relatively similar across the entire depth range, being generally flat with a few small burrows. Silt in the 25 – 30 m depth range had occasional shells (*Maoriculpus roseus*) visible on the surface, but in a low density of less than 1 per m^2. The sand showed a slight variation with depth. In depths less than 20 m, small regular small ripples (< 5 cm high) were commonly observed. Below 15 m depth small amounts of dead shell and shell fragments were observed on the substrate surface.

Table 2.6. Video description of major substrate features for reef, silt and sand by depth strata between 5 and 30 m.

Depth Range	Reef	Silt	Sand
5 – 10 m	Low profile reef with few small boulders and dense cover of algae, especially *Phyllospora comosa*	Flat substrate with a few small burrows	Flat substrate with regular small ripples, no shell matter
10 – 15 m	Low profile reef with dense cover of algae especially *Phyllospora comosa* and *Ecklonia radiata*	Flat substrate with a few small burrows	Flat substrate with regular small ripples
15 – 20 m	Low profile reef with medium density of algae *Ecklonia radiata*	Flat substrate with a few small burrows	Flat substrate with regular small ripples and small amount of shell fragments in furrows between ripples
20 – 25 m	Low profile reef with medium density of algae *Ecklonia radiata*	Flat substrate with a few small burrows	Flat substrate small amount of shell matter
25 – 30 m	Low profile reef with low to medium density of algae *Ecklonia radiate* and mixed red algae	Flat substrate with a few small burrows and occasional shell on surface	Flat substrate with small amount of shell matter

The E1 and E2 values calculated from 35 000 acoustic pings were examined for the effects of depth. The E1 values showed a slight increase with increasing depth for silt, and a slight decrease for reef habitat (Figure 2.11). The E1 values for sand showed an initial increase between 5 m and 15 m then a slight decrease from this depth to 30 metres. The peak in E1 values possibly represents the presence of both ripples and shell fragments in the 15 – 20 m depth range, whereas in the other depth ranges these are not present. Analysis of variance for the E1 index for each of these habitats showed the relationship between depth and E1 was highly significant in all cases (F-stat < 0.001). Tukeys-Kramer HSD tests between adjacent 5 m depth bins for each of these habitats showed a highly significant difference in the means ($P < 0.001$) except for the sand substrate for the 20 – 25 m and 25 – 30 m depth binds ($P = 0.279$).

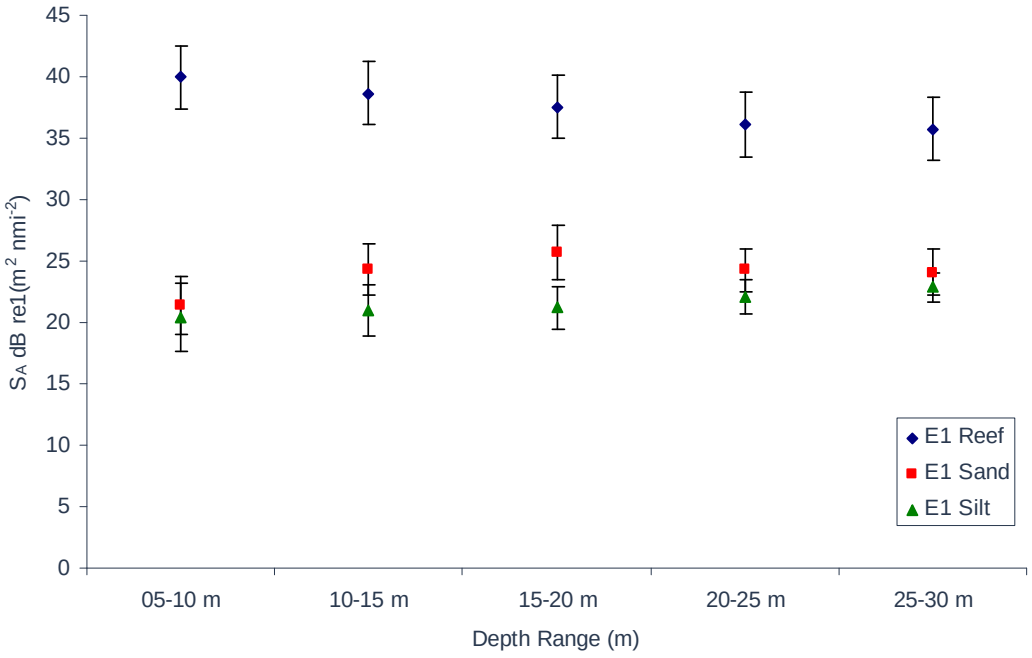

Figure 2.11. Depth trends in the E1 acoustic index for consolidated reef and unconsolidated sand habitats. Error bars show 95% confidence intervals.

The E2 values showed a similar trend for the reef and sand habitats, with both increasing with depth. The E2 values for the silt habitat showed an initial decrease in the 5 – 15 m depth range, followed by a slight increase to 30 m depth (Figure 2.12). The particle size information for the silt habitat identified an increase in the amount of fine sand matter in the 5 – 15 m depth range compared to the other depths. The elevated E2 indices in this range may reflect this difference. Analysis of variance showed that the relationship between depth and E2 was highly significant (F-stat <0.001). Tukey-Kramer HSD tests for each of the adjacent 5 m depth bins similarly showed highly significant differences ($P < 0.001$).

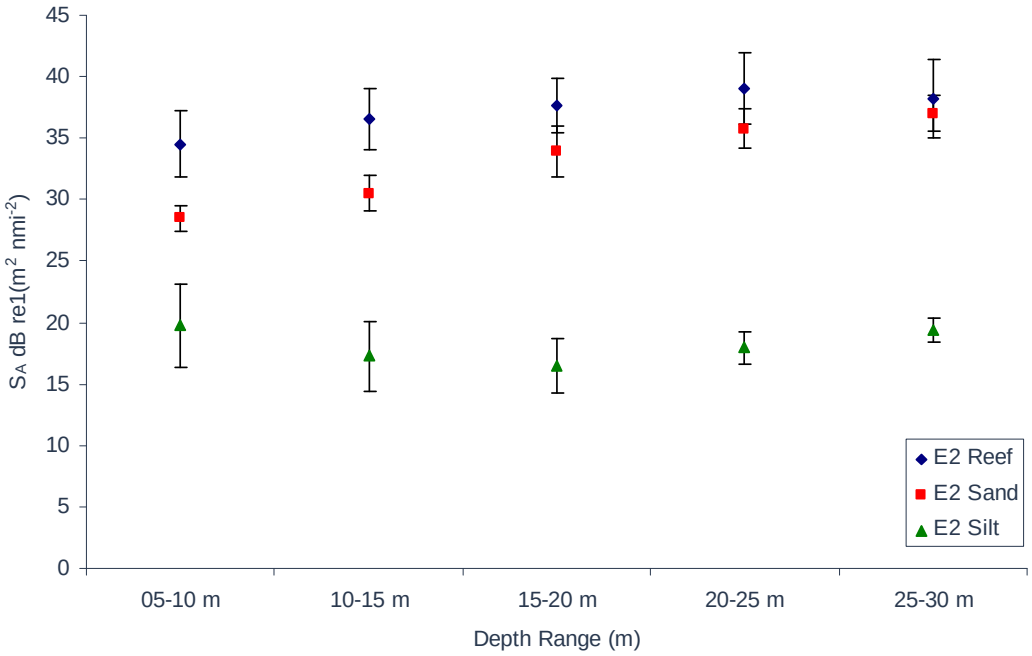

Figure 2.12. Depth trends in the E2 acoustic index for consolidated reef and unconsolidated sand habitats. Error bars give 95% CI.

The magnitude of the depth trend on the mean E1 and E2 values for each of the three habitats was between 2.5 and 4.5 dB, with the exception of the mean E2 value for sand, which was 8.6 dB (Table 2.7). This has the potential to influence the classification of this data and is discussed below.

Table 2.7. The magnitude of the depth dependence for the E1 and E2 indices (dB re1(m^2 nmi^{-2})) for reef, sand and silt habitat.

Substrate	E1	E2
Reef	4.2	4.5
Sand	4.3	8.6
Silt	2.5	3.2

2.3.3. Prevailing Conditions

The transition from calm to rough conditions had two effects that impacted on the measured acoustic scattering from the seafloor. Firstly, the presence of wind generated waves caused an increase in vessel pitch and roll. This has the effect of taking the acoustic axis off the normal incidence and thus changing the geometry of the acoustic wave interacting with the seafloor. Secondly wind speed above approximately 15 kts has the effect of causing “white caps”. These small breaking waves serve to entrain small air bubbles in the upper meter of the water column (Figure 2.13). These air bubbles act as small acoustic scatterers leading to both refraction and absorption of the acoustic energy from the transducer.

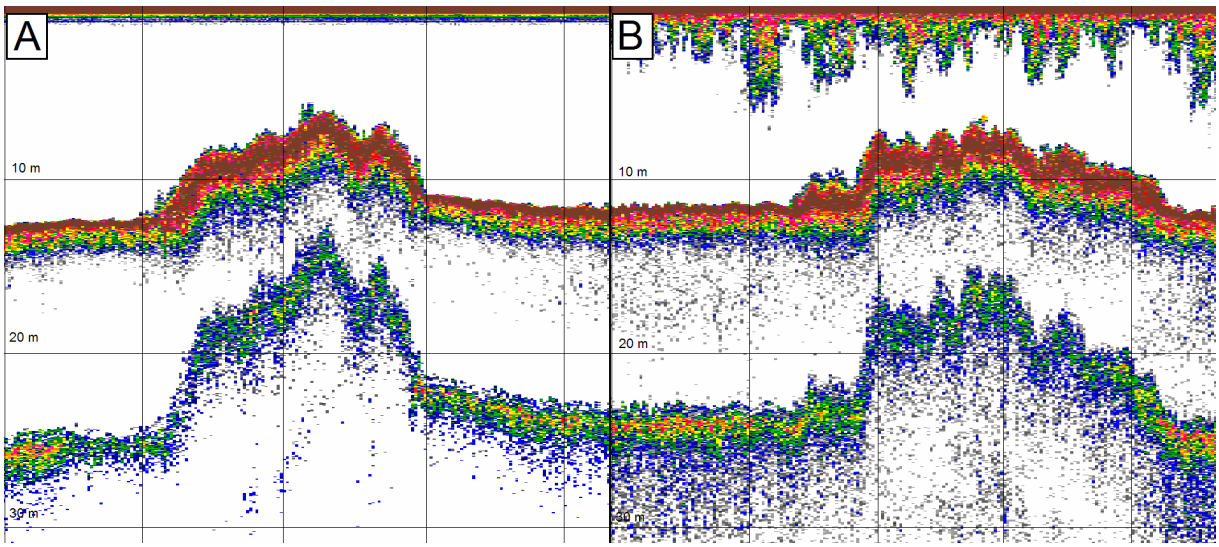

Figure 2.13. Calibrated volume reverberation (Sv) compensated echogram from Simrad ES60 120 kHz single beam echo sounder, set at 100 W, 0.256 ms pulse length, minimum Sv -60 dB showing two transects across a section of sand and reef substrate in (A) calm conditions (wind less than 5 kts, seas <0.5 m) and (B) rough conditions (wind greater than 15kts, seas >1m). The transects were generally within ± 10 m of each other, however were up to a maximum of 30 m apart. Vertical grid lines are spaced at 50 m, with horizontal grid lines spaced at 10 m.

Acoustic indices were compared for reef and sand in calm and rough conditions (Figure 2.14). Five hundred points in 10 m ± 1 m water depth were compared for each habitat in the two conditions. The difference between calm and rough conditions was more pronounced for the reef than for the sand. The reef in the rough conditions had weaker returns in the E1 and E2 indices (Table 2.8). The E1 for the sand habitat increased from calm to rough, while there was little change in the E2 (Table 2.8). T-tests on the effect of conditions on the E1 and E2 values for both reef and sand habitats showed a significant difference in the mean (Table 2.8).

Table 2.8. Mean (± S.E.) E1 and E2 values for reef and sand habitat in calm and rough conditions with t-test probability values.

Substrate	Conditions	Mean E1 (± S.E.) dB re1(m^2 nmi^{-2})	E1 P-value	Mean E2 (± S.E.) dB re1(m^2 nmi^{-2})	E2 P-value
Reef	Calm	34.6 ± 1.5	< 0.001	36.0 ± 1.5	< 0.001
Reef	Rough	32.4 ± 2.1		31.1 ± 2.0	
Sand	Calm	22.4 ± 1.2	< 0.001	30.5 ± 1.7	<0.001
Sand	Rough	24.4 ± 1.5		30.9 ± 1.9	

A comparison of the clustering of the E1 and E2 values for the reef and sand habitats in the two conditions showed that the separation between the reef and sand was greater in calm conditions than for rough conditions (Figure 2.14).

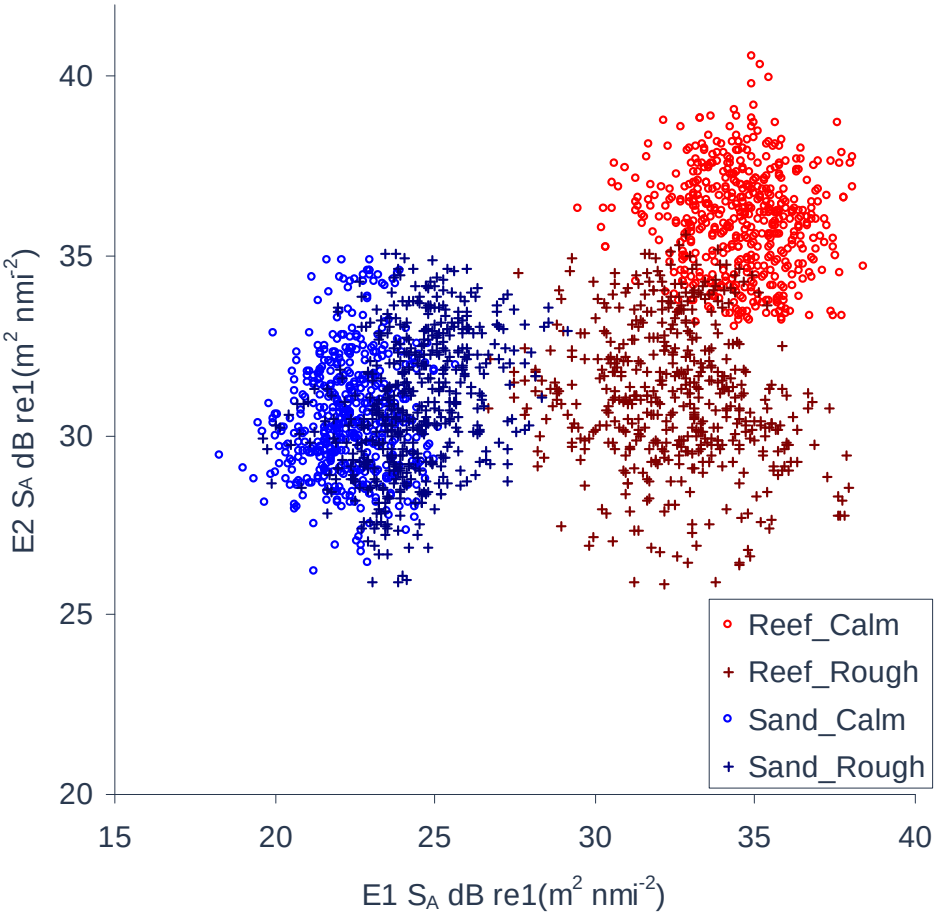

Figure 2.14. Cluster of 500 points at 10 m for reef and sand in calm (<5 kts, no swell) and rough (>15 kts, ~1 m swell) conditions. All points along ten meter depth contour.

2.3.4. Slope of bottom

The results of the slope analysis showed an increase in the E1 index with increasing slope and a decrease in the E2 index with increasing slope (Figure 2.15). The magnitude of these changes was 3.5 dB for the E1 index and 4.5 dB for the E2 index across the 45 degree slope range examined. Analysis of variance showed a significant effect of slope for both the E1 and E2 indices ($F < 0.001$).

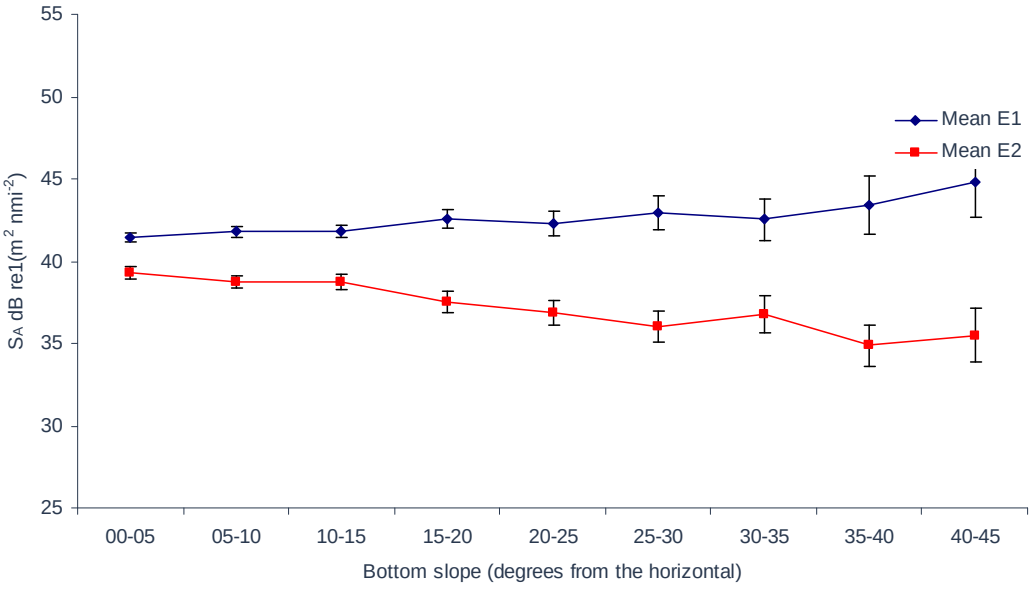

Figure 2.15. The average E1 (blue) and E2 (red) values (± 95% C.I.) for reef habitat of different slope.

Tukey-Kramer HSD tests were used to further examine the effect of slope on the E1 and E2 indices. Significant or highly significant differences were found in the means of both the E1 and E2 indices between many of the slope classes (Table 2.9). In general adjacent slope classes were not significantly different (i.e. 0 - 5 and 5 - 10 degrees). For the E2 indices no significant differences were found between the slopes greater than 15 degrees, presumably due to the increased variance of this measure with increasing slope (Figure 2.15). Note that increased variance was observed for both the E1 and E2 indices with increasing slope, with potential ramifications for classification accuracy.

Table 2.9. Summary of Tukey-Kramer HSD test p-values for analysis of slope effect on E1 and E2 values for reef habitat. Significant differences at the 0.05 level are indicated as *, with highly significant differences at the 0.01 level indicated as **.

Slope1	Slope2	E1 p-Value	Significance	E2 p-Value	Significance
00-05	05-10	0.077		0.445	
00-05	10-15	0.093		0.601	
00-05	15-20	<0.001	**	<0.001	**
00-05	20-25	<0.001	**	<0.001	**
00-05	25-30	<0.001	**	<0.001	**
00-05	30-35	<0.001	**	0.002	**
00-05	35-40	<0.001	**	<0.001	**
00-05	40-45	<0.001	**	<0.001	**
05-10	10-15	1		<0.001	**
05-10	15-20	<0.001	**	0.051	
05-10	20-25	0.127		<0.001	**
05-10	25-30	<0.001	**	<0.001	**
05-10	30-35	0.072		0.05	*
05-10	35-40	<0.001	**	<0.001	**
05-10	40-45	<0.001	**	0.005	**
10-15	15-20	<0.001	**	0.103	
10-15	20-25	0.28		0.003	**
10-15	25-30	<0.001	**	<0.001	**
10-15	30-35	0.132		0.069	
10-15	35-40	<0.001	**	<0.001	**
10-15	40-45	<0.001	**	0.007	**
15-20	20-25	0.924		0.935	
15-20	25-30	0.897		0.237	
15-20	30-35	<0.001	**	0.97	
15-20	35-40	0.114		0.024	
15-20	40-45	<0.001	**	0.355	
20-25	25-30	0.284		0.94	
20-25	30-35	0.992		1	
20-25	35-40	0.013	*	0.279	
20-25	40-45	<0.001	**	0.862	
25-30	30-35	0.975		0.994	
25-30	35-40	0.801		0.911	
25-30	40-45	<0.001	**	1	
30-35	35-40	0.288		0.546	
30-35	40-45	<0.001	**	0.951	
35-40	40-45	0.008		1	

2.4. Discussion

2.4.1. Vessel Speed

Changes in vessel speed were shown to significantly affect the computed E1 and E2 indices with both the E1 and E2 values decreasing with increasing vessel speed. Changes in the vessel speed resulted in measurable changes in both the vessel pitch and in the noise generated by the vessel. Changes in vessel pitch and acoustic noise due to vessel speed are known to influence single beam acoustic measurements of seafloor acoustic properties (Hamilton *et al.* 1999, Kloser *et al.* 2001b, von Szalay and McConnaughey 2002). Previously the E2 parameter of the RoxAnn system has been reported to be inversely related to speed (Hamilton

et al. 1999). However, the E1 parameter of the RoxAnn system, and the classification performance of the QTCView system have been reported to show no significant effect related to changes in vessel speed (Hamilton *et al.* 1999, von Szalay and McConnaughey 2002). The decrease in the E1 values with increased speed observed in this study contrasts with these previous findings, however this may be due to the type of vessel being used. The previous studies were all based on large displacement hull fisheries vessels, whilst this study was conducted from a small planing hull vessel. Small planing hull vessel responds differently to changes in vessel speed compared with the larger displacement hull vessels, with large changes in the pitch of the hull as the vessel approaches planning speed.

Changes in vessel pitch and roll associated with changes in vessel speed will result in the acoustic response of the seabed being measured off the normal angle of incidence, which is a general assumption when processing SBES data (Chivers 1990). Values of both E1 and E2 are likely to be affected when this assumption is violated, with this variation dependant on seabed type (Greenstreet *et al.* 1997). The vessel used in this study displayed measurable changes in the vessel pitch due to changes in vessel speed, especially at higher speeds. Further, at low speeds the vessel stability was also affected, leading to increased vessel pitch and roll. Changes in acoustic noise were observed in this study, primarily due to changes in engine revolutions per minute (rpm). Engine rpm were approximately 6 000 rpm at 2 kts, and increased to 20 000 rpm at 8 kts, with estimates of acoustic noise increasing at higher speeds. Finally, increasing speed can result in increased turbulence and aeration around the transducer and hull, which causes attenuation of the acoustic sound pulse (Kloser *et al.* 2001b). Aeration can also be increased at very low speeds, where the excessive pitch and roll of the vessel will act to increase turbulence and aeration around the transducer. The decrease in the E1 and E2 parameters measured in this study are likely to be a consequence of increased vessel pitch at higher speeds resulting in less acoustic energy being reflected directly back to the transducer face (i.e. the system is no longer operating as a normal incident acoustic system), and increased aeration around the transducer resulting in more attenuation of the acoustic signal. The effect of speed on the measured acoustic response of the seabed has important ramifications for the consistency in classification of single beam data.

2.4.2. Depth

Depth was found to be a significant factor affecting the acoustic values of the E1 and E2 parameters, although trends were not always consistent between habitats. Possible depth bias in single beam acoustic data have previously been reported, with both E1 and E2 values showing a trend to increase with depth (Greenstreet *et al.* 1997, Kloser *et al.* 2001b). This

study found the E1 index increased for both sand and silt, but decreased for reef with increasing depth. This difference between reef and the other substrates may reflect the differences in the scale of surface roughness of these habitats compared to the footprint size of the acoustic beam due to spherical spreading. For example the acoustic footprint of the E1 index used in this study forms an annulus with a maximum diameter of 5.8 m in 5 m depth and a maximum diameter of 34.6 m in 30 m depth. This creates a different measurement scale at different depths, with different scales of surface roughness potentially expressing in different ways at these different scales. As reef habitat generally displays a greater level of surface roughness and at a larger scale than both sand and silt, the effect of depth on E1 index is likely present differently for this substrate type.

The E2 values also showed a significant depth bias. This was generally of a similar magnitude as that of the E1 values, with the exception of sand, which showed a significant increase in the E2 value with depth. This is likely to reflect a change in the sediment composition, as video surveys in the study area found an increased amount of shell debris in some of the deeper parts of the transects. The presence of shell may increase the acoustic hardness of the seabed, and may also lead to increased acoustic roughness (Williams *et al.* 2001). This increase in shell was not apparent in the particle size data.

Differences in the acoustic response from the same composition and structure of seabed at different depths are due to beam spreading, and pulse length effects (Urick 1983, Pouliquen 2004). Several methods have been employed to account for these differences, the use of constant angular algorithms have been used to reduce the depth dependence of the E1 index (Kloser *et al.* 2001b), while adjusting energy values to a reference depth through time and power adjustments have also been suggested (Sánchez-Carnero *et al.* 2007).

It should be noted that the differences in depth trends seen in this study may also reflect actual differences in habitat type. It is difficult to find identical habitat in terms of physical and biological composition and structure across a wide range of depths, with depth often a strong structuring factor for benthic communities (Carruthers and Walker 1999, Connell and Lincoln-Smith 1999, Bell and Barnes 2000c, Bell *et al.* 2002, Goldberg and Kendrick 2004`). For example, the increased E2 values for the silt habitat in 5 meters may reflect the presence of additional biological or physical matter, either on or within the substrate, which would affect the acoustic response of the seabed.

Finally, the use of video and sediment grabs, which generally only sample small areas, to determine the seabed composition may not necessarily provide the information required to

ensure that the seabed is homogenous over the area being sampled by the acoustic system. This is especially an issue in deeper water where due to the increase in footprint size of the acoustic system with depth there is an increased chance of sampling more than one substrate type. For example in this study the footprint of the E1 index was an annulus with an inner diameter of 2.7 m and an outer diameter of 5.8 m in 5 m depth, and with an inner diameter of 16.1 m and an outer diameter of 34.6m in 30 m depth. Areas of homogenous seafloor will have similar echo statistics; in the field these areas were determined through visual inspection of the echo trace during site selection. It should be noted that this study did not attempt to match the exact location of a sediment and video sample to a single acoustic ping. Instead broad areas of similar seafloor based on a combination of video and sediment grab data and also a consistent acoustic response from the seabed were used.

2.4.3. Prevailing Conditions

The effect of prevailing conditions differed for the reef and sand habitats. The decrease in the E1 and E2 values for the reef reflects a combination of the attenuation and scattering of the sound pulse in the aerated top layer of the water and reflection of the sound pulse away from the transducer from the seafloor due to the pitch and roll of the vessel. The large difference in the E2 values for reef may also reflect different reef being sampled. While sample points were only compared when they were within ± 5 m for the two treatments, this may have resulted in structurally different parts of the reef being sampled. However, many of the points sampled were within less than ± 1 m of each other between the two treatments and even for these points there the E2 values differed considerable suggesting that there is indeed some environmental influence on the acoustic return from this substrate.

The slight increase of the E1 values in the sand habitat reflects a greater portion of the tail of the returning signal to the transducer due to the artificial roughness created by the pitching vessel. The unchanged E2 hardness values may reflect a combination of the smooth uniform sand substrate still reflecting the majority of the acoustic energy back to the transducer, compared to the more complex reef, which may reflect more of the energy away due to the angle of incidence. Previous studies have reported marked attenuation of the tail of the first echo and the whole second echo due to increased aeration around the vessels hull (Kloser *et al.* 2001b).

The separation between the mean of the sand and reef clusters in the calm weather was greater than for the rough conditions, which suggests that the discrimination ability of the single beam acoustics is reduced by adverse environmental conditions. This highlights the need for

mapping in only suitable conditions. Potential ways to reduce this effect include running the transducer deeper in the water column, mounting the transducer in a tow fish which decouples it from the vessel motion, or the use of a pitch and roll sensor to aid in the quality control of the data (Greenstreet *et al.* 1997). Putting the transducer deeper would potentially place it below the greatest region of aeration in the water column. However, operationally this has disadvantages for small vessels in shallow water, especially where rapidly changing depths due to reef may result in contact between the transducer and the seafloor. There are also potential effects of the scattering of the sound pulse from the rough sea surface and attenuation through the aerated surface water when calculating the second echo energy strength. The use of a pitch and roll sensor for quality control to allow the removal of data when it exceeds a certain angle off the normal incident has potential to help maintain data quality, although in a small vessel (<6m) the amount of pitch and roll rapidly increases when the swell gets over 1 m, such that the majority of data would be off the normal incident and thus in violation of this basic assumption required when processing SBES data (Greenstreet *et al.* 1997).

2.4.4. Slope of Bottom

The slope of the seafloor was found to have a significant effect on the E1 and E2 values. The E1 index was found to have a positive correlation with slope, while the E2 index was negatively correlated with slope. The E1 index is often correlated with bottom roughness, with increased bottom slope having a similar effect to roughness, while the E2 index is often correlated with bottom hardness, in this case a highly sloped bottom will result in more of the signal being reflected away from the transducer, resulting in a weaker acoustic return (Chivers 1990, Greenstreet *et al.* 1997). Slope has been shown to have an effect on the classification of SBES data in previous studies (Hamilton *et al.* 1999, Kloser *et al.* 2001b, von Szalay and McConnaughey 2002). These studies have highlighted the misclassification of substrate over areas of high profile but not attempted to quantify the effect on the raw acoustic indices. This study has shown that the effects of bottom slope appear to be relatively predictable, at least for a single substrate in a single depth range, presenting the possibility of developing corrections for slope into the classification of SBES data.

2.4.5. General Discussion

Changes in the measured acoustic response of the seafloor due to vessel speed, depth, prevailing conditions and slope all have the potential to lead to misclassification of SBES data. Classification of SBES data is generally achieved through attribution of habitat types to clusters of acoustic indices (E1 and E2 for *RoxAnn*, and the three Q values for *QTC View*)

(Greenstreet *et al.* 1997, Cholwek *et al.* 2000, Ellingsen *et al.* 2002, Freitas *et al.* 2003b, Humborstad *et al.* 2004b). The magnitude of the variation caused by changes in vessel speed, depth, prevailing conditions, and bottom slope were all found to be similar across the range of operational limits commonly encountered whilst mapping inshore coastal habitats in Tasmania.

For example both the E1 and E2 indices showed a decrease with increasing speed, with a magnitude of ~4 dB across the vessel speed range tested. The average acoustic signatures (combination of E1 and E2 indices) of reef, sand and silt in the 10 m to 15 m depth range are typically separated by between 14 – 22 dB (Figure 2.16). Thus a change of this magnitude in the E1 and E2 values would in most cases not affect the final classification for the reef sand and silt substrates examined in this study. However, the seafloor is comprised of a wide range a substrates including mixed substrates. Mixed substrates can occur at a variety of scales including having a mixture of substrates within the acoustic footprint of a single ping. The spectrum of seafloor types generally results in a cloud of acoustic signatures rather than discrete clusters for each substrate type. In these cases measurement error due to changes in vessel speed may have a significant impact on classification accuracy and repeatability. Changes in depth, prevailing conditions and bottom slope were also found to produce variation in the acoustic indices of between 2 and 8 dB, which could similarly result in an increase in misclassification of habitat type. Finally, it is unclear to what degree these factors are correlated or uncorrelated, thus there is a need to control and account for all of these factors in assessing classification accuracy.

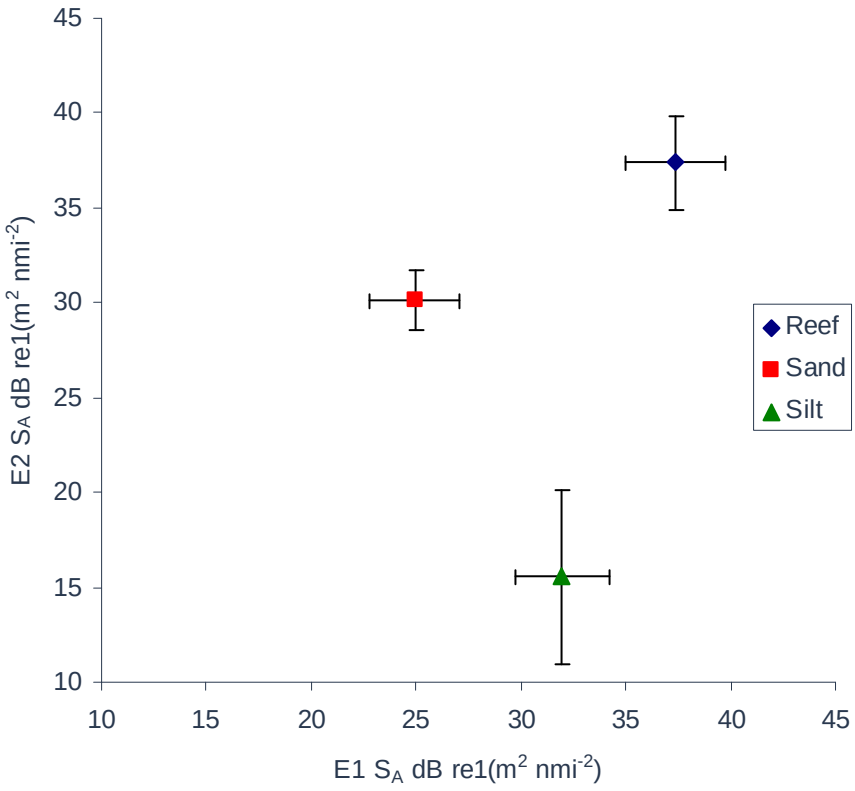

Figure 2.16. Plot of average E1 and E2 values for reef, sand and silt substrate in the 10 – 15 m depth range, with error bars showing standard deviation.

2.5. Conclusion

The measurements on the effects of vessel speed, depth, prevailing conditions, and bottom slope made in this chapter provide the basis for improving the consistency of SBES data. The importance of maintaining a consistent vessel speed, especially in small planning hull vessels, has been highlighted. Whilst it may be possible to develop a calibration for vessel speed based on the measures in this chapter, a more appropriate approach would to be eliminate the variation in the first place by maintaining a constant vessel speed both within and between surveys. Similarly the effect of adverse weather conditions on the quality of acoustic data suggests that operational procedures are the best method to tackle this source of error, limiting data collection to days where the weather will not influence the acoustic data.

The depth and bottom slope data on the other hand can not be controlled by operational procedures. Thus these two effects must be either absorbed into the final error budget, or alternatively calibrated in the data to improve the classification accuracy. For depth this presents several issues, as there appears to be a substrate dependent effect, and as the substrate is being interpreted from the acoustic data, this may have an effect on the capacity to provide a correction. The data however can be corrected for slope, however due to the natural level of

noise in the data this appeared to have little practical effect on improving the overall classification success.

In terms of classification of SBES data at the level of bio-geomorphic type and substratum/ecotype the level of variation due to the four factors investigated in this chapter need to be taken into account. For vessel speed and prevailing conditions these factors can be controlled through simple operational procedures, whilst for depth and bottom slope there will be a level of variation due to these factors, although this is generally within the level of noise typically exhibited in SBES data. Ultimately due to measurement bias and error fine scale differences in SBES data will be of limited use, therefore only large broad scale difference can be reliable and repeatedly achieved. These factors investigated in this chapter are likely to become more significant on classification at lower levels in the classification hierarchy, which are examined in the following chapters.

Chapter 3. Acoustic classification of unconsolidated sediment habitats using single beam acoustics.

3.1. Introduction

Knowledge of the distribution of benthic habitats is an essential part of management for any trawl or dredge fishery. Traditionally the distribution of these habitats has been inferred from the distribution of target and non target species examined using dredges, trawls, grabs and seafloor photography (Schwinghamer *et al.* 1996, Collie *et al.* 1997, Hall-Spencer *et al.* 1999, Collie *et al.* 2000, Hall-Spencer and Moore 2000). These techniques generally result in poor estimates of the key habitats across the whole fishing area (Committee of Ecosystem Effects of Fishing 2002). Acoustic mapping is an attractive option because it is non-destructive compared to dredge samples, rapid compared to video and grab samples, and provides spatial coverage at the scale required for management.

Acoustic approaches have been used in the past to identify scallop habitat and other shellfish habitat based on acoustic reflectance and environmental gradients. Both single beam and multi beam echo sounders have been used to detect and map scallop beds or potential scallop habitat (Kostylev *et al.* 2003, Pickrill and Todd 2003, Hutin *et al.* 2005). In Canada, the use of maps of potential scallop habitat based on multi beam echo sounder acoustic reflectance, surficial geology, and depth lead to a more efficient scallop industry, with up to a 75% reduction in effort to maintain the same catch levels (Pickrill and Todd 2003). An additional benefit is a reduction of benthic disturbance in non-scallop habitats (Pickrill and Todd 2003). Acoustically derived substrate information has also been used to better design surveys for stock assessment (Kostylev *et al.* 2003). Side scan sonar, which in turn provides a broad swath of backscatter data, has also been used to show the distribution and concentration of trawl furrows in soft unconsolidated substrates (Friedlander *et al.* 1999, Humborstad *et al.* 2004a) which allowed an independent measure of fishing intensity to be obtained relative to benthic habitats.

Soft sediment habitats are characterised by a combination of physical factors (e.g. particle size distribution, depth, currents and exposure) and biological factors (e.g. presence of plants, epifauna and infauna) (Morrison *et al.* 2001a, Ysebaert and Herman 2002, Stevens 2005). The acoustic detection of soft sediment habitats is based on differences in the reflection of sound energy due to differences in seafloor properties, with soft substrates generally having low reflectance at high incidence angles. Each the above mentioned factors will influence the reflection and scattering of sound energy at the water sediment interface. Sediment particle

size has been shown to correlate with acoustic response at certain frequencies, with particle size and porosity affecting the amount of energy returned (Greenstreet *et al.* 1997, Cholwek *et al.* 2000, Bates and Whitehead 2001, Brown *et al.* 2001, Kostylev *et al.* 2001, Morrison *et al.* 2001a, Ellingsen *et al.* 2002, Thrush *et al.* 2002, Freitas *et al.* 2003b, Freitas *et al.* 2005b). The presence of biota, surficial shell or surface roughness has also been shown to affect the acoustic response of the seabed (Stanic *et al.* 1989, Lee Long *et al.* 1998, Fenstermacher *et al.* 2001, Kloser *et al.* 2001b, Williams *et al.* 2001, Sabol *et al.* 2002).

The Tasmanian scallop fishery is moving towards spatially based management of the resource, utilising closed and opened areas to protect juvenile scallops and limit impact on non target species and habitats (Haddon *et al.* 2006). Sponge habitat is one such habitat that can be adversely impacted from scallop fishing activities (McConnaughey *et al.* 2000, Kefalas *et al.* 2003). Sponge habitat can occur across extensive areas of seafloor within this region (Butler *et al.* 2002, Jordan *et al.* 2005b), with sponge commonly encountered as bycatch within scallop dredges (Haddon *et al.* 2004, Haddon *et al.* 2005, Haddon *et al.* 2006). Soft sediment sponge habitat can be acoustically detected through differences in the acoustic response of the seafloor (Kloser *et al.* 2001b, Jordan *et al.* 2005b). Maps of sponge habitat within the scallop fishing zones would aid in the designation of no-fishing zones for the purpose of habitat protection.

This chapter focuses on Substratum/Ecotype and Modifiers levels in the hierarchical classification system presented in Chapter 1 (Table 1.1). It describes and investigation of the efficacy of single beam echo sounders to map the distribution of soft sediment habitats within a component of the Tasmanian scallop fishery, with a focus on the capacity of the system to detect and map the key habitats of sponge beds and scallop beds. The main objectives are to examine the statistical relationship between the acoustic backscatter indices E1 and E2 and key physical and biological properties of the seafloor. The SBES data are examined in relation to fishing effort data as a proxy for scallop habitat. The acoustic responses of the seabed are further compared to changes in sediment particle size parameters, surficial shell, and sponge cover. Finally, the capacity of the SBES to reproduce spatial patterns seen within soft sediment communities are compared to full coverage side scan sonar data for the same region.

3.2. Methods

3.2.1. Study Site

The study site was situated at 148° 24' E, 39° 51' S, approximately 10 km northeast of Babel Island, on the east coast of Flinders Island, Tasmania (Figure 3.1). The study site covered an area of approximately 2.5 by 3 km, with depths ranging from 37 m to 44 m. Previous dredge surveys have shown this area to be dominated by soft sediment habitats, with a mixture of scallop, sponge, dead shell and sand. The area was closed to scallop fishing in 1999 after the collapse of the scallop fishery in Tasmania and was due to open for fishing during the 2004 season.

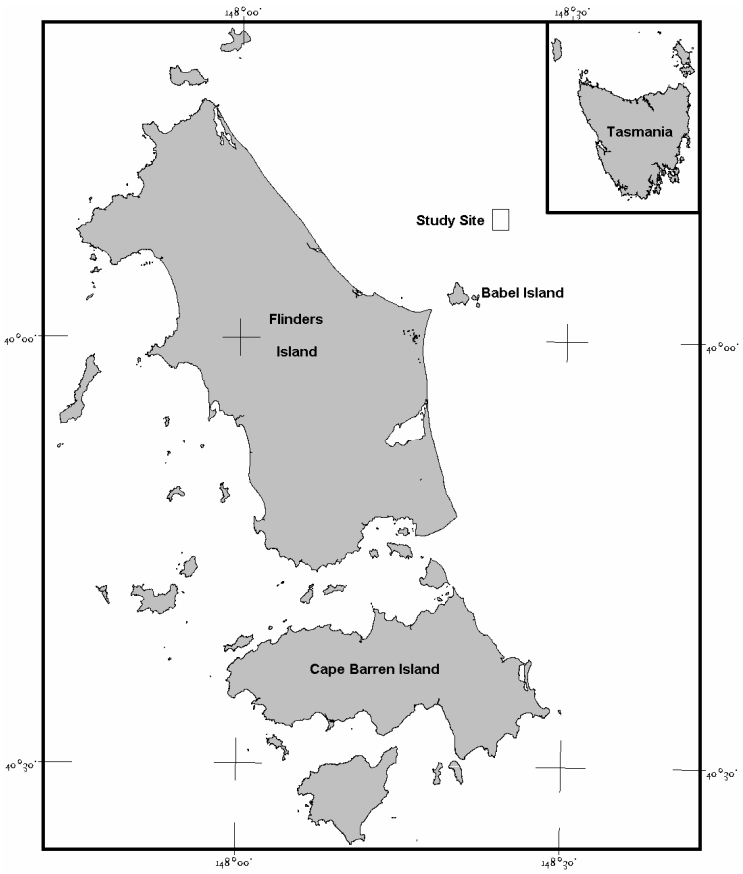

Figure 3.1. The location of study site off the north east of Flinders Island, Tasmania.

3.2.2. Field surveys

3.2.2.1. Acoustic

In December 2003 a single beam acoustic survey, with associated video and sediment sampling, was conducted from the FRV Challenger. This 20 meter vessel was fitted with a Simrad ES60 single beam echo sounder with a 120 kHz 10° transducer. The transducer was pole mounted on the starboard side of the vessel approximately 1.5 m below the surface of the water (Figure 3.2).

Figure 3.2. The pole mounted single beam transducer on the side of *FRV Challenger.*

The echo sounder was set to run at 500 W and 1.024 ms pulse length, with a ping rate of 1 ping per second. The raw data from the echo sounder, including the entire first and second echoes, were logged using the Simrad ES60 software (Version 1.5.0.73) to a laptop computer. A differential GPS was connected to the laptop to allow position information to be logged with the raw echogram. Based on visual inspection of the logged acoustic echogram, echo data with excessive noise, interference, or aeration under the transducer were excluded from further analysis.

The vessel was operated at approximately 6 kts following a series of parallel transects. Transects were conducted at 500 m spacing in the north south direction and 250 m spacing in the east west direction resulting in a grid across the study site. The ship's onboard navigation software, OceanVision, was used to plot position and maintain course.

3.2.2.2. Video and Sediment

Both underwater video and sediment grabs were used to collect ancillary data on the seabed composition and structure. Video transects were conducted at 13 stations throughout the study site based on randomly selected cells from a 250 m grid (Figure 3.3). An underwater digital video camera (MorphVision, NSW, Australia) linked to a miniDV digital video recorder at the surface was used to record imagery of the seafloor. The video camera was mounted in a

weighted tow fish and suspended from a davit over the side of the vessel. The camera was flown approximately 1 m above the seafloor, with this height monitored on the onboard video screen. The vessels position from the differential GPS was overlayed onto the video system to assist in the positioning of the video frames. Video transects were conducted for a minimum period of 5 minutes (up to 10 minutes), with the vessel allowed to drift with the prevailing conditions. The average length of the video transects was 130 m ± 22 m which is around 3 times the maximum diameter of the E1 footprint.

At 13 sampling stations, sediment grabs were collected using a Van Veen grab (Figure 3.3). A sub sample of each sediment grab was taken for particle size analysis, with the remainder characterised for the presence of large shell fragments and/or biota.

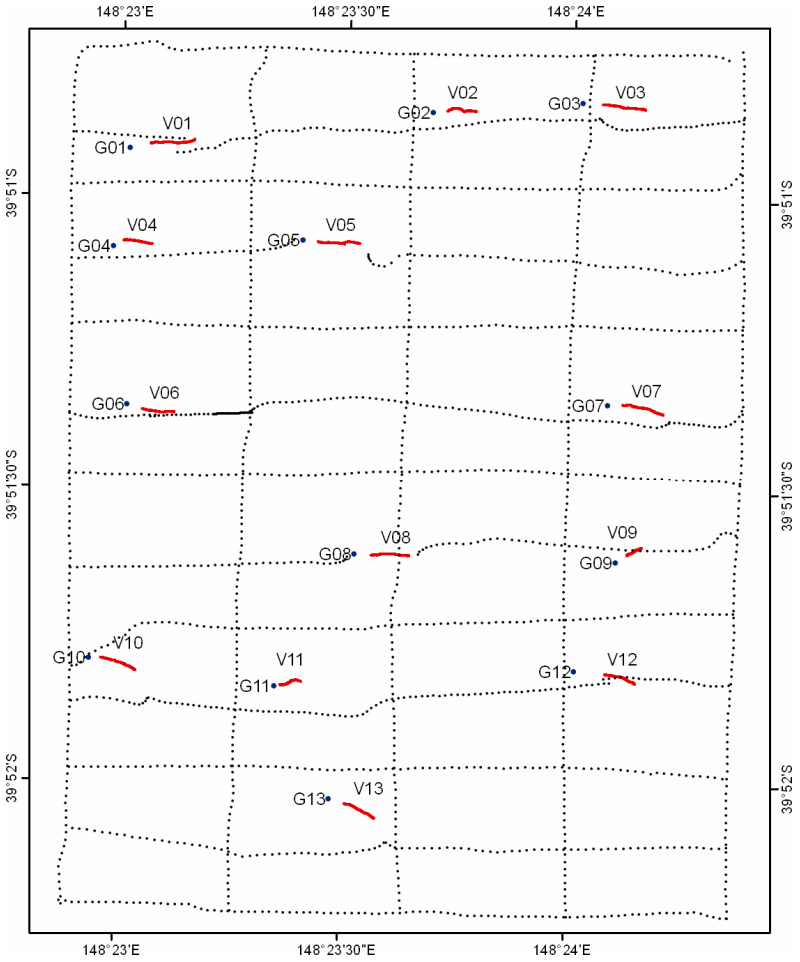

Figure 3.3. Location of the 13 sediment grabs (blue dots) and 13 video tows (red lines) in relation to the acoustic transects (black line) across the study site

3.2.3. Acoustic Processing

3.2.3.1. Bathymetry

Bathymetric data were recorded by the ES60 echo sounder. Logged data files were imported into Echoview 3.30, where the sounder detected bottom was checked for anomalies, corrected

for the transducer depth and exported as a comma delimited text file containing depth and position. These depth data were corrected for tidal variation based on the predicted tide heights from the National Tidal Facility (http://www.bom.gov.au/oceanography/tides/). The tidal cycle can be described by a harmonic equation:

$$D_i = D[h_1 + (h_2 - h_1) \times (\cos(\pi \times ((t - t_1)/(t_2 - t_1) + 1)) + 1)/2]$$

where D_i is corrected depth and D is measured depth, $h_{1,2}$ correspond to the heights of the high and low tides, $t_{1,2}$ are the times of the high and low tides, with t being the current time. This formula calculates the height of the tidal cycle for a given time and a given location and then applies this as a correction to the measured field data. All depth measures were corrected to Mean Sea Level based on the available standard port measurements (Port of George Town).

A bathymetric surface was generated from the tidally corrected depth data through the interpolation of depth (*z*) values using a Triangular Irregular Network (TIN) data model. Contours were created in ArcGIS 9.0 by interpolating the point data into a TIN and then creating contours from that TIN.

3.2.3.2. Acoustic Indices

The calibrated ES60 acoustic data were corrected for triangle wave (Section 2.2.2) and imported into Echoview 3.30 for post processing. Acoustic indices of seabed roughness (E1) and seabed hardness (E2) were calculated using the methods outlined in Section 2.2.3. Both indices were calculated over five successive pings and converted from s_A data (Nautical area scattering coefficient) to S_A (Nautical area scattering strength) using the following formula:

$$S_A = 10\log_{10}(s_A) \qquad \text{(MacLennan } et\ al. \text{ 2002)}$$

3.2.3.3. Video Processing

Video was converted to digital AVI format using a firewire capture card. A frame was grabbed off the video every 10 seconds for the first 5 minutes of the video tow using the software Video2Photo (PixelChain). This created 31 still frames, corresponding to a frame every 3 m ± 0.7 m. These frames were overlayed with an 8 by 8 cell grid giving a total of 49 line intercepts (Figure 3.4). The substrate at each of these intercepts was recorded as bare sand, shell, sponge, or other. This data was used to calculate the relative proportions of each of the components across the video drop.

The video data was also used to examine the patch length of different habitat components. In this case the entire length of each of the video transects was used to calculate the average patch length for the different substrate types. Each video transect was analysed, with changes

in substrate noted against the tracklog. The classified tracklog was then bought into a GIS and the average patch length for the different substrate types measured. Patch length was defined as the linear distance over which a continuous single substrate occurred.

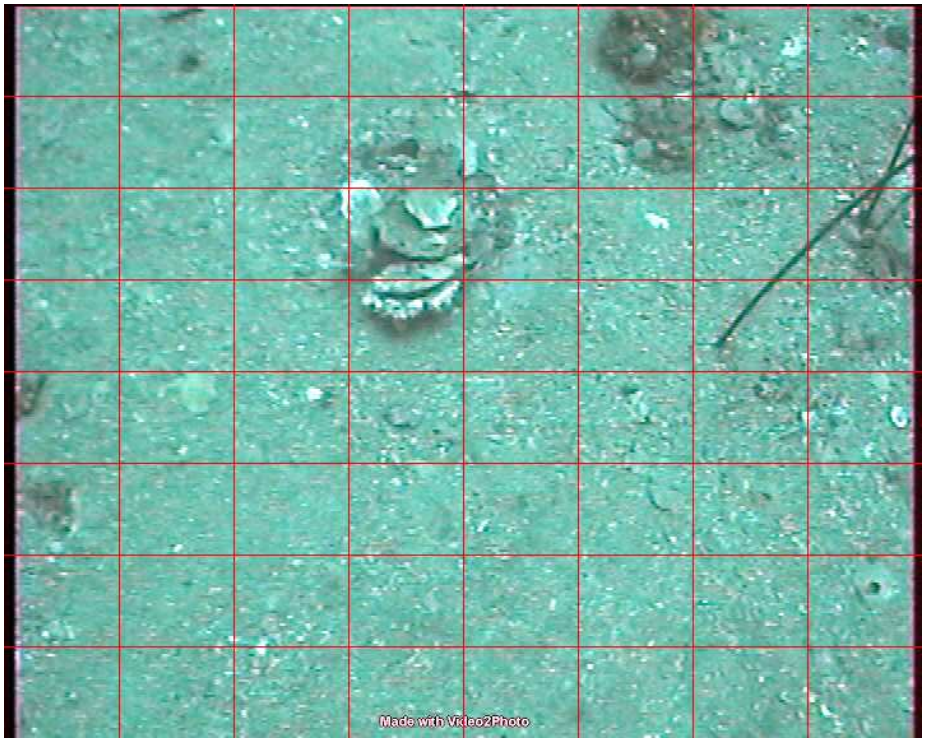

Figure 3.4. Example still frame grab from video with analysis grid overlay.

Multivariate correlation analysis in JMP (SAS Institute) was used to test for correlations between the acoustic indices E1 and E2 and the percentage of shell and sponge from the video analysis. The acoustic data and the analysed video data were aligned in a GIS, only points within ± 5 m were considered for the analysis. To avoid confounding effects, the shell and sponge were treated separately, such that any video that contained significant amounts of shell (>10%) was excluded from the sponge analysis and vice versa. This analysis calculated a correlation and associated probability for each relationship.

3.2.3.4. Sediment Processing

Sediment samples collected from the Van-Veen grab were processed for particle size distribution. Approximately 30 – 80 g from each sample was dried overnight at 80^{o} C. The dry samples were then weighed before being wet sieved through a series of stacked sieves (2 mm, 1 mm, 0.5 mm, 0.25 mm, 0.125 mm and 0.063 mm). The fraction in each sieve was then re-dried overnight at 80^{o} C before being weighed. The weight of the fraction less than 0.063 mm was calculated as the initial dried sample weight less the sum of the retained dried fractions. The dried weights were used to calculate the percentage of each fraction.

Sediment particle information was plotted to check for skewness and kurtosis. All samples

were well sorted and were normally distributed. Cumulative percentage particle size was plotted for each sample and Phi-50% values were calculated. This gave a measure of the mean particle size, which was used to classify the sediments on the Wentworth scale. Multivariate correlation analysis in JMP 7 was used to compare mean sediment particle size to the acoustic E1 and E2 indices.

3.2.3.5. Side Scan Sonar

The study site was surveyed using a GeoAcoustics 120 kHz side scan sonar (SSS) in March 2005. This allowed the spatial trends interpreted from the single beam acoustics to be compared to those detected by a swath system. The side scan was deployed from the FRV Challenger on 100 m of cable and towed approximately 25 m from the seafloor at 7 kts. The SSS was towed in a north-south direction with a 200 m transect spacing and range set at 200 m. This provided sufficient overlap to produce a good mosaic. The side scan data was slant range corrected, mosaiced and georeferenced by the commercial survey company Fugro Systems and provided as a binary image library file.

To compare the spatial trends in the E1 and E2 indices with the side scan sonar, the E1 and E2 indices were interpolated into surfaces. Variogram models for both indices were computed in the geo-statistical software Surfer 8 (Golden Software). For both indices a spherical model with nugget effect provided the best fit (Figure 3.5). The ordinary kriging algorithm in Surfer 8 was used to interpolate surfaces for both indices using these variogram models.

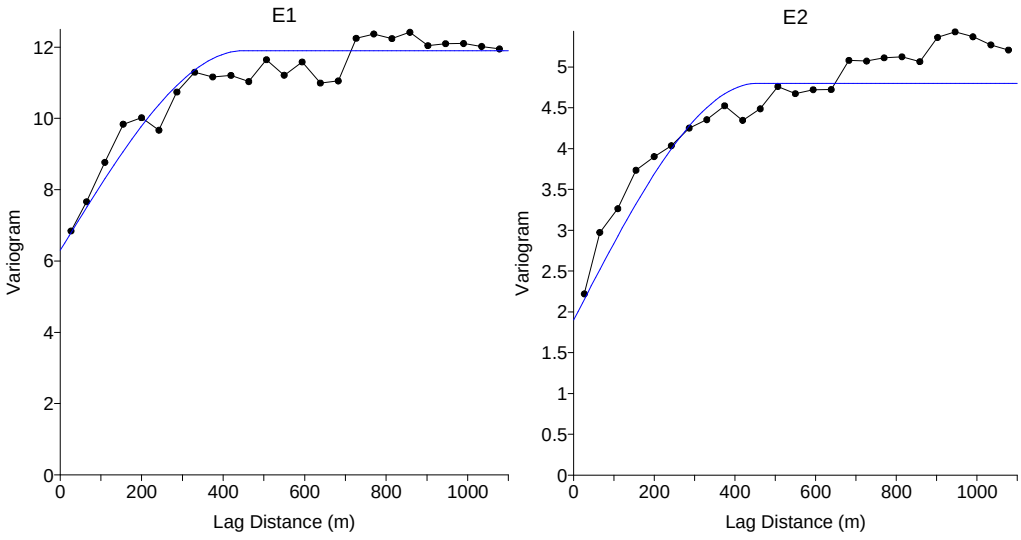

Figure 3.5. Variogram models computed from the E1 and E2 acoustic data.

3.2.4. Fishing Intensity

The scallop fleet is required by the fisheries regulators to have a Vessel Monitoring System (VMS). A VMS monitors the position of each fishing boat at a pole rate, determined by

management organisations, while they are out of port. Fishing effort in this study site was inferred from raw VMS data. It must be noted that individual VMS hits do not represent fishing activity; instead clusters of hits in close vicinity can be used to infer fishing activity. Due to the commercially sensitive nature of VMS data, the raw data could not be presented in this thesis.

To compute a relative measure of fishing effort across the site kernel analysis was used to calculate the core of the fishing effort and the extent of the fishing area in ArcView GIS using the animal movement extension (Hooge and Eichenlaub 2000). The core fishing zone was calculated as the smallest area that 50% of all VMS hits occurred, while the total fishing zone was calculated as the smallest area that 95% of all hits occurred. The level of fishing within this zone was comparable to that for the rest of the 2003/04 fishing season.

3.2.5. Classification

The acoustic E1 and E2 data were classified into acoustic classes based on the unsupervised clustering. The K-means algorithm in the statistical software package JMP (SAS Institute) was used to group the raw E1 and E2 data into clusters. This algorithm uses an iterative alternate fitting process to form the number of specified clusters. The K means algorithm was run for 2 to 7 clusters. The optimal number of classes was assessed by comparing the within cluster variance to the total variance for each of the number of clusters (Figure 3.6). Three clusters (explaining 70% of variance) were used for the subsequent analysis; the addition of more clusters only explained 10% of variance (Figure 3.6).

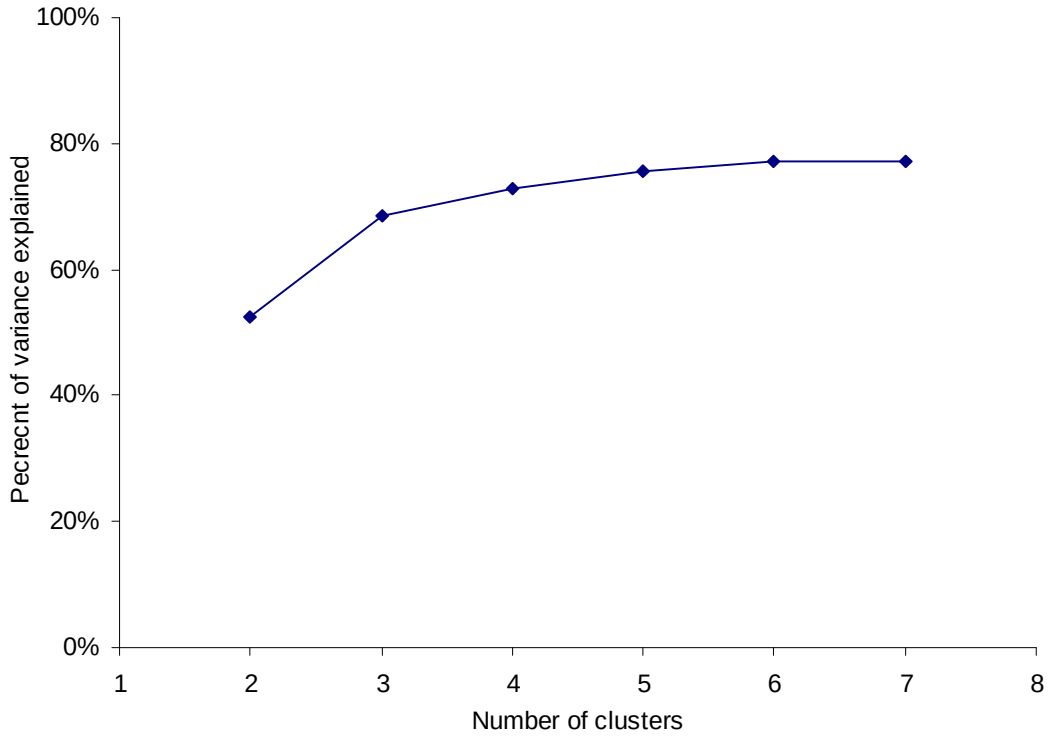

Figure 3.6. Graph of percentage of variance (ratio of cluster variance to total variance) for K-means clustering of E1 and E2 data for 2 to 7 clusters. The graph displays an elbow effect at 3 clusters indicating the optimal number of clusters.

The K-means algorithm provides a probability of membership for every data point to each of three computed clusters. To assist in the visualisation of the spatial trends in this data, surfaces of membership were interpolated for each of the clusters. Variogram models of the data were computed in the geo-statistical software Surfer 8 (Golden Software). The variogram models describe the degree of spatial dependence in the data and are used in kriging to account for spatial trends in the data. The variogram module in Surfer 8 allows the user to investigate different spatial models for the variogram and identify the model with best fit to the data. For clusters 1 and 2 a spherical model with nugget effect provided the best fit, however for cluster 3 a linear model with a nugget effect provided the best fit (Figure 3.7). Surfaces of probability of membership to each cluster were interpolated in Surfer 8 using these variogram models with the kriging algorithm.

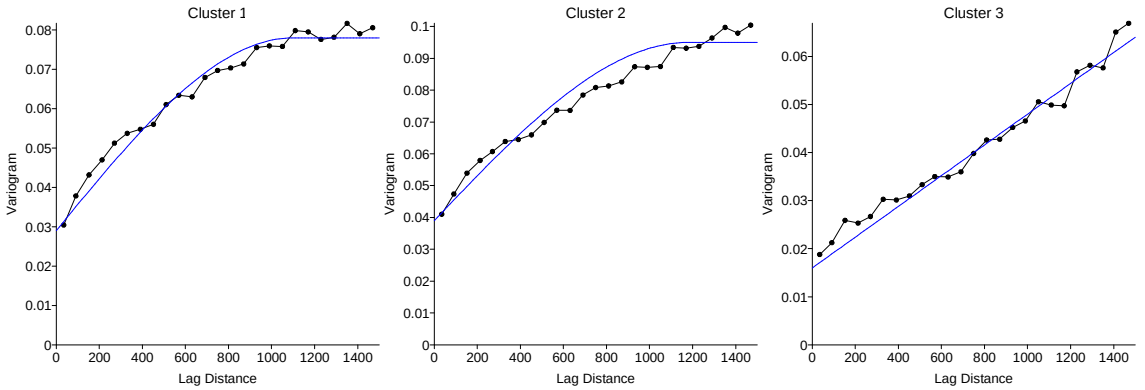

Figure 3.7. Variogram models computed from the probability of membership data for the three clusters identified by the K-means clustering. The black points and line represent the data while the blue line represents the model.

The ground truth data from the sediment samples and the underwater video analysis were related to the spatial distribution of the three clusters identified above. Analysis of variance was used to test for statistical relationships between the three clusters and mean particle size (Phi-50%), percent sponge cover, percent surficial shell cover, the two acoustic indices (E1 and E2) and depth. Finally, the cluster information and ground truth data were combined to make an interpreted map of habitat distribution which was related back to the fishing intensity information.

3.3. Results

3.3.1. Bathymetry

The bathymetry of the study site varied from 37 m to 44 m depth with contours running in a northwest to southeast direction. The majority of the study site was between 40 m and 42 m depth. The slope of the study region was very low, generally less than 1 degree.

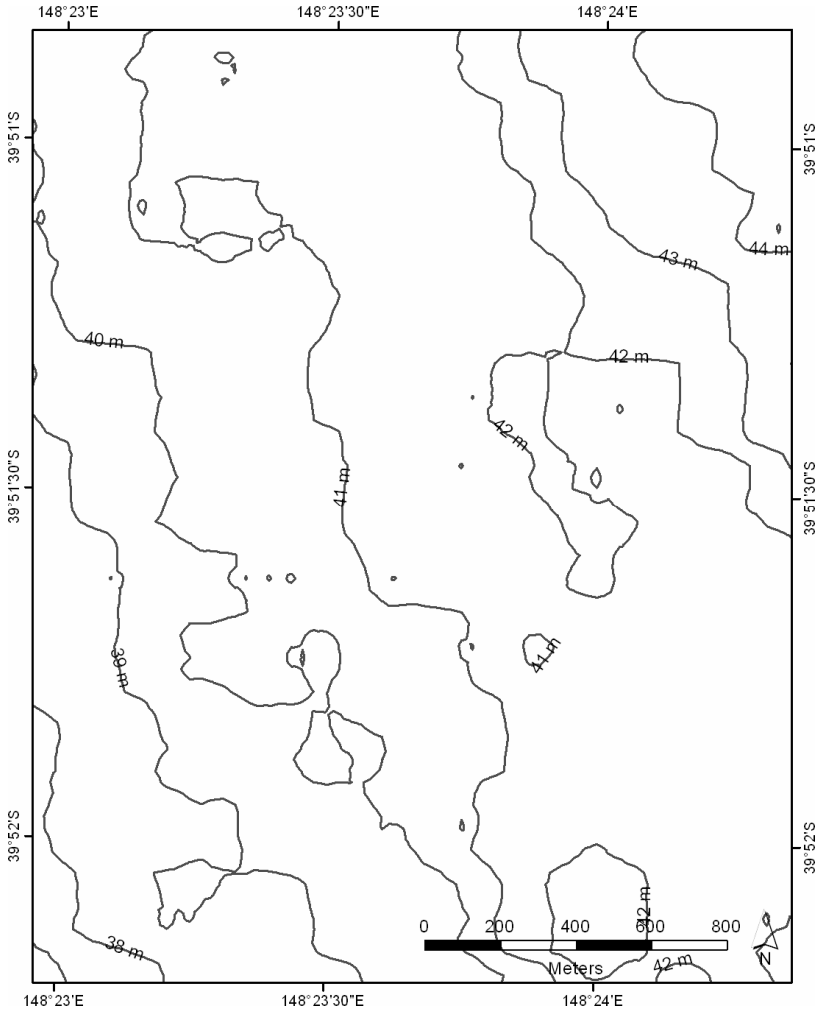

Figure 3.8. Interpolated bathymetry of the study site based on tidally corrected single beam echo soundings.

3.3.2. Video

The video data provided information on the structure of the seafloor including the presence of biota. The video confirmed that the sediment within this zone was dominated by sand, with areas of dead shell and areas of sponge. The attributed video track log data was used to calculate the average patch width of these habitats encountered within a GIS platform. The average width of shell patches was 63 m, with the average sponge patches 50 m. While live scallops were occasionally recorded on the underwater video, these were not observed frequently enough to be considered a 'habitat' type.

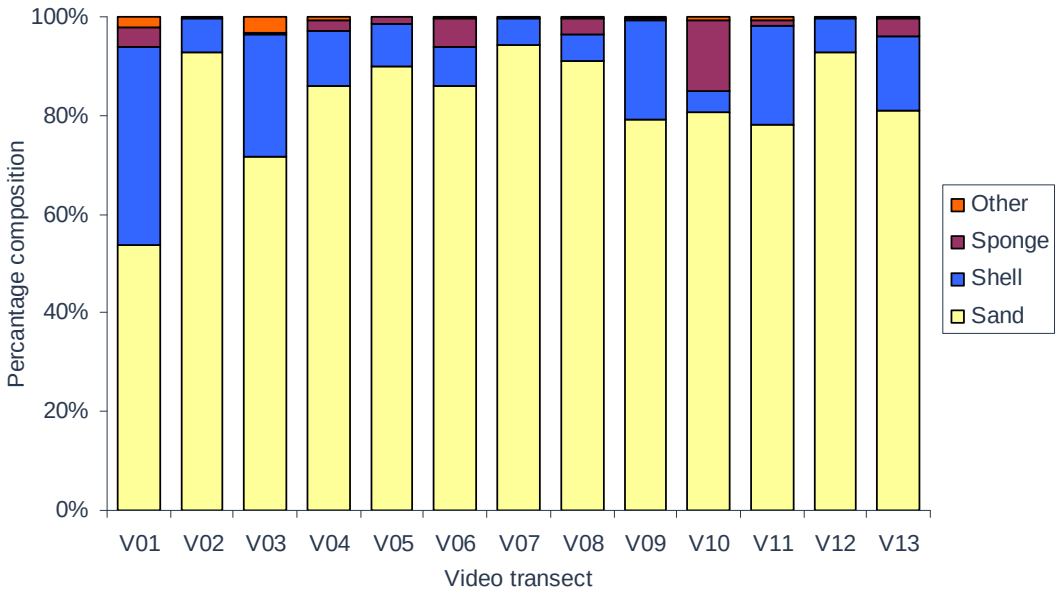

Figure 3.9. Summary of the percentage composition (sand, shell, sponge and other) for the 13 video transects based on point intercept analysis.

The point intercept analysis of the 13 video transects showed that sand was the most dominant substrate type in all cases. Surficial shell was present in all video transects, with several of the transects having significant amounts of shell (Figure 3.9). Sponge was generally either not present or only present with low cover, with the exception of video transect 10 which had around 14 % sponge cover (Figure 3.9). There were small amounts of 'other' substrate in several of the videos which was generally unidentified biotic organisms such as bryozoans.

The analysed video data were used to examine the relationship between E1 and E2 indices and the presence of shell and sponge with sand being identified as the underlying substrate in both cases. A multivariate correlation analysis was used to test for significant correlations between the acoustic indices and the amount of both shell and sponge cover. The amount of surficial shell, identified from the video, showed no significant correlation with either index ($p < 0.05$) (Table 3.1). The amount of sponge, identified from the video, had a significant positive correlation with the E1 index (0.98, $p < 0.01$), but none for the E2 index. (Table 3.2). There were insufficient amounts of the 'other' category observed in the video transects to examine for a relationship between this class and the two acoustic indices.

Table 3.1. Correlation analysis and associated probabilities for acoustic indices and amount of shell as identified from video analysis.

Acoustic Index	Correlation	Probability
E1	-0.021	0.99
E2	-0.524	0.15

Table 3.2. Correlation analysis and associated probabilities for acoustic indices and amount of sponge as identified from video analysis.

Acoustic Index	Correlation	Probability
E1	0.983	<0.01
E2	0.718	0.07

3.3.3. Sediment

Thirteen sediment samples were collected and processed for particle size from the study site. The sediment particle size distributions from these samples were very similar in structure (Figure 3.9); all were either classified as well sorted medium or coarse sands (Phi-50% 0.1 to 1.7) on the Wentworth scale (Table 3.3).

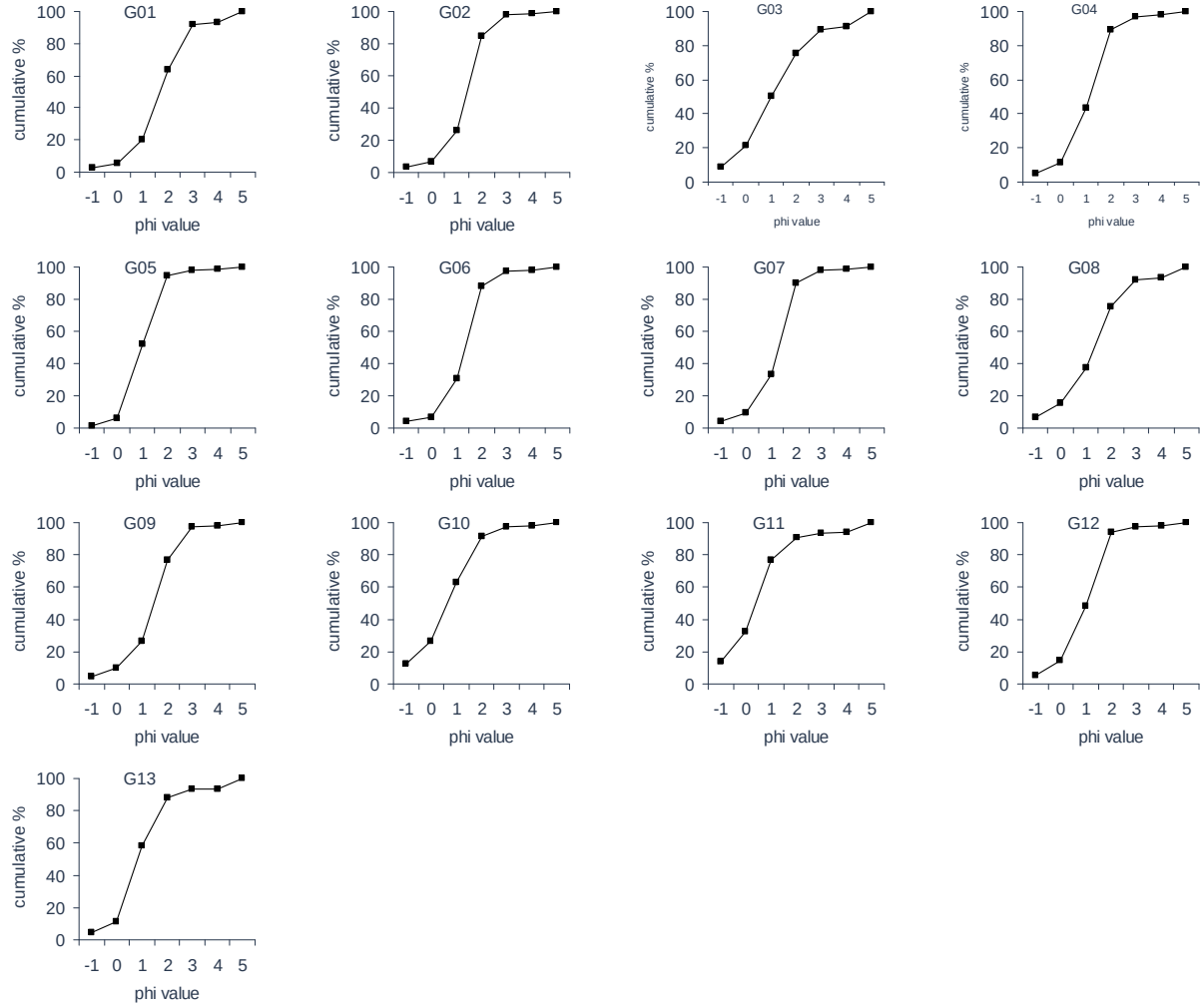

Figure 3.10. Cumulative percentage composition for particle size samples collected from within the study site.

Table 3.3. Phi-50 and Wentworth classification for the thirteen sediment samples collected from within the study site.

Sample No	Phi-50	Wentworth Classification
G01	1.70	Medium Sand
G02	1.40	Medium Sand
G03	1.00	Medium Sand
G04	1.15	Medium Sand
G05	0.95	Coarse Sand
G06	1.35	Medium Sand
G07	1.30	Medium Sand
G08	1.35	Medium Sand
G09	1.45	Medium Sand
G10	0.65	Coarse Sand
G11	0.40	Coarse Sand
G12	1.05	Medium Sand
G13	0.80	Coarse Sand

There was no significant correlation between particle size and depth (Table 3.4, Figure 3.11).

Table 3.4. Results of multivariate correlation analysis of mean particle size (Phi-50%) and the variables Depth, E1, and E2.

Variable	Correlation	Probability
Depth	0.32	0.18
E1	-0.52	<0.01
E2	-0.08	0.71

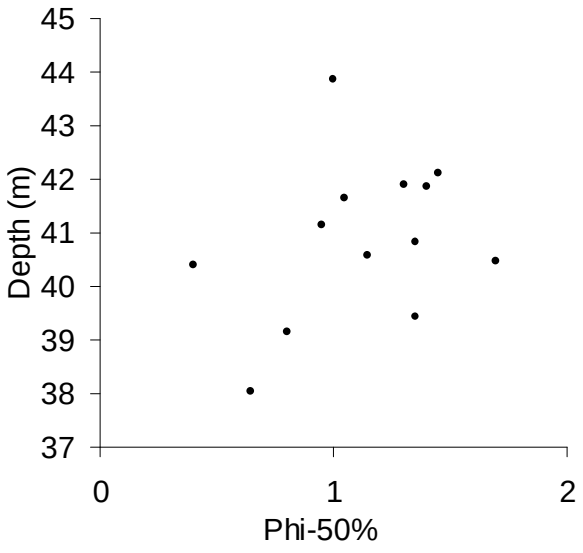

Figure 3.11. Mean sediment particle size (Phi-50%) versus depth for 13 sediment samples across study site.

The two acoustic indices, E1 and E2, were examined in relationship to the sediment particle size information. The Phi-50% value for each sample was used as a measure of mean sediment particle size for comparison with the acoustic indices. The E1 index showed a significant negative correlation with mean particle size trend ($P < 0.01$), with the energy in the tail of the first echo decreasing as the mean particle size decreased (Table 3.4, Figure 3.12).

The E2 index showed no significant correlation with mean particle size (Table 3.4, Figure 3.13).

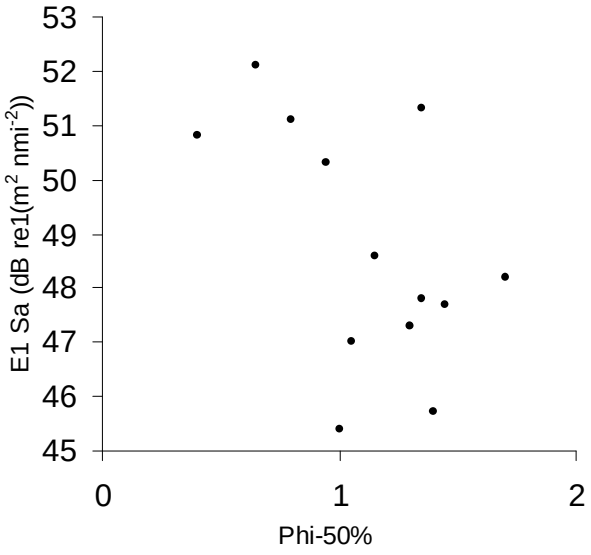

Figure 3.12. E1 acoustic index versus mean particle size (Phi-50%) for 13 sediment samples across study site.

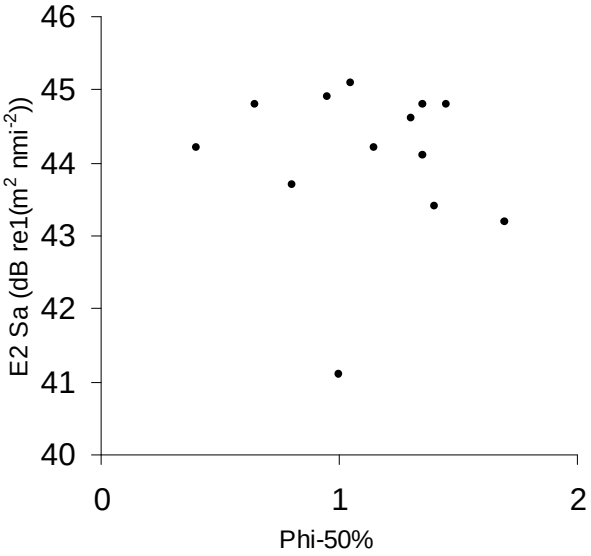

Figure 3.13. E2 acoustic index versus mean particle size (Phi-50%) for 13 sediment samples across study site.

3.3.4. Fishing Intensity

The fishing intensity as inferred from VMS data showed strong spatial trends across the study site. The majority of the fishing in this study site occurred on the eastern side of the site in approximately 42 m depth (Figure 3.14). Fishing within the study site was generally at a medium intensity compared to the other areas within the Tasmanian Scallop Fishery over the following fishing season (unpublished VMS data). There was a small amount of high intensity

fishing within the central part of the fished area.

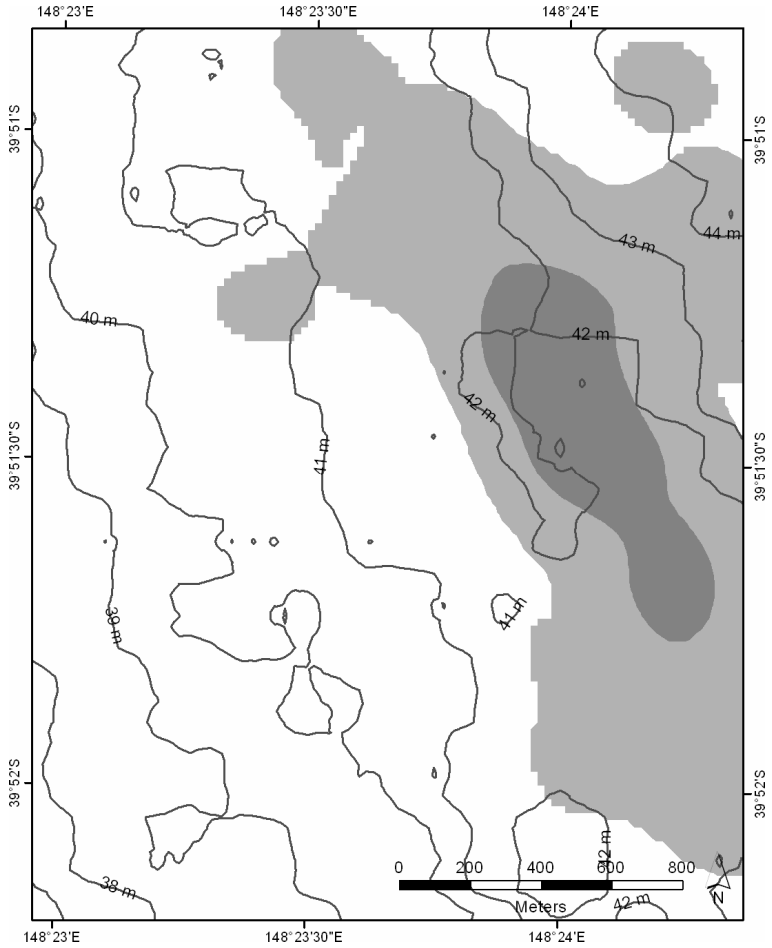

Figure 3.14. The spread of fishing effort across the study site for the 2003/2004 scallop fishing season as inferred from VMS data. The core fishing zone (dark grey) represents the smallest area containing 50% of all VMS hits, while the total fishing zone (light grey) represents the smallest area containing 95% of all VMS hits.

The acoustic response of the seabed in the three zones identified from the VMS analysis showed that there was overlap between the E1 and E2 values identified in each zone (Figure 3.15). The E1 and E2 values from the area with no fishing had the greatest variation, with the other two zones having reduced variation in the E1 and E2 values. Assuming that fishing effort reflects scallop abundance, this simple analysis shows that there is no E1 and E2 signature that delineates scallop habitat from non scallop habitat, rather that the acoustic values of scallop habitat are the same as that for other soft sediment habitat. The spatial distribution of all pings with E1 and E2 values corresponding to those identified from the core fishing zone showed no pattern across the study site (Figure 3.16).

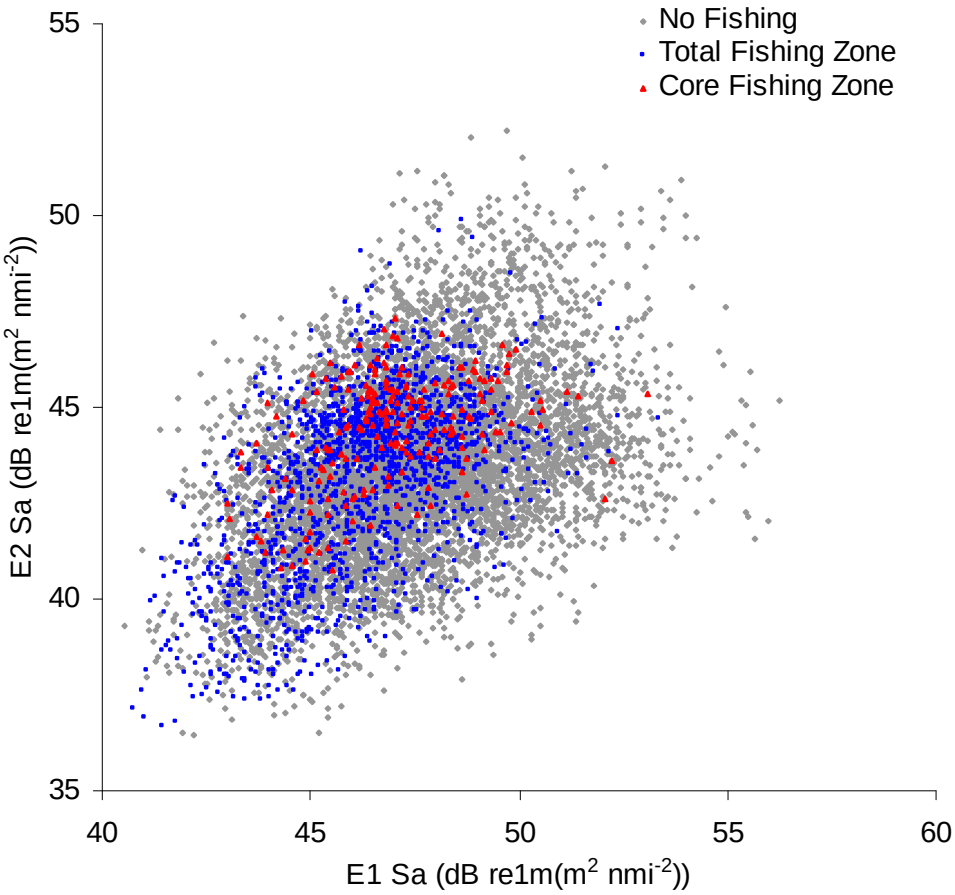

Figure 3.15. Acoustic response of the seabed in areas of no fishing, low and high fishing intensity.

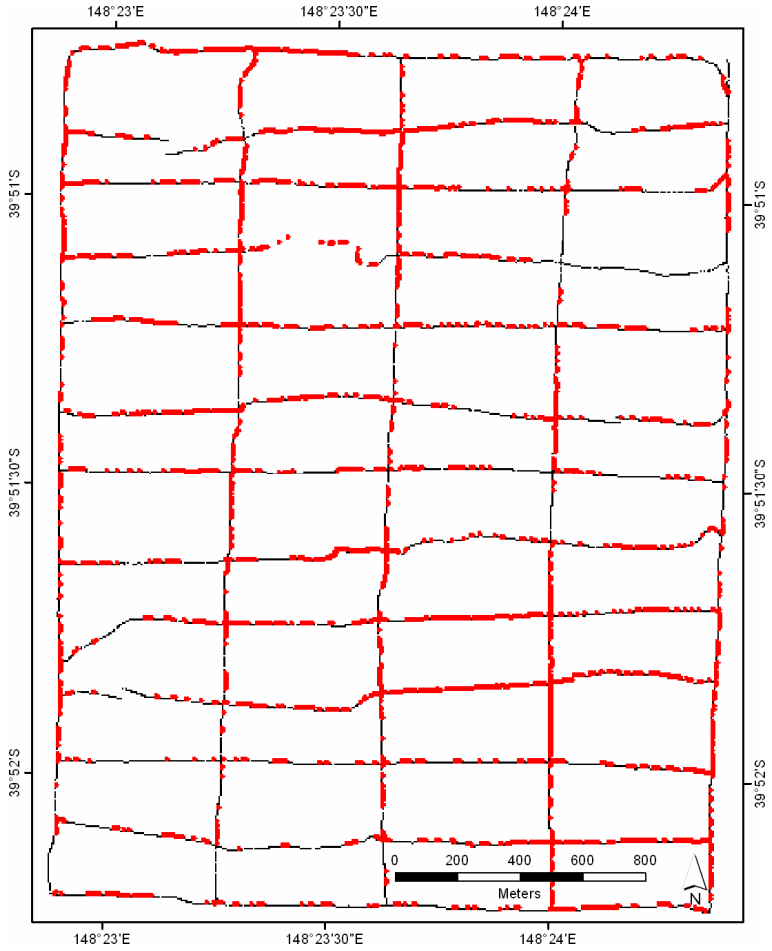

Figure 3.16. Distribution of acoustic pings with signature corresponding to that of the highest fishing intensity shown in red.

3.3.5. Acoustic Mapping

Both the E1 and E2 acoustic indices showed spatial trends across the study site. The patterns for both E1 and E2 were similar, with several linear features running in a northwest to southeast direction (Figure 3.17). The interpolated acoustic surfaces can be visually compared with side scan sonar taken in March of 2005 (Figure 3.18). As the side scan sonar data was collected several months after the single beam, and due to the inherent difficulty in making a direct comparison between the two instruments, no statistical comparison was attempted. However the side scan sonar data closely reflects the spatial trends seen in the E1 and E2 interpolated surfaces. It should be noted that there was very little dynamic range in the side scan sonar data and that the image contrast has been maximised to highlight the differences within the image.

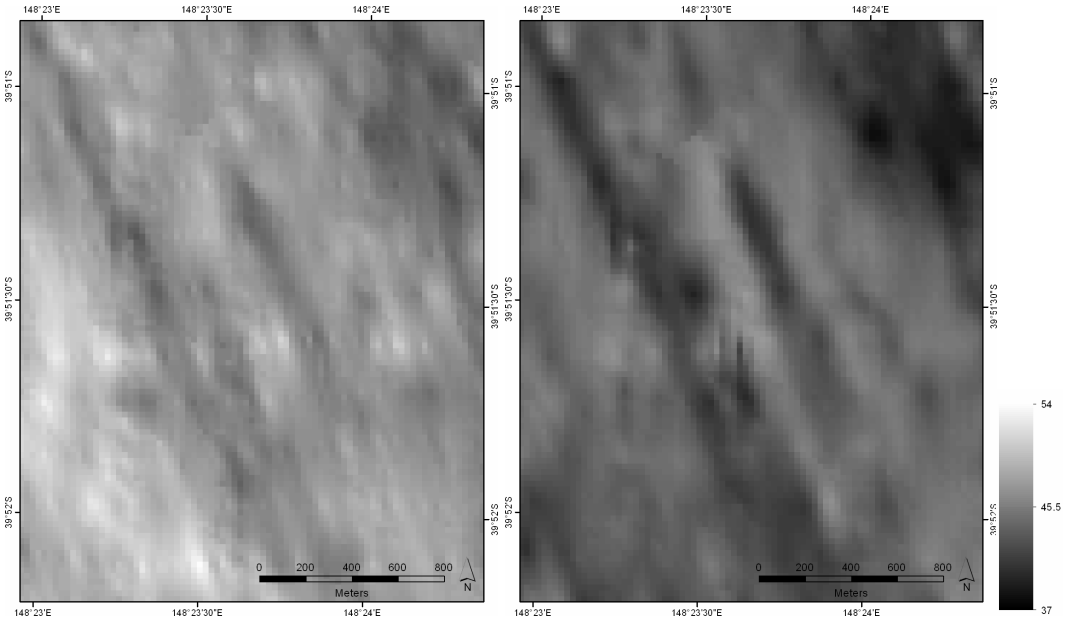

Figure 3.17. Interpolated surfaces of the E1 (left) and E2 (right) acoustic indices, lighter shades indicate areas of high acoustic reflectance, darker shades indicate areas of low acoustic reflectance.

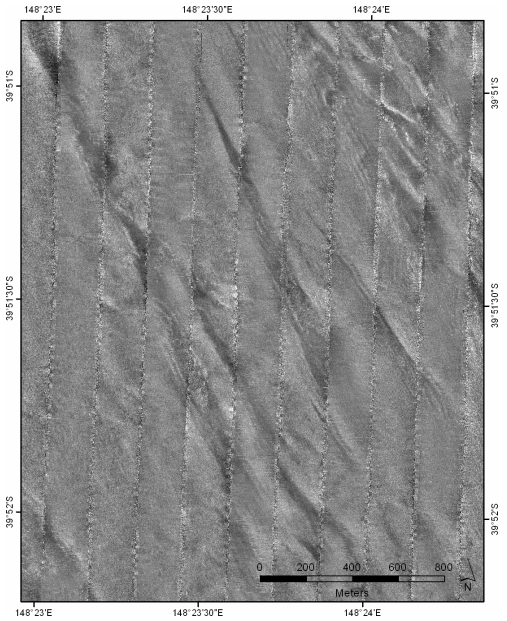

Figure 3.18. Geo-referenced side scan sonar image of the study site from March 2005, light indicates high reflectance, with dark indicating low reflectance.

The E1 and E2 acoustic data were segmented into three clusters using the K-means clustering algorithm. These three clusters displayed strong structuring in their spatial distribution (Figure 3.19). As for the interpolated E1 and E2 surfaces and the side scan sonar data, the classified acoustic data showed a northwest to southeast lineation in the gradient. The three clusters from the K-means algorithm explained approximately 70% of the variation in the acoustic data set. The hard class classification does not take into account the probability of membership to the three clusters. Instead there is the assumption that any given point belongs exclusively to one of the three clusters. Commonly, soft sediment habitats do not have crisp

boundaries, and as such a fuzzy classification would be more suitable.

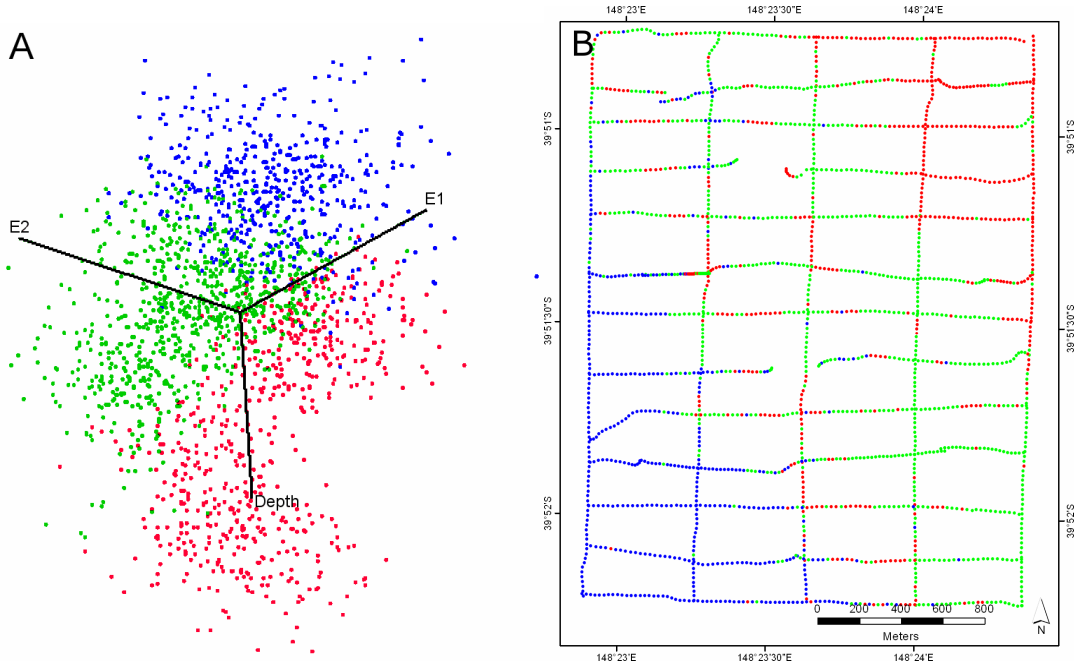

Figure 3.19. (A) K-means clusters identified based on E1, E2 and Depth and (B) distribution of hard classes based on 3 clusters.

The k-means algorithm provides a probability of membership for each point to each acoustic class. Thus every point will have a membership to each of the three clusters. This information can be used to visualise the confidence in the final classification. Kriging was used to interpolate the probability of cluster membership into continuous surfaces, henceforth referred to as acoustic classes. These three surfaces were colour coded from white to full colour (red, green or blue), with white representing 0% probability of membership and full colour 100% probability of membership. The three colour coded surfaces were then overlayed to form a probability map of acoustic classes, where solid colour represented a high probability of membership to that acoustic class and white represented a low probability or transition zone between acoustic classes.

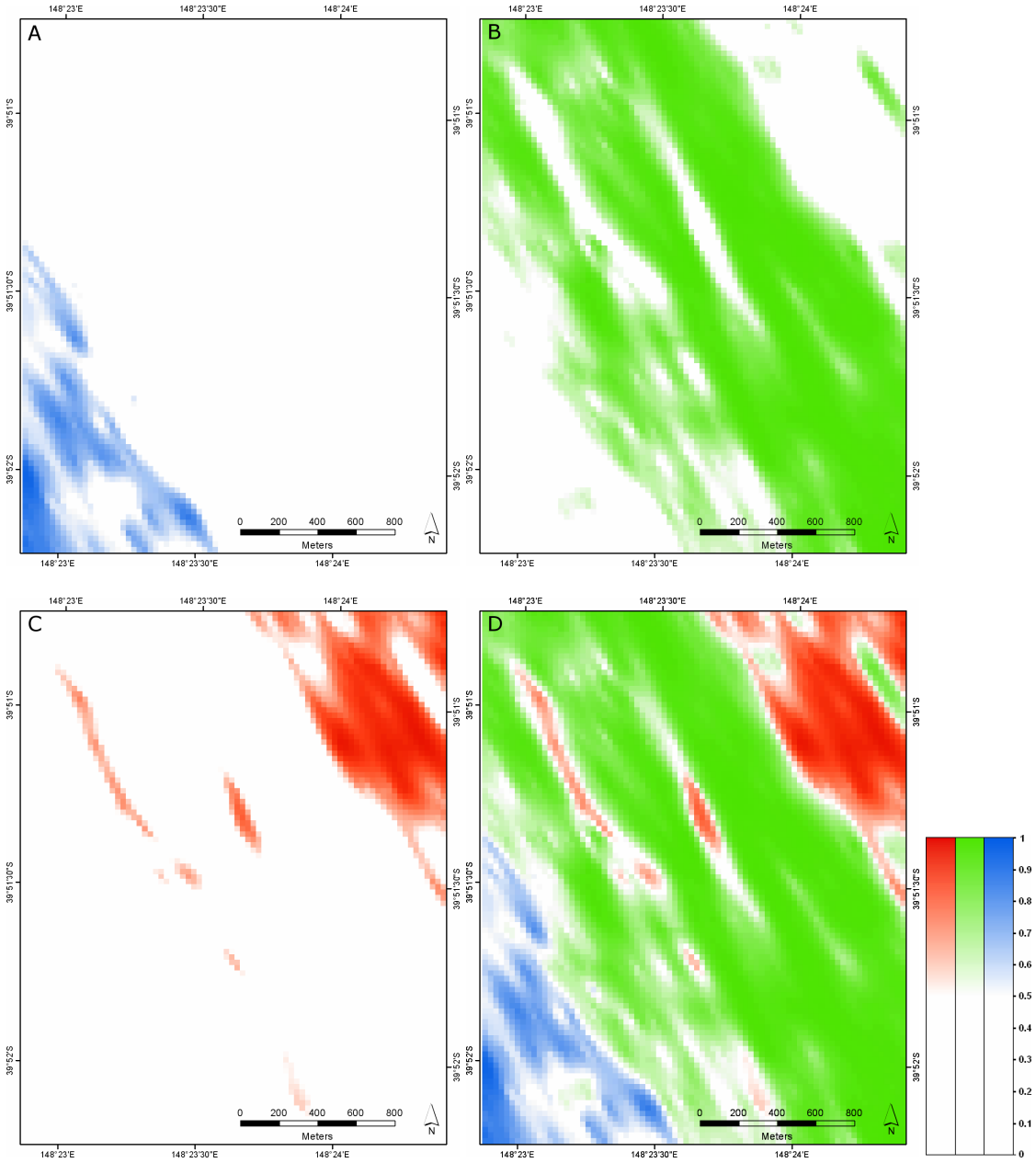

Figure 3.20. Interpolated probability surfaces for (A) cluster 1, (B) cluster 2, (C) cluster 3 and (D) combined probability surfaces.

3.3.6. Acoustic Classes and Ground Truth Data

To classify the three acoustic classes into substrate types, the video and sediment data were compared for areas where there was greater than 50% membership assigned to a given cluster. Acoustic class 1 was characterised by a larger mean sediment particle size than the other two classes, coarse sand versus medium sand (Table 3.5). Acoustic class 1 also had significantly more surface sponge than the other two acoustic classes, with over 10% cover (Table 3.5). There was a progression in shell cover from acoustic class 1 to acoustic class 3 in the amount of surficial shell cover, with acoustic class 1 having the smallest amount of surficial shell and acoustic class 3 having the largest amount of surficial shell with around 25% cover (Table

3.5). Depth was a strong covariate across all the classes, with differences in the mean depth of each of the three acoustic classes.

Table 3.5. Average sediment particle size (Phi-50%), percentage surficial sponge cover and percentage surficial shell cover of the 3 acoustic classes based on sediment and video analysis.

Variable	Acoustic Class 1 ± s.e.	Acoustic Class 2 ± s.e.	Acoustic Class 3 ± s.e.
Phi-50%	0.78 ± 0.05	1.14 ± 0.13	1.31 ± 0.21
% Sponge	10.9 ± 1.8	1.3 ± 0.5	0.3 ± 0.2
% Shell	8.7 ± 1.4	14.8 ± 1.4	24.9 ± 4.0
E1	43.93 ± 0.18	47.75 ± 0.06	45.64 ± 0.08
E2	43.93 ± 0.07	45.09 ± 0.05	41.19 ± 0.06
Depth	38.92 ±0.05	41.34 ± 0.03	42.24 ± 0.06

An examination of the statistical difference for mean particle size (Phi-50%), percent sponge, percent shell, E1, E2 and Depth for the three acoustic classes showed significant differences between each of these components (Table 3.6). These results indicate that there were some clear gradients across the study site, with these gradients running in a southwest/northeast direction. These gradients were present in depth, particle size, sponge cover and surficial shell cover and were reflected in the acoustic response of the seabed as measured by the E1 and E2 indices. Finally, this information was used to construct a habitat map for the study site which identifies the spatial distribution of the different substrate types and can be compared to the fishing intensity (Figure 3.21). When these habitats are compared to the distribution of fishing effort within the study site is can be seen that the highest intensity of fishing occurs on medium to coarse sand with low sponge and low to moderate amounts of surficial shell at around 42 m depth.

Table 3.6. Analysis of variance for mean particle size (Phi-50%), percent sponge, percent shell, E1, E2 and Depth for the three acoustic classes.

Variable	DF (class, error)	F Ratio	Probability
Phi-50%	2, 13	3.86	0.05
% Sponge	2, 206	40.9	<0.01
% Shell	2, 206	7.09	<0.01
E1	2, 1930	1046	<0.01
E2	2, 1930	1211	<0.01
Depth	2, 1930	1169	<0.01

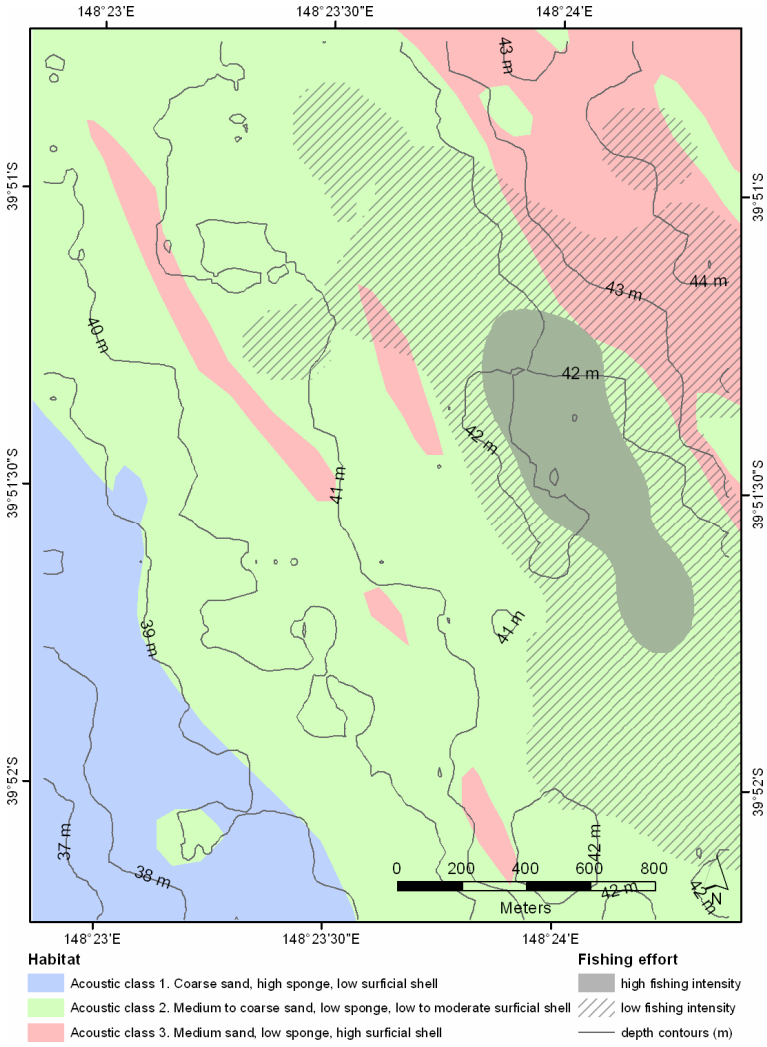

Figure 3.21. Habitat map of the study site showing the spatial distribution of habitats overlayed with the fishing intensity as inferred from VMS data.

3.4. Discussion

The single beam acoustic discrimination techniques outlined in this study were used to identify three acoustic classes of seafloor. When related to ground truth data, these acoustic classes could be described by a combination of physical and biological features of the seabed. There were significant differences in the acoustic response of each of these acoustic classes that could be related to density of sponge, mean sediment particle size and amount of surficial shell material all contributed to these acoustic classes. While the acoustic classes reflected the depth gradient across the study site, depth alone could not explain the differences in the E1 and E2 values for these classes.

The video ground truth data did not identify any areas of high scallop density however it is known from the VMS data from the subsequent fishing season that the study site did contain commercial quantities of scallops. In fact approximately 25% of the fishing effort off the east

coast of Flinders Island for the 2003/2004 fishing season occurred within the study site (unpublished VMS data). The area of highest scallop density as inferred from the VMS data did not have a unique acoustic signature. However the acoustic classes identified could be used to describe the potential for scallop habitat. This was demonstrated by the relationship between the fishing intensity inferred from VMS data and the distribution of the three acoustic classes. Based on the VMS data, the scallop bed within the study site appeared to be a small discrete bed, with less than 2 km by 1 km fished at medium to high intensity. This pattern was seen in all the VMS data for the scallop fishery; with relatively sparse points occurring where no scallops were found and high densities where beds were found (Haddon *et al.* 2006).

The majority of this fishing effort occurred in a narrow band on the eastern fringe of acoustic class 2 and a small amount in acoustic class 3 along the 42 m depth contour. This suggests that the distribution of scallops is not only defined by substrate type but also by environmental gradients such as depth, currents and exposure. In this case the prevalence of medium sands in itself did not constitute scallop habitat, but medium sand in 42 meters with the associated environmental factors seemed to be potential scallop habitat.

The current study shows that there is a potential to use single beam acoustics to identify potential scallop habitat. Studies in Canada has shown that maps of substrate and bathymetry derived from acoustic systems can be used identify areas likely to contain scallop habitat (Kostylev *et al.* 2003, Pickrill and Todd 2003). Assimilation of this type of information into the scallop fishery lead to a decrease of up to 75% in the time spent fishing, which has not only economic benefits, but also environmental benefits, leading to less contact on the seafloor, and thus less impact on other non scallop habitat (Pickrill and Todd 2003). SBES systems have also been shown to be able to differentiate between the substratum or biotopes associated with high scallop abundance (Kaiser *et al.* 1998).

Within this thesis scallop habitat did not appear to have a unique acoustic signature based on the indices examined. Hutin *et al.* (2005) found scallop beds were not able to be acoustically discriminated based on the proprietary QTCView, however were able to identify a unique signature from areas of dense scallop habitat based on analysis of depth corrected Sv backscatter data. Presumable the use of simple acoustic indices, such as the ones used in this chapter, do not have the resolution to discriminate subtle differences in the acoustic seabed response due to the presence of scallops. Further SBES are known to poorly discriminate large numbers of subtly different biotopes that merge into each other (Brown *et al.* 2001). The

study reported in this thesis was conducted in area containing a complex mosaic of soft sediment habitats, including bare sediment, sponge gardens, dead surficial shell, and scallop beds.

Whilst the study site was characterised as gently sloping, ranging in depth from 37 m to 44 m, depth was found to be a major factor in defining the three acoustic classes. The E1 index was shown to have a significant negative correlation with depth, whilst E2 index was not found to significantly relate to depth. It should be noted that there was a degree of overlap in depth distribution between each of these acoustic classes, especially between acoustic classes 2 and 3. Depth is known to be a major factor in determining seafloor habitats (Edgar and Barrett 2002, Hooper and Kennedy 2002), thus different depths are likely to have a range of different physical and biological characteristics which will also affect the acoustic response of the seafloor. The patterns in the acoustic classes derived from the SBES were also similar to those from the sidescan sonar system, providing further evidence that the different acoustic classes were not simple artefacts of changes in depth across the study site.

Sediment particle size did not show a strong relationship to depth in the study site. This is most probably due to the lack of a strong depth gradient within the study site and the limited range of particle sizes. The E1 or E2 acoustic indices also showed little relation to the mean particle size. Again this may reflect the lack of a large range of sediment types within the site, together with factors such as the amount of surficial shell and the presence of sponge influencing the acoustic response of the seabed. However, the three acoustic classes identified through the cluster analysis showed consistency in the sediment type contained within. Previous studies have shown acoustic variability to correspond with sediment particle size (Collins *et al.* 1996, Pinn and Robertson 1998, Hamilton *et al.* 1999, Freitas *et al.* 2003b). Many of these studies have had a wider variety of sediment types within their study areas, thus providing a larger spectrum across which to detect differences.

Sediment particle size is not the only factor that can affect the acoustic response of the seabed. The density of sponge and the amount of surficial shell also helped describe the identified acoustic categories in this study. Previously, acoustic diversity in QTC View data has been related to sediment particle size and the presence or absence of shell debris (Collins and Galloway 1998). The presence of distinct benthic communities has also been shown to influence the acoustic response of the seabed through bioturbation or the presence of surficial organisms (Caddell 1998, Pinn and Robertson 1998, Freitas *et al.* 2003a, Freitas *et al.* 2003b). High densities of sponge on soft sediment habitat have previously been identified using SBES,

based on increased energy in the tail of the first echo return and decreased energy in the second echo return, which can be related to increased roughness and decreased hardness of the seabed (Jordan *et al.* 2005b). A similar pattern was observed in this study.

The capacity to map sponge beds can have important benefits for the scallop industry. Sponge habitat is vulnerable to impact from mobile fishing gear, such as scallop dredges (McConnaughey *et al.* 2000, Kefalas *et al.* 2003). Thus knowledge on the distribution of sponge beds can allow these areas to be excluded from the fishery, providing them with protection. Within the Tasmanian scallop fishery scallop densities are generally low within areas of high sponge density (Haddon *et al.* 2005, Haddon *et al.* 2006). Thus the removal of these areas from the fishery is likely to have little negative impact on scallop catch rates, and may potentially lead to increased catch rates, due to less effort being directed to areas of low scallop abundance.

The current study used an unsupervised classification approach, where by clusters of similar E1 and E2 values were identified using k-means clustering and these were then related back to the ground truth data in order to describe acoustically distinct habitat types. An alternate approach would be to use a supervised classification approach. Supervised classification approaches identify acoustic signature for areas of known habitat type and then use these to classify the remainder of the data. Supervised classification methods have been successfully employed previously in seabed mapping (Sotheran *et al.* 1997, Foster-Smith *et al.* 2004b). One of the limitations of using a supervised classification approach is that they force the classification of data into the identified categories with varying degrees of uncertainty (Foster-Smith *et al.* 2004b) As soft sediment habitats can have overlapping characteristics and poorly defined boundaries between them creating fuzzy classes the identification of appropriate training sites can be problematic. Whilst not attempted within this study, a full supervised classification of the data presented in this chapter would provide a useful comparison to the unsupervised classification results.

The use of SBES to map the distribution of soft sediment habitats at fine scales is also limited by the resolution of the data both in terms of the footprint size of the acoustic beam and the interpolation between adjacent tracks. The footprint size of the acoustic beam increases with depth, for example in the current study the half beam power footprint size of the beam ranged from 6.5 to 7.7 m in diameter across the depth ranges surveyed. Whist the footprint of the E1 integration was an annulus ranging from inner diameter of 19.8 m to 23.6 m and an outer diameter of 42.7-50.8 m. As the footprint increases there is a greater likelihood of integrating

more than one habitat type in the acoustic return, especially in areas of heterogenous seafloor, which will affect both the classification accuracy and also the hierarchical level at which the habitat is able to be discriminated by the system. Further most of the acoustic energy is likely to be coming from angles closest to the central axis due to the beam pattern of the transducer thus changes in substrate composition at the outer edge of the footprint are less likely to affect the measured acoustic response using these simple metric.

Ideally the footprint size needs to be significantly smaller than the patch size of the substrate being sampled (Brown *et al.* 2005b). Secondly, SBES data consists of a series of points along the vessels path which need to be interpolated if a full coverage map is required. The track spacing needs to reflect heterogeneity of the substrate, with the heterogeneity being at least equal or greater than the track spacing (Brown *et al.* 2005b). In the current study the footprint size was generally smaller than the patch size of the different features as identified by the video, while the track spacing was at a scale smaller than the variability within the data based on the variogram modelling.

3.5. Conclusions

This chapter examined the classification of SBES data at the Substratum/Ecotype and Modifier levels in the classification hierarchy. The effects outlined in chapter 1 are likely to have a greater impact over classification of SBES data at this level, as the separation between acoustic classes was smaller than at higher levels in the classification, for example in the previous chapter the acoustic classes were generally separated by 10-20 dB (reef, sand silt), where as in this chapter the acoustic classes separated by less than 4 dB (subclasses of sand). For this level of classification, maintaining a constant vessel speed and consistent weather conditions for the duration of the survey is important. As the study site had only a small depth range and was generally flat (slope less than one degree) these two factors are likely to have had little impact on the classification results, however the E1 and E2 ranges for the acoustic classes may not be applicable to other areas in different depth ranges.

The techniques developed in this chapter delineated three acoustic seabed classes, which reflected differences in sponge density, mean sediment particle size, the amount of surficial shell, and depth. None of these categories related to areas of high scallop abundance as inferred from fisheries data. However, the distribution of fishing effort reflected the spatial distribution of these acoustic classes and the underlying bathymetry, with the areas of highest fishing effort located in a narrow depth range along the boundary of two of the acoustic classes.

Chapter 4. Acoustic detection of urchin barren habitat for broad scale distribution assessment

4.1. Introduction

Rocky reef systems are an important source of primary production in temperate waters, and support a large number species including many commercially important fish and invertebrate species. Much of the primary production is linked to large macroalgae beds which occur in the photic zone. Sea urchin barrens are an alternative habitat (at the modifier level of classification) state to algal dominated reef and have become increasingly common in many temperate regions throughout the world (Lang and Mann 1976, Mann 1977, Chapman 1981, Himmelman *et al.* 1983, Miller 1985, Hart and Scheibling 1988, Harris and Tyrrell 2001, Gagnon *et al.* 2004, Lauzon-Guay and Scheibling 2007), and have also been recorded in Australia (Andrew and O'Neill 2000, Fowler-Walker and Connell 2002). The destructive grazing of sea urchins on kelp beds can lead to reductions in both productivity and diversity on shallow temperate reef systems (Gagnon *et al.* 2004). These reef systems often support valuable fisheries that are adversely affected by the development of barrens.

In the past few decades there has been an increase in urchin barren formation in Tasmania (Edgar 1997). The common sea urchin, *Heliocidaris erythrogramma*, has been responsible for the formation of barrens in many sheltered bays (Valentine and Johnson 2005), while the long spined sea urchin, *Centrostephanus rodgersii*, has been progressively undergoing a range extension along the Tasmanian east coast, resulting in barrens in more exposed and previously productive areas of the coastline (Johnson *et al.* 2004). Previous attempts to document urchin barren distribution on the east coast of Tasmania have either focussed on characterising the broad scale trends in depth distribution (Johnson *et al.* 2004, Jordan *et al.* 2005a, Jordan *et al.* 2005b) or the fine scale structure of the barren algae interface (Johnson *et al.* 2004).

Commonly visual and optical techniques are used to detect algae and barren distributions on reef substrate; including diver surveys (Johnson *et al.* 2004), underwater video (Jordan *et al.* 2005a, Jordan *et al.* 2005b), and airborne remote sensing (Simms and Dubois 2001). The use of diver and video surveys provide highly detailed information on the species composition within a given area; however these techniques are generally limited in their spatial coverage. On the other hand, airborne optical remote sensing techniques can provide broad scale coverage but have limited penetration into to water column due to the rapid absorption of light by water, with maximum depths generally less than 10 m for the identification of algae on reef (Simms and Dubois 2001). As urchin barren on the east coast of Tasmania generally

range from between 5 and 25 m depth (Johnson *et al.* 2004), the use of airborne optical remote sensing is clearly limited in its application to urchin barren mapping. There is a need for techniques to be developed that have the capacity to identify the distribution of urchin barrens across broad geographic regions and depth ranges.

Single beam echo sounders (SBES) have been extensively used for substrate mapping (Greenstreet *et al.* 1997, Kloser *et al.* 2001b, von Szalay and McConnaughey 2002, Freitas *et al.* 2003b, Foster-Smith *et al.* 2004a). Commonly SBES have been used to map the distribution of soft sediment habitats (Greenstreet *et al.* 1997, Morrison *et al.* 2001a, Ellingsen *et al.* 2002, Freitas *et al.* 2003a), map the distribution of soft and hard substrate (Kloser *et al.* 2001b, Pickrill and Todd 2003, MacKinson *et al.* 2004), or map the distribution of biota (Pickrill and Todd 2003, Hutin *et al.* 2005). Several studies have reported on the capacity of SBES to detect the presence of algae as part of these classes (Anderson *et al.* 2002, Foster-Smith and Sotheran 2003). With the commercial Submersed Aquatic Vegetation (EcoSAV) module from BioSonics designed for detecting underwater vegetation using their SBES (Sabol *et al.* 2002). Limited work has also been done on developing acoustic signatures for common algae based on SBES data (Populus and Perrot 2007).

In the transition from native algae to barren a large amount of biomass is removed from above the seafloor (Tegner and Dayton 2000). On the east coast of Tasmania the algae *Phyllospora comosa* and *Ecklonia radiata* are the most common algae in the depth range commonly affected by urchin barrens (Jordan *et al.* 2005a, Jordan *et al.* 2005b, Lucieer *et al.* 2009). Both these species can form dense canopies up to 2 m above the seabed. *P. comosa* also has numerous small gas filled floats along its central axis, the impedance mismatch between the water and the air within these floats would be expected to provide a strong target for detection by a single beam echo sounder. This suggests that there should be a difference in the acoustic response above the seabed (sounder detected bottom) between algal dominated reef and barren reef.

Previous studies that have identified algal dominated reef have been based on proprietary systems including RoxAnn and QTC (Anderson *et al.* 2002, Foster-Smith and Sotheran 2003). These systems identify statistical differences in the acoustic return based on a series of acoustic indices. The RoxAnn system does not incorporate the region above the sounder detected bottom, while the QTC system does incorporate some parameters such as the rise of the first echo. Clearly while these systems have the capacity to identify reef with algae from non algal reef they are potentially not optimised for the task. The BioSonics EcoSAV module

on the other hand, does focus on the region above the seabed, with this system shown to successfully map seagrass distributions (BioSonics, Sabol *et al.* 2002). Species of algae with gas filled floats are expected to be strong acoustic targets, where integration of regions of the acoustic response above the seabed may lead to better segmentation of algal dominated reef and barren reef.

This chapter focuses on the modifier level of the hierarchical classification system presented in Chapter 1 (Table 1.1). A simple acoustic method for segmenting algal dominated reef from barren reef based on the processing of single beam echo sounder data is presented. The method involves the integration of the acoustic response above the seabed. The classification accuracy of this method is compared to that using traditional RoxAnn E1 and E2 indices (See Chapter 2 Section 2.2.3 for background on these indices). The echo shape method is compared across two sites, one characterised by simple low profile reef, while the other characterised by complex high profile reef. Finally, the usefulness of acoustic techniques for algae/barren mapping is investigated in terms of typical algal cover and algal and barren patch size on the east coast of Tasmania.

4.2. Methods

4.2.1. Study Site

Two regions were sampled in this study, one for development of methods (Lords Bluff), and a test region (Grants Point) (Figure 4.1). The methods development was conducted at Lords Bluff, on the east coast of Tasmania. The reef substrate at this location was known to have both urchin barren and dense stands of native algae (Valentine and Johnson 2003, Pederson and Johnson 2008). The reef was low profile and ranged from shore to a maximum of 15 m depth. The conditions at the time of the survey were calm to maximise the quality of the acoustic data. Two grounds within this site were surveyed, one where the urchin barren was known to be extensive and the other where stands of native algae dominated.

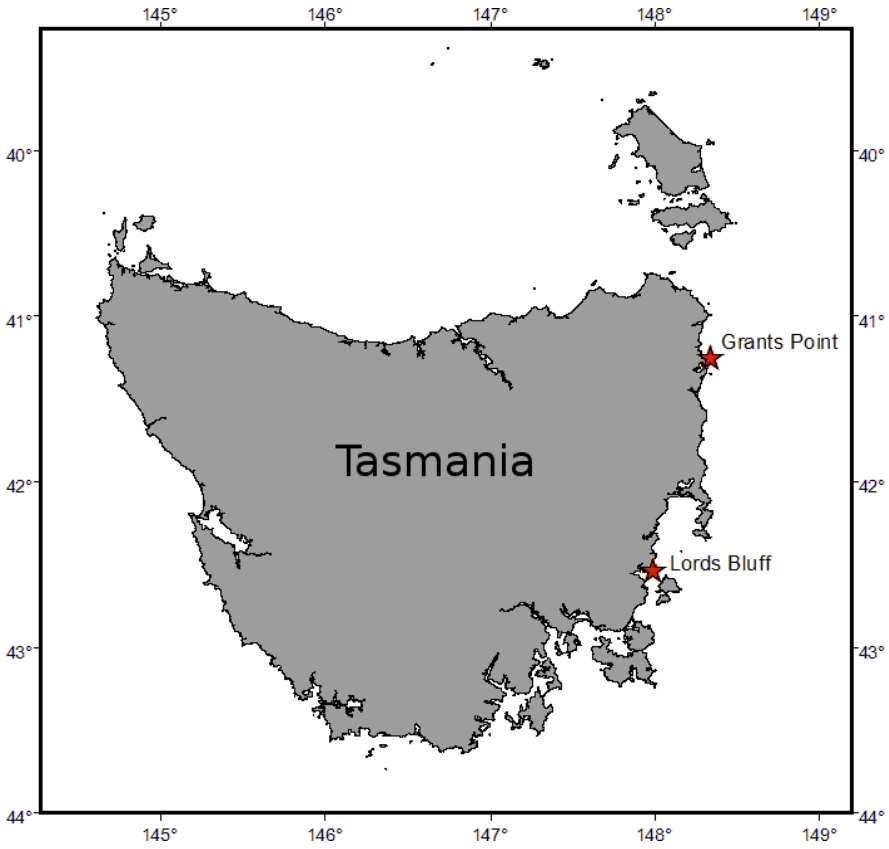

Figure 4.1. Location of the two study sites at Lords Bluff and Grants point on the east coast of Tasmania.

The signature development was then tested on data collected at a Grants Point, St Helens, on the upper east coast of Tasmania. This location was characterised by complex and steep granite reef, which extended to at least 30 m depth. Again this site was known to have a mix of large urchin barrens and dense native algal beds (Johnson *et al.* 2004, Jordan *et al.* 2005a). The conditions at the time of the survey were calm.

4.2.2. Field Surveys

The Lords Bluff site was surveyed using a combination of single beam acoustics and underwater video mounted on a 6.5 m aluminium vessel (*FRV Nubeena II*). A series of parallel transects approximately 20 m apart were run across the depth gradient using each system (Figure 4.2). Acoustic data were collected using a calibrated Simrad ES60 single beam echo sounder. A 120 kHz 10^{o} beam width transducer was pole-mounted to the side of the vessel directly beneath a differential GPS antenna. The echo sounder ping rate was set at 2 pings per second, with a pulse length of 0.256 ms and power output of 100 W. The echo sounder was calibrated using a standard tungsten carbide sphere (Foote *et al.* 1987). Positional information was acquired using an Omnilite 132 differential GPS, providing positional accuracy of ± 0.9 m r.m.s.. Vessel speed was maintained at 3 ms^{-1} for the acoustic surveys.

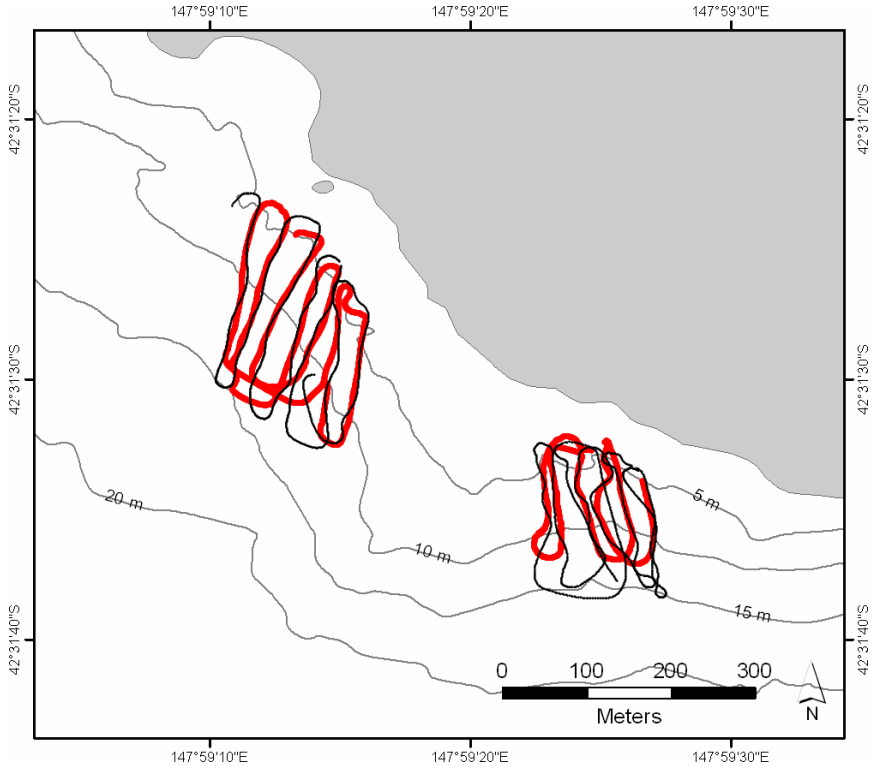

Figure 4.2. Map of the Lords Bluff study site showing the acoustic transects (black) and the video transects (red).

Underwater video was collected using a single CCD digital underwater video camera (MorphVision, NSW), mounted in a heavily weighted towfish and suspended below the vessel on a tow rope. The position of the camera system was monitored on the echo sounder to ensure it was beneath the vessel and maintained at approximately 1 m above the seabed using an electric winch. Vessel speed was maintained at 0.7 ms^{-1} to ensure the camera system remained directly beneath the vessel. Positional information from the differential GPS was directly overlayed onto the video signal and also logged to computer as a text file. The video data was recorded to miniDV cassette. Approximately 1 hour of video was collected across the two sites.

The Grants Point site was surveyed with the same acoustic and video systems as the Lords Bluff site, as part of a baseline mapping project. A series of parallel transects approximately 60 m apart were run across the depth gradient using the acoustic system. Several of these transects were also replicated using the underwater video system to provide ground truth information.

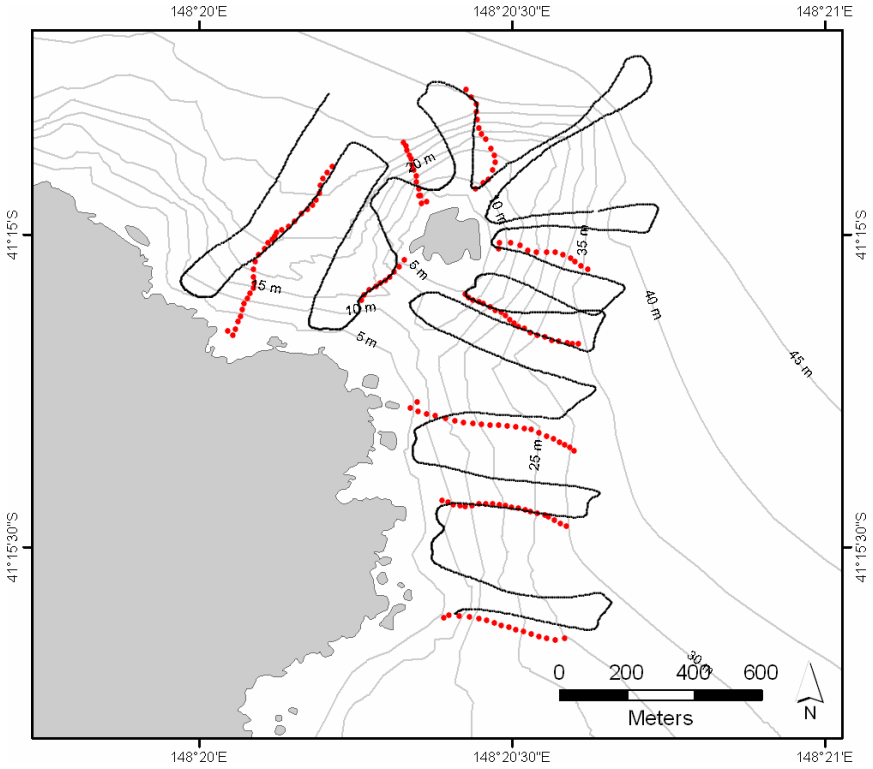

Figure 4.3. Map of the Grants Point study site showing the acoustic transects (black) and the video transects (red).

4.2.3. Data Analysis

Still images were captured from the underwater video footage at a rate of 2 frames per second (separation ~0.35 m). The images were analysed for percentage algal cover using a point intercept method. A 7 x 7 grid (49 intercept points) was overlayed on the images and percentage algal cover calculated according to the number of intercept points with algae present. The image data were then classified as either dense algae, where there was greater than 75% cover of macroalgae; barren, where there was less than 5% cover; or partial barren, where the cover fell between these two classes. The classified percentage cover data were recorded onto the vessel track log for comparison with the acoustic data.

The calibrated ES60 acoustic data were corrected for triangle wave (Section 2.2.2) and imported into Echoview 3.30 for post processing. The ES60 line pick algorithm failed to adequately detect the bottom in areas of dense algae. The sounder detected bottom was redefined using the line pick algorithm maximum Sv with backstep using the parameters outlined in Table 4.1. Acoustic indices of seabed roughness (E1) and seabed hardness (E2) were calculated based off the sounder detected bottom using the methods outlined in Section 2.2.3. The indices were calculated for each ping.

Table 4.1. Settings used for Maximum Sv with backstep algorithm in Echoview, used to calculate position of sounder detected bottom.

Setting	Unit	Value
Maximum Sv for good pick	dB	-25.00
Discrimination level	dB	-15.00
Backstep range	m	-0.15
Start depth	m	2.00
Stop depth	m	20.00

The E1 and E2 indices are integrations of the tail of the first seabed echo and the entire second seabed echo and, as such, potentially have low sensitivity to objects above the seafloor. A technique was developed to compare the shape of the echo return above the sounder detected bottom. A series of 12 integration regions were defined around the echo sounder detected bottom (SDB) in Echoview 3.30. These regions were defined by the pulse length in water ($c\tau$) 0.35 m, with six regions defined above the SDB and six regions defined below the SDB (Table 4.2). The average integral of each of these regions was calculated in Echoview 3.30 using a 1 ping grid. The integration results were exported to a text file for comparison with the video analysis.

Table 4.2. Definition of integration regions for echo shape, upper and lower bounding lines as defined by an offset from the sounder detected bottom (SDB).

Integration region	Lower limit (m)	Upper limit (m)
-6 pulses	SDB - 1.74	SDB - 2.09
-5 pulses	SDB - 1.39	SDB - 1.74
-4 pulses	SDB - 1.04	SDB - 1.39
-3 pulses	SDB - 0.70	SDB - 1.04
-2 pulses	SDB - 0.35	SDB - 0.70
-1 pulse	SDB	SDB - 0.35
+1 pulse	SDB + 0.35	SDB
+2 pulses	SDB + 0.70	SDB + 0.35
+3 pulses	SDB + 1.04	SDB + 0.70
+4 pulses	SDB + 1.39	SDB + 1.04
+5 pulses	SDB + 1.74	SDB + 1.39
+6 pulses	SDB + 2.09	SDB + 1.74

The acoustic indices (E1 and E2) and the echo shape data were imported into the GIS platform ArcView 3.2a. Within the GIS, the acoustic data was merged with the classified video data. To ensure spatial overlap the video and acoustics were only merged if they were within 1 meter of each other and the video showed homogenous classification for greater than 5 meters in either direction of the point. This resulted in a series of 515 points that encompassed both barren and algal dominated reef and ranged between 2 and 12 metres depth. These points were used to examine the acoustic response of these two habitat classes.

4.2.3.1. External validation site

The echo shape methods developed in the first part of this study were then tested at a second site, Grants Point, at St Helens, on the central east coast of Tasmania. The Grants Point study

site was characterised by more steeply sloping, and more complex reef than the Lords Bluff site. The reef at the Grants Point site also extended deeper than at Lords Bluff, to at least 30 m depth, thus allowing the testing of the echo shape method in deeper water where algal cover was potentially lower. A series of co-incident acoustic and video transects from St Helens were analysed using the methods developed at Lords Bluff. As for the Lords Bluff site only acoustic and video points within 1 meter of each other and at least 5 m of homogenous habitat were used, resulting in a total of 520 points for comparison.

Initial trials showed low classification success at the Grants Point site compared to the Lords Bluff site, which was attributed to poor performance of the Maximum Sv with backstep algorithm in attributing the sounder detected bottom in the complex reef more steeply sloping reef. This resulted in parts of the seafloor being integrated into the echo shape parameters and thus affecting the echo shape parameters. A second method to improve the bottom detection was trialled, which involved a series of masking steps within the Echoview software.

Firstly, the sounder detected bottom was smoothed over a 5 point moving average, the water column was then masked out at 1 m above the smoothed sounder detected bottom. A user specified threshold (-25 dB) was then applied to the masked echogram, where by any sample over the threshold was assigned a true class, and any sample below the threshold was assigned a false class. The -25 dB threshold was chosen as this represented the maximum value of detected algae Sv values from the Lords Bluff site, while still being below the maximum Sv level of the sounder detected bottom. The threshold mask was then used to mask a generated -10 dB echogram (which was an arbitrary value chosen to be below -25 dB maximum Sv level used in Maximum Sv with backstep algorithm). Finally the line pick algorithm, Maximum Sv with backstep, was used to pick a line over this new echogram using the original settings given in Table 4.1. The echo shape parameters were then calculated off this revised sounder detected bottom.

In order to examine the spatial structure of algal dominated and barren reef habitat, video data from the east coast of Tasmania was analysed to assess the average patch size of urchin barrens and to get a better understanding of algal cover by depth. A series of 126 video transects collected across reef substrate were analysed (Figure 4.4).

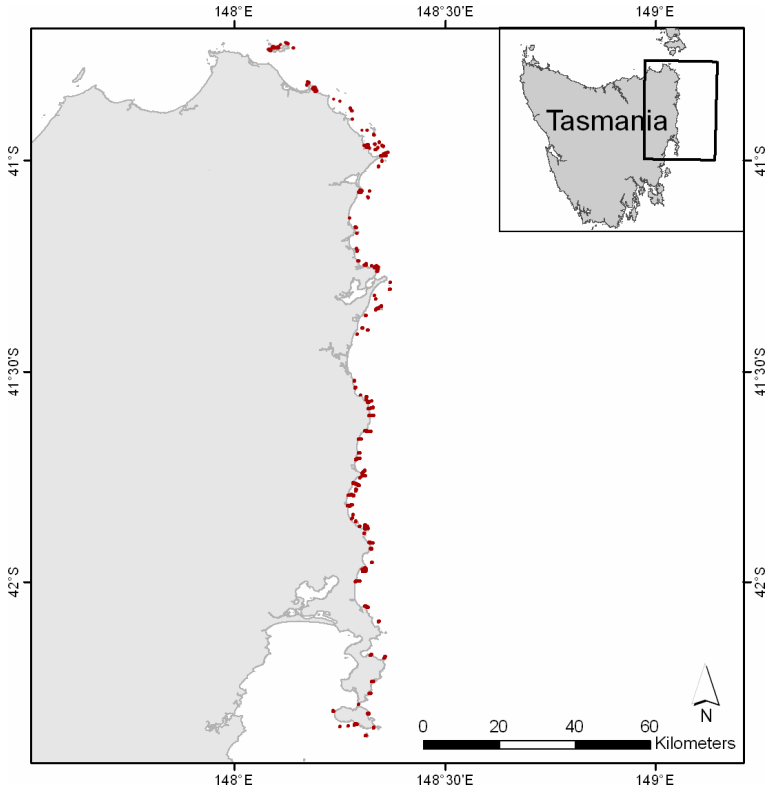

Figure 4.4. Location of 126 video transects (red dots) along the east coast of Tasmania used to estimate algal cover by depth and urchin barren patch size.

The algal cover was estimated based on the protocols outlined in Chapter 6.2.4.2.1. This involved analysing a set time period (4 seconds) of video every 10 seconds and attributing algal cover to the nearest 10% based on visual interpretation. The mean depth for this time period was then attributed to the algal cover data from the synchronised echo sounder data. The algal cover data was used to examine trends in algal cover by depth which could be related back to urchin barren depth distribution. Where urchin barrens were present, the videos were scored on a frame basis as either algae dominated reef or barren reef according to the same analysis techniques outlined above for the lords bluff site. The patch size of barren reef was calculated as the average distance of continuous barren observed on video and was based on the distance along the transect.

4.3. Results

4.3.1. Acoustic signature

The acoustic indices E1 and E2 displayed a large amount of overlap between algal dominated reef and barren reef (Figure 4.5). The means of the E1 index for algae dominated reef (38.3 ± 2.7 dB re1(m^2 nmi^{-2})) and barren reef (35.7 ± 3.0 dB re1(m^2 nmi^{-2})) were found to be significantly different at the 0.01% level based on t-tests. Similarly the means of the E2 index for algal dominated reef (38.6 ± 2.3) and barren reef (41.3 ± 2.0) were also found to be

significantly different at the 0.01% level based on t-tests. Confidence ellipses, encompassing 95% of the data, were separately defined for the algal dominated reef and barren reef E1 and E2 clusters. The area of overlap between these two confidence ellipses contained 69% of all algal dominated reef points and 79% of all barren reef points. Only 30% of algal dominated reef points and 18% of barren reef points fell exclusively within corresponding confidence ellipse. The remaining points for each class were misclassified. Hence the E1 and E2 indices were of little use for classifying acoustic data into algal dominated reef and barren reef.

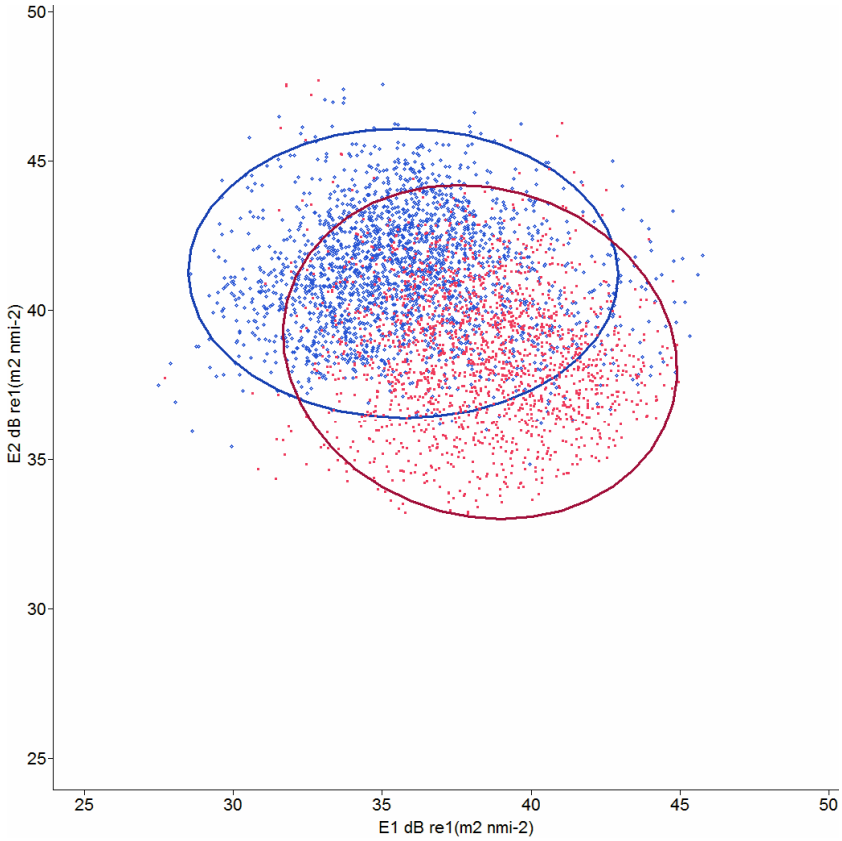

Figure 4.5. Scatter plot of average acoustic response (E1 and E2) of algae dominated reef (red square) and barren reef (blue diamond) showing a high degree of overlap between the two categories.

When the E1 and E2 data was classified based on the confidence ellipses the classification was dominated by the mixed class (Figure 4.6). Thus while there was a statistical difference between the mean E1 and E2 for algal dominated reef and barren reef, this could not be used to segment the two classes successfully due to the large amount of overlap between the two classes.

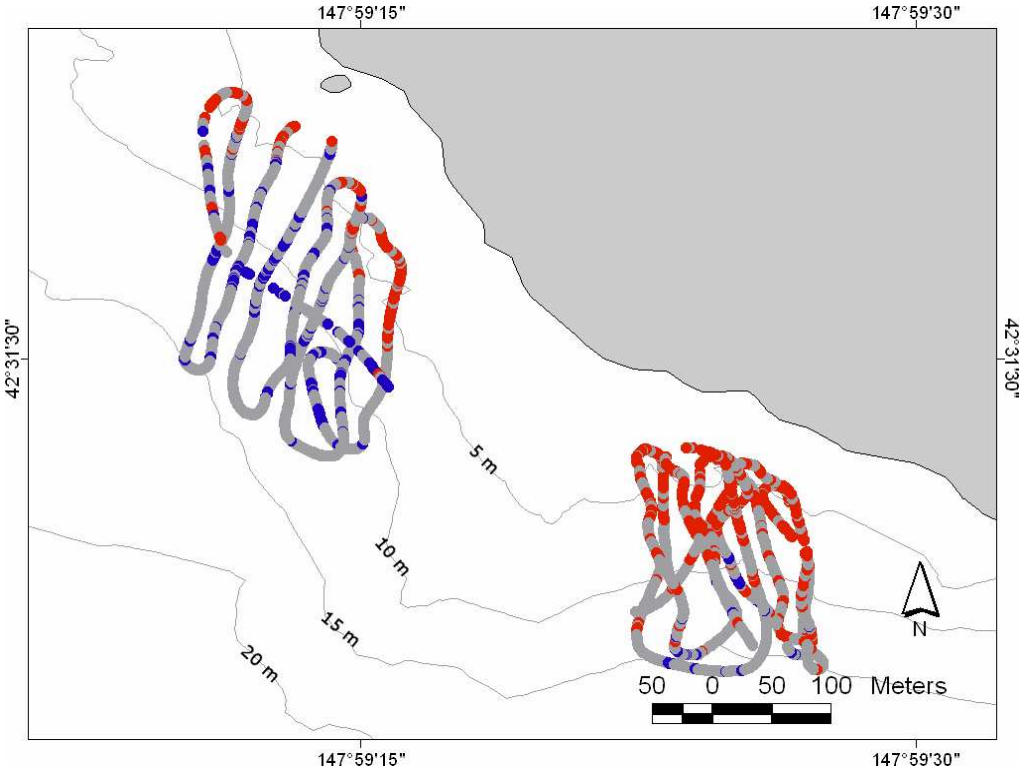

Figure 4.6. Predictive maps of urchin barren distribution at the Lord's Bluff study site based on classification of the single beam acoustics based on E1 and E2 indices. Red dots represent the algal class, blue dots represent the barren class, while grey dots represent where the two classes overlap.

The comparison of echo shape of barren versus algal dominated reef showed the greatest difference between -2 and -3 pulse lengths above the sounder detected bottom (Figure 4.7). This represents differences in the echo return from the algae and associated biota between the two habitats. The tail of the echo below the sounder detected bottom showed little differentiation between the two habitats. By -6 pulse lengths above the sounder detected bottom the average values of each of the habitats were again similar approximately -80 dB (Figure 4.7). There was little difference in the bin immediately above the sounder detected bottom, possibly due to partial integration of parts of the much stronger bottom echo in this bin saturating the return and masking the difference between the algae and barren signal.

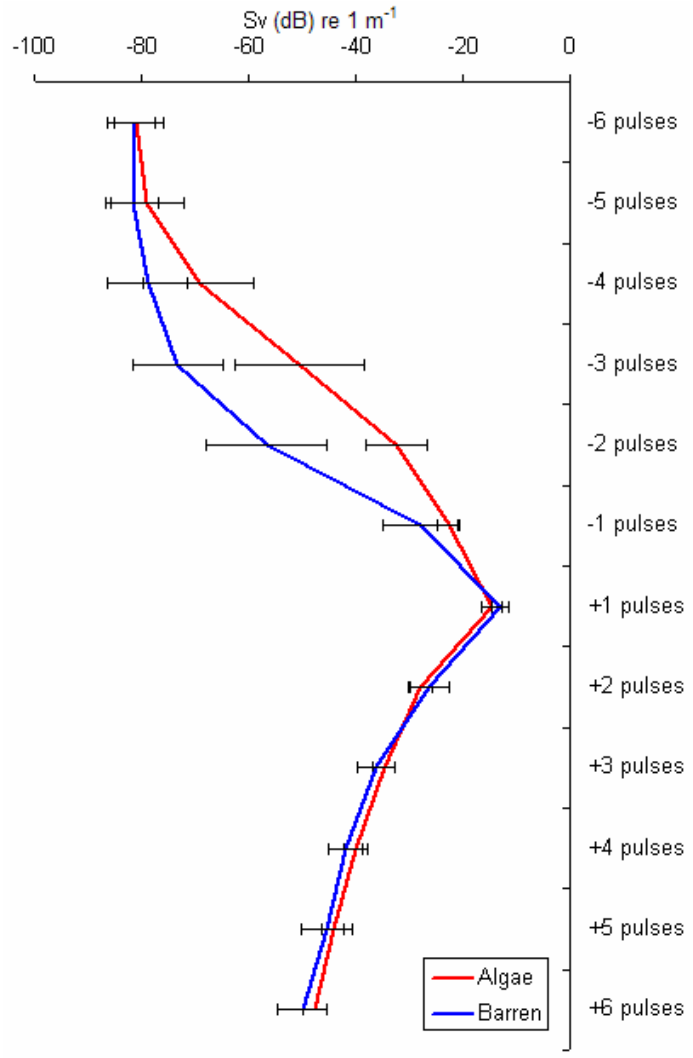

Figure 4.7. Comparison of average echo shape for algal dominated reef (red line) and barren reef (blue line) in 5 – 10 m depth range. Error bars give the standard deviation. Horizontal x axis gives the distance above and below the sounder detected bottom in pulse lengths. One pulse represents 0.35 m in seawater at a sound speed of 1500 ms^{-1}.

The data from the integration of the regions defined by -2 and -3 pulse length above the sounder detected bottom were used to classify the acoustic data into algal dominated reef and barren reef. Based on these indices the algae dominated reef and the barren reef separated out into two separate clusters (Figure 4.8). As for the E1 and E2 data, confidence ellipses encompassing 95% of the data were separately defined for the algal dominated reef and barren reef clusters. The degree of overlap was significantly less for the echo shape data compared to the E1 and E2 data (Figure 4.5, Figure 4.8). For both the algal dominated reef and barren reef classes, 79% of points fell exclusively within their corresponding confidence ellipses, a further 15% and 16% of points fell in the overlap between the two confidence ellipses respectively. The echo shape parameters defined by the integration of regions -2 and -3 pulse lengths above the sounder detected bottom were used to segment the acoustic data into algal dominated reef and barren reef.

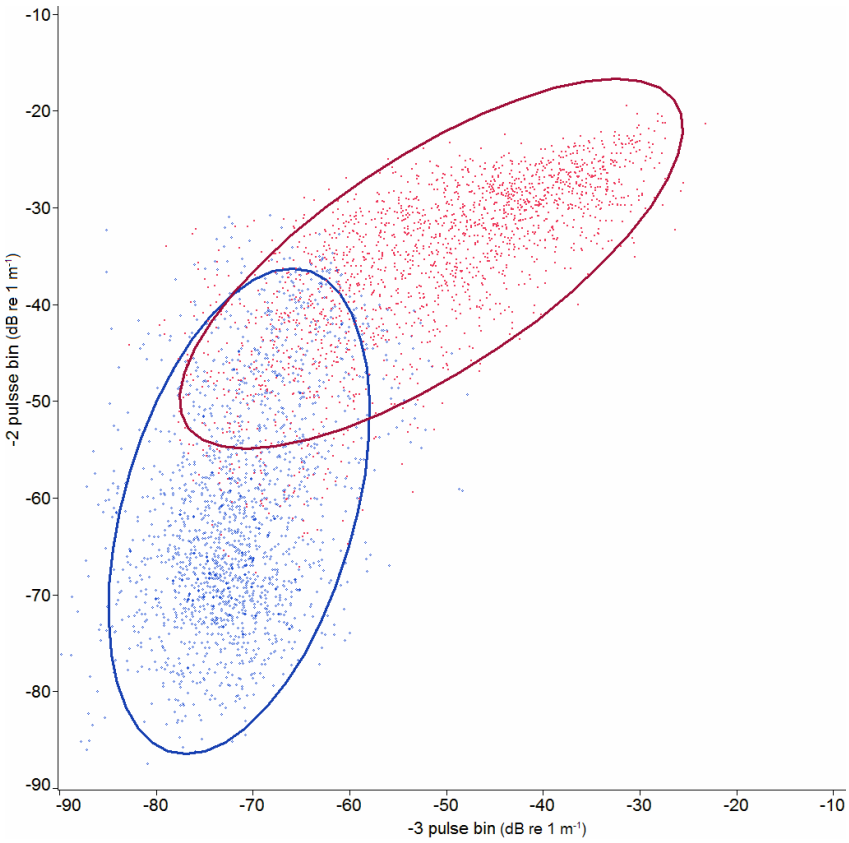

Figure 4.8. Scatter plot of integration values for -2 and -3 pulse lengths above the sounder detected bottom. Points are colour coded based on the video classification, with the red points representing algal dominated reef and the blue points representing barren reef. The red and blue ellipses indicate the 95% confidence ellipses for the algal dominated reef and barren reef respectively.

The classified video and acoustic data were used to construct predictive maps of the urchin barren distribution (Figure 4.9). These maps highlight that the urchin barren algal interface becomes deeper from the western to the eastern side of the study site. The urchins appear to be better adapted at grazing the algae *Ecklonia radiata*, which is replaced by the algae *Phyllospora comosa* in shallow more exposed water. Thus the pattern of barren formation is a reflection of the algal distribution, which in turn reflects an increase in exposure from the more sheltered western part of the bay to the exposed eastern point.

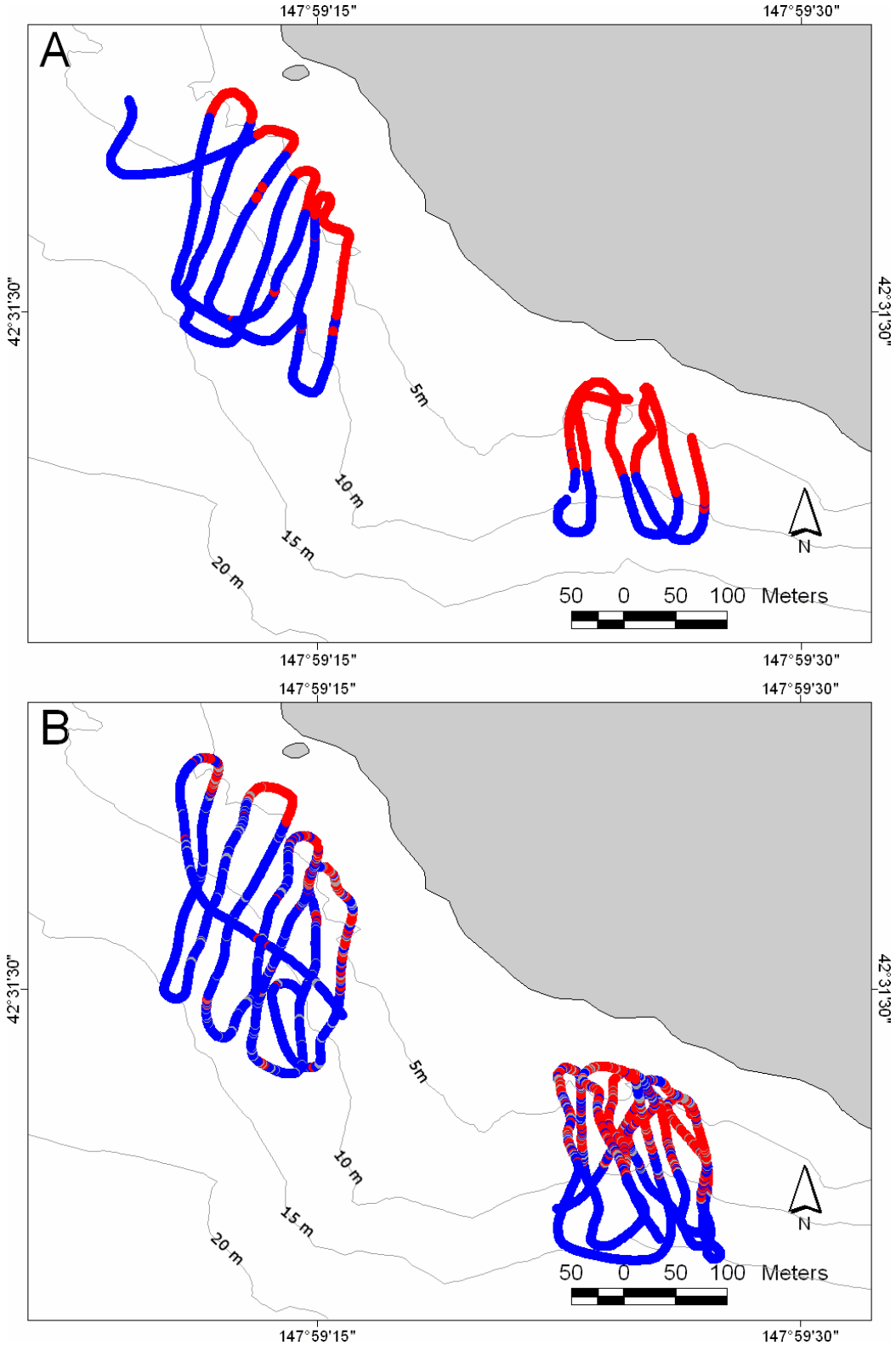

Figure 4.9. Predictive maps of urchin barren distribution at the Lord's Bluff study site based on (A) classification of the towed video and (B) classification of the single beam acoustics based on the echo shape parameters SDB-2 and SDB-3. Red dots represent algal dominated reef, blue dots represent barren reef, while grey dots represent where there was a mixture of algae and barren reef.

4.3.2. External validation

The echo shape method was tested at a second site at Grants Point on the upper east coast. This site was characterised by more complex reef extending to 30 m depth. The initial

calculation of the echo shape parameters, based on the Maximum Sv plus backstep algorithm, produced low classification success, with 61.1% of all points successfully classified. The algal dominated reef was classified successfully 86.4% of the time, while the barren reef only 45.3% of the time (Table 4.3). This was attributed to the poor performance of the line pick algorithm used to calculate the sounder detected bottom in the more complex reef at this site, resulting in significant parts of the seafloor being included in the echo shape parameters. The reef at this site was more complex and generally steeper than the reef at the Lords Bluff site. As shown in Chapter 2 slope of substrate can affect the acoustic return from the seafloor, in this case the slope of the seafloor resulted in parts of the seafloor to be integrated above the sounder detected bottom.

Table 4.3. Classification accuracy of echo shape algorithm based on sounder detected bottom (Maximum Sv with backstep) for urchin barren/algal dominated reef segmentation at the Grants Point study site.

		Echo shape classification	
		Algae	**Barren**
Video classification	**Algae**	86.4%	13.6%
	Barren	54.7%	45.3%

An alternate method was used to calculate the sounder detected bottom, referred to as the revised sounder detected bottom. A second set of echo shape parameters were calculated based on the revised sounder detected bottom. The classification accuracy increased to 86.4%. The classification accuracy for algal dominated reef, reduced to 72.2%, while the classification accuracy for barren reef increased to 94.3%.

Table 4.4. Classification accuracy of echo shape algorithm based on revised sounder detected bottom for urchin barren/algal dominated reef segmentation at the Grants Point study site.

		Echo shape classification	
		Algae	**Barren**
Video classification	**Algae**	72.2%	27.8%
	Barren	5.7%	94.3%

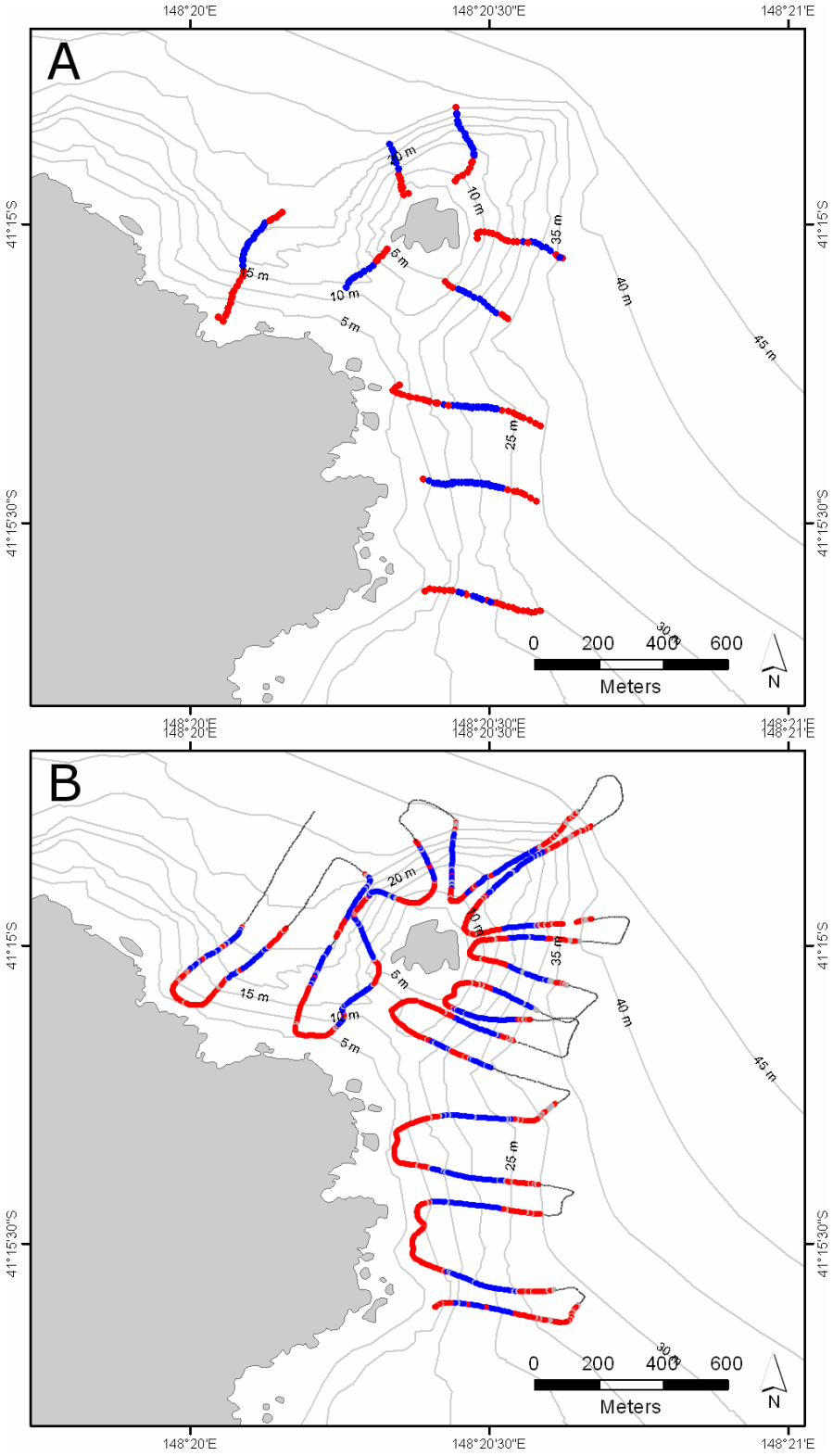

Figure 4.10. Predictive maps of urchin barren distribution at the Grants Point study site based on (A) classification of the towed video and (B) classification of the single beam acoustics based on the echo shape parameters SDB-2 and SDB-3 (revised sounder detected bottom method). Red dots represent algal dominated reef, blue dots represent barren reef, grey dots represent where there was a mixture of algae and barren reef, and small black dots represent transects across sand habitat.

4.3.3. Algal cover and barren patch size

To gain a better understanding of the trends in algal cover and urchin barren patch dynamics on the east coast of Tasmania a series of 126 video transects were analysed. There was a trend for reduced algal cover with depth. Between 0 and approximately 30 m depth the algal cover was high (average cover between 75% and 95%) (Figure 4.11). Below 30 m the algal cover rapidly decreased to below 50%, and by 35 – 40 m depth was less than 25%.

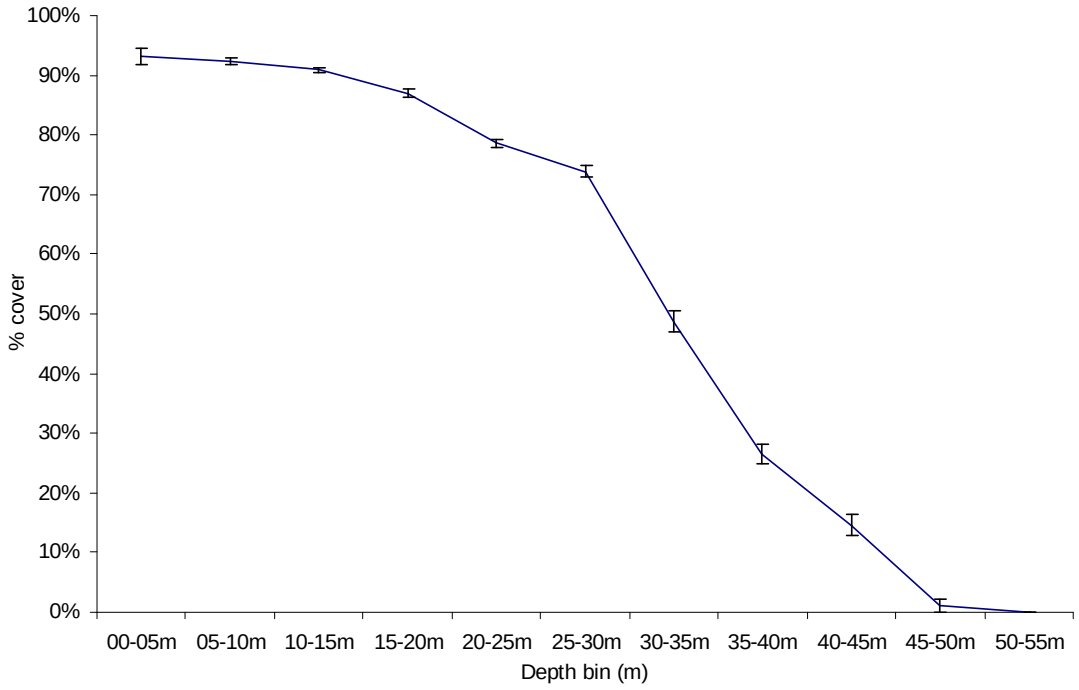

Figure 4.11. Average algal cover for Tasmanian east coast reefs based on analysis of 126 video transects (error bars indicate s.e.).

In the 126 video transects 26 urchin barrens were observed. The average barren patch size of these barrens, which was calculated as the distance of continuous barren recorded on the video were 79.3 m ± 10.8 m. The largest barren observed was 197 m, whilst the smallest was only 17 m across. It should be noted that smaller incipient barrens were observed, where urchins were grazing down the algae, however at these sites algae was still present albeit in low amounts, such that they were not recorded as full barren. The size of urchin barrens will have an influence on the sampling regime required to adequately recreate barren distribution from acoustic mapping.

4.4. Discussion

A simple method for the segmentation of algal dominated reef from barren reef was presented in this study. Integration of the acoustic data based on regions defined by 2 and 3 pulse lengths above the sounder detected bottom showed the largest separation between algal dominated reef and barren reef. Classification success for algal dominated reef and barren reef

was 79% for each class at the Lord Bluff site and 72% for algal dominated reef and 94% for barren reef at the Grants Point site.

The use of standard acoustic indices, E1 and E2, proved insufficient to separate algal dominated reef from non-algal dominated reef. These indices are based on integration of the first and second echo returns, which are generally influenced by the acoustic roughness and acoustic hardness of the seafloor (Chivers 1990, Magorrian *et al.* 1995). While algae can affect the amount of energy reflected and the scattering of that energy due to increased rugosity (Anderson *et al.* 2002), the rugosity and composition of the underlying substrate generally has the greatest influence on the E1 and E2 values.

The largest differences between the alga dominated and barren reef were between 2 and 3 pulse lengths above the sounder detected bottom, which equates to 0.384 m to 1.152 m above the sounder detected bottom. This region corresponds to the area of maximum algal biomass. The typical algae occurring along exposed coasts of eastern Tasmania are *Ecklonia radiata* and *Phyllospora comosa*, which attain maximum heights to 2.5 meters (Edgar 1997), however more typically the algal canopy extends 0.5 – 1.5 m above the seafloor. Integration of the bins above these generally resulted in a less distinct separation between the algal and barren reef, presumably as many of the algae do not reach this distance above the seafloor.

Integration of components of the echo return above the sounder detected bottom, corresponding to the region of macroalgae, were shown to be highly effective in the segmentation of algal dominated reef from barren reef. Several commercial acoustic systems have used components of the echo above the sounder detected bottom. These include the QTC View system, which applies a series of algorithms to the first echo return to create a series of 166 echo parameters (Collins 1996, Freitas *et al.* 2003b), and the BioSonics system with its EcoSAV module (Thorne 1998, Sabol *et al.* 2002).

The 166 echo parameters calculated by the QTC View system include parameters on the rise of the first echo, which based on this research would be the parameters most likely to show differences between algal dominated reef and barren reef. However, as the parameters are reduced using PCA as part of the classification process, and are rarely reported upon in the literature, this has not been explicitly shown for this system. Anderson *et al.* (2002) reported that maximum values in the principal component Q1 and minimum values in the principal component Q2 related to macroalgae on reef, highlighting that within some of 166 echo parameters there is the capacity to differentiate algae. The QTC View system has been reported to have classification accuracies around 60% for seagrass, algae and bare substratum

(Foster *et al.* 2006).

The BioSonics EcoSAV system on the other hand specifically targets the area above the sounder detected bottom. This system has been successfully used to map vegetation height and density from soft sediment substrates (BioSonics 2001, Sabol *et al.* 2002), however has had little published application to the assessment of vegetation or reef. As part of EcoSAV module, specific algorithms have been developed to improve the bottom detection in dense submersed aquatic vegetation (Sabol and Johnston 2001). The quality of the sounder detected bottom was shown to have a strong influence on the capacity of the echo shape method to segment algal dominated reef from barren reef, especially in areas of complex reef.

The sounder detected bottom is an estimation of the strongest echo return, which is generally assumed to come from the seafloor. A back step is often used to account for the spherical shape of the acoustic wave front. However, in certain cases significant portions of the seafloor echo may occur above the sounder detected bottom; this is especially the case where the seafloor is complex or steep (von Szalay and McConnaughey 2002). In these cases, echo return from the seafloor may be included in integration above the sounder detected bottom. The integration of echo return from the seafloor resulted in low segmentation when using the first echo shape parameter above the seafloor, while this was less of an issue when using the echo shape parameters defined by 2 and 3 pulse offsets above the sounder detected bottom.

At the Grants Point site the algorithm initially used to define the sounder detected bottom performed poorly in the steep and complex reef, resulting in large amounts of seafloor echo return being included in the calculation of the echo shape parameters, which reduced the classification success of this method. The slope of the reef at the Grants Point site was generally greater than the slope of the reef at the Lords Bluff site, and as shown in Chapter 2 slope can affect the acoustic return from the seabed. Even in this case where the target of the acoustic integration was above the seafloor, the methods had to be refined to account for the steeply sloping substrate. Improving the fit of the sounder detected bottom to the data using a revised bottom detection method resulted in increased classification success.

Algal cover was shown to decrease with depth on the east coast of Tasmania. There was a gradual decrease from 95% to 75% between 0 m and 30 m depth, with a rapid decrease to less than 50% cover below 35 m depth. The echo shape method showed no depth bias for the 0 – 30 m depth range tested at the Grants Point site. From the literature, the majority of urchin barrens on the east coast of Tasmania occur between 10 and 25 m depth (Jordan *et al.* 2005a), however barren have been recorded down to 35 m depth (Johnson *et al.* 2004). Clearly the

deep edge of some barrens extends below the area of dense algal growth, which will have some implications for the acoustic detection of this edge. However in the current study there appeared to be no depth related effect on the classification accuracy of the echo shape technique.

The echo shape technique developed in this chapter was able to segment barren reef from algal dominated reef where there were dense stands of large macroalgae. However it is not uncommon for turfing algae or encrusting invertebrates to dominate temperate reefs within some areas of Tasmania (Edgar 1984, Lucieer *et al.* 2009). Many of these turfing algae and encrusting invertebrates are low growing and will not provide an acoustic target sufficiently high in the water column for the echo shape approach to detect. The currently documented range for the sea urchin *Centrostephanus rodgersii* occurs predominantly down the east coast of Tasmania, where the large macroalgae are the dominant species in the 0 – 30 m depth range (Johnson *et al.* 2004, Jordan *et al.* 2005a, Lucieer *et al.* 2009). Another possible source of error when using the echo shape technique is the possibility of fish schools being incorrectly detected as algae.

Fish with swim bladders provide strong acoustic targets (MacLennan and Simmonds 1992). Within Tasmania fish such as the butterfly perch, *Caesioperca lepidoptera,* commonly form dense schools over reef habitats (Edgar 1997). Schools of this species show up strongly on the echo sounder trace. Generally schools of this species occur high enough off the seabed that they will not be detected using the echo shape technique. However there is the possibility that these or other fish may be misclassified as algae. This highlights the need for ancillary data, such as video, to confirm acoustic classifications and reduce the risk of errors in the final classification.

The use of SBES for the mapping of urchin barrens presents advantages over many existing techniques. Towed underwater video is a common tool for assessment of subtidal habitats (Norris *et al.* 1997, Barker *et al.* 1999). While towed video can be very useful for the identification of dominant biota and underlying substrate, it is not a practical tool for the systematic surveying of large geographic extents for the purpose of mapping. The acoustic system employed in this study could operate at speeds up to 6 times faster than the video system. Further, video has a large overhead in terms of post processing, with analysis of video being a labour intensive and time-consuming task. Due to these limitations, underwater video is more commonly used to support other mapping systems such as acoustics, providing highly detailed information on species and structure to aid in the interpretation of the acoustic data.

Alternatively satellite based optical remote sensing (Landsat TM and SPOT HRV) has been used to map the distribution of kelp from kelp free reef (Simms and Dubois 2001). These optical techniques were limited to a maximum depth of 6-7 meters. The attenuation of light in water is much greater than that of sound. This limit can be decreased by factors such as increased turbidity and sun glint (Mount 2005). Urchin barrens have been recorded to depths of 35 m in Tasmania, with the inner margin on exposed coasts between 5 and 10 m depth (Johnson *et al.* 2004, Jordan *et al.* 2005a). Hence the application of optical remote sensing is not appropriate for mapping these features.

There are limitations associated with the use of acoustic methods for urchin barren mapping. SBES data need to be interpolated to produce continuous coverage maps which are generally the desired result of mapping as they are easier to interpret than a string of classified points. Generally inverse distance weighting (IDW) and Kriging have been suggested as the most appropriate techniques for interpolation of SBES data (Guan *et al.* 1999, Valley *et al.* 2005). Regardless of the interpolation technique used, the final detail and accuracy of any interpolated map will still be reliant on the distribution and density of the base data. For SBES surveys this can be increased in one of two ways; along track through increased ping rates and, more importantly, through an increased number of parallel transects. Given that the average size of barrens on the east coast was calculated to be just less than 80 m wide, transect spacing required to capture this level of patchiness would need to be less than 80 m. This has important ramifications for sampling efficiency, as smaller transect spacing will lead to an increased cost to sample the same area due to the additional field time required.

4.5. Conclusion

The methods develop in this chapter were able to provide consistent segmentation of algal dominated reef from barren reef, which is at the modifier level of the hierarchical classification system. The ability to use SBES to map at this level of the classification hierarchy opens the way to produce detailed spatial representations of biologically relevant habitats in a relatively quick and cost effective manner when compared to diver surveys or towed video. There types of maps have relevance to biological conservation, fisheries assessments and ecological modelling.

Baseline information on the extent and distribution of urchin barrens is important for both their long term monitoring, and to gain a better understanding of the mechanisms involved in their establishment and growth. The use of acoustic systems to survey the extent of barren and algal dominated habitat provides a tool for the rapid assessment urchin barren distribution at a

broad scale. The acoustic segmentation techniques developed in this chapter will allow barrens to be identified in a consistent and quantitative manner, providing a baseline of algae/barren distribution for comparison over time.

Chapter 5. Acoustic Detection of Macrocystis

5.1. Introduction

Temperate reef ecosystems of southern Australia support a diverse range of macroalgal species, dominated by kelps (order Laminariales) and fucoid algae (order Fucales). Variability in algal abundance and composition on reefs are influenced by physical factors including depth and relief, level of exposure, siltation, light and hydrographic conditions, and biological factors such as sea urchin grazing and availability of algal recruits (Kennelly 1995). Kelp assemblages play an important role in ecosystem function, adding to primary production and habitat complexity (Steneck *et al.* 2002).

Species of *Macrocystis* are one of the key habitat forming kelps on temperate reefs along the west coasts of North and South America and at scattered locations in the southern hemisphere including South Africa, southern Australia, New Zealand and several subantarctic islands (Steneck *et al.* 2002). In southern Australian waters, two species of *Macrocystis* occur. *M. pyrifera* occurs along the east and south coasts of Tasmania, while *M. angustifolia* is limited to northern parts of Tasmania and parts of the Victorian and South Australian coasts (Edgar *et al.* 1997). The species are commonly known as giant string kelp as they can reach up to 45 m in length and grow down to 30 m depth (Steneck *et al.* 2002, Edwards 2004). Both species often appear as a distinct surface canopy.

Throughout much of its distribution *Macrocystis* exhibits seasonal variations in growth. At high latitudes growth is limited by light availability during winter (Hurd *et al.* 2004), while at low latitudes growth is limited by high water temperature and reduced nutrients during summer (Brown *et al.* 1997). The Tasmanian kelp exhibits a similar growth pattern, with maximum growth in the winter months when cold, nutrient rich, sub-Antarctic water dominate the coast, followed by dieback in the summer months when the warmer, nutrient poor East Australian Current (EAC) waters dominate (Edyvane 2003). There are also large interannual variations in the growth of this species (Steneck *et al.* 2002), particularly off the Californian coast where variability has been related to El Nino-Southern Oscillation (ENSO) and Pacific Decadal Oscillation (Kinlan 2003). Most fluctuations in kelp abundance are in response to changes in environmental conditions, either increased water temperature and/or decreased nutrients (Tegner and Dayton 1987, Grove *et al.* 2002, Steneck *et al.* 2002). Losses can also result from catastrophic storm events (Simms and Dubois 2001) and increased turbidity (North *et al.* 1993). Similar fluctuations in *Macrocystis* abundance are known to occur in Tasmania, with losses attributed to the increased dominance of warm nutrient-poor

EAC waters associated with ENSO events (Edyvane 2003). The ecological consequences of such fluctuations can result in changes in community structure, with implications including a decrease in commercial fish stocks and an increase in urchin barrens (Tegner *et al.* 2001, Kinlan 2003).

Aerial photography and satellite remote sensing have commonly been used to monitor kelp distribution and estimate standing crop (Jensen *et al.* 1980, Deysher 1993, Simms and Dubois 2001). These systems use optical sensors, either colour, infrared or multispectral to image the kelp, all of which are limited by light attenuation in water, restricting their detection ability to the surface or the first few metres of the water column. Satellite remote sensing has been used to differentiate kelp down to 7 metres of water (Simms and Dubois 2001), although more commonly aerial photography is used to map only the surface canopy of kelp beds (North *et al.* 1993). Such measures of surface canopy have been used as an estimate of giant kelp biovolume or biomass (North *et al.* 1993) and these estimates are usually the basis for assessing temporal variations in kelp abundance.

As aerial remote sensing techniques do not effectively identify the sub-surface component of the giant kelp bed, many estimates of biovolume may underestimate kelp abundance. For example, large-scale dieback of giant kelp occurred along sections of the Baja Californian Coast during the El Nino of 1997-1998. However in deep water (25 - 40 m) off the coast of northern Baja California the giant kelp was largely unaffected during this warming event due to local hydrographic conditions, but was not detectable with traditional remote sensing methods (Ladah and Zertuche-González 2004).

Estimates of giant kelp abundance from aerial photography can also be influenced by seasonal variability in canopy abundance, storms, tides and currents. Estimates of maximum kelp bed area from a series of surveys have been used to reduce this variability (North *et al.* 1993). However this can be a costly exercise and often resources are only available for a single survey.

An alternative remote sensing technique to estimate subtidal floral abundance involves the use of underwater acoustics, with early research focussed on the detection and measurement of plant height, and biovolume or biomass for species of aquatic macrophytes (Duarte 1987, Thomas *et al.* 1990).

Macrocystis has a large number of gas filled floats (pneumatocysts) along the length of its main axis. These floats are typically 1-2 cm in diameter and there can be 20 to 30 floats on an average size plant (Zimmerman and Robertson 1985). These floats act as air water interfaces

of high acoustic impedance resulting in high acoustic energy backscattered to an acoustic system (MacLennan and Simmonds 1992). This suggests that *Macrocystis* is an ideal species to be detected using active acoustic techniques.

Underwater video is an alternative technique that may be used to detect submerged aquatic vegetation (Norris *et al.* 1997). The use of video allows direct identification of plant species. As video is an optical tool, it is limited by light attenuation in the water column.

As with Chapter 4, this chapter focuses on the Modifier level of the hierarchical classification. However, unlike Chapter 4, this chapter attempts to develop methods to assess the distribution of a single species of algae. This study investigates the capacity of single beam acoustics and underwater video to determine the distribution and extent of sub-surface *Macrocystis pyrifera*. These estimates of the sub-surface canopy are compared to estimates of the surface canopy derived from aerial photography to examine the potential error inherent in reliance on only the latter method for kelp mapping and monitoring.

5.2. Methods

5.2.1. Study Site

George III reef is located in southeast Tasmania at approximately 43^{o}30’ S, 146^{o}59’ E (Figure 5.1). The reef is surrounded by sand and covers an area of approximately 44 ha. It extends from 2 m at its shallowest point to 24 m on its outer margin. The reef is dominated by macroalgae, namely *Durvillaea potatotorum*, *Phyllospora comosa*, *Ecklonia radiata*, *Caulerpa* sp, mixed reds and coralline algae. The reef is partially sheltered from the predominantly south-westerly swell by the mainland of Tasmania and the nearby Actaeon Islands. However, it still has a low to medium wave exposure (Barrett *et al.* 2001). This reef was known to have dense stands of *Macrocystis* with both surface and sub-surface plants from previous surveys (Barrett *et al.* 2001).

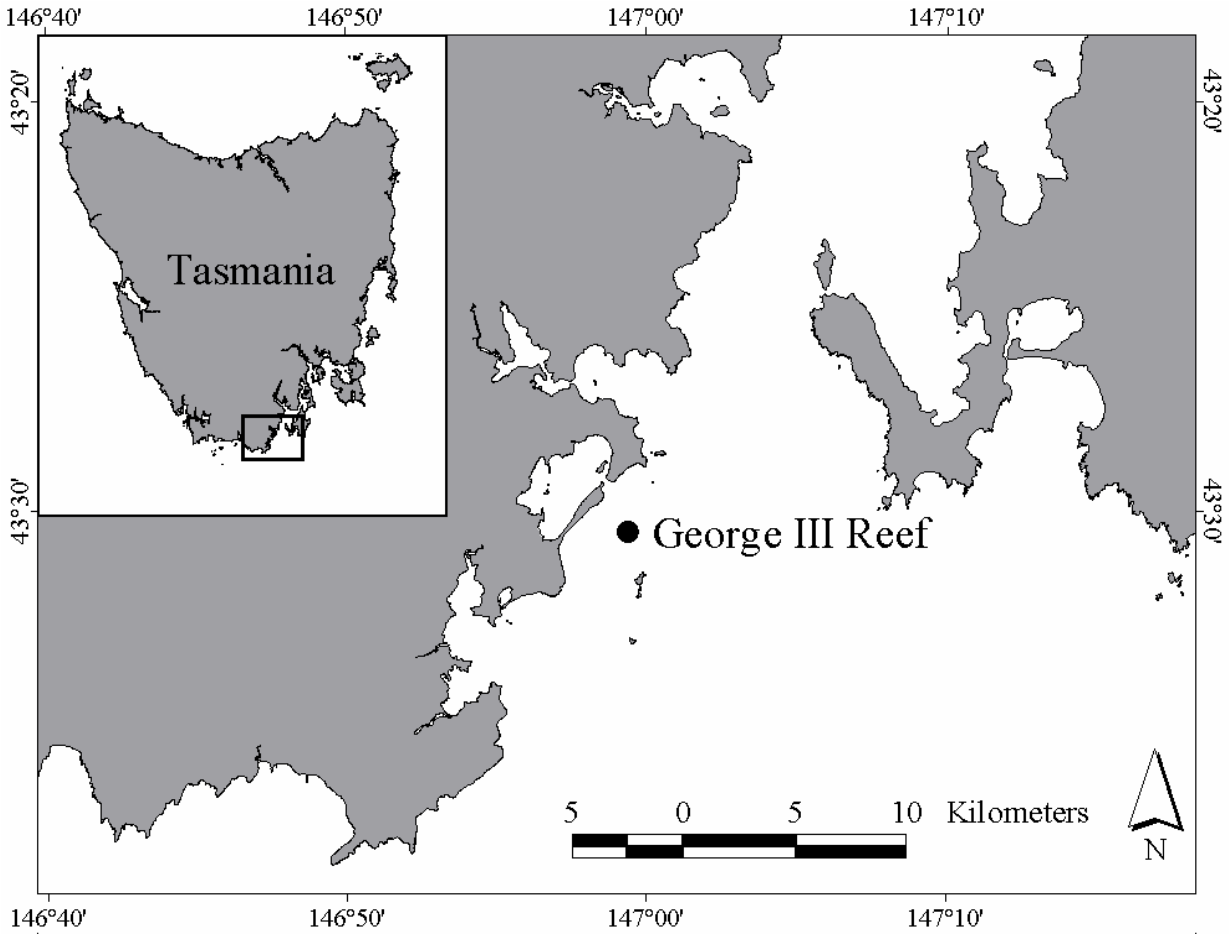

Figure 5.1. Location of George III Reef study site in southern Tasmania.

5.2.2. Definitions

This study uses a series of metrics that were calculated from the aerial photography and the raw acoustic data to describe parameters of the surveyed kelp bed. These are defined below (Table 5.1).

Table 5.1. Definitions of metrics calculated from the aerial photography and acoustic data used to describe kelp bed parameters. (See section 5.2.3.2 for a detailed explanation of how these metrics were calculated).

Measure	Method	Definition
Canopy Area	Aerial Photography	The numerical extent of individual plants and canopies (square meters).
Bed Area	Aerial Photography	The geographical extent of surface kelp within its own perimeter (square meters).
Relative Density Index (RDI)	Aerial Photography	The ratio of Canopy Area to Bed Area
Basal Bed Area	Acoustics	The geographical extent of kelp (surface and sub-surface) within its own perimeter (square meters).
Canopy Depth	Acoustics	The depth of kelp plants below the sea surface (meters)
Kelp Density Index (KDI)	Acoustics	The density of kelp plants within the Basal Bed Area as a ratio of detected to non-detected.

5.2.3. Methods: Aerial Photography

5.2.3.1. Field

An aerial photographic survey of the study site was conducted on the 26th November 2004. A Cessna 172 was fitted with a vertically mounted Canon 300D digital camera (Canon, Australia). This camera was fitted with a standard EF-S 18-55mm lens. The focal length was set to 24 mm for the photographic run. The size of the captured images was set to 3072 x 2048 pixels, which, at the flying height of 2286 m, resulted in a ground resolution of 0.704 m x 0.702 m per pixel. The photographic run was conducted between 8 am and 10 am when the sun angle was between 20º and 30º, to reduce the effect of sun glint in the images.

A vessel was simultaneously mapping the kelp distribution from the water. This vessel deployed four large marker buoys around the perimeter of the reef to act as ground control points. The position of these buoys was measured using differential GPS. These buoys were all greater than 1 m diameter and bright pink, ensuring that they would be detected in the aerial photography at the given flying height and pixel resolution of the camera. These buoys were used to georeference the aerial photographs using the methods described by (Finkbeiner *et al.* 2001).

5.2.3.2. Analysis

A single image with little sun glint and good contrast was selected from the digital aerial photographs taken in the aerial survey. The image was rectified using ArcGIS 8.0 (ESRI, Ca, USA), using the position of the four marker buoys and the vessel at the time the image was taken. A first order affine transformation was used to rectify the image. The residual error on control points was 5.06 m (RMS).

This image was visually classified into regions containing kelp and those without by onscreen digitising in ArcView. Polygons were drawn around groups of pixels visually interpreted to be kelp based on colour, shape, and contrast. The smallest polygon digitised using this technique was 10 pixels (approximately 6 m^2). This technique was subjective, relying on the operator to consistently define boundaries around surface kelp where the boundaries were often not crisp. The need for a quantitative and repeatable technique of image segmentation led to the investigation of the colour bands and band ratios.

A white mask was placed over non-target areas of the image using Adobe Photoshop 5.0 (Adobe Systems Inc., USA). This new image was then imported into ArcView 3.2a (ESRI, Ca, USA) with the original world file. The masked image was converted to a grid, with each colour band (red, green and blue) converted to a grid of the same cell size (pixel size) and

value (RGB pixel value, 0-255). A user-defined threshold was separately applied to each of these grids to maximise the correlation with the visually classified polygons. Band 2, the green band, had the best correlation with the visually classified polygons, the other two bands had no optimal threshold. Band ratios were also investigated, with the Band 3 / Band 2 ratio providing the best correlation with the visually classified polygons, however this provided no improvement over the threshold of the green band.

From the threshold grid data several measures were computed. The first was canopy area, defined as the numerical extent (m^2) of individual plants and canopies, calculated as the sum of the area of pixels identified as kelp from the aerial photograph. The next measure was bed area (planimetric area), defined as the geographical extent of surface kelp within its own perimeter. To calculate this measure, a boundary was drawn around the outer perimeter of all identified kelp plants and canopies; plants and canopies were linked if they were within 50 m of each other. This provided a measure of the total surface area that the kelp was influencing. For the bed area measure, a relative density index (RDI) was also calculated. This was a measure of the ratio of the canopy area to the bed area:

$$RDI=\text{canopy area/bed area}$$

This gives the proportion of the bed area that is actually occupied by kelp plants. The measure will be 1 when there is 100% cover.

5.2.4. Methods: Video and Acoustics

5.2.4.1. Field

Acoustic field surveys of the *Macrocystis* bed were conducted simultaneously with aerial photographic surveys. A combination of normal incidence SBES and vertical underwater video was used to survey the kelp bed. The surveys were conducted on a high tide.

The SBES system was the same as that described for Chapter 2. A 120 kHz, 10º single beam Simrad ES60 echo sounder (Kongsberg Maritime, Norway) was pole mounted to the side of a 6 m vessel. The transducer face was approximately 0.5 m below the surface, with a vertical orientation. The echo sounder was set with a power output of 100 W, a pulse length of 0.256 ms, and a sample rate of 2 pings per second. The system was calibrated using a standard 38.1 mm tungsten carbide sphere using standard methods (Foote *et al.* 1987).

Parallel transects separated by approximately 50 – 100 m were driven at 2 ms^{-1} across the study site (Figure 5.2). An Omnilite132 differential GPS (Fugro Spatial) linked into ArcPad 6.0 (ESRI, Ca, USA) was used for navigation around the study site. The raw acoustic data

was logged and post processed in Echoview 3.30 acoustic software (SonarData, Hobart, Australia).

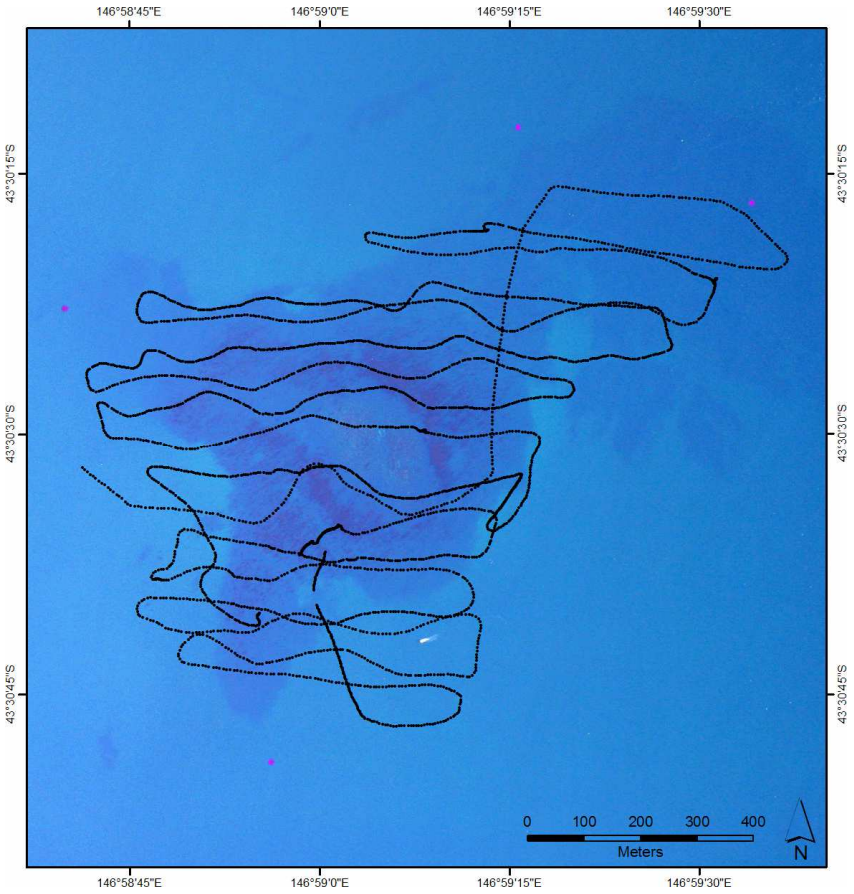

Figure 5.2. Acoustic transects across George III reef overlayed on aerial photograph

A downward looking sub-surface video camera (MorphVision, NSW, Australia) was attached to the acoustic transducer (approximately 0.5 m below the surface). The camera recorded a visual record of *Macrocystis* plants as they passed below the transducer face. The video was stamped with time, date and DGPS position using a genlock video overlay device (VinGenII). This footage was recorded to miniDV tape for further analysis.

5.2.4.2. Analysis

The underwater video footage was reviewed in the laboratory for the presence/absence of kelp and the approximate number of kelp plants. The footage was converted to digital format (AVI) using a DVRaptor firewire capture card (Canopus Inc. USA). A still image was captured off the video every second and labelled with a sequential number using the program Video2photo (PixelChain). This corresponded to a video sample point every 1.9 m ± 0.4 m along the track log. The video frames were scored for presence/absence of *Macrocystis* and the number of plants (1 for one plant, 2 for two plants and 3 for three or more plants). When kelp fronds obscured the camera's field of view, the video frame was scored as unknown and excluded

from any subsequent analysis. All data was entered into an excel spreadsheet containing the track log details. In all, 7853 images were reviewed for kelp parameters, of which 2262 had visible kelp.

5.2.4.3. Acoustic processing

The calibrated ES60 acoustic data were corrected for triangle wave (Section 2.2.2) and imported into Echoview 3.30 for post processing.

Ringdown in the echogram masked the kelp signal close to the transducer. The ringdown region of the echogram filled approximately the top 1.5 meters of the echogram. The constancy of this region was used separate return from kelp and the background ringdown. The raw Sv values for each ping were exported, and a moving average was calculated for each of the top 40 samples across a window 500 pings. Pings where the kelp reached the ringdown were excluded from this calculation. This averaged ringdown was then subtracted from the initial echogram, to create a new echogram (Figure 5.3).

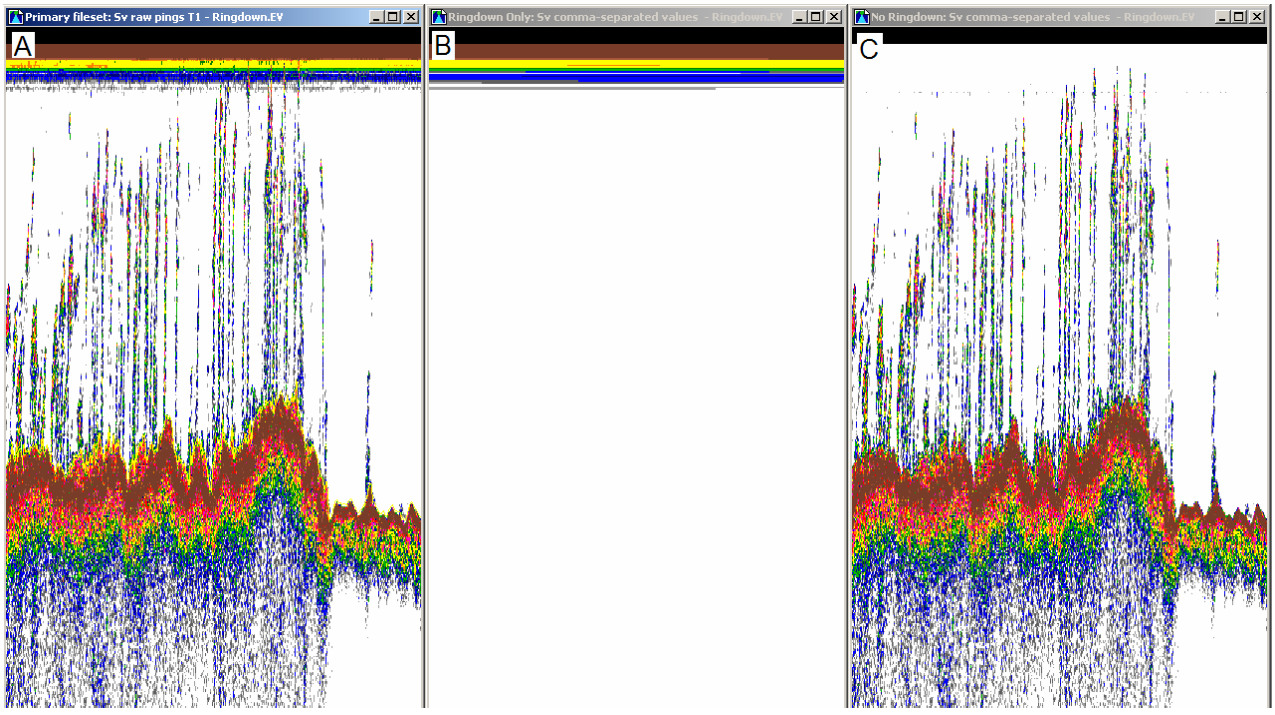

Figure 5.3. Stepwise removal of ringdown to reveal signal (A) original echogram (B) ringdown averaged across upper most 40 samples for 500 sequential pings with areas of kelp excluded (C) ringdown subtracted from original echogram

5.2.4.4. Echogram segmentation

Segmentation of the echogram into kelp and non-kelp regions was examined using a number of different techniques.

5.2.4.5. Visual Interpretation

Macrocystis appears visually on the raw echogram as a series of vertical lines running through the water column from the bottom echo towards the surface (Figure 5.4).

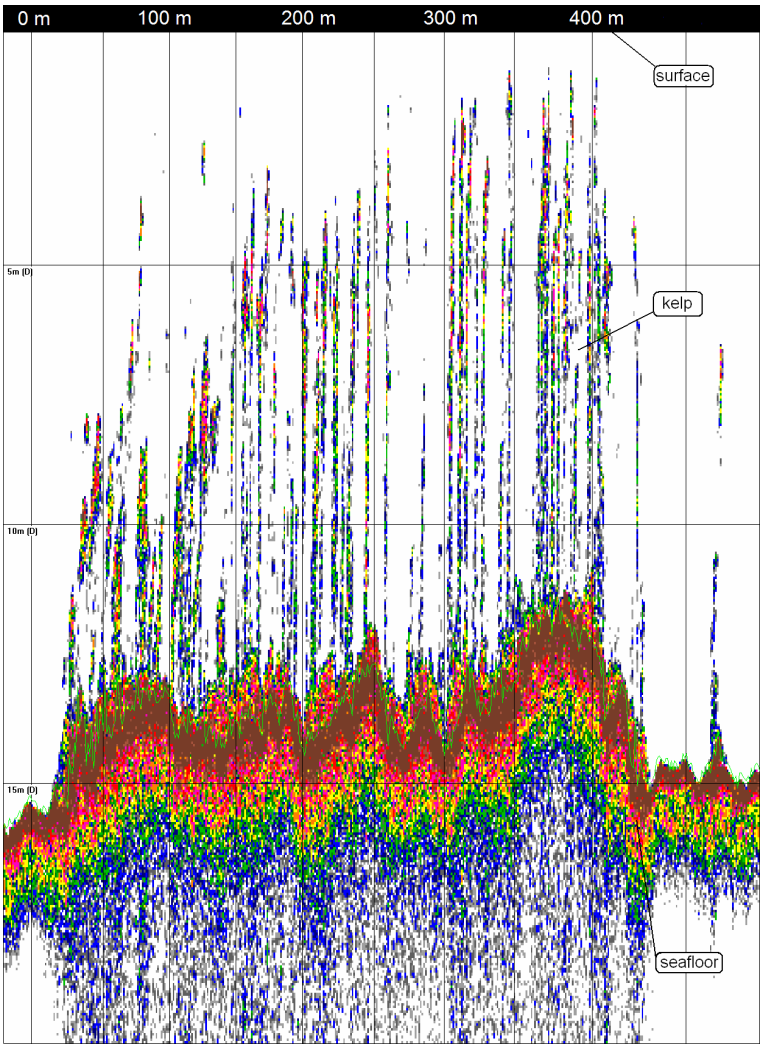

Figure 5.4. Acoustic echogram from Simrad ES60 running at 120 kHz, showing *Macrocystis pyrifera* plants (kelp) as distinct vertical lines in the water column above the bottom echo return.

The presence of kelp was determined visually from the echogram in the software package Echoview 3.30. Kelp was deemed present where linear structures with a height greater than 2 m were visible in the water column above the –60 dB threshold. A user defined line was drawn across the top of these structures and linked where plants were closer than 10m.

Where no plants were present this line was not defined, resulting in no depth being attributed where kelp was not present. This visual interpretation line was exported to an excel spreadsheet for subsequent comparison with the automatically detected canopy.

5.2.4.6. Schools Detect

The schools detect technique used the schools detect algorithm of Echoview 3.30 to identify areas of kelp and then the line pick function to trace across the top of these identified kelp areas.

The schools detect algorithm is based on the shoal analysis and patch estimation system (SHAPES) (Barange 1994, Coetzee 2000). The following sequential steps segment the echogram into target and non-target regions, in this case kelp from non-kelp: A matrix is overlayed across the data; a threshold is then applied to this matrix to remove unwanted noise. Cells that meet this threshold are then joined, taking into account a continuity factor. Schools that are smaller than a pre-determined size as imputed by the user are discarded.

The matrix used in this study was a 1 ping by 1 sample grid, with a -60 dB threshold applied. Regions were recorded if they exceeded this threshold over a minimum height of 2 m and a minimum length (horizontal) of 1 m. Regions were linked if they were within 5 m vertically of each other and if they were within 10 m horizontally of each other, resulting in a number of regions covering the areas of echogram that met these criteria. Each of the regions was visually examined to confirm that it corresponded to kelp based on appearance, bottom depth, attachment to the seafloor, and underlying substrate.

The regions were converted to a boolean true or false using the region bitmap command. These regions were used to mask a 1 dB echogram (from the data generator) to create an echogram of the regions with 1 dB value. The line pick algorithm (max dB with backstep) was used to draw a line across the top of these regions, representing the upper limit of kelp detection with these settings. This line was exported to a text file using the export line command.

Schools detected from the SBES data were assumed to be kelp, with visual inspection of the schools used to confirm the classification, and exclude any detected schools that did not appear to be kelp. To examine whether this school validation could be automated, 20 days of acoustic data covering reef and sand substrates between 0 and 40 m depth were analysed using the schools detect methods as outlined above. This data was collected using the same acoustic system outlined above. A total of 206 schools were detected that could be visually classified as either kelp or fish. The kelp class was assigned to schools that visually corresponded to kelp in the echogram and were coincident with areas identified as kelp from either aerial photography or underwater video transects. The fish class was assigned to schools that did not visually correspond to kelp in the echogram and had been identified as

being fish (or definitely not kelp), by either multiple acoustic transects crossing the same area and not detecting the same school, or video transects being conducted either identifying fish schools or identifying that kelp wasn't present. Thus the fish class while likely to be fish in most instances may contain additional non-kelp acoustic targets. For each of these schools the underlying substrate (reef or sand), bottom depth and attachment to substrate were scored. These data were examined for consistent trends between kelp and fish schools.

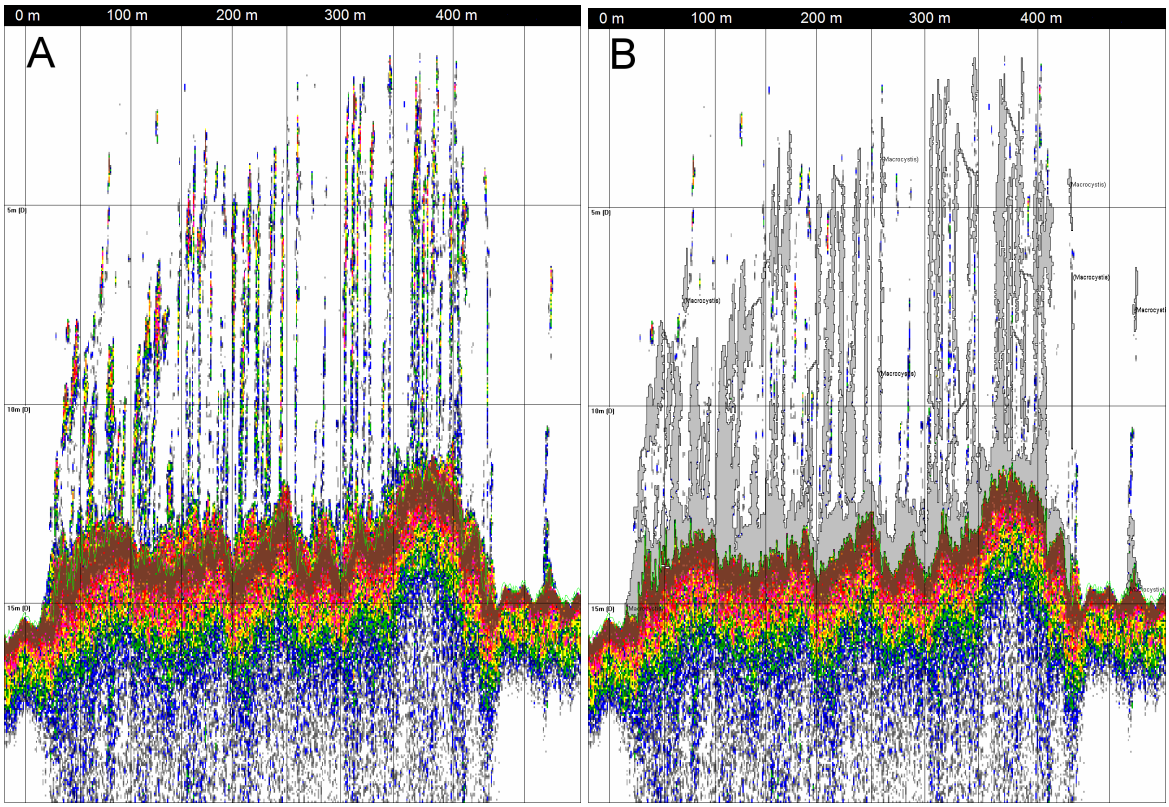

Figure 5.5. (A) Sample echogram showing kelp as vertical bands in the water column and (B) the resulting regions (shaded grey) calculated from the schools detect algorithm.

5.2.4.7. Echo Integration

The Simrad ES60 echo sounder outputs S_v data (volume backscattering strength). The S_v data is calculated from the return energy measured at the transducer based on the following formula;

$$S_v(R, P_r) = P_r + 20\log R + 2\alpha R - 10\log(\frac{P_t G_0^2 \lambda^2 c \tau \psi}{32\pi^2}) - 10\log(F_{Sv})$$

Where:

R the corrected range (m)

P_r is the received power (dB re 1 W)

P_t is transmitted power (W)

α is the absorption coefficient (dB/m)

G_0 is the transducer peak gain

λ is the wavelength (m)

c is the speed of sound (m/s)

τ is the transmit pulse duration (s)

ψ is the Equivalent Two-way beam angle (Steradians)

FS_v is a filter correction as defined by Simrad

Echo integration is the calculation of the mean S_v over a defined volume, and is commonly used for estimating the abundance of fish in mid-water fish schools (MacLennan and Simmonds 1992). Echo integration operates by calculating the accumulated energy returning to the transducer across a time gate (t1 to t2), which corresponds to a target range (ct1/2 and ct2/2) (MacLennan and Simmonds 1992). In this study echo integration was calculated for a target range defined by the top of the echogram and 1 m above the seafloor (to remove the influence of the seafloor). This integration was run over a single ping grid and the resulting S_v values were classed as either kelp or non-kelp based on a user-defined threshold (-60dB), which corresponded to the display threshold used for the visual echo interpretation.

5.2.4.8. Echo Shape

The presence of kelp in the water column will affect the shape of the returning echo for each ping. The echo shape can be calculated in Echoview by integration of regions of the water column between the top of the echogram and 1 m above the sounder detected bottom. Due to the changing depths, between 2 and 25 m within the study site, shape as a proportion of total depth was chosen as the most representative measure. Integration regions were defined between lines based on the percentage of the depth at 10% intervals. This resulted in a series of 10 Sv values that described the echo shape between the bottom of the ringdown and 1 m above the sounder detected bottom.

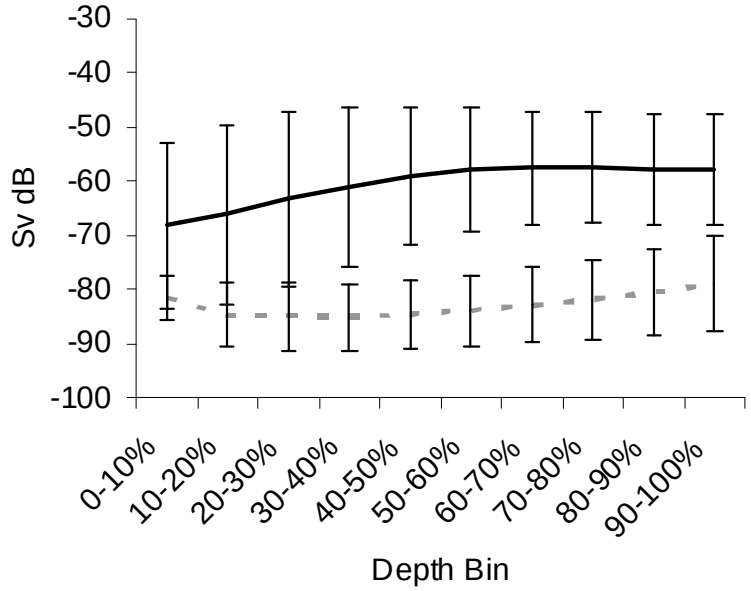

Figure 5.6. Comparison of the average echo shape for points classified as kelp (solid black line) versus points classified as no kelp (dotted grey line). Error bars give the standard deviation for each of the classes.

The 10 echo shape parameters were separated into two classes using the *k*-means clustering algorithm in the statistical software, JMP 5.1 (SAS Institute, USA). The *k*-means approach to clustering performs an iterative alternating fitting process to form the number of specified clusters. The *k*-means method first selects a set of *n* points called cluster seeds as a first guess of the means of the clusters. Each observation is assigned to the nearest seed to form a set of temporary clusters. The seeds are then replaced by the cluster means, the points are reassigned, and the process continues until no further changes occur in the clusters. These classes were then attributed as kelp or no kelp based on comparison with the classified video data. The average shape of these two classes showed considerable deviation, especially in the depth below the 30-40% bin (Figure 5.6).

5.2.4.9. Comparison with aerial photography

The classified data from the video and acoustic systems was not able to be compared 1 to 1 with pixels in the aerial photograph due to the cumulative effect of positional error in collecting both the acoustic data and rectifying the aerial photograph. Instead the interpolated basal bed area derived from each system was compared. Similar to the aerial photographic the basal bed area was derived by joining data points that were within 50 m of each other in a GIS platform. The basal bed area was then calculated in the GIS for comparison between the different methods.

5.3. Results

5.3.1. Aerial Photography

The aerial photographic survey identified a large area of surface kelp covering much of George III Reef. The surface kelp was visible in the image as darker patches on the surface and formed a ring around the shallowest central part of the reef. Two areas of dense canopy to the northeast and southwest were identified, with numerous smaller canopies and plants joining and surrounding these two dense canopies to form this ring (Figure 5.7).

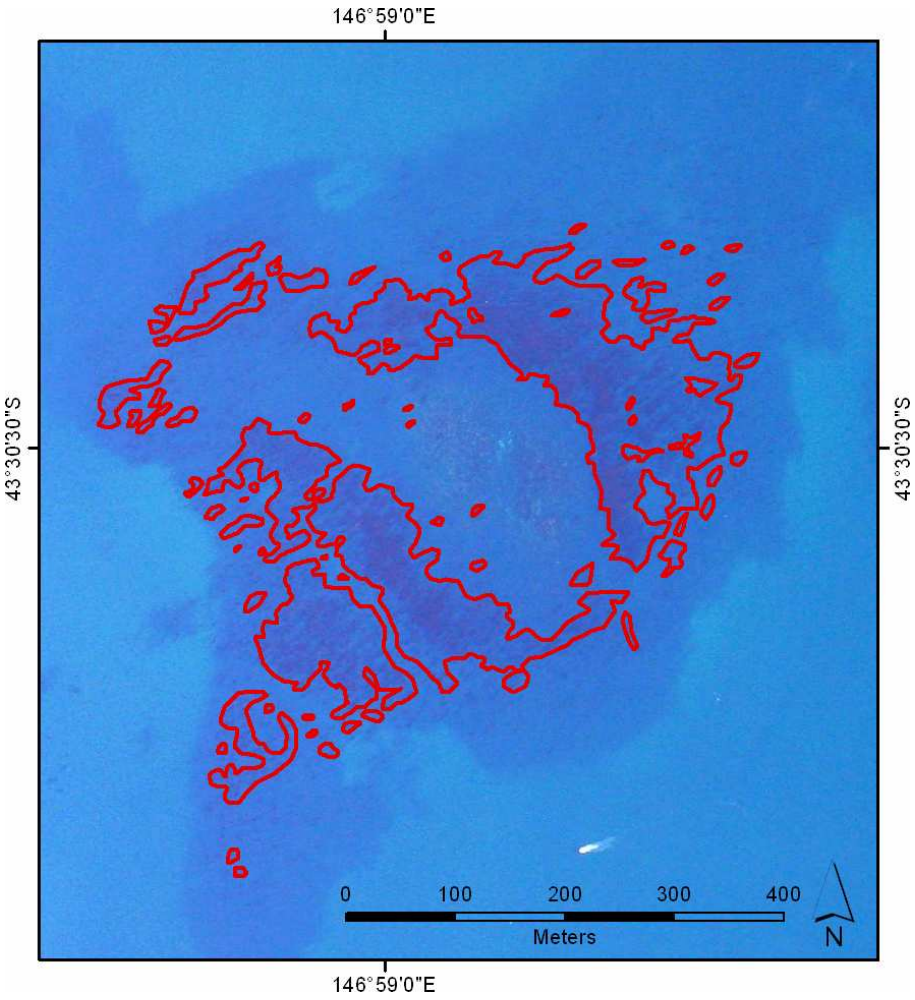

Figure 5.7. Aerial Photograph of George III Reef showing ring of *Macrocystis pyrifera* outlined in red.

A visual classification of the image was undertaken. A skilled operator digitised areas of the image, containing surface kelp, based on the colour and contrast of the pixels. Visual classification relies on subjective judgements by the operator, which are open to errors of omission and commission. Repeatable techniques for the segmentation of the image were investigated.

Segmentation of pixels corresponding to surface kelp in the image was achieved by splitting the image into separate colour bands (red, green and blue). A user determined threshold was

applied to each band with a view to achieving the best correlation with the user defined visual classification. The red and the blue bands had no optimal thresholds, with high error of commission (Table 5.2). The green band, with a threshold set between 80-112, showed good correlation with the visual classification (Figure 5.8, Table 5.2). Band ratios were also examined, with the ratio of band 3 divided by band 2 resulting in the best correlation with the visual classification (Figure 5.8, Table 5.2). The green band and the band 3/2 ratio both had high errors of omission (24 – 28%). These errors of omission probably reflect errors of commission in the visual classification process due to the inability of a human operator to digitise below the scale of groups of pixels; resulting in fine scale structuring being lost and causing a general overestimate in the area of kelp identified using this technique. The green band was chosen due to its lower error of commission (Table 5.2).

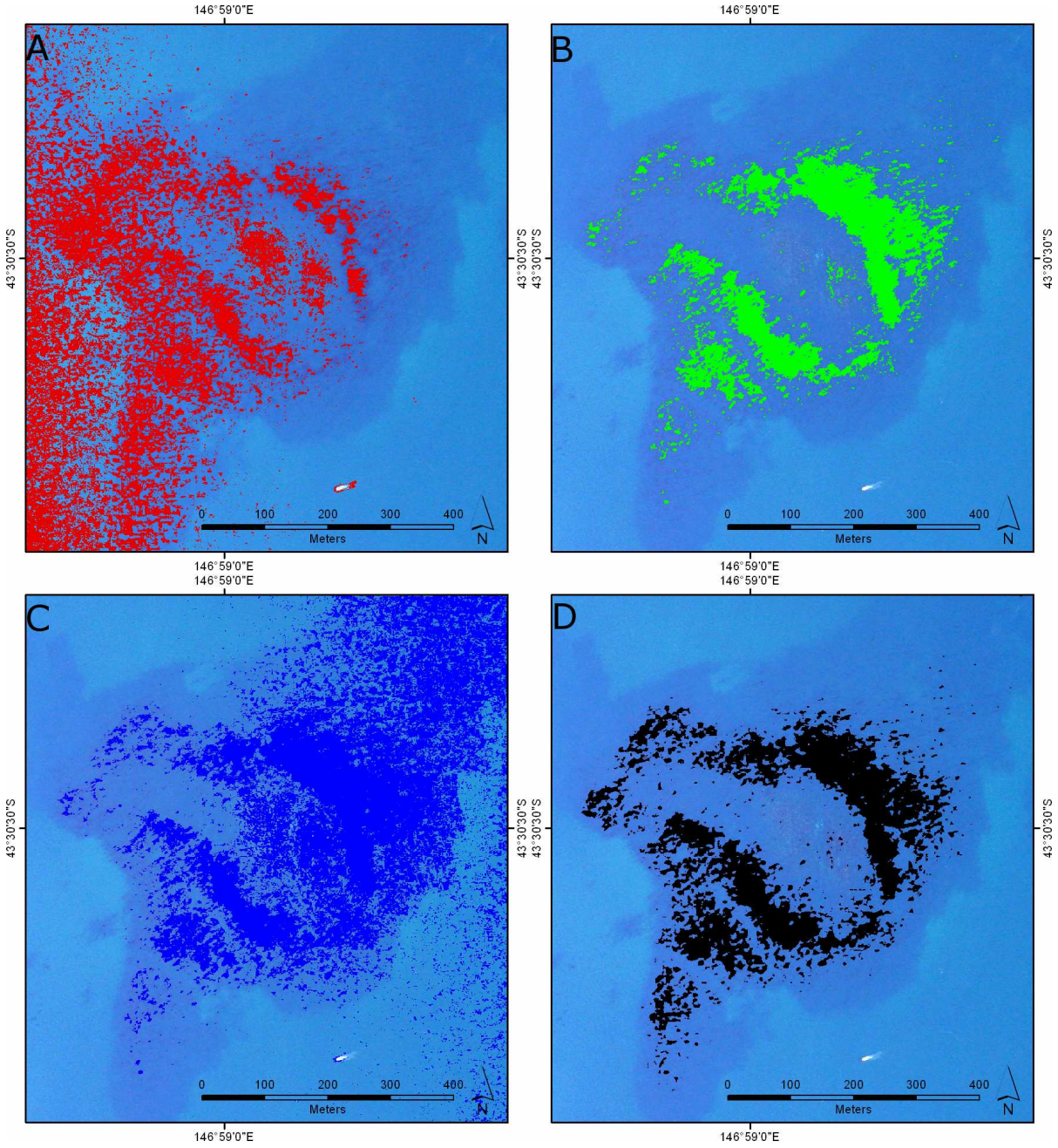

Figure 5.8. Kelp detection in the red, green and blue bands. The following thresholds were applied, red 65-90; green 80-110; and blue 150-215. The black indicates the band 3 /2 ratio in the range 1.89 to 2.41.

Table 5.2. Comparison of the performance of kelp segmentation for an aerial photograph of George III reef, using visual, band threshold and band ratio techniques.

	Total Area detected (ha)	Comparison with Visual (%)	Errors of Commission (%)	Errors of Omission (%)
Visual	8.3	100	0	0
Band 1 (red)	16.2	43.4	152.0	56.7
Band 2 (green)	6.4	72.4	4.8	27.7
Band 3 (blue)	18.3	78.8	141.9	21.3
Band Ratio(3/2)	7.8	75.7	18.6	24.4

Both the green band and the band ration (3/2) compared well with the visual classification, with over 72% classification accuracy. The green band had lower error of commission, and

was thus chosen for comparison with the acoustic data. From the green band data, statistics on the canopy area, kelp bed area and relative density index (RDI) were calculated. The canopy area was found to be 6.4 ha. The kelp bed area, calculated as the water surface area occupied by this kelp, was defined by drawing a polygon around all plants. This was done at various joining scales of 30 m, 50 m and 70 m. The subsequent areas were 11.8, 13.4, and 14.2 ha respectively. (Figure 5.9). The corresponding RDI of 0.54, 0.48 and 0.45.

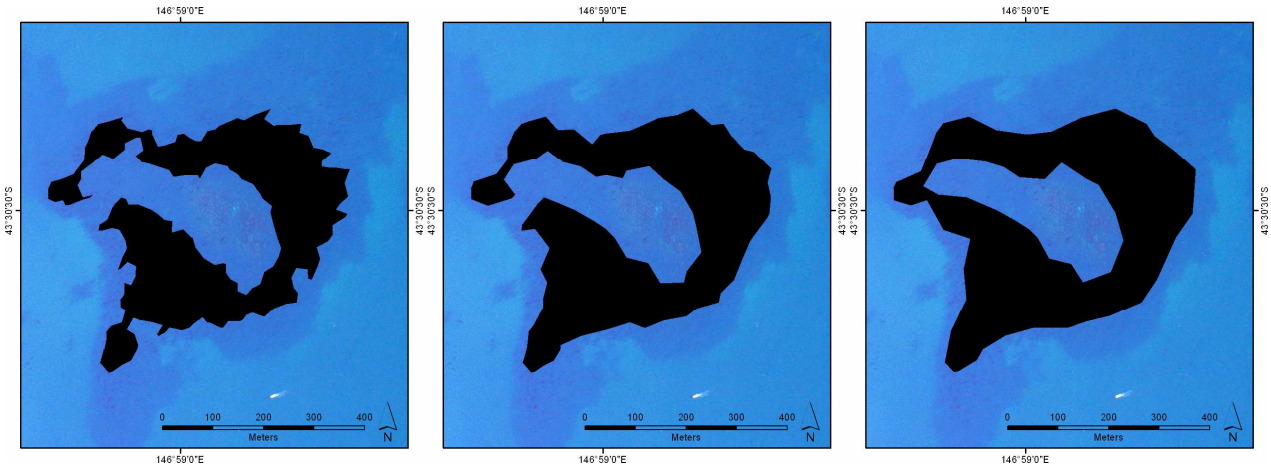

Figure 5.9. Kelp bed area base on (A) 30 m, (B) 50 m and (C) 70 m joining distances from green for George III Reef.

5.3.2. Video and Acoustics

Visual interpretation of the acoustic echogram is the simplest form of segmentation. This is a subjective technique that relies on a skilled operator to pick kelp from non-kelp based on visual differences in the echogram. A comparison of the classified underwater video and the visual interpretation of the acoustic echogram showed that the acoustic system detected more kelp than the video system. A total of 3128 GPS points were attributed as having kelp present by either one or both of the video and/or acoustic systems. Of these, 27.7% were attributed using the acoustics but not the video, while 3.5% were attributed using the video but not the acoustics. The remaining 68.8% were attributed using both techniques.

5.3.2.1. Automated detection of kelp from acoustics

A need for more repeatable techniques for segmentation of the acoustic echogram into kelp and non-kelp regions led to the investigation of a number of automated segmentation techniques. Three automated segmentation techniques were examined: Schools detect, echo integration and echo shape. The performance of these was compared against the underwater video and the visual interpretation of the acoustics (Table 5.3). The visual interpretation and the schools detect techniques attributed more points as kelp than the other techniques; this was especially the case in depths greater than 10 meters, where the kelp frequently did not

reach the surface (Table 5.3). It should be noted that the performance of the video system decreased with depth, such that only six points were attributed as kelp in greater than 15 m depth using this system, compared with 90 - 212 for the acoustic system (Table 5.3).

Table 5.3. Comparison of the number of points attributed as kelp in 5 meter depth bins for the video and acoustic systems.

	0-5 m	5-10 m	10-15 m	15-20 m	Total
Video	70	1916	2532	6	4524
Visual Interpretation	67	1991	3811	166	6035
Schools Detect	73	2061	3955	212	6301
Integration	78	1738	3115	161	5092
Echo Shape	58	1883	3289	91	5321

The overall performance of the acoustic segmentation techniques compared to the video ranged from 83 to 96% correlation in kelp detection, with the schools detect technique having the strongest correlation (Table 5.4). When divided into five meter depth bins, the visual interpretation and the schools detect techniques had the strongest correlation in all depth ranges. The integration and the echo shape techniques had poor correlation in less than five meters and greater than 15 meters, with 50% or less agreement between these techniques and the video classification (Table 5.4). The values for depths greater than 15 meters are based on comparison with only six points attributed as kelp from the video. Due to this low number of points, these values are likely to be less reflective of the overall accuracy.

Table 5.4. Comparison of the percentage agreement between the video classification and the four acoustic segmentation techniques across 5 meter depth bins and total agreement across all depth ranges.

	0-5 m	5-10 m	10-15 m	15-20 m	Total
Visual Interpretation	70%	95%	96%	100%	95%
Schools Detect	76%	97%	97%	67%	96%
Integration	43%	91%	89%	50%	89%
Echo Shape	43%	86%	82%	33%	83%

The distribution of the points identified as kelp using each of these techniques (video and acoustics) showed similar spatial trends (Figure 5.10). The major differences were for the echo integration and echo shape techniques, which in some of the deeper areas attributed kelp in locations that were not attributed using the other techniques. The echo integration and the echo shape techniques also attributed more kelp points in the shallower water than the other acoustic techniques.

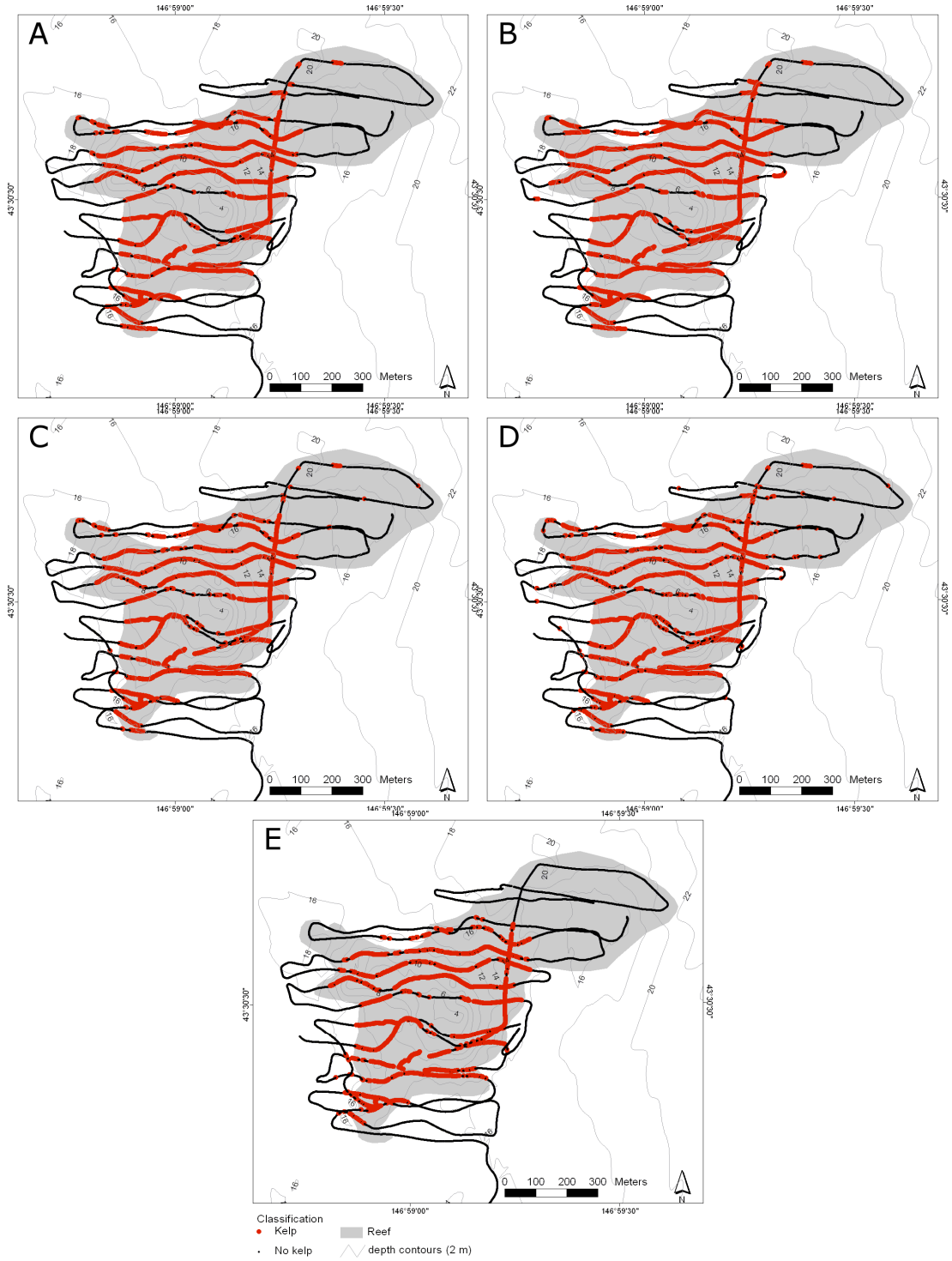

Figure 5.10. Segmentation results of acoustic data based on (A) visual segmentation, (B) Schools Detect, (C) Echo Shape, (D) Integration and (E) Video. Black crosses indicate where kelp was identified in the echogram using each of the techniques (or the corresponding video frames for the underwater video (E)).

The schools detect method resulted in a number of regions identified within the echogram data that were visually identified as kelp. Analysis of 206 regions detected by this method in the 0 – 40 m depth range over reef and sand habitat identified several consistent differences between schools containing kelp and schools containing fish. At the substrate level, 100% of all kelp regions detected were above reef substrate, compared to 65.7% of fish school regions

detected above reef substrate, with the remainder above sand substrate. Of the regions detected above reef substrate 99.3% of all kelp were attached to the substrate, where as only 34.1% of fish schools were attached to the substrate. Finally, there was a separation of fish and kelp regions by bottom depth, with fish schools occurring deeper than kelp regions (Figure 5.11). Based on the above parameters, kelp regions could be automatically segmented from fish regions based on attachment to a reef substrate with less than 20 m depth. This accounted for 99.3% of all kelp schools, with only 6% of fish schools fitting these criteria.

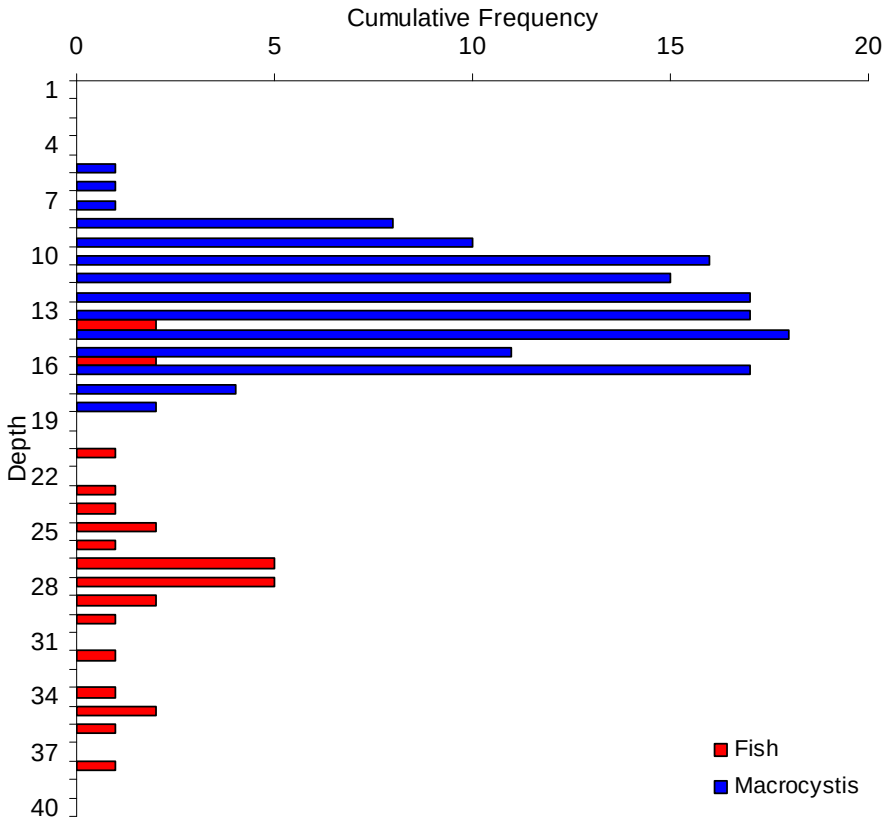

Figure 5.11. Frequency histogram of bottom depth for fish and kelp regions detected using the schools detect method.

5.3.2.2. Comparison of Video, Acoustics and Aerial Photography

Due to the potential for positional error in the order of ± 1 m for the differential GPS (RMS 0.9) and a further ± 5 m in the rectification of the aerial photograph (RMS 5.1). A direct acoustic point to photo pixel comparison was not appropriate. Instead comparison of bed-wise statistics is made to compare the three techniques.

The kelp distribution point data from the video and acoustics (schools detect technique) were used to interpolate maps of the basal bed area for the kelp. The computed area of the kelp bed based on the acoustic system was 18% more than for the video system, (28.8 ha compared to 23.5 ha) (Table 5.5). The basal bed area derived from both these systems was greater than that

derived from the aerial photography (13.4 ha) (Table 5.5 and Figure 5.12.). The kelp density index of the acoustically derived basal bed area was calculated as 0.91. When the density was calculated for the bed area as identified from the aerial photography the KDI was 0.95. This is significantly higher than the RDI of 0.48 when calculated from the aerial photography only. However this includes all the surface and sub-surface plants in the calculation.

Table 5.5. Comparison of calculated basal bed area for the video, acoustic and aerial photography.

Method	Basal Bed Area (ha)
Video	23.5
Acoustics	28.8
Aerial Photography	13.4

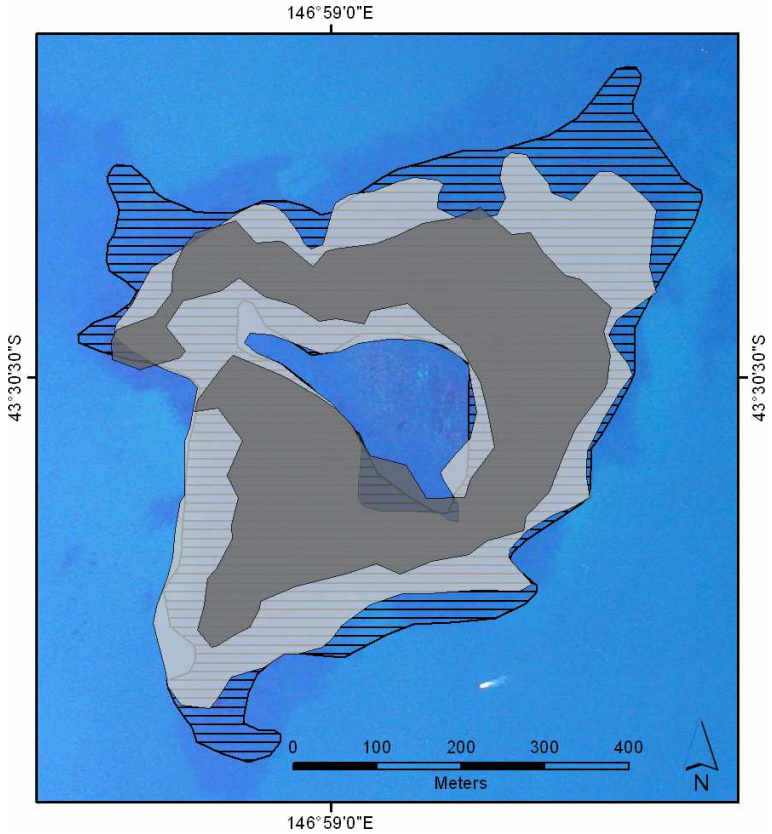

Figure 5.12. Map of George III Reef with basal bed area as derived from aerial photography (black shading), underwater video (grey shading), and single beam acoustics (diagonal lines)

5.3.2.3. Detection of canopy height

The visual interpretation and schools detect techniques for acoustic kelp detection provide measures of canopy height for a given plant or cluster of plants. There was a strong correlation (R2 = 0.84) between the detected canopy heights using these two techniques (Figure 5.13). Where differences existed in estimated plant height, the visual technique tended to estimate lower canopy heights for the kelp than the schools detect technique. Measures of canopy height using these techniques relate to the point where the plants intercept the acoustic

beam. Due to the conical nature of the beam, plants are less likely to intercept the beam closer to the transducer, meaning these may generally be underestimates of plant height.

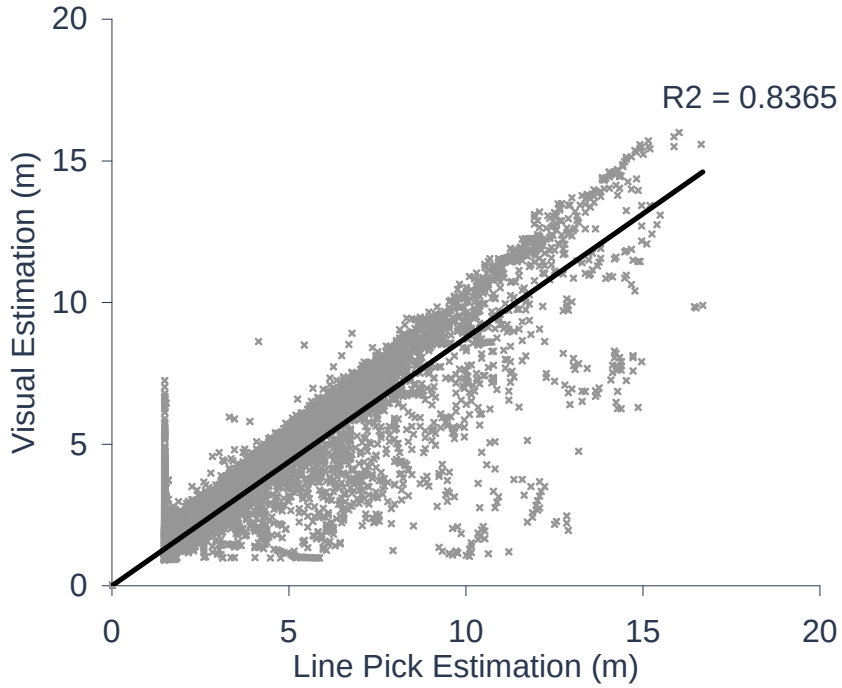

Figure 5.13. Comparison of the visual and line pick estimates of kelp canopy height for George III Reef showing a general agreement between the two techniques in estimating canopy height.

A comparison of the canopy depth for points detected by both video and acoustics with those detected only by acoustics shows that the average depth of the canopy was considerably deeper for the acoustically detected points than for points detected by both the video and the acoustics (Figure 5.14). This highlights the depth limitation of the video system.

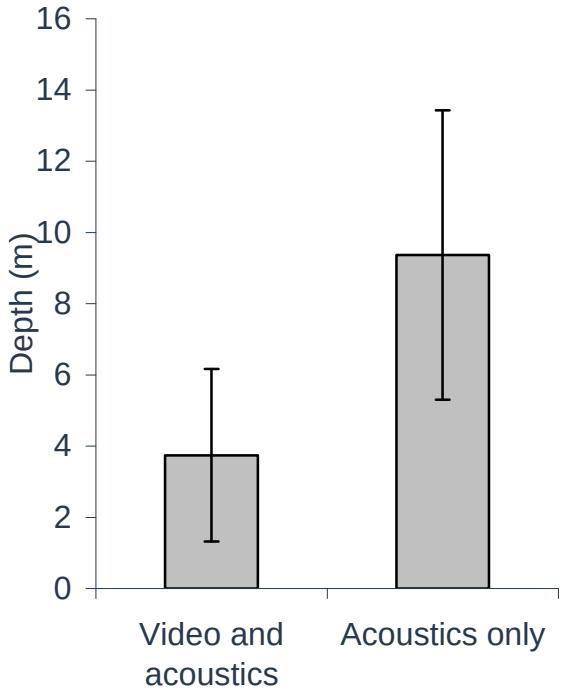

Figure 5.14. Comparison of the average Canopy Depth for kelp points attributed from both the video and acoustics with those attributed from the acoustics only (schools detect technique).

5.4. Discussion

The sub-surface component of *Macrocystis pyrifera* beds contributes to the size and stability of these beds. This study examined the capacity of underwater video and single beam acoustics to be used to detect and map the sub-surface canopy of *Macrocystis* beds, and thus to complement more traditional optical remote sensing techniques. Both the video and the acoustic technologies detected sub-surface kelp that was not visible in aerial photography. The acoustic system performed better than the video system, as it was not limited by the attenuation of light through the water column. The computed basal bed area of kelp derived from acoustics was more than twice that derived from aerial photography.

The underwater video provided positive identification of *Macrocystis* plants that were close to the camera, but identification became more difficult as distance between the plant and the lens increased, until a threshold where light attenuation made it impossible to detect plants from the background. The processing of the video was also time consuming, requiring each frame to be scored for presence/absence of kelp. This scoring was subjective in nature and open to potential operator bias, especially where the distance from the camera to the kelp was large. The underwater video also required a relatively slow boat speed, as the quality of the video decreases with the speed of the boat, with blurred images caused by high boat speed and slow shutter speed.

Underwater video has been used in the past to map submersed aquatic vegetation (Norris *et al.* 1997). However in that case towed video was used to map seagrass, which has a relatively consistent growth structure and a size that relates well to the field of view of the camera. The growth habit of *Macrocystis* is not as consistent, with plants ranging from 1 m to 15 m at the study site. This also means that many of the plants are larger than the field of view of the camera. A towed video could not be used, as it would frequently snag on the large kelp plants, making it impractical to efficiently cover large areas of dense kelp.

The acoustic system was not limited by attenuation in this depth range, with a sounder at 120 kHz able to detect the seafloor to a maximum of 800 m (Simrad 2004). Where present, *Macrocystis* appeared in the echogram as distinct vertical structures above the seafloor. This study examined four techniques for the segmentation of the echogram into kelp and non-kelp, which all achieved over 80% agreement with classification of the video data.

The visual segmentation was good at detecting plants in all depth ranges when compared to the video. It relied on a skilled operator to make subjective judgements when identifying individual plants or clusters of plants in the echogram. This leads to problems with repeatability.

The schools detect technique closely replicated the visual segmentation technique. Using the schools detect technique removed operator subjectivity. This technique is not uniquely identifying kelp, rather it will segment the echogram into regions that match the input criteria for minimum height and width of targets. The regions created in this process need to be checked to confirm they are kelp. These checks may include the depth (kelp grows to a maximum of 25 – 30 m in Tasmania); the substrate (*Macrocystis* requires a rocky reef substrate), the reef profile (*Macrocystis* generally prefers low profile substrate (Patton *et al.* 1994)), and the shape of the echogram. A comparison of substrate, bottom depth, and attachment to the substrate parameters for regions visually identified as kelp or fish showed these parameters could be used to automate classification of regions with a high degree of accuracy. However, it is unclear if these relationships would always hold true, as several species of fish seasonally school on inshore reefs in Tasmania (Edgar 1997).

Both the visual segmentation and the schools detect techniques provide an estimation of the height of the plants. This height related to the maximum height at which the plant intersected the acoustic beam and not necessarily the maximum height of the plant. Measures of plant height derived from acoustics may be useful in monitoring change in bed growth over time. Further validation of this acoustically measured height is required in order to relate these back

to actual plant heights. This is beyond the scope of this study. The system is limited in that it can only detect kelp below the transducer face and below the ring down. This equates to approximately 1 – 1.5 m (or 0.5 m where the ring down was minimised) with the setup used in this study, thus this system cannot map the surface canopy of the kelp to compare directly with estimates from aerial photography and remote sensing techniques. The geometry of the transducer beam pattern also means the chance of detecting the top of the plant decreases as it nears the transducer. The relationship between these acoustic estimates of plant height and actual plant height needs to be investigated, as this type of information would be valuable in characterising kelp beds.

The echo integration and echo shape techniques tended to misclassify the amount of kelp in shallow water when compared to the video classification. While these two techniques identified similar amounts of kelp to the video interpretation in less than 5 meters (78 and 58 points respectively, compared to 70 points using the video), only 43% of these points were the same as the video, meaning high errors of omission and commission. In contrast, the visual interpretation and schools detect techniques achieved 70% and 76% agreement respectively in this depth zone. The relatively small amount of water between the transducer and the seafloor in less than five meters of water probably resulted in the poor performance of the echo integration and the echo shape techniques. In these depths the unintentional inclusion of small amounts of other algal species (e.g. *Phyllospora comosa* and/or *Durvillaea potatorum*) would have a proportionally greater effect than in deeper water.

Likewise in depths greater than 10 meters the echo integration and echo shape techniques performed worse than the visual interpretation and the schools detect techniques when compared to the video classification. It should be noted here that in deeper water the performance of the video rapidly decreased due to light attenuation. In depths greater than 10 meters the kelp often did not reach the surface, which would affect the classification of kelp based on the echo integration and echo shape techniques.

The major weakness of the echo shape technique was the large depth range and variable plant size of the *Macrocystis*. A proportional approach was taken to divide the water column into 10 equal bins. This approach attempted to correct for depth, such that the shape of a ping in 5 m of water with 100% kelp would be similar to that in 10 m with 100% kelp. However, using this technique the shape of a ping with a 5m plant in 5 m of water would look different from a 5 m plant in 10 m of water. The reverse of using fixed depth bins would allow the shape to be consistent for plant height but different for 100% plants in different depths. Similar issues

have been highlighted in using shape parameters in fish school classification, where many of the descriptors used do not work well across large ranges of school sizes (Reid *et al.* 2000).

The echo integration technique had similar problems with the shallow and deep water kelp segmentation. This technique provided a rapid technique for quickly identifying potential kelp, and could be used to detect regions of the echogram that may contain kelp for closer examination with one of the first two techniques. Echo integration techniques are commonly used for acoustic detection of fish species (MacLennan and Simmonds 1992), however in previous studies, they have been shown to not reliably predict the biovolume of submersed aquatic vegetation in previous studies (Sabol *et al.* 2002). This was attributed to the wide range of species, densities, heights, and conditions within the sample set (Sabol *et al.* 2002). The current study had a wide range of depths (3 - 25 m), plant heights (3 - 14 m) and potentially fish species in addition to the kelp, which may have confounded the echo integration.

Transducer ring down presented a final difficulty with the segmentation of the echogram. The top 1.5 m of the echogram contained ring down above the display threshold. Kelp could be discerned from this background noise, and could have been included using the visual segmentation technique, however for the automated techniques the ring down had to be masked out. A technique to minimise the ringdown and leave the kelp signal was shown to reveal kelp to within 0.5 m of the transducer face.

A working model for the segmentation of the echogram into kelp and non-kelp would include the following steps: 1) Correct the raw echogram for transducer ring down, mask pings in the echogram where the bottom is deeper than the maximum growing depth of the kelp. 2) Run a preliminary echo integration to detect potential areas of kelp. 3) Run the schools detect over areas identified as potential kelp from this echo integration. 4) Visually check the identified schools to ensure that they appear kelp like in the echogram and are over reef substrate.

All the acoustic techniques investigated assume that the kelp is the only acoustic reflecting object in the water column. Several groups of schooling fish species can commonly occur both within kelp forests and in the open water (Edgar 1997), and other species of algae occur closer to the bottom and may be attributed incorrectly as *Macrocystis pyrifera* when using these simple acoustic techniques. In this study the downward looking camera did not detect any schools of fish, and the characteristic trace of the kelp and fish schools look different when visually inspected. Areas of doubt can be flagged or excluded from any analysis.

Acoustic detection of giant string kelp can provide valuable information about the sub-surface component of kelp beds that may otherwise not be detected in aerial photographic surveys. Aerial photographic techniques are only able to detect kelp that exhibits a surface or near surface canopy (North *et al.* 1993, Simms and Dubois 2001). The acoustic techniques used in this study were could be used to detect kelp with a sub-surface canopy. The extra penetration of the acoustic system led to over twice the area of kelp being detected with this system compared to the aerial photograph. This has important implications when using remote sensing techniques to monitor the distribution of kelp beds over time.

The limitation of optical systems is primarily related to the attenuation of light through the water column. Airborne optical systems have been used to map seagrass beds in up to 15 - 20 m of water (Pasquilini *et al.* 1998), and depths of up to 6 - 7 m have been achieved for mapping kelp using satellite remote sensing (Simms and Dubois 2001). This difference probably reflects difference in contrast, with seagrass having a higher contrast to its background (sand), than kelp does to its background (reef/other algae).

Aerial photographic surveys generally only map the surface canopy of the kelp beds (North *et al.* 1993), and commonly use infrared photography, which is limited to a few millimetres penetration into the water column (Jensen *et al.* 1980). This lack of penetration into the water column means that aerial photography and satellite-based remote sensing techniques have the potential to miss significant amounts of kelp, and possible entire beds if they have no surface canopy. Deep beds that do not have surface canopies have been shown to provide important refuge for kelp during both warming and storm events (Ladah and Zertuche-González 2004).

The results of aerial photographic surveys, which detect only the surface kelp, can also be affected by the environmental conditions at the time of the survey. The area of surface kelp canopies are affected by seasonal changes, storms, tides and currents (North *et al.* 1993). This means that aerial photographic surveys can potentially produce different results for the same bed over a relatively short time frame if environmental conditions are different between the two surveys. Past studies have used the maximum kelp bed area from a series of several photographic runs in a single year to account for this (North *et al.* 1993). However, this is not always practical due to the cost of aerial photographic runs.

The acoustic approaches investigated in this study are less affected by environmental conditions than aerial photographic techniques. These systems are also less affected by attenuation through the water column than optical systems. Depending on the operating frequency used, acoustic systems can reliably penetrate from hundreds of meters to several

kilometres. The acoustic techniques examined here detected kelp canopy that was several meters below the surface and not detectable in the aerial photography. The use of this information to estimate the Basal Bed Area would provide a more stable estimate of the area of kelp than the Surface Bed Area estimates from aerial photographic surveys. Hence, this measure may be more useful when investigating seasonal and long term changes in kelp distribution and abundance.

However, there are several disadvantages to the use of acoustics over aerial photography for base line kelp mapping. The coverage of the acoustic system is low compared to aerial photography (Kenny *et al.* 2003). An aerial photographic run can typically cover tens to hundreds of kilometres in a relatively short period of time. The acoustic surveys conducted here only covered an area of approximately one square kilometre in 2 hours. For this reason, the acoustic system does not present itself as an alternative to aerial photography for large scale kelp mapping. The two techniques provide complementary data, one on the broad scale distribution of the kelp canopy (Jensen *et al.* 1980, North *et al.* 1993), and the other on the relationship between the canopy area and the basal area.

Single beam acoustic systems require interpolation between points if complete coverage maps are to be produced (Pinn and Robertson 2003, Valley *et al.* 2005). The number of transects and spacing will often depend on the patchiness and scale at which the kelp needs to be mapped (Pinn and Robertson 2003). In this study an arbitrary transect spacing of 50 m was chosen. This captured the broad distribution patterns of the kelp, but did not capture the fine scale structuring.

The acoustic system is difficult to operate in dense surface kelp, with entanglement of the transducer a commonly encountered problem. It is possible to provide some form of protection to the transducer to help prevent these entanglements (Kvitek *et al.* 1999), however certain areas of kelp canopy can be so dense that they become impassable to a small vessel and thus will not be sampled by the acoustics. Despite these disadvantages the use of single beam acoustics to map sub-surface kelp beds will complement optical remote sensing techniques and lead to more robust estimates of kelp bed areas and change detection.

5.5. Conclusions

The methods developed in this chapter for the segmentation of sub-surface giant kelp distribution from SBES data have demonstrated that for certain species of marine algae it is possible to use acoustic systems to rapidly map distribution. The methods are only applicable to situations where there is a large amount of plant biomass in the water column. These

methods enable mapping at the modifier level of the hierarchical classification system from a SBES system, and were shown to be more effective than both underwater video and aerial photography in this circumstance. Further investigation may lead to biomass/biovolume estimates that can be calculated from SBES data, which will further enhance the usefulness of this tool for kelp bed mapping and assessment.

Chapter 6. Video assessment methods for the analysis of temperate rocky reef algal community structure

6.1. Introduction

Macroalgal assemblages are generally characterised by the dominance of a few large canopy species, in most cases easy to identify "in situ", and the presence of many other understorey species that are more difficult to identify to species level, but with a relatively low percentage of the total algal biomass (Puente and Juanes 2008). These characteristic species are often used as a qualitative descriptor of habitat (Shears *et al.* 2004), and have been shown to be a useful habitat surrogate that represents a component of marine biodiversity (Edgar 1983, Tuya *et al.* 2008). Further, the dominant canopy structure has been shown to be a useful predictor of algal understorey composition and structure (Irving and Connell 2006) and also biodiversity (Bertness *et al.* 1999).

The extent and distribution of algal species is influenced by a range of physical environmental factors including substrate characteristics (Patton *et al.* 1994), depth (Schiel and Foster 1986, Underwood *et al.* 1991), wave exposure (Siddon and Witman 2003, Tuya *et al.* 2008), current flow (Duggins *et al.* 2001), light intensity (Reed and Foster 1984, Brown *et al.* 1997), temperature (Schiel and Foster 1986, Hart and Scheibling 1988, Ladah and Zertuche-González 2004), turbidity (Tegner *et al.* 2001), and nutrient availability (Schiel and Foster 1986, Tegner and Dayton 1991, Tegner *et al.* 2001). These factors operate at different spatial scales, ranging from 100s of kilometres (temperature and nutrients) to 100s of meters (exposure). Often these factors are interlinked, for example wave exposure and light availability decreases with depth. Competition and grazing pressure will also work to control the distribution of an algal species (Breen and Mann 1976, Harold and Reed 1985, Schiel and Foster 1986, Hart and Scheibling 1988, Gagnon *et al.* 2004). A combination of these factors interact to determine algal community structure and will result in distinct algal communities across reef systems, with the composition of algal communities having an important influence on the associated fauna (Choat and Ayling 1987, Shears *et al.* 2004, Preciado and Maldonado 2005, Tuya *et al.* 2008).

Within Australia the structure of algal communities is controlled by a number of factors, with regional differences in whether algal biomass is controlled by top down or bottom up processes (Fowler-Walker and Connell 2002, Connell and Irving 2008). This results in regional patterns in algal cover and patchiness (Connell and Irving 2008). Changes in algal cover can influence both the fish and invertebrate communities (Edgar *et al.* 2004), and

conversely changes in the fish and invertebrate communities can affect the macroalgal cover (Barrett *et al.* 2009). Further local scale changes in exposure will also act to structure the composition rocky reef communities (Edgar 1984). The implication for researchers and managers is that there needs to be both a local understanding of the factors affecting algal community structure and also the capacity to put this into a regional context (Connell and Irving 2008).

Mapping the extent of seabed habitat using acoustic methods generally only identifies substrate type (see Chapter 2, and Chapter 3), and therefore further biodiversity assessment would benefit from the characterisation of macroalgal community composition across reef habitat, especially the habitat forming canopy species. Diver surveys are commonly used to collect information on macroalgal composition; however divers are generally limited by depth and time and thus diver surveys generally have low spatial coverage (Kenyon *et al.* 2006). Towed video presents an alternative technique for the collection of information on macroalgal composition and extent, and is not limited by constraints of depth and time, and is therefore able to provide broader coverage of the seabed. Underwater video generally leads to a loss of taxonomic resolution compared to divers (Kenyon *et al.* 2006), with only the larger dominant species often identified. Loss of taxonomic resolution with video is due to the low resolution of the video, resulting in an inability to examine the specific parts of the algae required to differentiate two or more similar species. However, for the large canopy forming species, which are used to define the specific habitat type, video generally provides sufficient resolution for taxonomic identification (Jordan *et al.* 2005a, Lucieer *et al.* 2009).

Video is generally converted to a series of still images prior to analysis, these still images are low in resolution, with PAL format used in this study with a pixel resolution of 720 x 576 pixels. Several analysis techniques adopted for analysis of underwater imaging data, including point count (Foster *et al.* 1991, Carleton and Done 1995, Kohler and Gill 2006), and percentage cover estimates (Bernhardt and Griffing 2001, Kenyon *et al.* 2006). Point counts may be randomly generated or in a fixed grid, with each point identified to the lowest taxonomic level (Kohler and Gill 2006). The proportion of points for each taxonomic unit is used to calculate community composition and percentage cover statistics (Kohler and Gill 2006). An alternative analysis technique is to estimate the percentage cover of algae directly from the video or captured still images. Percentage cover estimates have been achieved through digitising (Kenyon *et al.* 2006), colour segmentation (Bernhardt and Griffing 2001), and visual estimation (Valentine *et al.* 2004). As the majority of published underwater video

studies have been on coral reef assessment, there is a need to assess video analysis methods for algal community structure studies.

The use of remotely operated cameras to assess the seabed requires accurate positioning of the camera system if data is to be compared to acoustic data or other environmental data. Positional accuracy is important when evaluating the spatial distribution of macroalgae, as algal composition can rapidly change across short distances, especially across depth gradients. Positional accuracy can be achieved through the use of a heavily weighted towfish to maintain camera position directly beneath the vessel for shallow water deployments (Norris *et al.* 1997), or through the use of acoustic positioning systems. Where either of these are not possible, the position of the camera system may be estimated based on the layback, either as a function of tow cable length (Sutton and O'Keeffe 2007), or based as a function of depth (Kenyon *et al.* 2006).

This chapter investigates the capacity for underwater video to be used to collect data on temperate rocky reef macroalgal community structure. The chapter focuses on classification of shallow rocky reef habitats at a level below that achievable using the SBES system from previous chapters (Chapter 2, Chapter 4). The application of video analysis methods is examined in regards to processing time, correlation and taxonomic resolution. The resulting data is compared between three biogeographically separate sections of the Tasmanian coastline defined at a scale of 100's of kilometres (Edgar *et al.* 1997). Finally, the data from one of these biogeographical regions is examined to determine if video sampling methods have the capacity to detect smaller scale spatial differences in algal community structure (at a scale of 10's of kilometres).

6.2. Methods

6.2.1. Underwater video system

An underwater video camera (MorphVision, NSW, Australia) was mounted in a heavily weighted tow fish. The camera had a focal length of 3.7 mm and a CCD size of 3.6 mm x 2.7 mm. The horizontal field of view of this camera was 0.97 m at an object distance of 1 m. The underwater video camera was connected to the surface via an umbilical cable which allowed real-time viewing. The video was recorded to miniDV cassette in PAL format (720 x 576 pixels). Positional information from an Omnilite132 differential GPS (dGPS) was overlayed onto the top of the recorded video images using an overlay device (BlackBox Systems, UK) and also logged to computer as an ASCI text file. Depth information was provided from a Simrad ES60 single beam echo sounder (as described in section 2.2.1), and was logged to

computer with the positional information from the Onmilite132 dGPS (Figure 6.1).

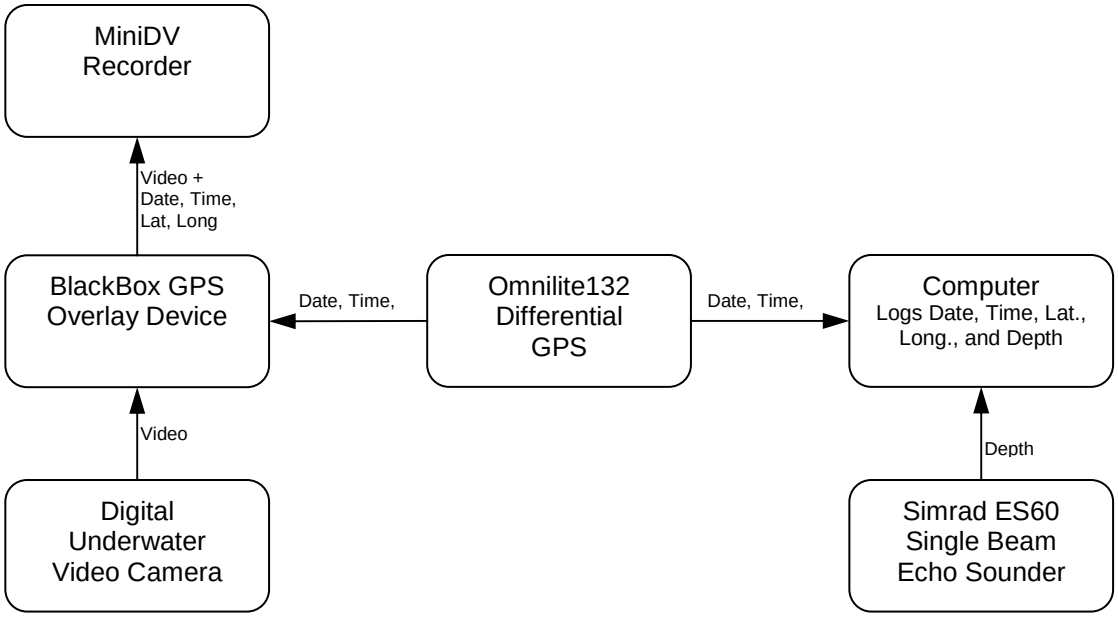

Figure 6.1. Schematic layout of underwater video system showing links with positioning components; arrows indicate the direction of data flow.

6.2.2. Field Deployment

In the field the video system was deployed over the side of a 6.5 m aluminium vessel (*FRV Nubeena II*) using an electric winch. The height of the system was adjusted using the electric winch and monitored both on the echo sounder output and in the video output to maintain it approximately 1m above the seafloor (Figure 6.2). The camera was mounted in the tow fish on an angle of approximately 70 degrees from the horizontal. This created an oblique field of view with the top of the field of view approximately 1.3 times the bottom of the field of view (Figure 6.3). At an object distance of 1 m the area sampled was approximately 1 m^2.

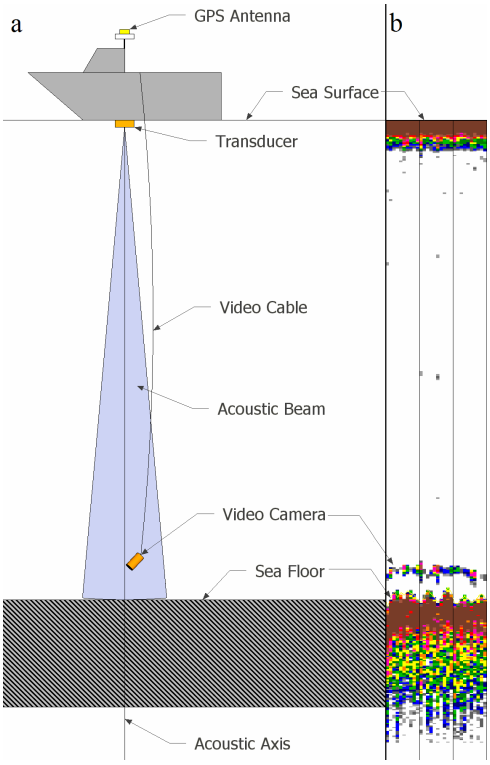

Figure 6.2. (a) Schematic of underwater camera positioning system showing location of the GPS antenna, acoustic transducer and video camera, (b) echo trace from the echo sounder clearly showing the echo return from the underwater camera above the seafloor echo return

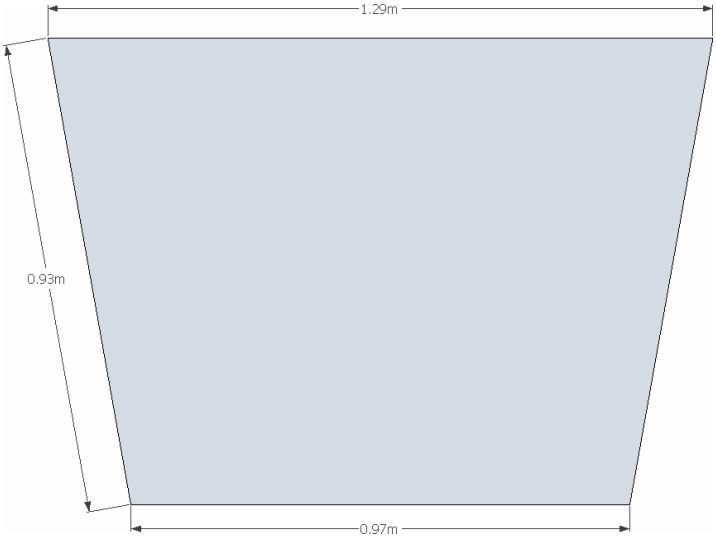

Figure 6.3. Dimensions of the projected field of view for the underwater video camera at 1 m object distance.

The video signal was recorded at the surface using a miniDV recorder. Video transects were generally run across the depth gradient to encompass the depth extent of rocky reef. Video transects were conducted at approximately 1 meter per second. The minimum operating depth was limited by the draft of the vessel. In exceptionally sheltered areas this minimum was approximately 1 m depth although more typically was 3 m depth, and on some exposed coast 5 m depth.

6.2.3. Positional Accuracy

The positional accuracy of the underwater video system was assessed by comparison of the position of reef-sand boundaries identified between the video and the acoustic system (Figure 6.4). The video system was deployed consistent section 6.2.2. The acoustic data was simultaneously logged and acoustic indices calculated (see section 2.2.3). Boundaries were identified by changes in the E1 and E2 indices consistent with the clusters identified in chapter 2 for reef and sand, with these interpretations confirmed by visual observation of the echogram. Only crossings where the reef-sand edge was easily identified in both the video and the acoustic echogram, at a constant depth and with a relatively rapid transition were used in the assessment. From 200 video transects a total of 61 boundary crossings were identified that satisfied these criteria. These ranged in depth from 2 m to 40 m. The difference between the acoustically detected boundary and that detected from the video were calculated in a GIS platform. These were plotted against depth and used to determine the camera system lag distance with depth. While vessel speed will also affect the lag distance, the video surveys were all conducted at a relatively constant speed (90% were within the range of 0.9 ms^{-1}±0.2 ms^{-1}). Only transects conducted at 0.9ms ± 0.2 ms^{-1} were included in the analysis. It should be noted that spherical spreading of the acoustic beam will result in a lessening of the spatial precision of the depth measure with increased depth.

The relationship between depth and layback was used to calculate a correction for layback based on the given depth, and this was then used to calculate the position of the camera based on the vessels logged position using the following procedure. The bearing was calculated for adjacent records within the vessel track log based on Equation 1 (below), a smoothing algorithm was then applied to remove errors due to the effect of vessel motion (pitch and roll). The smoothing algorithm averaged the preceding 10 bearings to calculate a smoothed bearing for a given point. A back bearing was then calculated based on the smoothed bearing (Equation 2). The corrected layback coupled with the back bearing was then used to calculate the corrected position of the video camera in relation to the vessel (Equation 3).

Equation 1

$$Bearing = 360/2\pi(ATAN((x_2 - x_1 + 1\times10^{-10})/(y_2 - y_1 + 1\times10^{-10})))$$

Where $x_{1,2}$ are the two sequential x co-ordinates of the vessel track log (in eastings)

$y_{1,2}$ are the two sequential y co-ordinates of the vessel track log (in northings)

1×10^{-10} is a very small number which prevents both x_2-x_1 and y_2-y_1 from equalling 0.

The calculated bearing is then converted to a back bearing based on Equation 2

Equation 2

$$BackBearing\phi_b = IF(y_2 - y_1 < 0, IF(x_2 - x_1 > 0, Bearing + 360, Bearing), Bearing + 180)$$

The back bearing and the layback correction were then used to calculate the corrected positions for the video (X_c and Y_c) using Equation 3.

Equation 3

$$X_c = \sin\phi_b \times D + X$$
$$Y_c = \cos\phi_b \times D + Y$$

Where ϕ_b is the back bearing

D is the Layback distance

X/Y are the original coordinates (easting and northing)

6.2.4. Single video field assessment methods

Visual analysis of underwater video is inherently a time consuming task. Several techniques were used to analyse the underwater video, and were assessed based on the detail extracted and time taken to complete. These included both qualitative and quantitative approaches. Each approach gave a different level of information about the community structure. The analysis approaches were divided into two categories: frame based and time based. Frame based analysis used frame grabs from the video as the base unit of analysis, analysing these as a series of still images. Time based analysis analyses a set time of video and used these as the base unit of analysis. In all the methods the algae was scored against a standard set of species/taxonomic groups.

6.2.4.1. Frame based analysis

Frames were grabbed off the video using the frame grabbing software Video2Photo (PixelChain). One frame for every 4 seconds of video was exported, which equated to approximately 1 frame every 1 m ± 0.1m of transect. This was the minimum distance that ensured that there was no overlap between subsequent frames. These frames were sequentially numbered and used for analysis.

6.2.4.1.1. Frame based point intercept

A grid with 49 point intercepts was overlayed on each video frame grab using the software analysis package Coral Point Count with Excel (Kohler and Gill 2006). This program allows a fixed or random grid of points to be overlaid on a series of images, with the features under the points identified and recorded to an Excel file. The algae/biota under each intercept was

identified to the lowest taxonomic level. The point intercept data was then used to make estimates of total percentage cover for each of the dominant species or group. Where the algae under a point intercept could not be determined that intercept was scored as unknown. Where frame grabs were of poor quality (due to motion blurring or poor light) they were excluded from the analysis. The time taken to score each frame was measured and used to compute the time taken to analyse 1 hour of video for this method.

6.2.4.1.2. Frame based percentage cover

The same frame grabs used in the point intercept method were analysed using abundance estimates. For each frame the percentage cover of each algal species or group was estimated to the nearest 10%. Where a species was present but, less than 10% cover it was scored a 1%. Where frame grabs were of poor quality (due to motion blurring or poor light) they were excluded from the analysis. The time taken to score each frame was measured and used to compute the time taken to analyse 1 hour of video for this method.

6.2.4.2. Time based analysis

The time based analysis used a period of time as opposed to frames as the base unit of analysis used by the previous two methods (section 6.2.4.1.1 and section 6.2.4.1.2). For this analysis the base unit of time was 4 seconds, which corresponded to approximately 1 m ± 0.1 m of linear distance. The start of the time period was offset by 2 seconds from the still image capture locations, such that the still images analysed in the previous two methods fell in the middle of the time analysis period.

6.2.4.2.1. Time based percentage cover

Each time unit of video was analysed for the dominant algal species/groups. For each algal species/group the cover was estimated to the nearest 10% across the time unit. Where a species was present but was less than 10% it was scored as 1%. The time taken to score each time unit was measured and used to compute the time taken to analyse 1 hour of video for this method.

6.2.4.2.2. Time based presence/absence

The second method of time based analysis examined each time unit for the presence/absence of algal species/algal group. If a species/group was present within a time period it was scored as ‘1’ and if absent it was scored as ‘0’. Algal cover was estimated based on the percentage of time an algae was observed at a given depth range. Again the time taken to score each time unit was measured and used to compute the time taken to analyse 1 hour of video for this method.

6.2.4.3. Comparison of methods

The four analysis methods were compared for consistency in classification and for the time taken to process. Ten transects were processed using each of the four methods. For each method the time taken to analyse 1 hour of video was measured. These times were compared to give a measure of processing overhead. The algal cover data summarized by depth bin for each of these transects was then compared for correlations.

6.2.5. Analysis of algal data

Distribution of algae by depth was assessed for sections of the north, east and south coasts of Tasmania (Figure 6.4). A series of 270 video transects were conducted across reef habitat within these areas between September 2003 and August 2007. The time based percentage cover technique was used due to its increased time efficiency whilst being comparable to the frame based methods. The algae were analysed for the percentage composition across 5 m depth bins for each of the three areas (north coast, east coast, and south coast). Data were summarized at the transect level, to create a table of average cover by species for each transect in each five meter depth range.

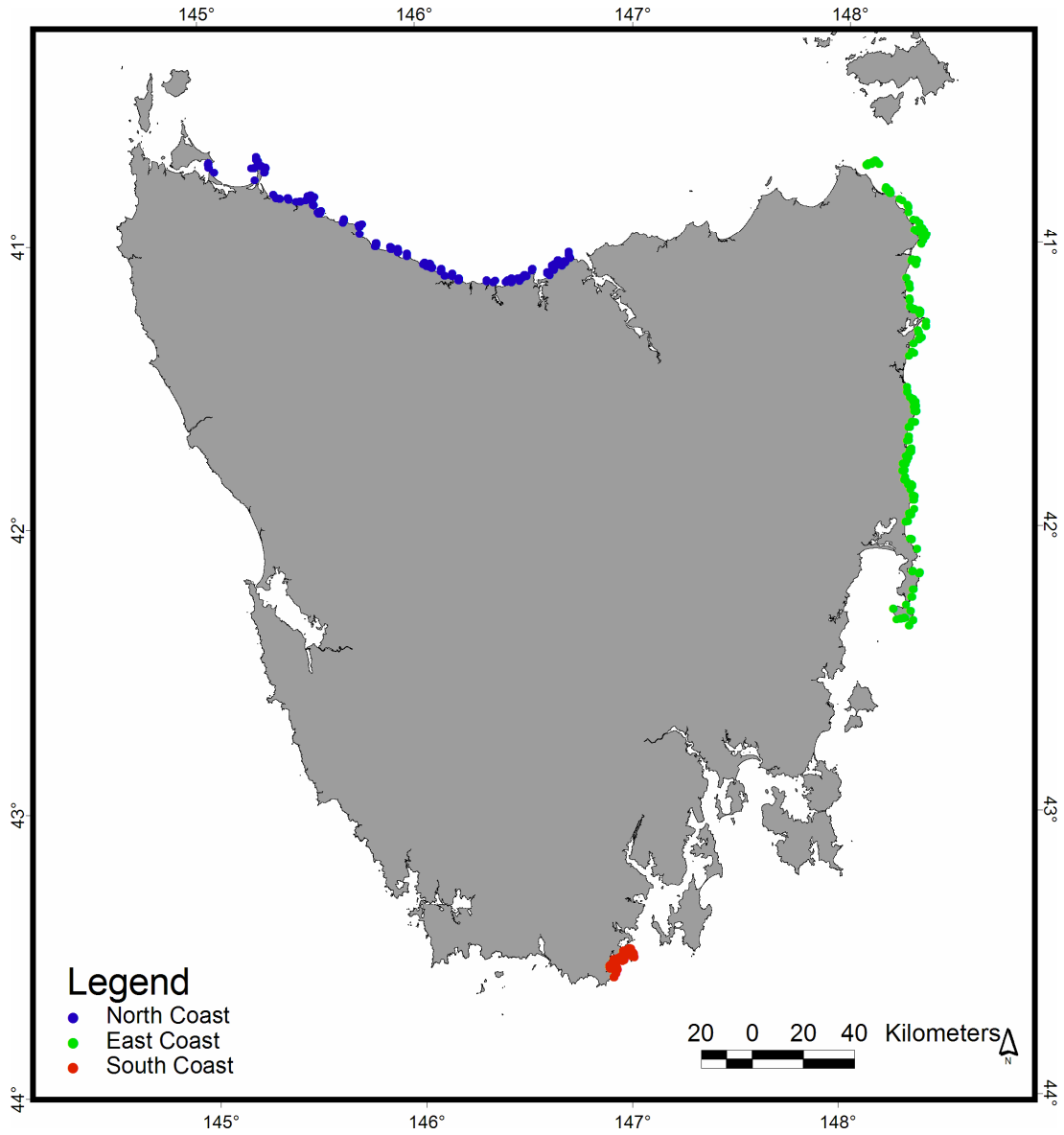

Figure 6.4. Location of video transects around the north (blue), east (green) and south (red) coasts of Tasmania for comparison of algal communities

Bray-Curtis similarities were calculated for each pair of data in the software PRIMER 6 (Prime-E Limited). Multi-Dimensional Scaling (MDS) was used to examine for differences between the three regions and by depth strata based on the similarity data. SIMPER analysis was conducted to examine which species contributed to the differences between the three regions. A two-way crossed design was adopted for the SIMPER analysis PRIMER 6, with region and depth set as the factors. SIMPER analysis uses the Bray-Curtis measure of similarity, to break down the contribution of each species to the observed similarity (or dissimilarity) between samples and allows the identification of species that are most important in creating the observed pattern of similarity.

To test the capacity of video for detection of algal community differences at a scale of 10s of kilometres, data from the east coast were analysed. The east coast was chosen as it contained

a relatively straight coastline with a strong latitudinal gradient, and corresponding exposure and temperature effects. The coastline was divided into five arbitrary sections of approximately 40 km each for the analysis (Figure 6.5). This level of division was chosen as it allowed a high degree of replication within each section, with a minimum of 20 video transects per section. As for the regional analysis, SIMPER analysis was used to examine for similarities and differences in the species cover by section. Again, a two-way crossed design was used with section and depth as the factors.

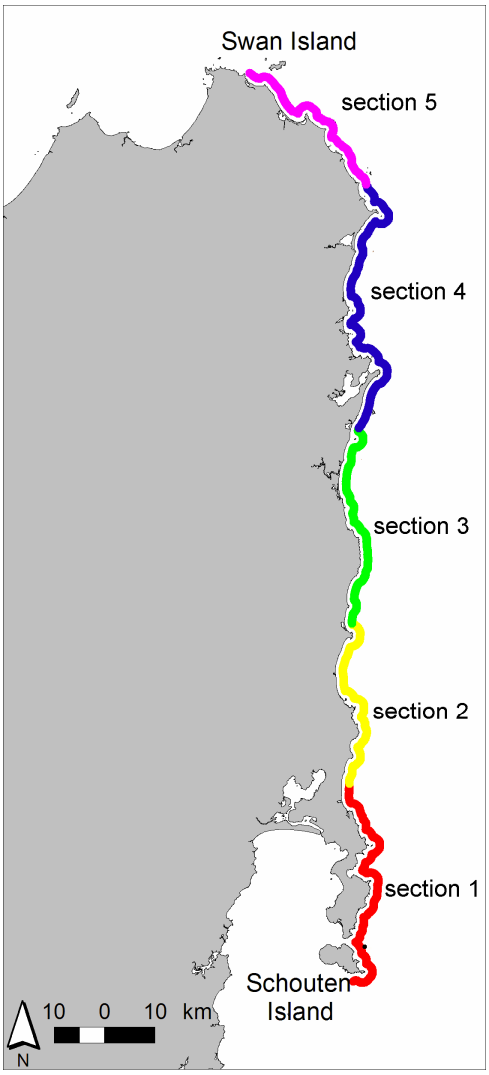

Figure 6.5. Location of the five analysis sections for the east coast algal analysis.

For species which showed strong dissimilarities in cover between sections from the SIMPER analysis, ANOVA was used to examine statistical differences by depth bin. The depth distribution from the major canopy species *Durvillaea potatorum*, *Phyllospora comosa* and *Ecklonia radiata* were compared between the sections. ANOVA was conducted for each of these species by section for each depth bin, with paired T-tests used to examine for groupings where significant differences existed. Only records where there was 25% cover or greater for

each species were included in the depth analysis, as this removed the effect of single plants occurring deeper than the majority of the species distribution.

6.3. Results

6.3.1. Positional Accuracy

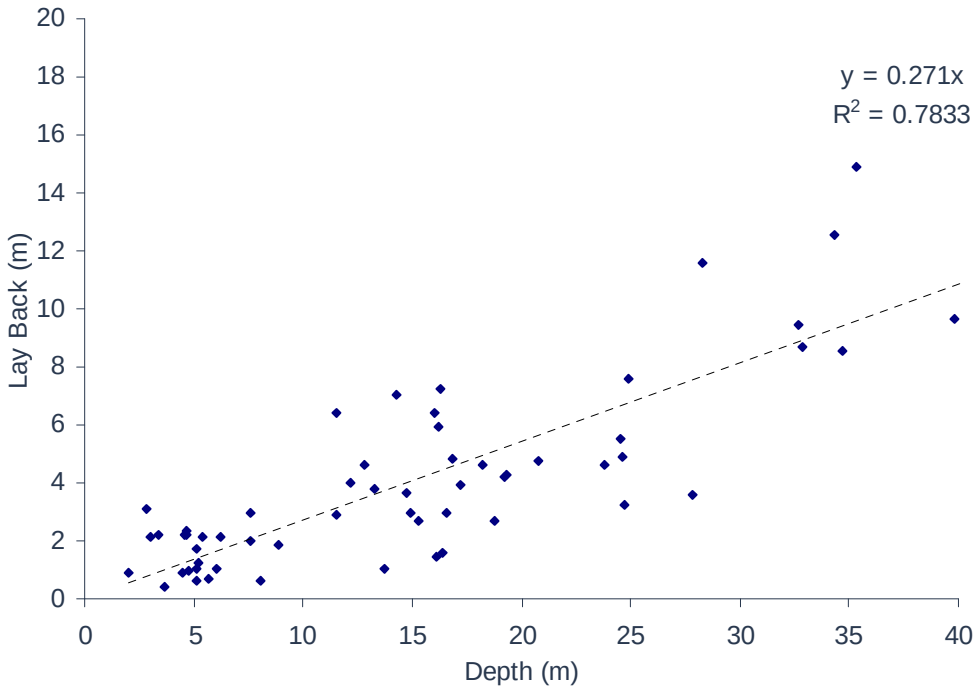

Figure 6.6. Plot of estimated lay back (video vs. acoustic) versus depth for 61 reef-sand boundary crossings

Estimates of video layback based on comparison of the video and acoustic data showed a strong linear relationship with depth within the depth range of 0 m – 40 m (Figure 6.6). This relationship was used to estimate the video camera distance behind the vessel. This distance was coupled with the back bearing data to estimate the position of the video in relation to the vessel. When unsmoothed back bearing data was used, the estimated video position changed rapidly around the vessel track log due to the pitch and roll of the vessel. When this back bearing data was smoothed these large jumps in estimated video position were removed (Figure 6.7). Correcting the video position for depth resulted in an estimated positional error for the video system of 0.271 times the depth. Thus in 20 m depth the video was within ± 2.5 m of the estimated position. Positional error of this magnitude corresponded with a potential depth error of 0.37 m ± 0.54 m. The positional error calculated using this method is in addition to GPS error, and should be incorporated into any error budget as such. This method also assumes that the camera system is directly behind the vessel, which in many cases may not be the case.

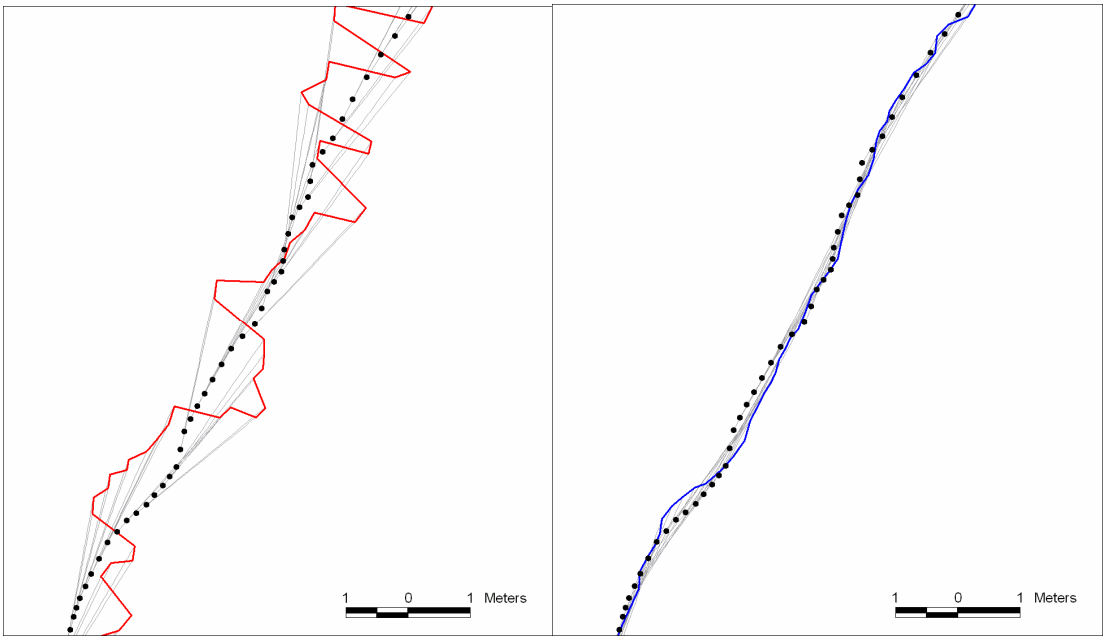

Figure 6.7. View of vessel track log (black dots) with estimated video track log with (a) no smoothing of back bearing (red line), and (b) smoothed back bearing (blue line). Grey lines link the points on the vessel tracklog with the corresponding points of the video tracklog

6.3.2. Comparison of the analysis methods

Four methods were examined to analyse the video for algal cover. The efficiency of these methods was compared, based on the time taken to analyse 1 hour of video. Most of the methods took between 2- 3 hours to process 1 hour of video, however the frame based point intercept took close to 6 hours to process 1 hour of video (Table 6.1). The Time based presence/absence was slightly quicker than the frame based 10% cover method, while the time based 10% cover method was slower, taking almost 50 % longer to analyse, but was still twice as quick as the frame based point intercept method.

Table 6.1. Comparison of time taken to analyse 1 hour of video for the four analysis methods

Method	Time/hour video	Data type
Frame 10% cover	2.0 ± 1.8	Percentage cover in 10% bins
Frame Point Intercept	5.9 ± 4.9	Percentage cover in 2% bins
Time 10% cover	2.9 ± 2.3	Percentage cover in 10% bins
Time Presence/absence	1.9 ± 0.8	Percentage cover based on% time observed

A comparison of the classified algae from 10 randomly selected video transects was made. Very little difference between the cover estimates from the Frame 10% Cover, Frame point intercept and Time 10% cover methods was observed (Table 6.2), while the estimates from the Time presence/absence method varied from the other three methods. These correlations were relatively similar over the 10 transects analysed hence low standard deviations. The strong correlation between the Frame 10%, Frame Point Intercept and Time 10% methods can be seen when the algal cover data for one of the 10 transects is presented graphically in 5 m depth bins (Figure 6.8). The patterns of the graphs are similar for each of these three methods,

and differ from that of the Time Presence/absence method (Figure 6.8).

Table 6.2. Comparison of correlation between analysis methods based on analysis of 10 transects

Method 1	Method 2	Average Correlation ± Standard Deviation
Frame 10%	Frame Point Intercept	98.2% ± 1.6%
Frame 10%	Time 10%	98.5% ± 0.8%
Frame 10%	Time Presence/Absence	74.5% ± 2.5%
Frame Point Intercept	Time 10%	98.1% ± 1.2%
Frame Point Intercept	Time Presence/Absence	73.1% ± 2.7%
Time 10%	Time Presence/Absence	76.5% ± 2.1%

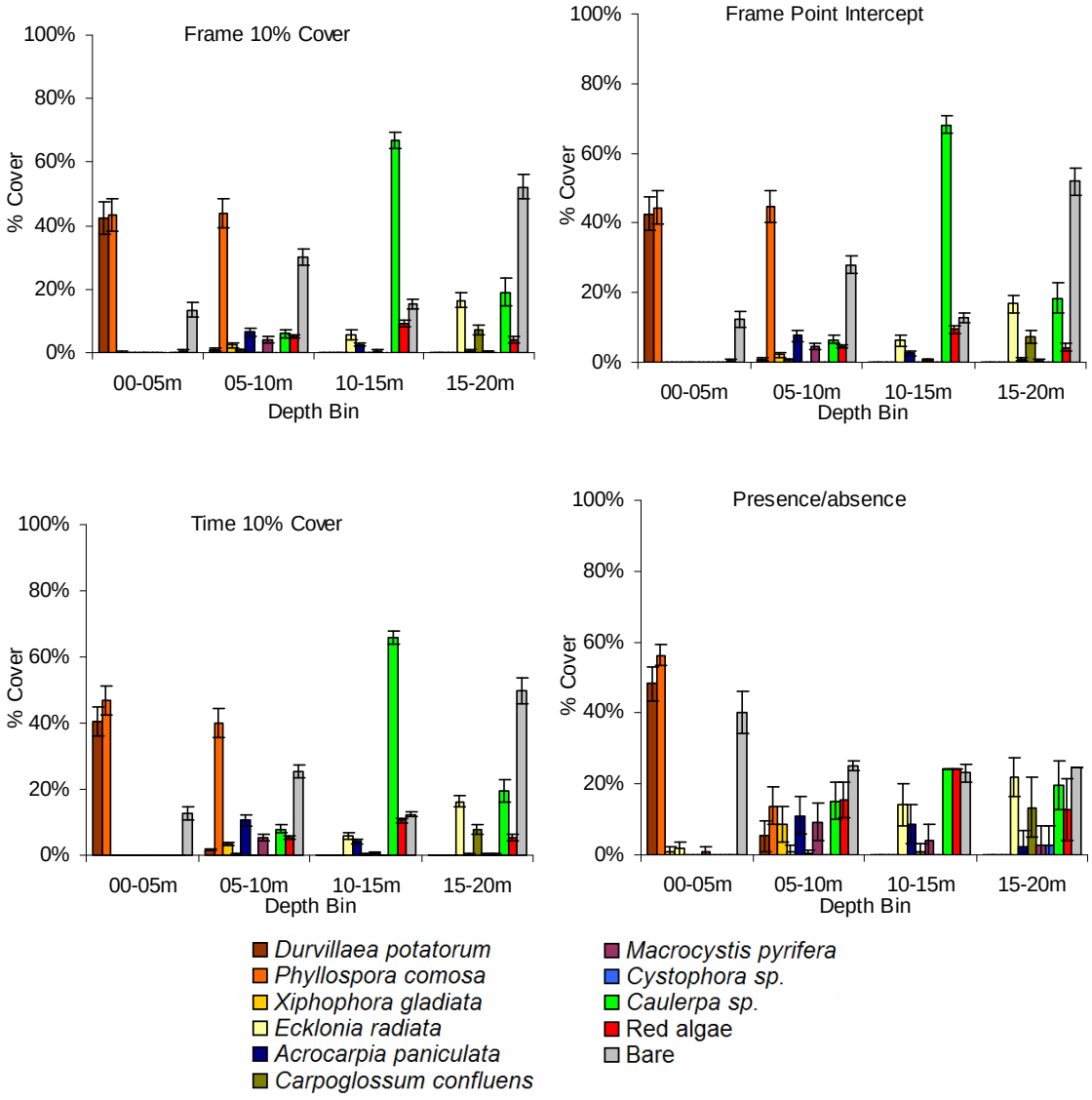

Figure 6.8. An example of the algal cover estimates based on the four methods of analysis for one of the 10 transect analysed. Only data for algal species/groups that were present at greater than 1% in at least one depth bin are presented in these figures.

Due to the low resolution of consumer digital video, coupled with the motion video, not all algae could be identified, either due to excessive camera motion, poor lighting/visibility, or too great a camera object distance. This was often more noticeable in the still frame grabs. To assess the capacity of each analysis method to identify all the algae in each frame/time unit, the number of unidentified attributes was compared between each of the methods. The frame

based methods had a higher proportion of unidentified algae than the time based methods (Table 6.3). This was especially the case for the frame based point intercept method, which had 2.6% unidentified algae, versus 1.2 – 1.3% for the time based methods (Table 6.3). Frame based methods rely on the quality of a single frame grab, which can be affected by shadowing, excessive camera movement and long camera range. In the time based methods there was a lower probability of unidentified algae as there were 100 frames within each time period, creating a greater chance of identifying an algal species within several frames.

Table 6.3. Average percentage of unclassified algae for the four video analysis methods with standard error.

Method	% Unidentified
Frame 10% cover	2.2% ± 1.3%
Frame Point Intercept	2.6% ± 1.5%
Time 10% cover	1.3% ± 0.9%
Time Presence/absence	1.2% ± 0.8%

Based on the above comparisons of the four analysis methods. Each method was rated for processing time, correlation with the other methods and the amount of unidentified algae (Table 6.4). The time based presence/absence method did not correlate well with the other three methods. This method is better suited to gathering information on the distribution of species, such as depth distribution. Of the remaining three, the frame based point intercept method had a high overhead in terms of processing with a ratio of approximately 6:1 (hours of processing to hours of video) compared to the remainder of methods that were less than 3:1. The two frame based methods also had a higher percentage of unidentified data, approximately twice that of the frame based methods. The comparison of the four methods suggests that the time based percentage cover method is the best for analysis of algal data from video for this chapter, balancing processing time with accuracy.

Table 6.4. Summary of the four video processing methods for processing time, correlation with other methods and percentage unidentified algae. + indicates good performance, ~ indicated average perfomance, and - indicates poor performance.

Method	Processing Time	Correlation	Unidentified Algae
Frame 10% cover	+	+	-
Frame Point Intercept	-	+	-
Time 10% cover	~	+	+
Time Presence/absence	+	-	+

6.3.2.1. Structure of algal community between north, east and south coasts of Tasmania

The structure of rocky reef algal communities within the three regions were compared based on 270 video transects. These transects equated to approximately 100 linear kilometres, evenly divided between the three regions. The algal communities showed visual differences when plotted by 5 m depth bins, both across depth and between the regions (Figure 6.9,

Figure 6.10, and Figure 6.11). Differences were observed in the total algal cover, species composition and species cover both within and between the three regions.

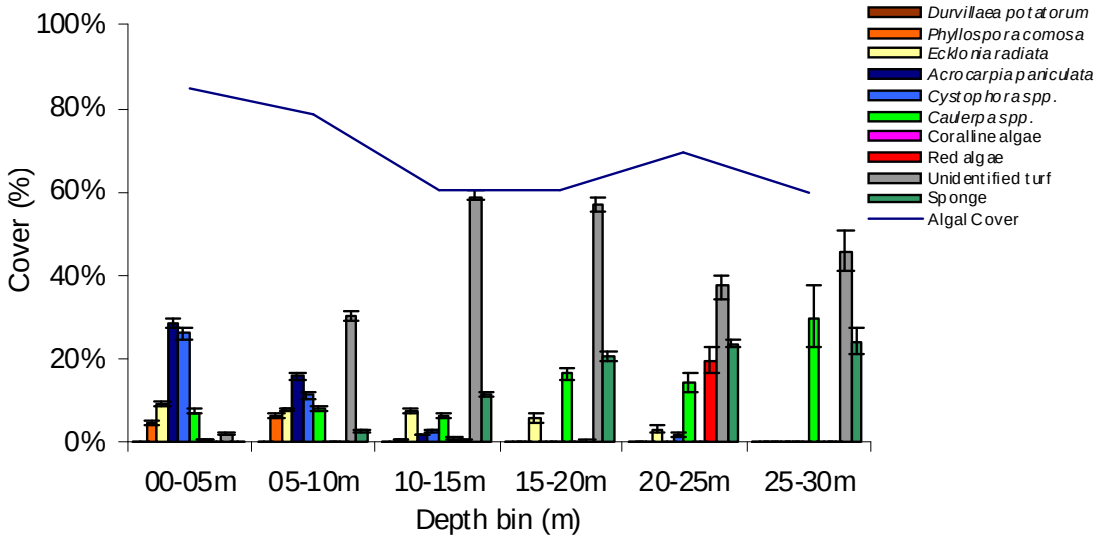

Figure 6.9. Average algal cover for dominant canopy species by depth (5 m bins) for the north coast of Tasmania. Error bars give standard error. Only data for algal species/groups that were present at greater than 1% in at least one depth bin are presented in these figures.

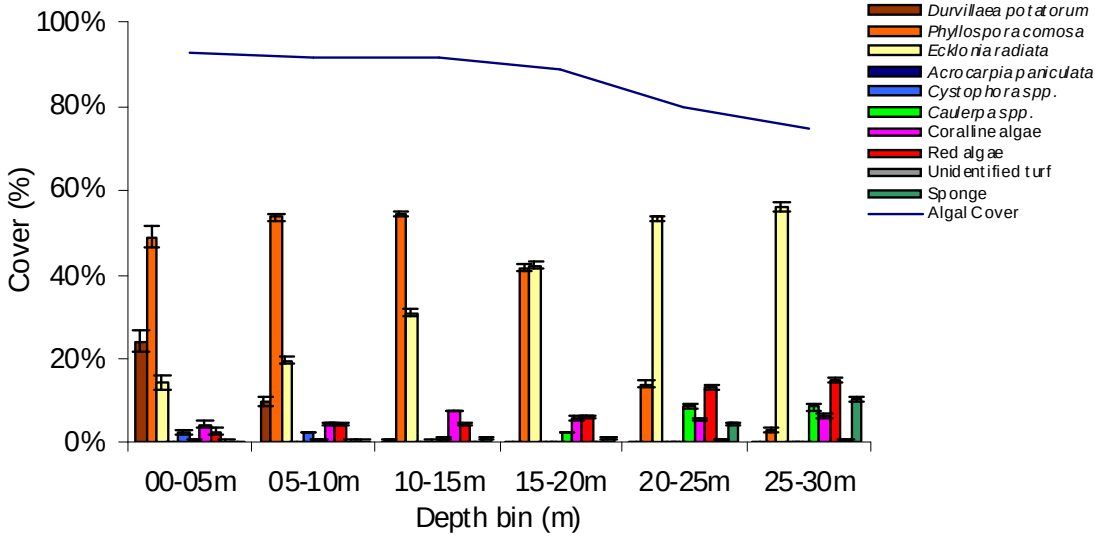

Figure 6.10. Average algal cover for dominant canopy species by depth (5 m bins) for the east coast of Tasmania. Error bars give standard error. Only data for algal species/groups that were present at greater than 1% in at least one depth bin are presented in these figures.

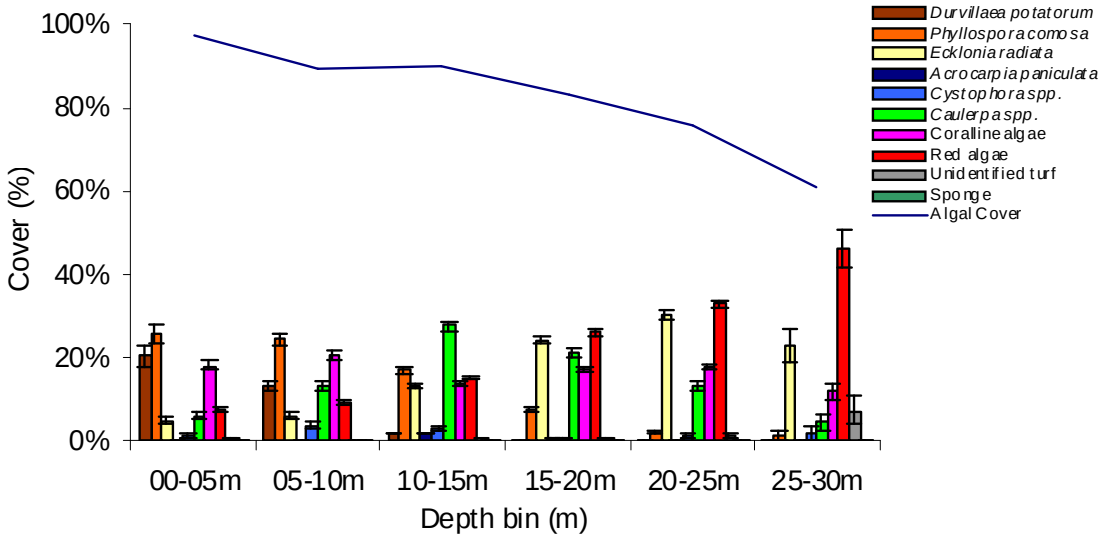

Figure 6.11. Average algal cover for dominant canopy species by depth (5 m bins) for the south coast of Tasmania. Error bars give standard error. Only data for algal species/groups that were present at greater than 1% in at least one depth bin are presented in these figures.

Algal assemblage from the north coast showed significant separation from samples from the east and south coasts (Figure 6.12). The samples from the south and east coasts showed a large amount of overlap. In all cases there was a large amount of scatter for clusters from a given region. The majority of this scatter is explained by depth related trends in algal distribution (Figure 6.13). The data for the south and east coasts tended to cluster more tightly in the shallower depths (0 – 20 m depth) than the data along the north coast. It should also be noted that there was very little data below 20 m depth along the north coast, as this is generally the maximum depth of reef along this coastline. For this reason comparison between the regions was conducted on data in the 0 – 20 m depth range.

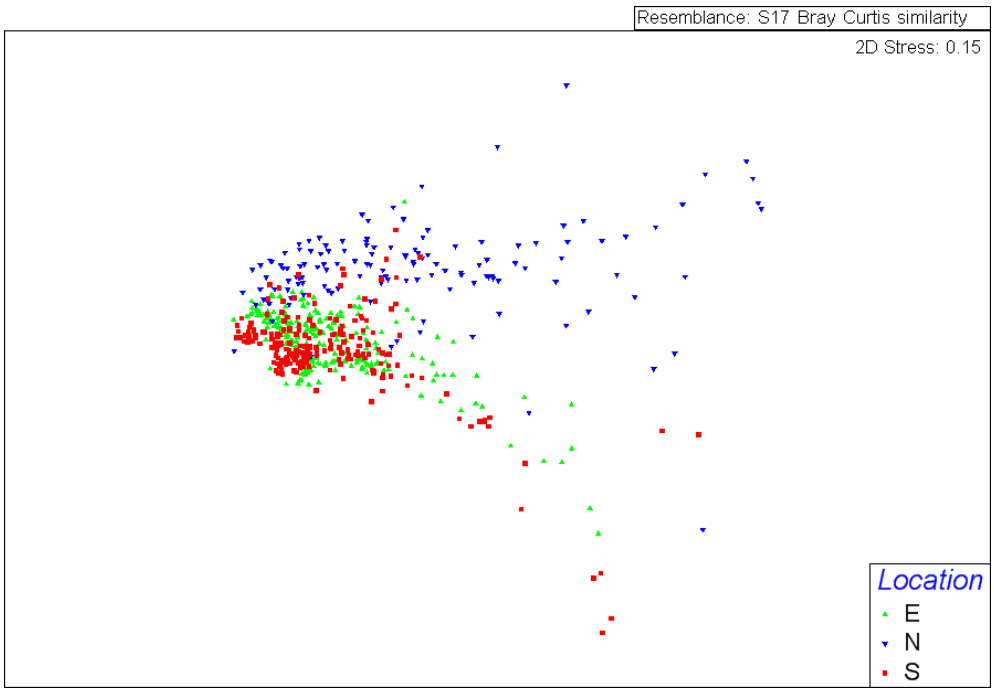

Figure 6.12. Multi-Dimensional Scaling plot comparing video data from the north, east and south coasts of Tasmania for data in the 0 - 30 m depth range colours represent the different regions.

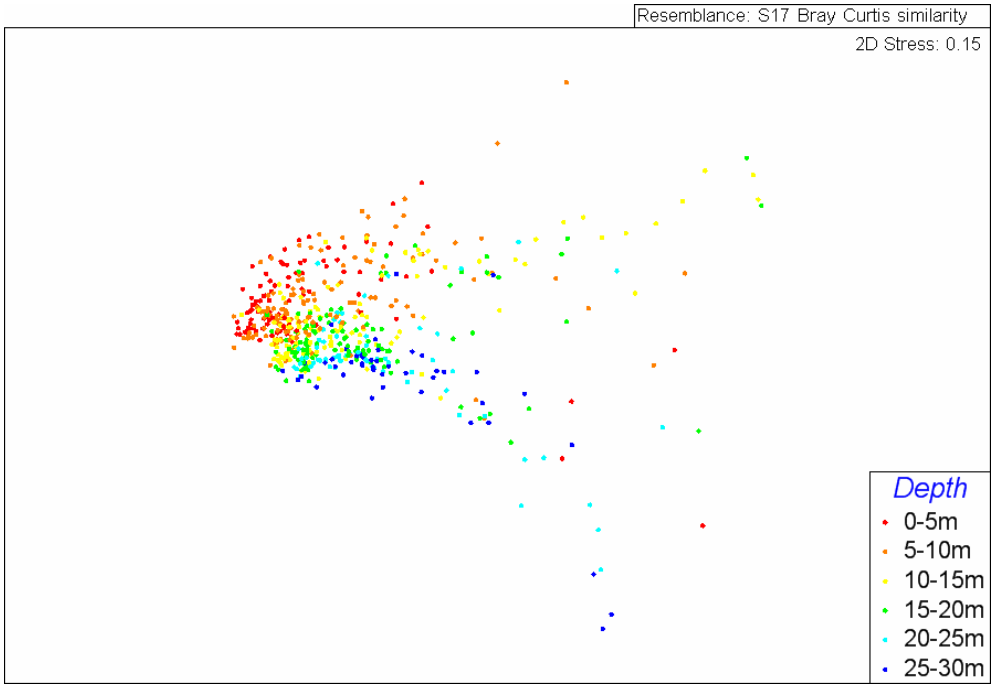

Figure 6.13. Multi-Dimensional Scaling plot comparing video data from the north, east and south coasts of Tasmania for data in the 0 - 30 m depth range colours represent 5 m depth bins from 0 to 30 m depth.

The differences between the algal communities within and between each section were analysed using SIMPER analysis. The east and south coast data showed the highest within group similarity of 59 and 55% respectively, while the north coast was the lowest at 36%. For the east coast *Phyllospora comosa* and *Ecklonia radiata* accounted for 89% of the similarity (Table 6.5); for the north coast unidentified turfing algae, *Acrocarpia paniculata*, *Cystophora*

spp., *Caulerpa* spp., and *Ecklonia radiata* accounted for 89% of the similarity (Table 6.6); while for the south coast *Caulerpa* spp., Coralline algae, *Phyllospora comosa*, red algae, and *Ecklonia radiata* accounted for 92% of the similarity (Table 6.7).

Table 6.5. Within group similarity (Bray-Curtis) percent contribution by species/group (top ten) for the east coast algal video data. The within group similarity for the east coast is 59.3%.

Species/group	Abundance (average)	Similarity (average)	Similarity (Stdev)	Percent contribution	Cumulative percent
Ecklonia radiata	0.38	27.10	1.36	45.70	45.70
Phyllospora comosa	0.37	25.94	1.01	43.73	89.43
Red algae	0.07	2.88	0.53	4.86	94.29
Coraline algae	0.04	1.41	0.45	2.38	96.67
Durvillaea potatorum	0.04	0.68	0.15	1.15	97.82
Caulerpa spp.	0.03	0.68	0.21	1.14	98.97
Sponge	0.02	0.37	0.15	0.62	99.59
Cystophora spp.	0.01	0.19	0.11	0.31	99.90
Turfing brown algae	0.01	0.04	0.06	0.06	99.96
Polysiphonia spp.	0.00	0.01	0.03	0.01	99.97

Table 6.6. Within group similarity (Bray-Curtis) percent contribution by species/group (top ten) for the north coast algal video data. The within group similarity for the north coast is 36.3%.

Species/group	Abundance (average)	Similarity (average)	Similarity (Stdev)	Percent contribution	Cumulative percent
Unidentified turf	0.30	14.23	0.58	39.17	39.17
Acrocarpia paniculata	0.13	7.20	0.56	19.82	59.00
Cystophora spp.	0.12	6.06	0.56	16.68	75.68
Caulerpa spp.	0.10	2.65	0.52	7.30	82.98
Ecklonia radiata	0.07	2.10	0.43	5.79	88.76
Sponge	0.07	1.66	0.32	4.57	93.33
Sargassum spp.	0.04	0.78	0.20	2.15	95.48
Phyllospora comosa	0.04	0.58	0.11	1.61	97.09
Caulocystis spp.	0.02	0.45	0.25	1.24	98.33
Carpoglossum confluens	0.01	0.18	0.17	0.51	98.84

Table 6.7. Within group similarity (Bray-Curtis) percent contribution by species/group (top ten) for the south coast algal video data. The within group similarity for the south coast is 55.1%.

Species/group	Abundance (average)	Similarity (average)	Similarity (Stdev)	Percent contribution	Cumulative percent
Caulerpa spp.	0.18	12.00	0.93	21.77	21.77
Coraline algae	0.18	10.68	1.15	19.38	41.14
Red algae	0.18	10.44	1.02	18.94	60.08
Phyllospora comosa	0.15	9.30	0.94	16.87	76.95
Ecklonia radiata	0.14	8.37	0.89	15.18	92.13
Durvillaea potatorum	0.08	3.20	0.35	5.80	97.92
Xiphophora spp.	0.01	0.43	0.35	0.78	98.70
Macrocystis pyrifera	0.01	0.30	0.30	0.55	99.25
Acrocarpia paniculata	0.01	0.12	0.15	0.22	99.48
Carpoglossum confluens	0.01	0.11	0.19	0.21	99.69

A pair wise comparison of the dissimilarity between the regions showed high dissimilarity between the east and north coasts, and south and north coasts, 90 and 89% dissimilarity respectively, with 63% dissimilarity between the south and east coasts. The main

species/groups contributing to the dissimilarity between the east and north coasts were *Phyllospora comosa*, unidentified turf and *Ecklonia radiata* (Table 6.8); the main species/groups contributing to the dissimilarity between the east and south coasts were *Phyllospora comosa*, *Ecklonia radiata* and *Caulerpa* spp. (Table 6.9); while the main species/groups contributing to the dissimilarity between the north and south coasts were unidentified turf, *Phyllospora comosa*, coralline algae and *Caulerpa* spp. (Table 6.10).

Table 6.8. Between group similarity (Bray-Curtis) percent contribution by species/group (top ten) for the east and north coast algal video data. The between group similarity for the east and north coast is 89.7%.

Species/group	East Abundance (average)	North Abundance (average)	Dissimilarity (average)	Similarity (Stdev)	Percent contribution	Cumulative percent
Phyllospora comosa	0.37	0.04	23.65	1.69	26.36	26.36
Unidentified turf	0.00	0.30	16.25	0.96	18.12	44.48
Ecklonia radiata	0.38	0.07	13.15	1.16	14.66	59.14
Acrocarpia paniculata	0.00	0.13	6.35	0.62	7.07	66.22
Cystophora spp.	0.01	0.12	5.58	0.64	6.22	72.44
Caulerpa spp.	0.03	0.10	4.74	0.72	5.28	77.72
Sponge	0.02	0.07	3.36	0.59	3.74	81.47
Durvillaea potatorum	0.04	0.00	3.14	0.38	3.50	84.97
Red algae	0.07	0.01	2.68	0.56	2.99	87.95
Sargassum spp.	0.00	0.04	2.39	0.31	2.66	90.62

Table 6.9. Between group similarity (Bray-Curtis) percent contribution by species/group (top ten) for the east and south coast algal video data. The between group similarity for the east and south coast is 62.8%.

Species/group	East Abundance (average)	South Abundance (average)	Dissimilarity (average)	Similarity (Stdev)	Percent contribution	Cumulative percent
Phyllospora comosa	0.37	0.15	15.69	1.34	25.00	25.00
Ecklonia radiata	0.38	0.14	12.56	1.19	20.01	45.01
Caulerpa spp.	0.03	0.18	9.27	1.10	14.77	59.78
Coraline algae	0.04	0.18	7.61	1.19	12.12	71.90
Red algae	0.07	0.18	6.90	1.09	11.00	82.89
Durvillaea potatorum	0.04	0.08	4.17	0.52	6.64	89.53
Cystophora spp.	0.01	0.01	1.36	0.36	2.17	91.70
Xiphophora spp.	0.00	0.01	0.79	0.49	1.25	92.95
Macrocystis pyrifera	0.00	0.01	0.71	0.46	1.13	94.09
Sponge	0.02	0.00	0.54	0.26	0.86	94.95

Table 6.10. Between group similarity (Bray-Curtis) percent contribution by species/group (top ten) for the north and south coast algal video data. The between group similarity for the north and south coast is 88.9%.

Species/group	North Abundance (average)	South Abundance (average)	Dissimilarity (average)	Similarity (Stdev)	Percent contribution	Cumulative percent
Unidentified turf	0.30	0.01	17.07	0.99	19.20	19.20
Phyllospora comosa	0.04	0.15	9.72	1.21	10.93	30.13
Coraline algae	0.00	0.18	9.54	1.31	10.73	40.86
Caulerpa spp.	0.10	0.18	8.36	1.09	9.41	50.27
Ecklonia radiata	0.07	0.14	6.42	0.97	7.23	57.49
Acrocarpia paniculata	0.13	0.01	6.19	0.63	6.97	64.46
Durvillaea potatorum	0.00	0.08	6.13	0.65	6.90	71.36
Red algae	0.01	0.18	6.08	1.18	6.83	78.19
Cystophora spp.	0.12	0.01	5.62	0.64	6.32	84.51
Sponge	0.07	0.00	3.65	0.61	4.10	88.61

The east coast region was divided into 5 sections to examine algal community structure at a finer spatial scale. The algal communities showed visual differences in community structure when plotted by five meter depth bin (Figure 6.14). It should be noted that only species/groups with greater than 5% cover within a single depth bin are included in these plots, however these groups were included in the subsequent analysis.

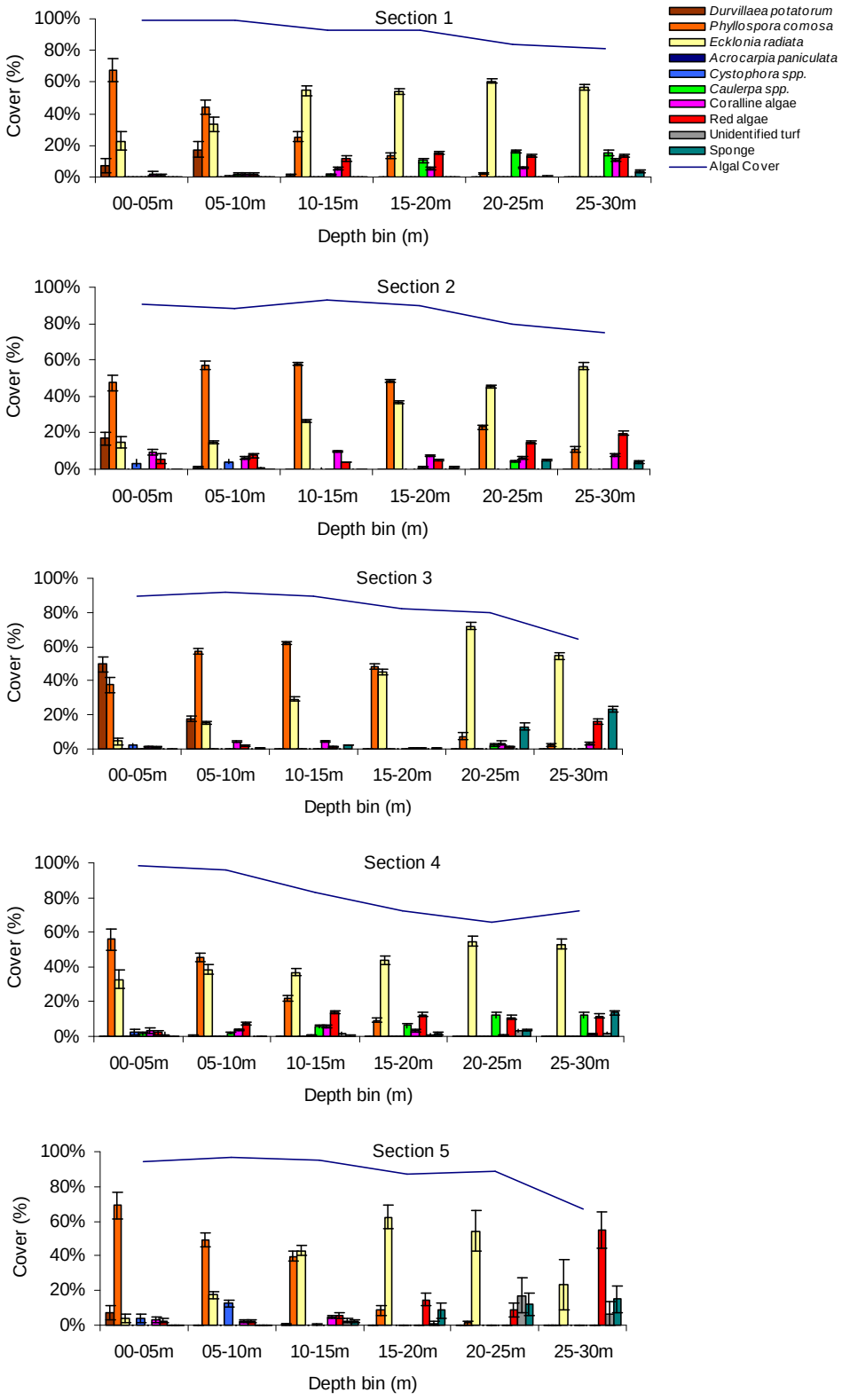

Figure 6.14. Mean algal cover for dominant algal species by 5 m depth bin for the five analysis sections on the east coast of Tasmania derived from video analysis. Error bars indicate standard error. Only data for algal species/groups that were present at greater than 1% in at least one depth bin are presented in these figures.

Analysis using SIMPER showed an average similarity within section of between 60 and 70%. The dissimilarity between pairs of groups ranged from 34 and 50% (Table 6.11), with differences in *Phyllospora comosa* and *Ecklonia radiata* cover generally accounting for at

least 50% of this dissimilarity, with *Durvillaea potatorum* also accounting for a large proportion of the dissimilarity in several cases. These three species were examined for significant differences in cover by 5 m depth range between the five sections.

Table 6.11. Pair-wise comparison of dissimilarity (% dissimilarity) for algal communities in the five analysis sections on the east coast of Tasmania based on SIMPER analysis.

		section				
		1	**2**	**3**	**4**	**5**
Section	**1**	-	47.1	45.5	38.0	49.6
	2	47.1	-	34.1	47.2	39.9
	3	45.5	34.1	-	45.8	39.2
	4	38.0	47.2	45.8	-	46.2
	5	49.6	39.9	39.2	46.2	-

Significant differences in the cover of *D. potatorum* were observed in the 0 – 10 m depth range, for *P. comosa* between 10 and 30 m depth and for *E. radiata* between 10 and 20 m and again between 25 and 30 m between the five sections based on ANOVA. Paired T-tests were used to test which sections were significantly different and which sections grouped together based on the cover of theses three species. For *D. potatorum* in the 0 – 5 m depth range sections 1, 2 and 3, and sections 1, 4 and 5 formed groups, with significant differences observed between all other combinations of sections. In the 5 – 10 m depth range sections 1 and 3 were significantly different from each other and all other sections (Figure 6.15).

Table 6.12. Probability values (ANOVA) for significant differences between sections of cover for *Durvillaea potatorum*, *Phyllospora comosa*, and *Ecklonia radiata* by 5 m depth bin. * denotes significant differences observed.

Depth range	*D. potatorum*	*P. comosa*	*E. radiata*
00-05m	<0.05*	0.75	0.16
05-10m	<0.01*	0.07	0.16
10-15m	0.12	<0.01*	<0.01*
15-20m	0.58	<0.01*	<0.01*
20-25m	-	<0.01*	0.24
25-30m	-	<0.05*	0.43

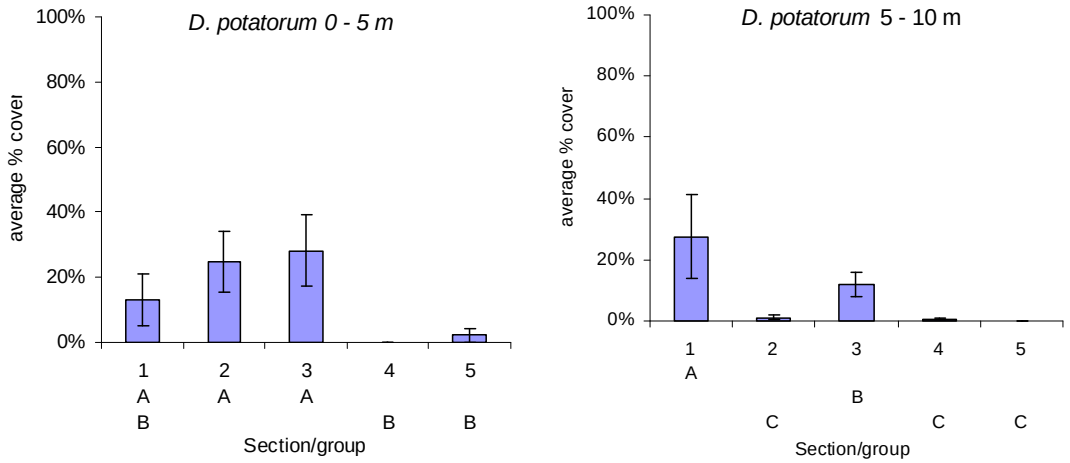

Figure 6.15. Plots of mean cover by section for *D. potatorum* for 5 m depth bins where significant differences were observed using ANOVA. Sections not connected by the same letter (under the x-axis) are significantly different. Error bars indicate standard error.

E. radiata cover showed significant differences in the 10 – 20 m depth range. In 10 – 15 m depth range sections 1 and 5, and sections 2, 3 and 4 formed groups, with significant differences observed between all other combinations of sections. In the 15 – 20 m depth range sections 1, 3 and 5, and sections 2, 3, 4 and 5 formed groups, with significant differences observed between all other combinations of sections (Figure 6.16).

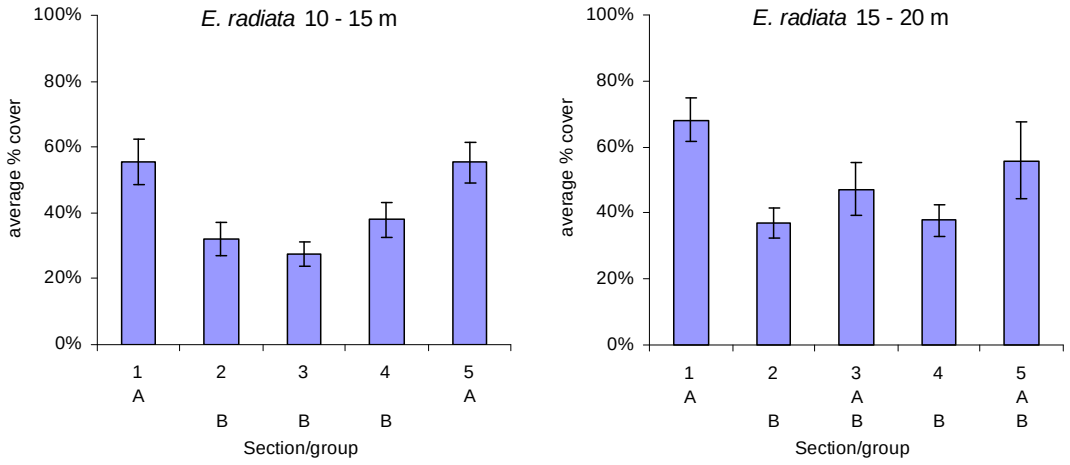

Figure 6.16. Plots of mean cover by section for *E. radiata* for 5 m depth bins where significant differences were observed using ANOVA. Sections not connected by the same letter (under the x-axis) are significantly different. Error bars indicate standard error.

P. comosa cover showed significant differences in the 10 – 30 m depth range. In the 10 – 15 m depth range sections 2 and 3, and sections 1 and 4 formed groups, with significant differences observed between all other combinations of sections. In the 15 – 20 m depth range again sections 2 and 3 formed a group, with sections 1, 4 and 5 also forming a group, with significant differences observed between all other combinations of sections. Similarly, sections 2 and 3 again grouped together in the 20 – 25 m depth range, with sections 1, 3 and 5

and sections 1, 4 and 5 also forming groups, significant differences were observed between all other combinations of sections. In the 25 – 30 m depth range sections 2, 3 and 5 formed a group, as did sections 1, 3, 4 and 5, with significant differences between all other combinations of sections (Figure 6.17).

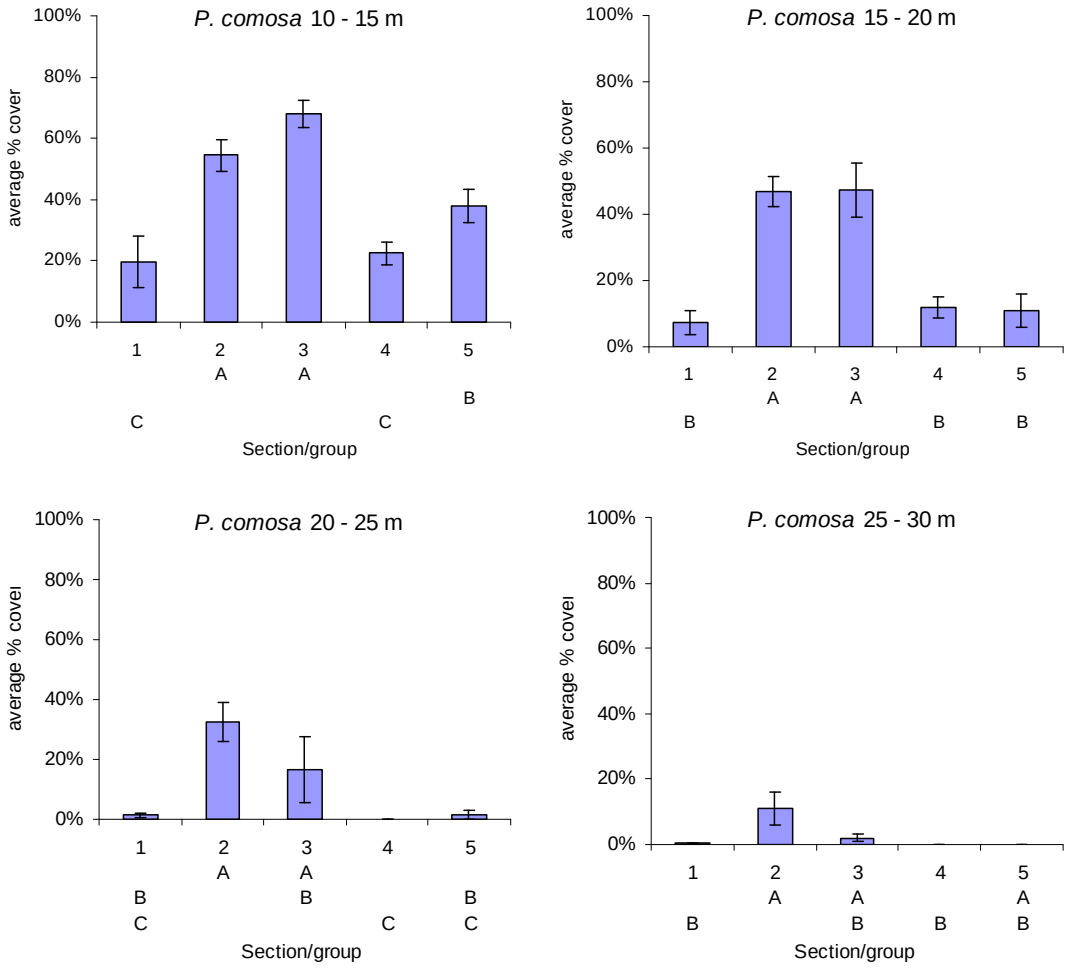

Figure 6.17. Plots of mean cover by section for *P. comosa*, for 5 m depth bins where significant differences were observed using ANOVA. Sections not connected by the same letter (under the x-axis) are significantly different. Error bars indicate standard error.

The depth distribution of the three dominant algae was also examined by section. The depth distribution of *D. potatorum* showed a significant difference across the sections (ANOVA, df = 3, F = 16.65, P < 0.01), with this species tending to have a deeper distribution in the sections 1 and 3, and a shallower distribution in sections 2 and 5, *D. potatorum* was not observed at sufficient levels in section 4 to be included in this analysis. Sections 2 and 5 formed a statistical group, with significant differences observed in all other combinations of sections (Figure 6.18). There was a trend for a decrease in the average depth distribution of *D. potatorum* in the more northern sections.

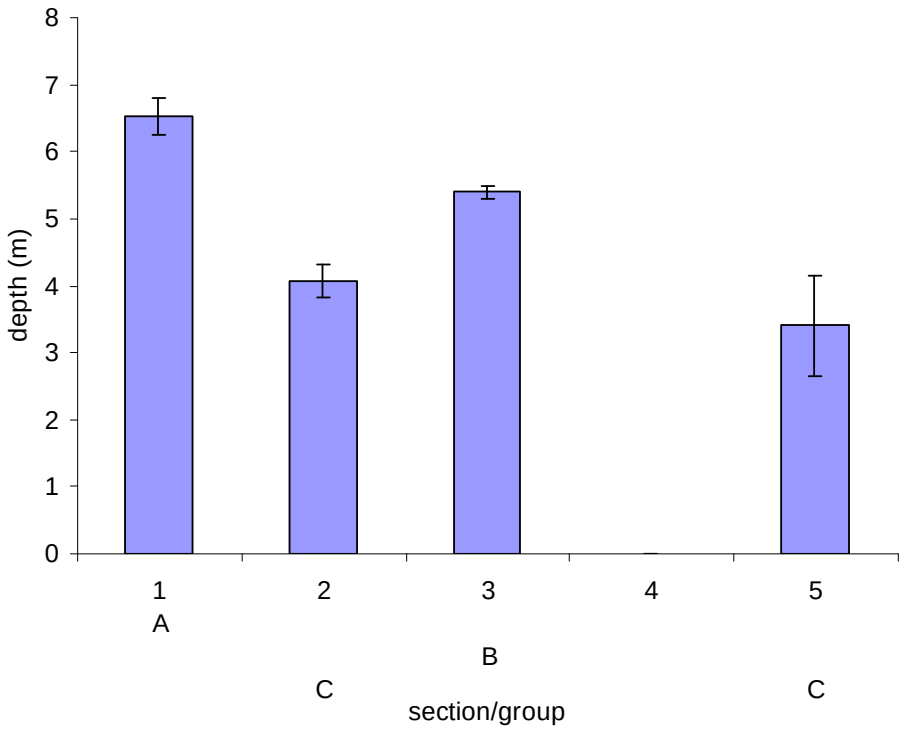

Figure 6.18. Average depth of *D. potatorum* by section. Sections not connected by the same letter (under the x-axis) are significantly different. Error bars indicate standard error.

The depth distribution of *P. comosa* showed significant differences in the average depth distribution across the sections (ANOVA, df = 4, F = 131.7, P < 0.01). Sections 1 and 3 grouped together, with significant differences between the remaining combinations of sections (Figure 6.19). As for the *D. potatorum* there was a general trend for a decrease in the average depth distribution of *P. comosa* in the more northern sections.

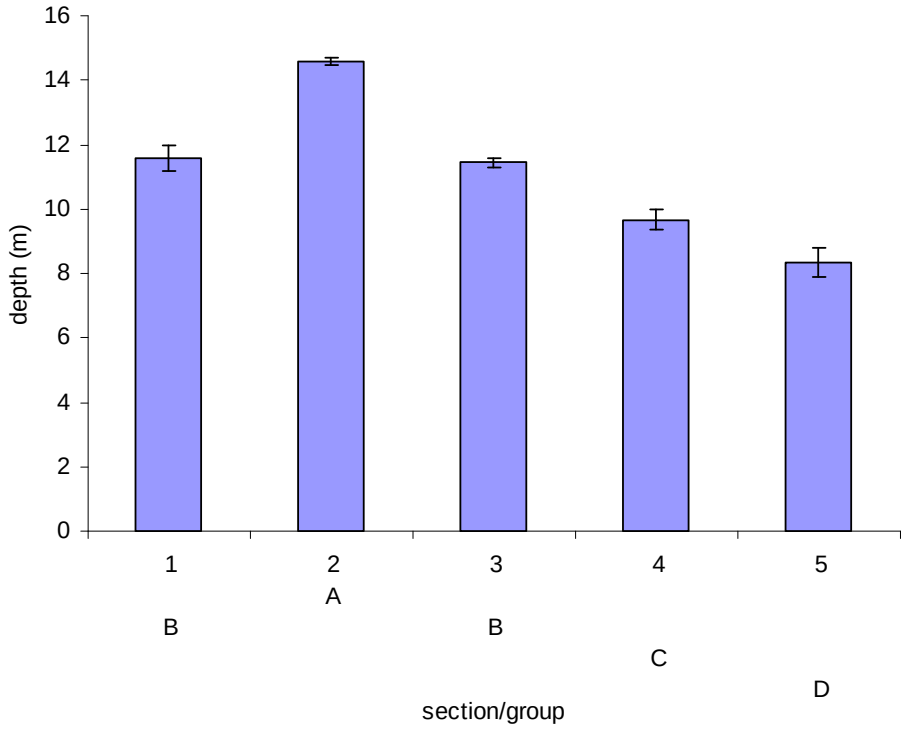

Figure 6.19. Average depth of *P. comosa* by section. Sections not connected by the same letter (under the x-axis) are significantly different. Error bars indicate standard error.

The depth distribution of *E. radiata* showed significant differences in the average depth distribution across the sections (ANOVA, df = 4, F = 190.1, P = < 0.01). Sections 2 and 4 formed a statistical group, with significant difference shown between the remaining combinations of sections (Figure 6.20). As for both *D. potatorum* and *P. comosa* there was a trend for a shallower depth distribution in the more northern sections.

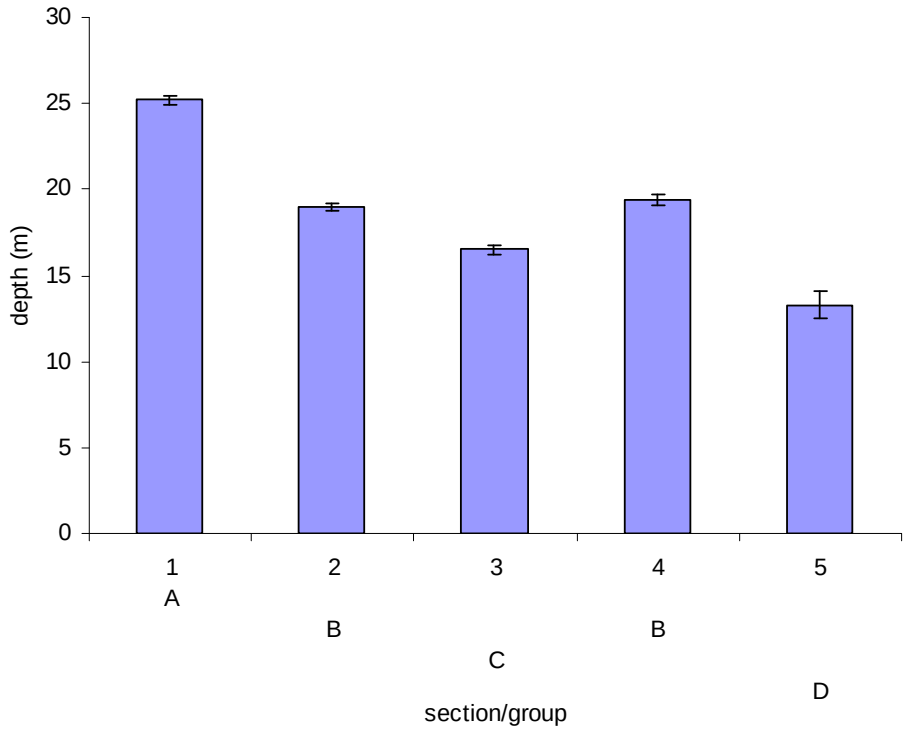

Figure 6.20. Average depth of *E. radiata* by section. Sections not connected by the same letter (under the x-axis) are significantly different. Error bars indicate standard error.

6.4. Discussion

Temperate reef algal communities are important for the biodiversity of reef systems. These communities provide a source of primary production, shelter, and structure that support a large number of other species (Schiel and Foster 1986). This chapter examined methods to analyse underwater video data, which in turn could be used to describe patterns in algal community structure. Three of the methods examined had a strong correlation, while a fourth did not correlate as well. The three methods with strong correlation differed in the processing time and the amount of unclassified data obtained. This suggests that, at least for algal community structure at this spatial and taxonomic level, the method of analysis is not critical to the outcome of the analysis.

In order to relate the video frames to the depth collected from the acoustic sounder the positional accuracy of the video system was estimated based on the crossing of easy to distinguish reef/sand boundaries simultaneously with the video and acoustic systems. This comparison showed that while the video system was generally directly beneath the vessel in shallow water, it was up to 15 m behind the vessel in deeper water. In many cases this meant that the video was outside the half beam power acoustic footprint and thus a positional correction was needed to relate the video footage to the depths from the acoustic sounder.

There is also the possibility that the video camera, being inside the acoustic beam could affect the measured depth from the seabed, however the camera system was generally on the outside of the acoustic beam, whilst the strongest returns are generally along the central axis and it is these strongest returns that are used to calculate the sounder detected bottom. A simple linear correction model was developed to account for this layback. Alternatively the use of acoustic positioning technology could be used to more accurately account for the layback of the video system.

Four video analysis methods were compared, with the frame based point intercept, frame based percentage cover, and the time based percentage cover methods strongly correlated. The two frame based methods were limited by the quality of the frames grabbed from the video. This led to problems with the identification of algal groups, with a higher proportion of unclassified algae with these two methods. The time based methods had less problems with unidentified algae, as algae that was blurred or obscured in one frame were generally visible and identifiable in subsequent frames. The frame based analysis methods would benefit from higher resolution video or purpose taken still images. The real strength of video is the continuous stream of data, rather than the high detail within each frame. Thus the time based analysis method has the potential to better capture detailed information from the video by working to its strengths.

The processing time for each of the four methods varied from a ratio of approximately 2:1 for the frame based percentage cover and time based presence/absence methods (2 hour processing for each hour of video) to a maximum of 6:1 for the frame based point intercept method, with the time based percentage cover method in the middle with a ratio of 2.9:1. Point intercept methods are commonly used to assess cover of organisms from still images (Drummond and Connell 2005, Kohler and Gill 2006); however the high overhead in term of processing may be prohibitive for many large datasets that are collected using underwater video. While this is the most quantitative method, it correlated very well with the two percentage cover methods, such that these are potentially a viable alternative for a more rapid analysis of the video.

All the analysis methods required a trained operator to estimate the cover of each algal to the lowest taxonomic level, and for the time and frame based percentage cover methods estimate cover, which involves a degree of subjectivity. Onscreen digitising (Kenyon *et al.* 2006) and colour segmentation (Bernhardt and Griffing 2001) methods present alternate methods of calculating percentage cover from still images. These were initially investigated, however

were found to be difficult to apply to algal community structure due to a combination of the complex 3 dimensional matrix formed by various layers of the algal in the canopy, and the similarity in colour between many of the algal species, coupled with shadowing and variable water quality and lighting.

When selecting a method for the analysis of video, consideration should be given to the type of questions being asked of the data. The frame based point intercept methods of analysis, being the most quantitative, would be best suited to long term change detection (Foster *et al.* 1991, Kohler and Gill 2006), where a statistically robust estimate of cover needs to be made; however this is at the cost of increased processing time. The percentage cover methods (Kenyon *et al.* 2006), with their lower processing times were better suited to the description of algal community structure across broad regions. It has also been shown that the scale of measurement may be more important than the method used when monitoring subtidal communities (Parravicini *et al.* 2009). The scale of measurement must reflect the structure of the community being monitored.

The taxonomic resolution of video is known to be less than for comparable diver surveys (Kenyon *et al.* 2006). However, the loss of taxonomic resolution is balanced against increased coverage when compared to diver surveys, with the additional benefit of a permanent record which can be re-analysed in the future (Carleton and Done 1995). For algal community structure the taxonomic resolution that can be collected from video is generally limited to large macroalgal species or genera. In this study most of the large brown macroalgae could be identified to either species or genus level, however many of the smaller turfing algae could not be consistently identified and were thus attributed to a category of turfing algae. Similarly, the red and coralline algae could not be consistently identified to species level and were thus grouped at a higher taxonomic level. Resolution could potentially be improved by using still cameras or hi-definition digital video. However, there will always be a loss in the taxonomic resolution compared to diver surveys.

The underwater video data were used to characterise the dominant canopy species and genera, however these algae generally obscured the smaller understorey algal. Algal canopy structure has been shown to be a large and predictable influence on the understorey structure (Melville and Connell 2001, Irving and Connell 2006). Knowledge of the canopy structure can therefore be used to develop assembly rules to predict the understorey structure (Irving and Connell 2006). Thus, knowledge of the canopy species could potentially be used to predict the entire algal assemblage at a given location. Taxonomic resolution at a similar level to that obtained

from video in this chapter, has previously been shown to be sufficient for use as a biological indicator for monitoring algal communities (Puente and Juanes 2008).

Commonly, qualitative descriptors based on dominant algal canopy species are used to define habitat on temperate rocky reefs (Schiel and Foster 1986, Underwood *et al.* 1991, Shears *et al.* 2004). For example, habitats on shallow temperate reefs have been defined as urchin barrens, kelp forests, mixed algae or sponge garden to name a few (Shears *et al.* 2004). These descriptors are generally defined subjectively; they have been quantified and validated through diver surveys in previous studies (Shears *et al.* 2004). Underwater video assessment, which allows the rapid collection of dominant algal species data, would allow definition and validation of habitat at broader scales than diver surveys.

The time based percentage cover method was used to analyse rocky reef video data from three broad geographic regions of the Tasmania coastline. Differences in the algal community structure were observed between each of these three regions. Reefs on the north coast were dominated by a mix of turfing algae, *Acrocarpia paniculata*, *Cystophora* spp., *Caulerpa* spp., and *Ecklonia radiate*; reefs on the east coast were dominated by *Phyllospora comosa* and *E. radiata*; and reefs on the south coast dominated by *Caulerpa* spp., Coralline algae, *P. comosa*, red algae, and *E. radiata*. These differences in community structure reflect differences in the environmental conditions around the coastline including water temperature (Rochford 1975, Jeffrey *et al.* 1990), nutrients (Harris *et al.* 1987, Jeffrey *et al.* 1990), and exposure (Edgar *et al.* 1997, Barrett *et al.* 2001, Jordan *et al.* 2005a). Environmental conditions will also affect the fish and invertebrate communities (Edgar 1984).

The three regions examined in this chapter have previously been designated into different bioregions based on a analysis of fish, invertebrate and algal presence/absence data from 5 m depth, with the north coast having greater separation than the other two sections of coast (Edgar *et al.* 1997). The differences found through analysis of video data from this chapter showed similar trends, with a different suite of species and a different algal structure along the north coast compared to the south and east coasts. The east coast and south coasts contained a similar suite of algal species, although the composition of these species differed with depth.

The analysis of the east coast video data at a smaller scale showed differences in the algal community structure along this coastline. Significant differences were observed in the cover and depth distribution for the three dominant structuring species, *Durvillaea potatorum*, *Phyllospora comosa* and *Ecklonia radiata*. There was a trend for each of these three species to show a decreasing depth distribution from south to north. Broadly speaking there is a

similar level of exposure on the east coast between Schouten Island and Swan Island. However, the exposure to large southerly swells is greater in the south than the north, with extremes of wave exposure that potentially have as much influence as temperature on the distribution of biota at the regional scale (Edgar *et al.* 1997). Increased exposure has previously been shown to increase the minimum, average and maximum depth distribution for each of these species within the Bruny Bioregion, to the south of this region (Barrett *et al.* 2001). Small scale coastal features may also help explain the observed patterns, with local exposure affected by the angle of the coast. The southern part of this coastline has a greater number of rocky headlands, with parts of Schouten Island and the Freycinet Peninsula having a southerly aspect. The middle parts of this coast generally have an easterly aspect, while the northern parts have a north easterly aspect.

A strong latitudinal gradient in algal cover has been observed on mainland Australia (Connell and Irving 2008). Algal canopy cover was shown to decrease with increasing latitude, with almost no canopy algae present at the southern most site (Eden, NSW) due to the presence of extensive urchin barrens, (*Centrostephanus rodgersii*). The range of this species has extended down the Tasmanian east coast over the last few decades (Johnson *et al.* 2004). The presence of these urchin barrens was visible in the algal cover data from section 4 on the east coast of Tasmania, with a decrease in algal cover in the 10 – 25 m depth range compared to other sites along the east coast. Large barrens due to this species have been documented at the Kent Group of islands in Bass Strait (Jordan *et al.* 2005b). The north coast algal data also showed low algal cover, however this species has not been documented on the north coast of Tasmania, presumably due to the predominantly westerly current flow preventing distribution of larvae along this coastline (Cresswell 2000). The low algal cover along this coastline is more likely related to water quality and exposure gradients.

6.5. Conclusions

The analysis of underwater video for the classification of algal community structure has been shown to be useful for the detection of broad scale differences in community structure at the bioregional level, and also within a selected bioregion. Of the four analysis methods compared in this chapter, three were found to have strong correlation when used to analyse the dominant algae at this spatial scale. The choice of which method is ultimately used will depend upon the type of analysis being conducted. In terms of hierarchical classification of seabed habitats, underwater video provides the capacity to include algal species information as a habitat descriptor, which allows habitat classification at lower levels than from SBES, as

discussed in the previous chapters.

Chapter 7. Development of stereo video techniques for classifying sponge beds based on functional morphology

7.1. Introduction

Sponges (Phylum Porifera) play an important role in marine ecosystems, forming complex structures on the sea floor that provide refuge and habitat for many fish and invertebrate species. Sponge biodiversity is affected by environmental conditions including depth, slope, current, and water conditions (Roberts and Davis 1996, Bell and Barnes 2000b, Bell and Barnes 2000a, Bell *et al.* 2002, Hooper and Kennedy 2002). In order to assess biodiversity, a measure of species composition and species distribution is required. However the taxonomy of sponges is inherently difficult, with colour, shape and size often variable within single species (Bell and Barnes 2001, Bell *et al.* 2002), confounding visual identification. Sponge functional morphology has been shown to be a useful surrogate for sponge biodiversity (Bell and Barnes 2001, Bell and Barnes 2002).

Measures of diversity in sponge functional morphology have been related to species diversity in both tropical (Bell and Barnes 2002) and temperate regions (Bell and Barnes 2001). Sampling sponge morphological diversity is less time consuming, and requires no specialist knowledge when compared to sampling sponge species diversity (Bell and Barnes 2001). Information on the diversity of sponges is a key component of conservation, with the role of marine sponges often overlooked in importance (Bell 2008). For conservation planning issues, such as marine protected areas planning, information on biodiversity is required (Ward *et al.* 1999, Hooper and Kennedy 2002). While information on species diversity is preferred, potential indicator groups have been shown to also be useful as a surrogate for species diversity (Gladstone 2002). Thus there is the potential to use sponge morphological diversity as a surrogate for species diversity in such situations.

To develop a repeatable classification of sponge functional morphology a quantitative measurement of sponge morphometric characteristics is required. Due to the vulnerability and slow growth of many sponge species, it is preferable to make *in situ* measurements than remove the sponges for measurements. *In situ* measurements using conventional methods, such as diver surveys, are not always possible due to the excessive sampling time required and depth limitations (Roberts and Davis 1996). The use of remotely controlled cameras to collect morphometric information would decrease the field time required and remove depth limitations.

Information collected using underwater camera systems can include presence/absence information, counts of target species/objects, or measurements. With multiple exposures and appropriate camera geometry, highly detailed 3D models can be reconstructed using photogrammetric techniques (Eos Systems Inc 2000, Cocito *et al.* 2003). Hence photogrammetry may prove a powerful tool for the classification of sponges. The use of a photogrammetric system to make measurements involves system design, construction, calibration, and validation. System design requires specification of the required spatial accuracy of the targets to be measured and their range.

In-water photogrammetry presents complications that are additional to those of terrestrial photogrammetry as light travelling through water is subject to both attenuation and refraction (Thorndike 1967, McNeil 1968, Jerlov 1976). Water attenuates light at a much greater rate than in air, with different wavelengths attenuating at different rates. The presence of particulate material, such as phytoplankton or suspended sediment, increases the rate of absorption. Due to the high absorption of light in water, underwater photogrammetry is only practical at close ranges (Rebikoff 1975, Moore 1976). This has implications for the scale of targets that can be sampled using underwater photogrammetry. In certain environments with high particulate loads, the level of absorption may be so high that it is impractical to use a photogrammetric solution.

A second major complication in underwater photogrammetry is the optical effect of the refractive surfaces at the water-port or water-lens interfaces, as seawater has a higher refractive index than air (approximately 1.33 compared with 1) (Stanley 1971, Schiebener *et al.* 1990, Yunus 1992). Refractive effects at the boundary between the water and the camera port or camera lens will alter the optical properties of the camera, causing a change in the effective focal length and, potentially, introducing large and complicated image distortions.

These distortions can be minimised by using specially designed ports, lenses or lens adaptors (Thorndike 1950, Ivanoff and Cherney 1960, Hopkins and Edgerton 1961, Wakimoto 1967), and by calibrating the camera for use underwater rather than in air. System calibration is a necessary requirement in order to use cameras for underwater photogrammetry, and is also an important step in the assessment of the accuracy and precision of a system.

A single camera, single exposure system can be used when only two-dimensional measurements on a planar or near-planar surface are required. For single camera, single exposure photography, the calibration is often derived using a reference scale in the field of view of the camera (Bergstedt and Anderson 1990, Barker *et al.* 2001, Pitcher *et al.* 2001,

Stokesbury 2002). This can be by way of a reference quadrat attached to the camera (Torlegard 1974, Fryer 1983, Williams and Leach 2001, Stokesbury 2002), projected laser marks (Barker *et al.* 2001, Pitcher *et al.* 2001), or some other form of scale (Collie *et al.* 2000, Willis and Babcock 2000, Parsons *et al.* 2004). Certain applications allow the camera to be mounted a set distance from the seafloor, such as on a sled, providing a standard field of view that can be calibrated to allow measurements (Martin and Martin 2002). Single camera, single exposure systems are generally limited to simple 2-dimensional measurements including length, planar area, and density estimates.

Multiple cameras or multiple exposure stations are used when three-dimensional measurements are required. A single-camera multiple-exposure system can be used to obtain 3-dimensional measurements provided sufficient information is known about the camera's interior orientation (focal length, image plane dimensions, lens distortions) and exterior orientation (camera position and orientation at each exposure station). The exterior orientation data can be known either by measuring the cameras' pitch, roll and rotation and position in a reference coordinate system (real world or other) (Green *et al.* 2002) or by deriving these values from the known location of control points in the field of view (Fryer and Done 1982, Tao and Hu 2002, Cocito *et al.* 2003). Single camera, multiple exposure systems are limited to stationary objects and they require the target object to maintain its position and geometry during multiple exposures.

Alternatively, simultaneous exposures from multiple cameras can be employed. Most commonly this photogrammetric solution involves a stereo camera (two cameras in a fixed geometry), however more than two cameras can be used in the case of complex objects. Stereo camera systems have been successfully employed in the measurement of highly mobile organisms (Klimley and Brown 1983, Bräger *et al.* 1999, Harvey *et al.* 2001), and also fine scale 3D modelling of targets (Hale and Cook 1962, Moore 1976, Doucette *et al.* 2001). Multiple camera systems with fixed geometry can be calibrated before measurement and then deployed in the field. This greatly reduces or eliminates the need for any control or reference targets in the field of view of the cameras, because accurate 3-dimensional measurements can be derived from stereo-photography acquired using a calibrated stereo-camera.

A summary of the types of camera systems used in underwater applications, and the types of measurements obtainable from these systems is provided in (Table 7.1).

Table 7.1. Summary of types of photogrammetric systems and the types of measurements obtained.

Number of Cameras	Number of Exposure	Scale	Use
Single	Single	Fixed frame or lasers	2D measurements
Single	multiple	Fixed scale object	3D measurement and models
Single	multiple	Fixed height from seafloor plus orientation information	2D measurement Image mosaic
Two (Stereo Video)	Single	Known Geometry and camera info	3D measurement
Multiple	multiple	Known camera geometry and camera info	3D measurement and model

The choice of an appropriate system will depend upon the specific application, including the types of measurements, accuracy, and whether 3D visualisation, or 3D models are required. 3D measurements are often the desired result of a photogrammetric solution. This may be simple measures of height, width and breadth, or the construction of 3D models. For 3D measurement and modelling, two or more exposures are required. A pair of images, such as from a stereo camera system, can be used to derive 3 dimensional measurements of a target. However, they cannot normally be used to create a 3 dimensional model of a solid object. This will require multiple exposures from a variety of locations surrounding the object. These may be multiple stereo pairs, which allows for stereo-viewing of the surfaces, or multiple single-exposures. As a general rule, increasing the number of images to cover the target from all angles will increase the accuracy and fidelity of the derived data (Eos Systems Inc 2000).

To make measurements from an image (image space), a point on the image must be related to a point in the real world (object space), either in 2 or 3 dimensions. For 2-dimensional measurement, this may only require a rescaling of the image, however lens calibration may be required. For 3-dimensional measurement, this will rely on knowing the internal geometry of the camera, and so it is necessary to use a calibrated camera.

Video cameras can be used to collect a continuous stream of single or stereo-camera images. This is advantageous when the targets are moving, are inaccessible to divers, or when the camera is remotely operated. Useful images from the recorded stream can be selected and processed. However, the use of video rather than still image cameras does present some challenges, especially the low resolution of video, typically 720 x 576 for a standard definition PAL camera (approximately 0.5 Megapixels), compared to 5 – 10 Mega pixels for a digital still camera at the time of writing. Video from digital video cameras is typically interlaced, where each frame is made up of two alternating frames known as fields, each containing half the information to make up a full frame. Each field will be separated in time based on the frame rate, in the case of PAL video $1/25^{th}$ of a second. Thus, if the camera or target moves during image acquisition, there will be artefacts apparent in the frames. There

are a number of processes that can be used to help reduce these artefacts when still-frames are captured off video. These normally either duplicate or interpolate one of the fields to hide the artefact – a process that generates a visually better image but that can introduce photogrammetric errors.

This final data chapter examines the characterisation of sponge community structure, which is at the modifier level of the hierarchical classification system (Chapter 1 Table 1.1). This chapter will investigate the capacity of a photogrammetric system to accurately measure morphometric features of sponges. These morphometric features will then be related to predefined functional groups (Bell and Barnes 2001) and also used to investigate the morphological differences in sponges between two sites.

7.2. Methods

7.2.1. Definitions

For consistency the following definitions and symbols have been adopted in this chapter.

Table 7.2. A list of definitions and symbols used in this chapter.

Symbol	Unit	Description
f	mm	focal length
x_p	mm	principal point x-coordinate
y_p	mm	principal point y-coordinate
K_1	-	radial lens distortion 1st component
K_2	-	radial lens distortion 2nd component
P_1	-	decentering lens distortion 1st component
P_2	-	decentering lens distortion 2nd component
r	mm	Radial distance from principal point
x	mm	x-image point
y	mm	y-image point
xc	mm	Corrected x-image point
yc	mm	Corrected y-image point
XL	mm	Exposure station position X-coordinate
YL	mm	Exposure station position Y-coordinate
ZL	mm	Exposure station position Z-coordinate
ω	degrees	Omega - Camera station rotation around x-axis
φ	degrees	Phi - Camera station rotation around y-axis
κ	degrees	Kappa - Camera station rotation around z-axis

7.2.2. Stereo video system design and construction

A stereoscopic video system was constructed for the photogrammetric measurement of sponge morphology. This system comprised a pair of Sony TRV22e video cameras in Amphibico underwater housings with standard 0.55x lens ports. The cameras were mounted in a rigid frame with a parallel orientation (Figure 7.1). The whole stereo video system was then mounted in a tow fish for field deployments. The stereo system was attached in the towfish so that the cameras were mounted in a near vertical orientation to the seafloor (approximately 75 degrees from the horizontal). This orientation was preferred to a directly

vertical orientation (90 degrees from the horizontal) as it allowed both the base and top of most targets to be recorded simultaneously in a single stereo pairs, thus allowing measurements of height to be made.

Figure 7.1. The stereo video system mounted inside a tow fish

The Sony TRV22e cameras were set up as shown in Table 7.3. These settings were checked at the start of each survey to ensure the system setup was consistent between surveys. The two cameras were mounted in the housings, which in turn were mounted in a fixed stereo video geometry.

The video footage between each of the cameras was synchronised using flashing LEDs, with a single red LED mounted in each of the housings. These LED's were mounted to the edge of the field of view (to the left for the left camera and the right for the right camera) so that they would not affect that part of the image used for the stereo measurement. A cable connection between the two housings linked these LEDs to a control circuit. This circuit was designed to flash the LEDs simultaneously for $1/25^{th}$ of a second every 10 seconds.

Table 7.3. Settings of the Sony TRV22e miniDV digital cameras as used in the calibration and surveys of sponge metrics.

Setting	Value
Focal Length in Housing (Max Wide Angle)	3.7 mm
Zoom	Set to maximum wide angle
CCD resolution (WxH)	720 x 576 pixels
CCD size (WxH)	3.7 x 2.7 mm
Focus	Manual, fixed
Exposure	Auto
Steady Shot	Off
Camera Base	0.35 m

Still images were captured from the video footage using the Adobe Premiere Version 6.02 (Adobe Systems Incorporated, USA) and a DVRaptor capture card (Canopus Co. USA). The

still images were captured as bitmap files and then Adobe Photoshop Elements (Adobe Systems Incorporated, USA) was used to remove the effect of video interlace from the images prior to importing into the photogrammetric software. The “Video de-interlace” filter was used to interpolate the odd field from the even field.

7.2.3. Camera Calibration

Camera calibration was conducted as a two-step process. Firstly each of the cameras used to construct the stereo camera system were calibrated separately to provide interior orientation information. The interior orientation accounts the ray path from the lens to the imaging plane of the camera and can be used to account for lens distortions. The stereo camera system was then calibrated for exterior orientation, which was used to “hardwire” the relative camera position into the photogrammetry software PhotoModeler Pro 4.0 (Eos Systems Inc. Canada). The exterior orientation is the relative orientation of each camera to a reference point, in the case of a stereo camera system this is the orientation of one camera to the other.

The individual cameras that were used to construct the stereo camera system were calibrated using Camera Calibrator 4.0 software, which is part of the PhotoModeler Pro 4.0 package. This program uses a calibration slide (Figure 7.2) as a reference surface that can be photographed and used with the calibration software. The calibration slide was printed onto waterproof A4 paper, and images of this printed copy were captured separately by each of the two cameras at an object distance of approximately 70 cm whilst submerged in a saltwater tank. The protocols outlined in the PhotoModeler Pro 4.0 manual (Eos Systems Inc. 2000) were used to acquire the calibration photos and perform the calibration. The results of the camera calibration were saved in a calibration file for each camera for subsequent use with PhotoModeler.

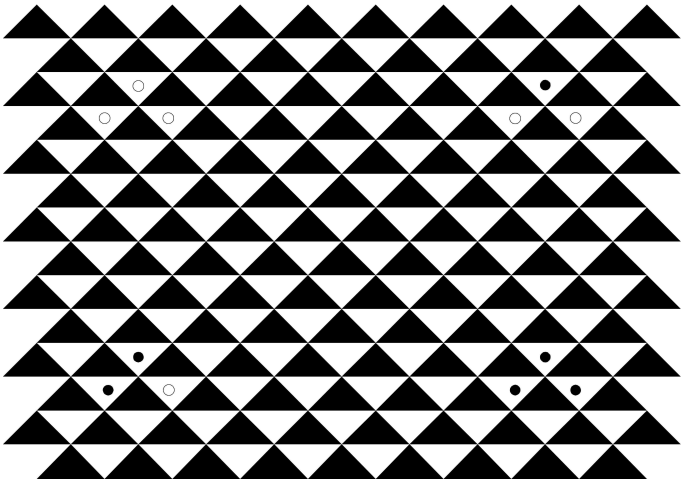

Figure 7.2. Calibration slide for use with Camera Calibrator 4.0 software to calculate camera calibration parameters (Eos Systems Inc 2000).

The Camera Calibrator 4.0 software was used to calculate the focal length, principal point coordinates, digitising scale, and lens distortion parameters for each camera. Lens distortion in PhotoModeler is described by a set of four values. Two of these (K_1 and K_2) describe the radial lens distortion, while the other two (P_1 and P_2) describe the decentering lens distortion (Eos Systems Inc 2000). The radial distortion is normally the major component of lens distortion. PhotoModeler uses an unbalanced formulation for radial lens distortion. This is given by:

$$dr = K_1 r^2 + K_2 r^4 \qquad \text{(Eos Systems Inc 2000)}$$

Where dr = radial distortion at a distance r from the principal point

r = radial distance from the principal point

K_1, K_2 = parameters of the radial lens distortion

Decentering lens distortion normally contributes a smaller amount to total lens distortion than radial distortion. Decentring distortion is described by:

$$\begin{aligned} dpx &= P_1(r^2 + 2x^2) + 2P_2 xy \\ dpy &= P_2(r^2 + 2y^2) + 2P_1 xy \end{aligned} \qquad \text{(Eos Systems Inc 2000)}$$

Where dpx, dpy = decentering lens distortion in x and y respectively

r = radial distance from the principal point

x, y = any given point in the image, where (0,0) is the principal point

P_1, P_2 = parameters of decentering lens distortion

PhotoModeler calculates the correction for any given point (x,y) on the imaging surface using the following:

$$\begin{aligned} xc &= x + drx + dpx \\ yc &= y + dry + dpy \end{aligned} \qquad \text{(Eos Systems Inc 2000)}$$

Where xc, yc are the corrected image point coordinates,

drx is the x component of the radial lens distortion correction,

dry is the y component of the radial lens distortion correction,

dpx is the x component of the decentering lens distortion correction, and

dpy is the y component of the decentering lens distortion correction.

7.2.4. Capture of stereo pairs

For both the stereo camera calibration exercises and the field surveys, the stereo camera system was deployed with the sync lights flashing and with both cameras set to record. The video from both cameras was captured to a computer hard drive using a DV Raptor capture card (Canopus), and Adobe Premiere 6.0 (Adobe) as AVI files using the Canopus DVRaptor DV codec. The video was captured as interlaced digital video with a frame rate of 25 frames per second and a video size of 720 x 576 pixels (native PAL DV format).

The video was synchronised based on the firing of the flashing sync lights. The *export still image* option of Adobe Premiere was used to export corresponding stereo pairs. As the recorded video was interlaced, the images were exported using the lower field first option as Windows bitmap files with the dimensions of 720x576 pixels. These images contained artefacts from the interlaced video. The effect of this video interlace was removed using the image processing package Photoshop Elements (Adobe). The Video De-Interlace filter was applied using the 'interpolate the odd field' setting. This resulted in the odd field being removed with the missing data then interpolated between adjacent even fields.

7.2.5. Estimated system precision

The precision of a stereo video system is related to the focal length of the cameras, the separation and orientation of the cameras, and the precision with which points appearing in each image can be measured in image space. The ability to precisely measure the location of a point on both images of the stereo pair is known as the pointing precision. Errors in pointing precision will result in increased X,Y and Z standard errors. The result of these errors will be more pronounced in the Z plane than the X and Y planes. The accuracy in X, Y, and Z can be estimated based on the following formulas (Abdel-Aziz 1974):

$$m_X = \frac{D}{C}\frac{(1+\tan\alpha\tan\phi)}{(1-\tan[\alpha-\phi]\tan\phi}m$$

$$m_Y = \frac{D}{C}\frac{\sec\phi}{(1-\tan[\alpha-\phi]\tan\phi}m$$

$$m_Z = \frac{D/C}{B/D}\sqrt{2}\frac{(1+\tan\alpha\tan\phi)}{(1-\tan[\alpha-\phi]\tan\phi}m$$

If the optical axes are parallel, then these formulas simplify to (Abdel-Aziz 1974):

$$m_X = \frac{D}{C} m$$

$$m_Y = \frac{D}{C} m$$

$$m_Z = \frac{\sqrt{2}D}{B} m_x$$

where m_X, m_Y, mz_z are the expected standard deviation in X, Y, Z object space co-ordinates,

m is the accuracy (estimated standard deviation) of a measured image coordinate,

C is the principal distance of the camera, for this propose equivalent to focal length f

D is the object distance to the central point of the object,

B is the camera base distance,

ϕ is half the convergence of the camera pair,

α is $\tan^{-1}(B/2D)$.

7.2.6. System Calibration and Validation

The stereo video system geometry was calibrated using a fixed calibration frame (Figure 7.3). This frame comprised a grid 5 x 5 points (5 mm diameter) separated by 75 mm in both the X and Y planes, with several of points extended in the Z plane. Four were extended 125 mm above the base plane, and the central point was extended 250 mm above the base plane. The calibration frame was deployed on the bottom of a saltwater tank, with the camera system held in water approximately 750 mm above the array. The synchronisation lights were activated and the cameras set to record the calibration frame to miniDV cassette for several minutes from a variety of different angles.

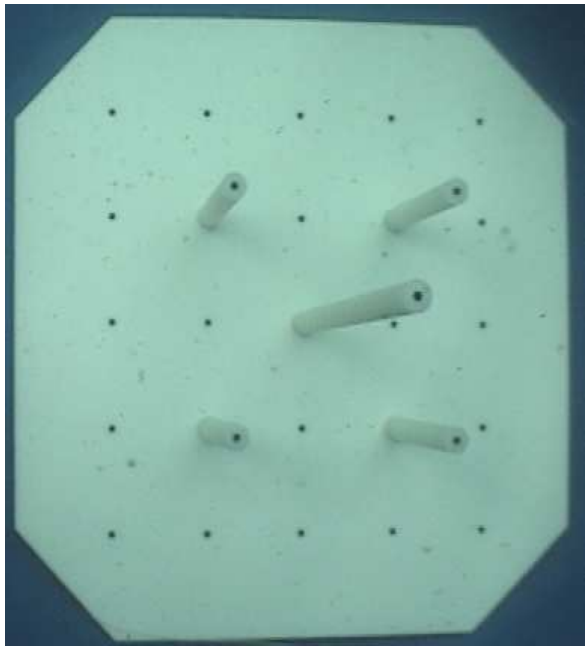

Figure 7.3. The fixed calibration frame used to calibrate the stereo video geometry in PhotoModeler.

Nine stereo pairs were selected from the calibration footage using the method outlined in section 7.2.4. These stereo pairs were selected to ensure that the calibration frame was imaged from a variety of angles and orientations. The stereo pairs were loaded into 9 separate PhotoModeler Pro 4.0 projects. The camera calibration files from the individual camera calibrations were used to provide camera information for both the images in the stereo pair. A control point file, giving the X, Y, and Z co-ordinates of the control frame was imported into the project. The 25 control points were then marked on each of the images using the sub-pixel marking mode. The project was processed for camera orientation, which determines the position and orientation of the cameras relative to the calibration frame (Figure 7.4).

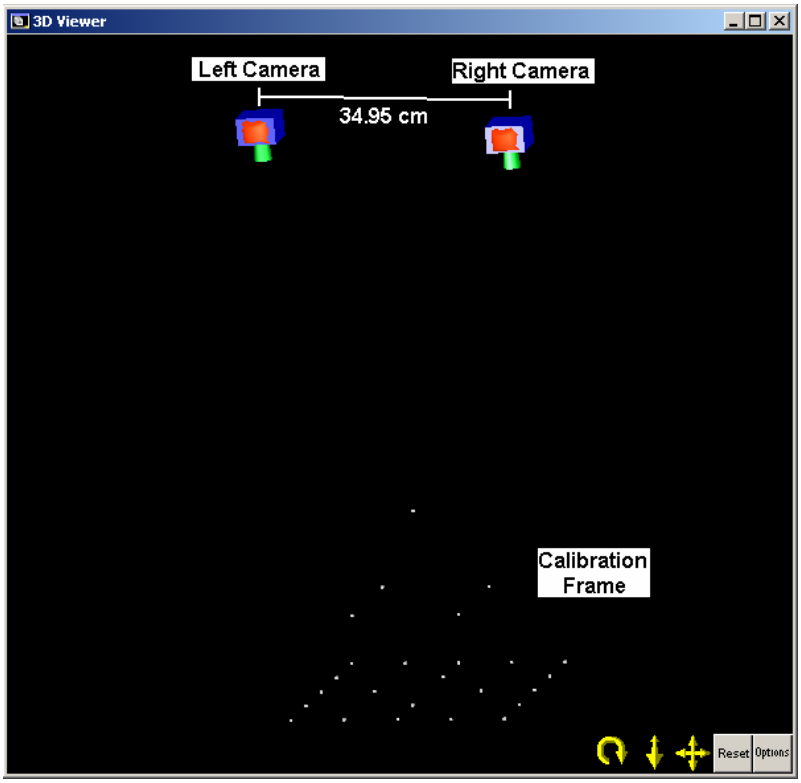

Figure 7.4. 3D view of stereo model showing the control points on the calibration frame and the calculated camera stations with associated camera separation distance (PhotoModeler Pro 4.0).

7.2.7. Measured system precision and accuracy

To test system precision the computed camera station information from six of the calibration projects was used to estimate the control point positions from one of the nine other stereo pairs (Table 7.4). To achieve this, the control points in each image were marked using the sub-pixel marker mode, however in this instance these points were not assigned the control frame X, Y, and Z co-ordinates. Instead the co-ordinates for these points were calculated in PhotoModeler based on the calibrated interior orientation (camera calibration) data and 'hardwired' exterior orientation (location and angular orientation) data. These calculated point co-ordinates were then exported to a text file for comparison. As these point co-ordinates were relative to the camera station they needed to be transformed into a consistent co-ordinate system for comparison. A least squares rigid motion transformation was run in MatLab 6.5 (The MathWorks Inc.) to fit the measured control points to the control frame X, Y, and Z co-ordinates. This routine solved for 3 rotations and 3 translations around the X, Y and Z axis using a least squares rigid motion.

Table 7.4. Calibration model and corresponding stereo pairs used for comparison of calibration stability.

Model	Stereo Pair
1	5
2	3
4	1
6	8
7	9
8	4

The precision of the camera system was assessed by repeated measurement of the position of the 25 points of the calibration frame using the calibrated system in PhotoModeler4.0. For one of the stereo pairs each point was marked and measured 6 times with the resulting point co-ordinates exported for comparison.

7.2.8. Field Surveys

Field surveys were conducted at two locations. The first site was off Babel Island on the North East coast of Flinders Island (Figure 7.5). This site was on soft sediment in approximately 38 m water depth. The second site was off Rocky Cape (Figure 7.5). This site was on reef in approximately 24 m water depth.

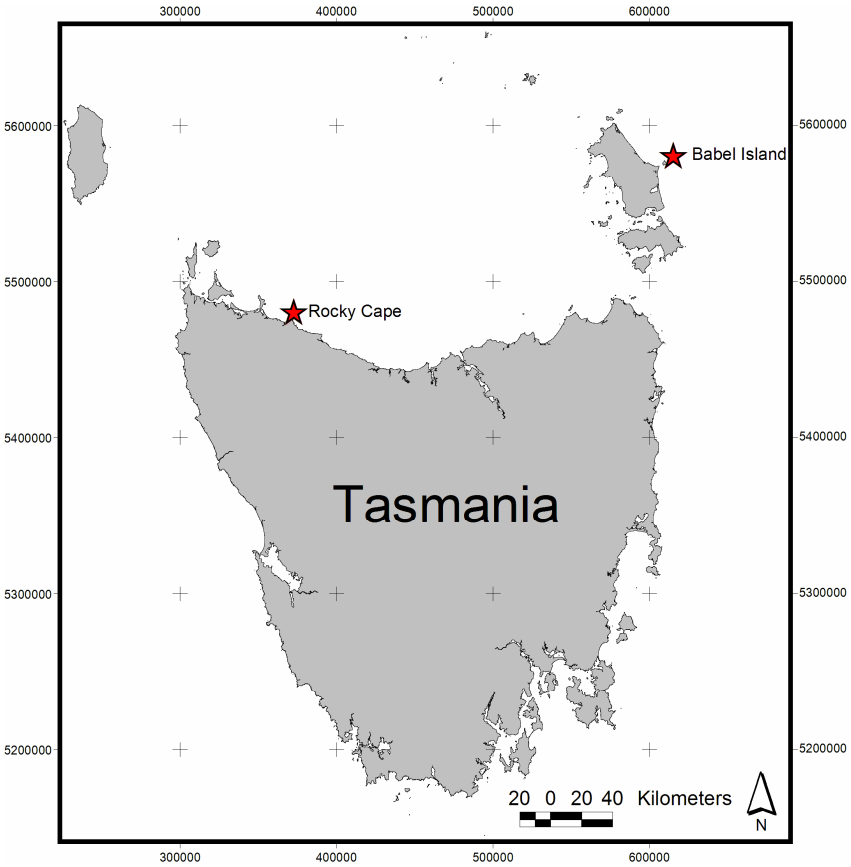

Figure 7.5. Map of Tasmania showing two field survey sites at Rocky Cape and Babel Island.

Prior to deployment at each site the camera system was setup and the calibration frame recorded to monitor the system stability. The system was then left intact until deployment. At

each site the camera system was lowered to the seafloor using an electric winch and held approximately 1 m above the seafloor. The system was left to record for approximately 1 hour, while the vessel was allowed to drift. A separate underwater video camera on an umbilical was attached to the stereo system to provide real-time images to the vessel. This was used to ensure the camera system was an appropriate height from the seafloor and that suitable sponge habitat was present. Artificial lighting was provided by a pair of 50 W halogen lights mounted off axis to reduce backscatter from particulate matter in the water column.

7.2.9. Measurement of sponges

At each site 100 stereo video pairs were processed in PhotoModeler 4.0 using the parameters from the camera calibration to hardwire the system geometry. Each sponge was visually classified into one of the 9 morphological variants described by Bell and Barnes (2001) (Figure 7.6). For each sponge a series of metrics were then measured including height, width, branch lengths and angles (Table 7.5).

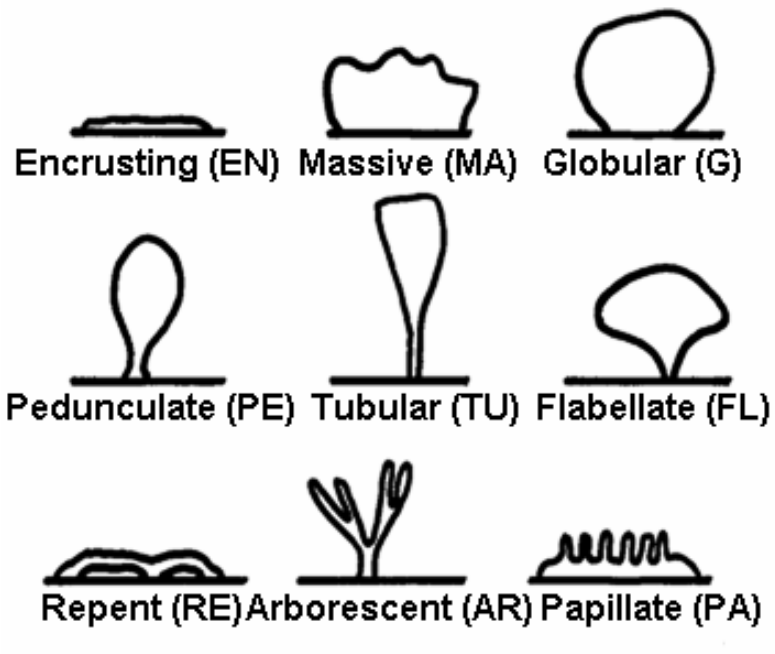

Figure 7.6. Nine morphological variants described by Bell and Barnes 2001

Table 7.5. Sponge metrics measured in PhotoModeler

Metric	Description
Growth Habit	EN,MA,G,PE,TU,FL,RE,AR,PA (see Figure 7.6)
Height	Maximum height from the sea floor
Width	Maximum width
Width of base	The width of the attachment to the sediment
Branching	Yes/No
Primary/secondary branching	Primary/Secondary
Number of Branches	Count of total branches
Length of trunk	Length of trunk for branching sponges
Length of primary Branch	Average length of primary branch
Width of primary branches	Average measure of the width of the primary branches at the widest point mid way up the branch
Width to depth ratio of primary branches	The ratio of the width of the branches to the depth at the mid point of the primary branches
Primary Branching Angle	Average branching angle of primary branches
Length of secondary Branch	Average length of secondary branches
Width of secondary branches	Average measure of the width of the secondary branches at the widest point mid way up the branch
Width to depth ratio of secondary branches	The ratio of the width of the branches to the depth at the mid point of the secondary branches
Secondary Branching Angle	Average branching angle of secondary branches
Number of pores	Count of the number of visible pores
Width of pores	Average width of pores
Colour	The RGB (Red, Green, Blue) colour value

7.2.10. Analysis of functional structure

Of the nine morphological variants described by Bell and Barnes (2001) eight were observed in this study, with papillate sponges absent. Of these remaining eight variants, pedunculate sponges were only observed on one occasion so have been removed from the analysis. All of the remaining seven variants were present at the Babel Island survey site, with only five present at the Rocky Cape site (Arborescent, Flabellate, Globula, Massive, and Tubular). Discriminant analysis in JMP (SAS Institute) was used to examine the relationship between the measured metrics and the functional groups. Discriminant analysis is a method of predicting some level of a one-way classification based on known values of the responses. The technique is based on how close a set of measurement variables are to the multivariate means of the levels being predicted.

The community composition data was compiled from three sub-sites at each location based on the classification of functional morphology from the stereo video system. Paired T-tests were used to examine differences in the mean composition of each functional group between the two locations. For the functional groups that occurred at both of the sample sites, a comparison of the metrics was used to investigate differences in the gross morphology

between the two sites. Analysis of variance (ANOVA) was used to examine for differences in growth and branching metrics.

7.3. Results

7.3.1. Camera Calibration

The magnitude of the radial lens distortions for each of the cameras was similar, with the left camera showing only slightly higher distortions than the right camera (Figure 7.7). The radial distortion was typically less than 50 μm within 1.5 mm of the principal point, increasing to a maximum of up to 100 μm at the edge of the imaging array.

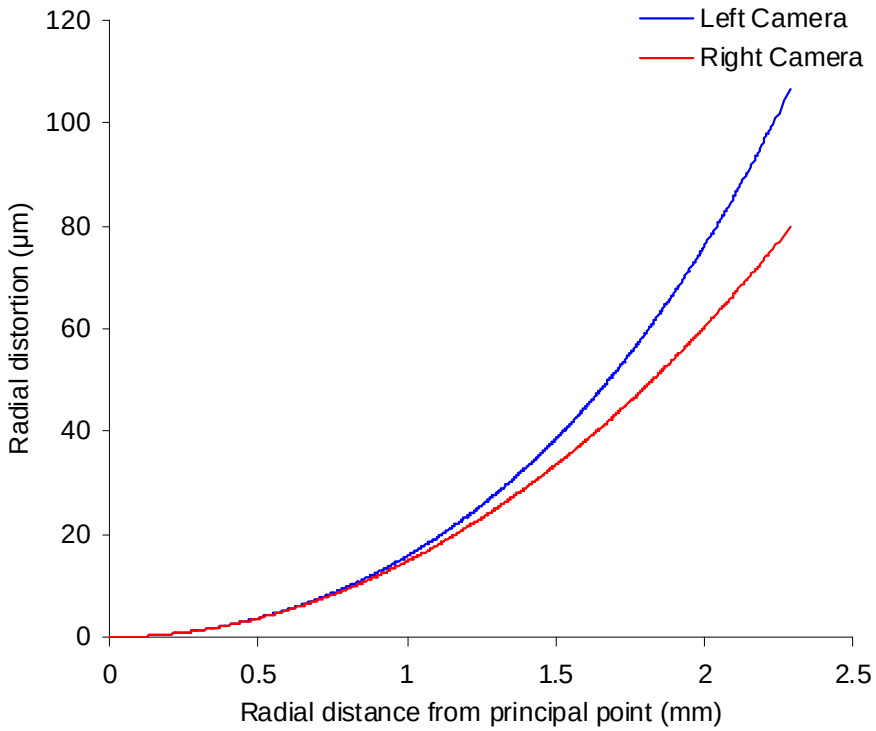

Figure 7.7. Radial distortion for left and right cameras based on Camera Calibration 4.0 calculations

A summary of the camera calibration results for the left and right cameras is provided in Table 7.6

Table 7.6. Summary of camera calibration results from Camera Calibrator 4.0 for the left and right stereo video cameras.

Parameter	Left Camera	Right Camera
Focal Length (mm)	3.2147	3.2868
Format Width (mm)	3.6908	3.7133
Format Height (mm)	2.7	2.7
Principal Point *x* (mm)	1.8481	1.8178
Principal Point *y* (mm)	1.3316	1.3534
K_1	0.0147	0.01462
K_2	0.001069	0.0001075
P_1	-0.0019	0.0003304
P_2	0.00075	0.0003537

The predicted precision of the stereo system is affected by the camera separation (camera base)

and the pointing precision. Changes in camera base have two effects, firstly the amount of overlap between adjacent photos decreases with increasing camera base. At an object distance of 1 m, a camera base of 0.1 m will give an overlap of 90%, while a camera base of 0.55 m will give an overlap of 43%. The region of overlap dictates the size of the resulting stereo model, with an overlap between 60 and 80% commonly used. The x and y accuracy remains fixed regardless of the camera base for a fixed object distance, while the z accuracy is a function of the camera base (Figure 7.8).

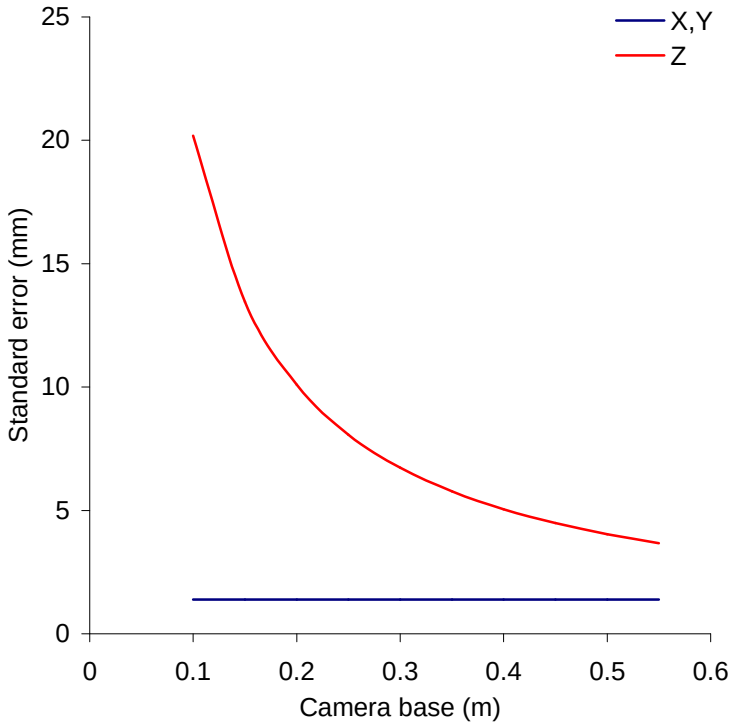

Figure 7.8. Predicted accuracy m_x, m_y and m_z (standard error) of the stereo video system for camera base distance between 0.1 and 0.55 m and object distance of 1 m and pointing precision of 1 pixel.

The Z precision increases with increasing camera base, but with a reduced stereo-overlap and a smaller volume within which 3-dimensional measurements can be acquired. The optimal camera base will thus be where the Z precision falls within an acceptable range, whilst still maintaining a sufficient stereo model size (Figure 7.9). For this system, at an object distance of 1 m and a pointing precision of 1 pixel, camera bases between 0.2 and 0.4 m will result in a stereo model with greater than 60% overlap and a Z standard error (m_z) of less than 10 mm.

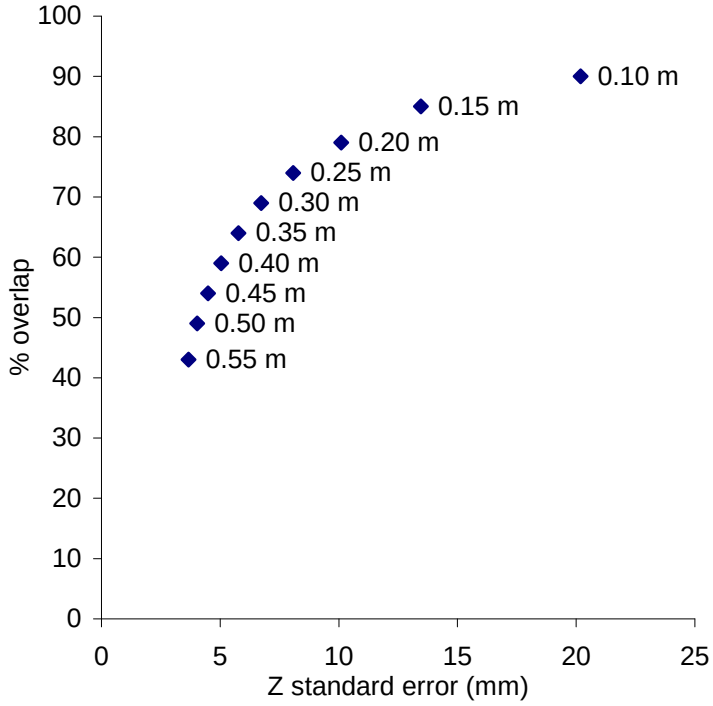

Figure 7.9. Predicted Z standard error (m_z) as a function of image overlap (%) for camera bases between 0.1 m and 0.55 m (labels) and an object distance of 1 m and a pointing precision of 1 pixel.

Degrading the pointing precision from 1 pixel to 2 pixels resulted in a doubling in the Z standard error while increasing it to 10 pixels resulted in an order of magnitude increase in the Z standard error from 13.5 mm to 135 mm (Figure 7.10). The X and Y standard error increased in the same manner, however a pointing precision of 10 pixels still resulted in predicted X and Y standard errors less than 14 mm (Figure 7.10).

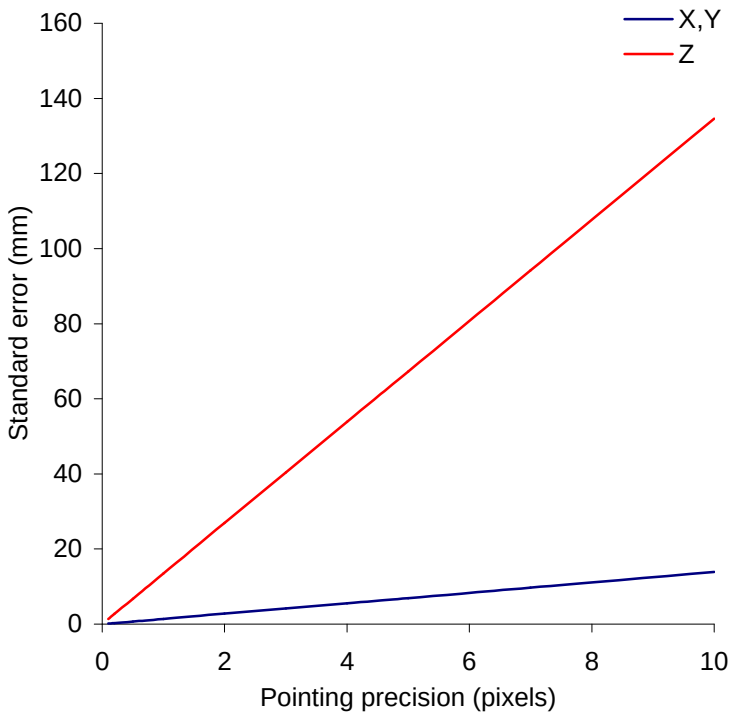

Figure 7.10. Predicted x, y and z accuracy of stereo video system for pointing prescision between 0.1 and 10 pixels, with camera base 0.35 m and object distance of 1 m.

Based on the above considerations, the stereo video system was set up with a 0.35 m camera base. This system was then calibrated to derive interior and exterior orientation parameters and to provide an empirical estimate of the system's precision and accuracy.

7.3.2. System Validation

The exterior orientation of the system was calculated using a rigid frame, and computed in PhotoModeler. This information was used to 'hardwire' the exterior orientation of the stereo video system in PhotoModeler. A series of nine calibration trials were conducted, each produced different relative camera station information based on the orientation of the calibration frame to the camera system. A comparison of the camera separation distance for each of these calibration projects showed this to be highly consistent, 34.95 cm ± 0.5 mm (average ± S.E.).

The data from the nine calibration trials was then used to assess the accuracy of the system. Exterior orientation information from six of the trials was used to calculate the position of the control points from the randomly selected photos from one of the other trials. To allow comparison of the results a least squares rigid motion transformation was used to align the measured control point data. The average error on the control points following transformation was 1.41 mm ± 0.09 mm, with the maximum error for any single control point 3.07 mm ± 0.42 mm. The greatest error was for those points that extended into the Z plane, which is to be

expected (Table 7.7).

Table 7.7. Summary of stereo video system accuracy assessment using fixed calibration frame.

Control Point ID	X	Y	Z	Average Error (mm)	Standard Error (mm)
1001	0	0	0	1.22	0.32
1002	7.5	0	0	0.89	0.25
1003	15	0	0	1.11	0.16
1004	22.5	0	0	1.04	0.25
1005	30	0	0	1.45	0.34
1006	0	7.5	0	1.08	0.32
1007	7.5	7.5	12.5	3.07	0.42
1008	15	7.5	0	0.42	0.14
1009	22.5	7.5	12.5	1.91	0.41
1010	30	7.5	0	1.03	0.30
1011	0	15	0	1.19	0.32
1012	7.5	15	0	1.72	0.21
1013	15	15	25	2.35	0.86
1014	22.5	15	0	0.86	0.28
1015	30	15	0	1.05	0.23
1016	0	22.5	0	1.47	0.35
1017	7.5	22.5	12.5	1.03	0.12
1018	15	22.5	0	1.59	0.63
1019	22.5	22.5	12.5	2.43	0.53
1020	30	22.5	0	1.09	0.19
1021	0	30	0	1.99	0.30
1022	7.5	30	0	1.14	0.35
1023	15	30	0	1.22	0.24
1024	22.5	30	0	1.26	0.00
1025	30	30	0	1.33	0.50
			Total	1.41	0.09

The repeatability of measurements obtained from the system was used to estimate the precision. The precision was calculated as the maximum measurement error in X, Y, and Z based on six repeated measurements of the control frame (Table 7.8).

Table 7.8. Maximum measurement error (mm) in the X, Y, and Z dimensions based on repeated marking of targets.

X	Y	Z
0.31	0.68	0.96

7.3.3. Field measurements of functional groupings

Of the nine functional groupings described in Bell and Barnes (2001), seven of these were observed and measured across the two study sites (Table 7.9). The most common functional group was the arborescent sponges, which represented approximately 40% of all the sponges. The least common functional groupings were the repent and tubular which each represented less than 5% of all the sponges. Large variations in the gross sponge morphometric measures were observed both within and between all functional groups (Table 7.9). Branching was

observed in the majority of arborescent sponges (93.2%), and a small proportion of massive sponges (8.0%), with only one specimen of tubular sponge exhibited branching. Visible pores (osculum/ostium) were observed on all tubular sponges (100%), slightly over half globular sponges (57.1%) and approximately one third of massive sponges (32%).

Table 7.9. Summary of sponge metrics (mean and standard deviation) by functional grouping based on stereo video measurement (AR = arborescent, EN = encrusting, FL = flabellate, G = globular, MA = massive, RE = repent, and TU =tubular).

Metric	AR	EN	FL	G	MA	RE	TU
No. Observations	88	24	24	28	50	10	8
Height (cm)	25.2 ± 14.2	2.8 ± 2.7	14.9 ± 7.5	6.6 ± 4.2	11.9 ± 10.1	2.9 ± 2	7.7 ± 4.7
Width (cm)	17.8 ± 12	11.4 ± 4.5	18.9 ± 9.7	10.1 ± 4.9	12.9 ± 6.3	17.7 ± 7.4	14.6 ± 14.9
Breadth (cm)	8.2 ± 9.7	9.4 ± 3.2	6.6 ± 8.6	8.2 ± 4.8	6.6 ± 4.9	6.1 ± 3.5	6 ± 5.5
Width of Base (cm)	6.4 ± 4.4	11.9 ± 4	7.5 ± 4.9	10.7 ± 8.6	10.7 ± 6.7	15.6 ± 6.5	13 ± 15.7
% Sponges with Branching (%)	93.2	0	0	0	8.0	0	12.5
% Sponges with Pores (%)	0	0	0	57.1	32	0	100
RED	168.4 ± 40.2	171.8 ± 29.7	129.2 ± 46	152.3 ± 53.5	184.8 ± 40.6	165.8 ± 25.6	170.3 ± 13.4
GREEN	137.1 ± 26.1	130.1 ± 28.3	116.1 ± 22.7	153.8 ± 39.5	142.6 ± 27.7	123.4 ± 23.9	138 ± 9.2
BLUE	115.4 ± 25.4	110.3 ± 23.9	100.6 ± 20.3	118.9 ± 29.4	102.4 ± 40.1	104 ± 15.6	106 ± 14.2

Of those sponges that exhibited branching, the majority exhibited only primary branching (Table 7.10). Secondary branching was only observed in the arborescent functional group (23.4%). Average primary branch length was longer in the arborescent functional group than in the globular or tubular functional groups, however this difference was not significant. There was little difference in the average width of the branches or the average branching angle between any of these functional groups. Average branching length, average branching width and average branching angle showed no significant difference between the primary and secondary branching.

Table 7.10. Summary of branching metrics by functional grouping for all sponges exhibiting primary and/or secondary branching (AR = arborescent, G = globular, and TU =tubular).

Metric	AR	G	TU
% Primary Branching	75.6	100	100
% Secondary Branching	23.4	0	0
Number of Branches	8.1 ± 7.3	6.5 ± 1.8	7 ± 0
Primary Branch Length	14.6 ± 7.6	4.9 ± 1.8	2.7 ± 0
Primary Branch Width	2.3 ± 1.5	2.8 ± 0.7	1.3 ± 0
Primary Branching Angle	37.1 ± 29.6	35.1 ± 32.1	34.7 ± 0
Secondary Branching Length	11.6 ± 9	-	-
Secondary Branching Width	2.6 ± 2.5	-	-
Secondary Branching Angle	44.9 ± 41.9	-	-

Three of the functional groupings had visible pores (globular, massive and tubular), however there were no significant differences in the means of either the number of pores or the width of the pores between these groups (Table 7.11).

Table 7.11. Summary of pore metrics for all sponges with visible pores by functional grouping. (AR = arborescent, G = globular, and TU =tubular).

Metric	G	MA	TU
Number of Pores	9.9 ± 10.0	5.0 ± 2.4	8.8 ± 8
Width of Pores (cm)	1.0 ± 0.8	0.7 ± 0.3	1.1 ± 0.5

The discriminant analysis using the 19 morphological metrics, and a further four derived metrics showed varying degrees of separation of the seven morphometric sponge types (Figure 7.11). The arborescent variant showed the greatest separation from the other groups, with the flabellate variant also separating out. The remaining variants had a high degree of overlap when using the 19 morphological metrics. Canonical 1 described 76.6% of the variation, while Canonical 2 described a further 12.4% of the variation, with 100% of the variation described by the first 6 canonicals. Canonical 1 had strong positive correlations with sponge branching, and whether a sponge displayed primary/secondary branching, and strong negative correlation with secondary branch width. Canonical 2 had strong positive correlations with the width of pores on the sponge and whether a sponge displayed primary/secondary branching and a strong negative correlation with sponge branching.

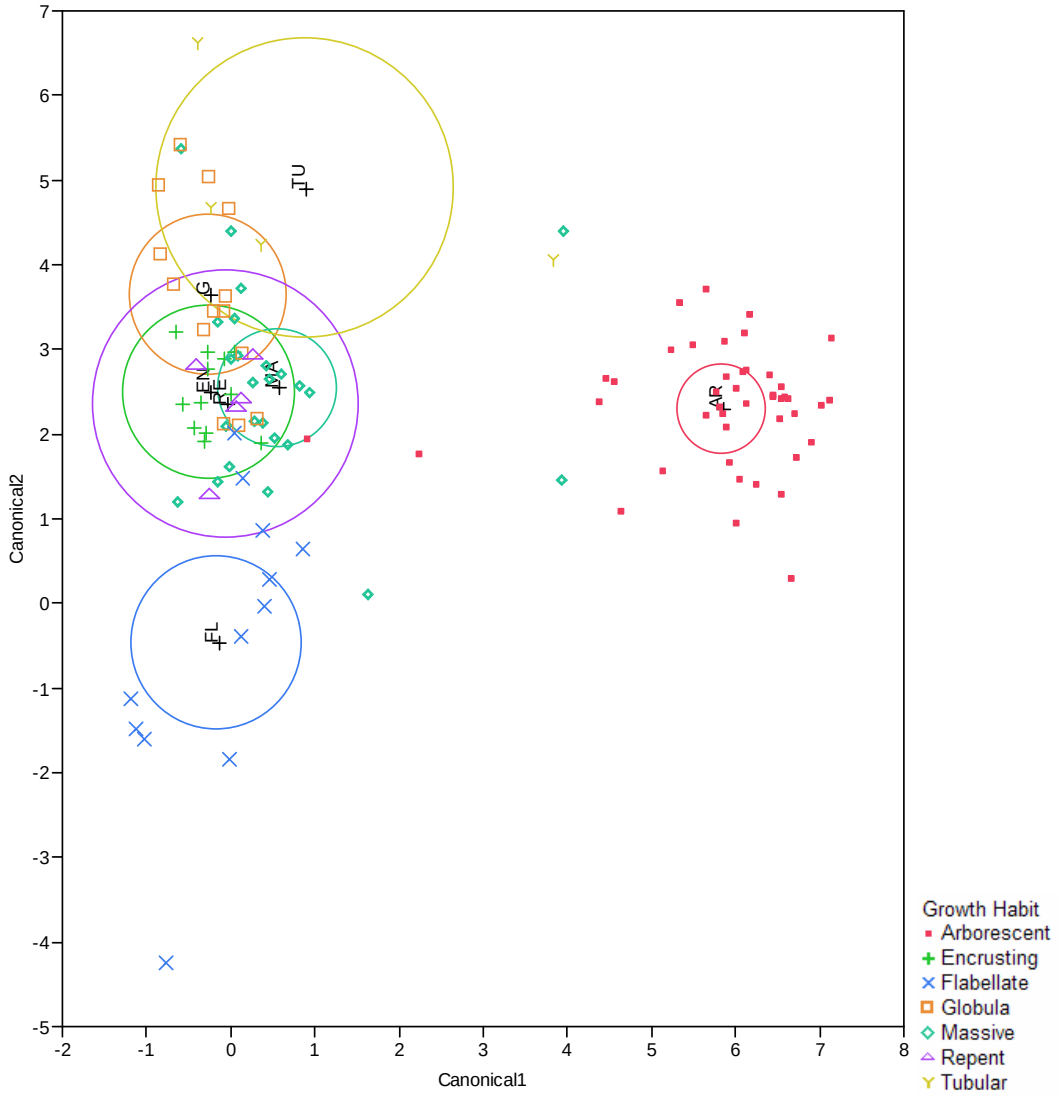

Figure 7.11. Results of discriminant analysis showing the separation of the seven morphological variants based on the 19 morphometric measurements. The coloured ellipses represent mean confidence limit

Overall classification accuracy based on the discriminant analysis was 76.7%. Comparison of the classification accuracy of the seven morphological variants by comparing the actual class with the predicted class from the discriminant analysis showed classification success greater than 80% for the arborescent, encrusting, flabellate and repent variants (Table 7.12). The remaining 3 variants had between 56 and 75% classification success. Of these three, the globular and massive variants were commonly classified as encrusting (28.6% and 12.0% respectively), the tubular variant was also commonly classified as globular (25%). The repent variant, whilst classifying correctly 80% of the time, also classified as encrusting 20% of the time.

Table 7.12. Actual versus predicted morphological variant matrix for the seven morphological variants based on discriminant analysis.

		Predicted						
		Arborescent	**Encrusting**	**Flabellate**	**Globular**	**Massive**	**Repent**	**Tubular**
Actual	**Arborescent**	95.5	0.0	0.0	0.0	4.5	0.0	0.0
	Encrusting	0.0	83.3	0.0	0.0	8.3	8.3	0.0
	Flabellate	0.0	8.3	83.3	0.0	8.3	0.0	0.0
	Globular	0.0	28.6	0.0	57.1	7.1	0.0	7.1
	Massive	8.0	12.0	0.0	8.0	56.0	8.0	8.0
	Repent	0.0	20.0	0.0	0.0	0.0	80.0	0.0
	Tubular	0.0	0.0	0.0	25.0	0.0	0.0	75.0

7.3.4. Comparison of sponges at two sites

The sponge communities at the two sites surveyed differed markedly in their functional group composition (Figure 7.12). The soft sediment site at Babel Island was dominated by arborescent sponges, with a lesser amount of massive and encrusting sponges, while the consolidated sediment site at Rocky Cape was dominated by a mix of globular, massive and, to a lesser extent, arborescent and flabellate sponges. Encrusting and repent sponges were found at Babel Island but were not observed at Rocky Cape. Significant differences in the percentage composition were observed for arborescent, encrusting, globular, massive and repent sponges between the two sites.

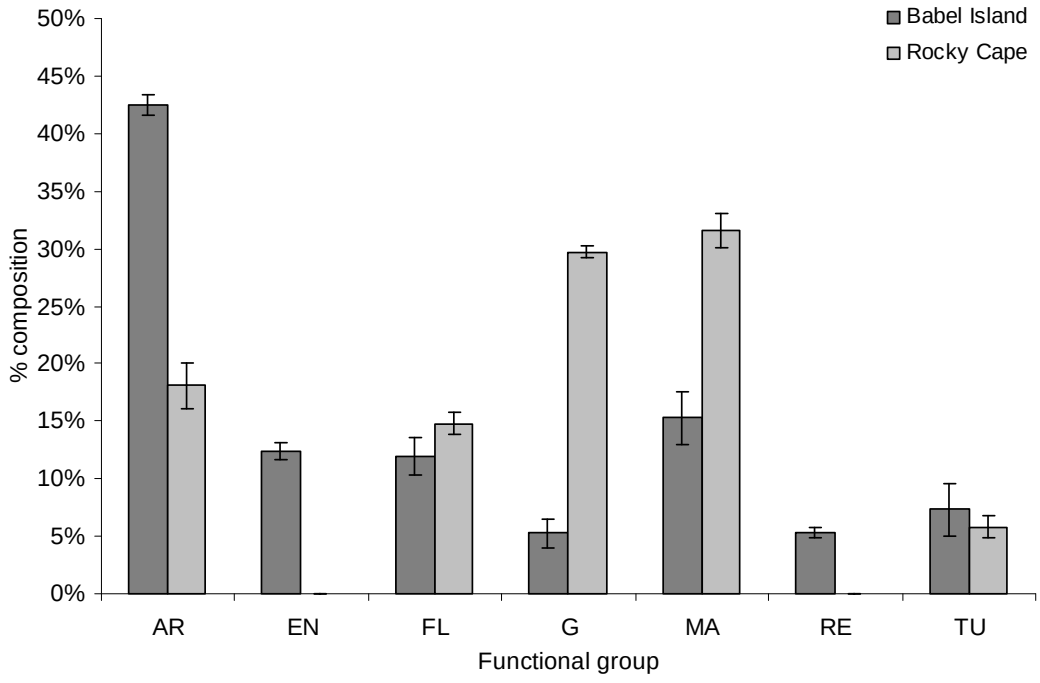

Figure 7.12. Mean percentage composition of sponge functional groups at the two surveyed sites (AR = arborescent, EN = encrusting, FL = flabellate, G = globular, MA = massive, RE = repent, and TU =tubular). Error bars give standard error

Comparison of the morphometric measurements of the four most common functional groups between the two sites showed general differences (Table 7.13). The average height of the arborescent, flabellate, and massive functional groups were greater at the Babel Island site,

with the average height of the globular functional group greater at the Rocky Cape site. Similarly, differences were observed in the average width, breadth, and width of base between groups at the two sites. Significant differences in the means were observed between the two sites for the breadth of flabellate sponges, and for the height, width, and width of the base for massive sponges.

Table 7.13. Mean and standard deviation of the metrics: height, width, breadth and width of base for two sites (Babel Island and Rocky Cape) as measured by photogrammetric analysis of stereo video (AR = arborescent, FL = flabellate, G = globular, and MA = massive). (* indicates significant difference at p = 0.05).

	Data Set	AR	FL	G	MA
Height	Babel Island	26.3 ± 14.5	17.6 ± 7.6	5.1 ± 2.7	14.4 ± 10.7*
	Rocky Cape	16.6 ± 7.9	9.4 ± 3.4	8.2 ± 5	5.6 ± 4.1
Width	Babel Island	18.2 ± 12.5	15.3 ± 6.5	8.2 ± 3.4	14.9 ± 6*
	Rocky Cape	14.6 ± 6.8	26.3 ± 11.9	12 ± 5.8	7.6 ± 3.5
Breadth	Babel Island	8.2 ± 10.2	2.2 ± 1.3*	6.6 ± 3.7	7.4 ± 5.4
	Rocky Cape	8.1 ± 5	15.6 ± 10.3	9.7 ± 5.6	4.4 ± 2.5
Width of Base	Babel Island	6.7 ± 4.5	6.5 ± 2.8	8.4 ± 3.3	12.6 ± 6.6*
	Rocky Cape	4.3 ± 3.2	9.6 ± 7.9	13 ± 11.7	5.9 ± 4.1

The branching morphology of the arborescent group was also compared between the two sites. Secondary branching was more common at the Rocky Cape site, 40% compared to 12.8% at Babel Island. The mean number of branches was higher at Rocky Cape, however there was large variation, especially at Babel Island. The average branching length, width and branching angles for both primary and secondary branches showed little difference between the sites, with a large amount of standard deviation in all these metrics.

Table 7.14. Comparison of branching morphology statistics (average and standard deviation) for arborescent sponges at Babel Island and Rocky Cape.

Metric	Babel Island	Rocky Cape
% Primary Branching	87.2%	60.0%
% Secondary Branching	12.8%	40.0%
Number of Branches	7.4 ± 7.4	13 ± 4.5
Primary Branch Length	13.9 ± 8.5	11.7 ± 6.1
Primary Branch Width	2.1 ± 1.6	1.5 ± 0.7
Primary Branching Angle	35 ± 31.7	24 ± 8.1
Secondary Branching Length	2.2 ± 6.2	4.1 ± 5.6
Secondary Branching Width	0.5 ± 1.6	0.7 ± 1.1
Secondary Branching Angle	8.2 ± 25.7	7.6 ± 10.4

7.4. Discussion

The role of sponges in marine ecosystems is often overlooked in research, monitoring and conservation programmes (Bell 2008). Information on sponge biodiversity is required for conservation planning issues such as marine protected area planning. Studies on sponge biodiversity in eastern Australia have shown that both species richness and taxonomic composition are highly heterogeneous over small spatial scales (10's of kilometres) and are also affected by factors including depth and distance from the coast (Roberts and Davis 1996,

Hooper and Kennedy 2002). In Tasmanian waters, sponge distribution has been documented at a broad scale in Bass Strait (Butler *et al.* 2002), and also in targeted mapping (Jordan *et al.* 2005b), however the distribution of sponge biodiversity has not been examined. As functional morphology has been shown to be a useful surrogate for species diversity in both temperate and tropical studies (Bell and Barnes 2001, Bell and Barnes 2002), the methods developed in this chapter present the possibility of incorporating diversity in sponge functional morphology into marine conservation planning.

This chapter investigated the use of stereo video to measure sponge metrics, and subsequent capacity to assist in defining sponge functional morphology. The chapter consisted of two parts, accuracy assessment of the stereo system, and field measurement of sponge morphology. A stereo camera system was developed using low cost consumer grade digital video cameras.

Based on the algorithms of (Abdel-Aziz 1974), the expected accuracy of the stereo video system developed for this study was approximately 1 mm in the X and Y planes and 5 mm in the Z plane (object distance of 1 m and pointing precision of 1 pixel). Tank based calibration and accuracy assessment of the system showed error values within this range. The repeated calibration of this system showed very little variation in the geometry and calibration parameters of the system. Stereo video systems have previously been shown to be stable both within and between deployments (Harvey and Shortis 1998). The stereo video system used throughout this study was maintained in a rigid frame, with the camera housing permanently attached.

One of the major operational considerations in designing a stereo video system is matching the accuracy of the system to the scale of measurement required. This is a balancing act between the resolution of the cameras used, the size of the target organisms and the required field of view. This study chose to construct a system using digital video cameras as opposed to still cameras. This was primarily due to the nature of the target organisms. Due to the depth of the sponge beds, diving was not a feasible option for data collection. Thus the system had to be remotely operated. The use of video allowed a large number of stereo pairs to be collected (25 per second), which allowed stereo pairs to be selected to maximise their usefulness. A pair of still cameras would have increased the resolution of the images but result in far fewer stereo pairs to select appropriate pairs for measuring.

One of the challenges in designing this system was matching the scale of the cameras system geometry with that of the targets. Sponges within both study sites varied in size from <5cm to

75 cm in height, meaning the system required the capacity to make accurate measurements across this range. The camera base is one of the critical factors in determining the precision of measurement of any such system, with a larger camera base improving the overall measurement precision (Shortis *et al.* 2001). Countering this is a reduction in the area covered by the stereo model at close ranges. Thus determining an appropriate camera base is critical in the design of a stereo camera system. Theoretical estimates provided by the algorithms of (Abdel-Aziz 1974) proved useful in determining the appropriate settings, with tank based trials supporting these predictions.

The sponge measurements collected in this study were not an exhaustive list of possible measurements. These were selected as they represent broad morphological metrics and were easily measured on most stereo pairs. It is well known that multiple convergent photos gives the optimum accuracy in close range photogrammetry (Chong and Stratford 2002). The use of a single pair of cameras limits the capacity to make accurate measures across all dimensions because not all of a sponge will be visible in a single stereo pair.

Of nine functional groups outlined by (Bell and Barnes 2001), seven were encountered within this study. For some groups, including the arborescent, encrusting, flabellate and repent, greater than 80% were successfully predicted based on discriminant analysis, while, for other groups, including the globular and massive this was between 50 and 60%. These low accuracies may be a reflection of two main factors. Firstly the metrics chosen may not be diagnostic for a particular group, for example tubular sponges consisting of one or a series of long sponge fingers with a large terminal pore. Whilst this may be easy to visually determine, creating a series of metrics to differentiae this from other sponge variants is more problematic. Secondly, and possibly more importantly, is the plasticity in sponge morphology (Ackers *et al.* 1992, Bell and Barnes 2000c, Bell and Barnes 2001). The morphology of a single particular species has been shown to vary in relation to factors including bathymetry and flow regime (Bell and Barnes 2000c). This can create difficulties in attributing a sponge to a single particular functional group. Sponges may often display traits of one or more of the functional groups, and often it can become a subjective decision when trying to visually classify a sponge into one of these groups. The use of the stereo-video techniques from this chapter has the advantage that classification can become a more objective process.

Sponge communities at two locations were classified using these methods. These locations were characterised by differences in substrate, depth and exposure. Overall there was found to be a significant difference in composition of functional groups between the two sites.

Environmental factors including depth, exposure, and flow regime have previously been shown to affect the distribution of sponge morphological diversity (Bell and Barnes 2000c). Sponges communities on the east coast of Australia have been shown to increase in species richness with increasing depth, particularly in the case of erect or massive species (Roberts and Davis 1996). This was the case for the large arborescent sponges in this study, with this group more common at the deeper site at Babel Island. The large erect arborescent, flabellate and massive sponges were also found to be larger at Babel Island, than the shallower Rocky Cape location. Similar trends have been shown on hard substrates, presumably due to increased turbulence due to wave action in the shallower depths adversely affecting these larger erect sponge growth types (de Kluijver 1993).

Interestingly encrusting sponges were only encountered at the soft sediment site at Babel Island and not on the reef substrate at Rocky Cape. Generally encrusting sponges are more abundant in shallow depths, where they can better cope with the turbulence, and decrease in deeper water where they may be more susceptible to smothering by sedimentation (Peattie and Hoare 1981, Roberts and Davis 1996). While depth is often a strong structuring factor, there are other factors that can influence the distribution of sponges. For example distance from the coast has been shown to influence sponge species diversity, with an increase in diversity with distance from the coast reported in a number of studies (de Voogd *et al.* 1999, Hooper and Kennedy 2002). Sponge communities close to the coast may be subject to including increased nutrients and siltation from land based runoff. In this study the Rocky Cape site was directly on the coast, while the Babel Island site was ten kilometres offshore, which may mean there is more sedimentation at the Rocky Cape site resulting in the absence of encrusting sponges.

7.5. Conclusion

The classification of sponge functional morphology as a surrogate for species diversity provides a pathway for more easily including information about sponge biodiversity in marine conservation planning. The techniques developed within this chapter have shown that a simple stereo video system can provide accurate and useful measurements of sponge morphology that can be used to assist in the classification of functional morphology. This will allow sponge beds to be classified at lower levels of the classification hierarchy. The methods described in this chapter can provide additional information, such as sponge size, which would otherwise not be recorded in simple visual classification of sponge morphology. The

use of photogrammetric classification may also help to remove some of the subjectivity when attributing sponges to functional groupings.

The sponge metric data may also prove useful for monitoring sponge communities over time. Having quantitative measures of sponge morphology will allow information on sponge growth, or damage due to disturbance, to be monitored through time. Finally, this study has shown that a highly accurate stereo-video system can be built with relatively low cost digital video cameras. Further improvements in digital video, including high definition digital video, will increase the accuracy and precision of such systems, primarily through increased resolution of the images.

Chapter 8. General Discussion

This thesis has examined the application of single beam echo sounders and underwater video systems in the mapping and assessment of temperate marine benthic habitats. Each system was examined in the context of a hierarchical classification system (Jordan *et al.* 2005b), with the capacity of each of these systems to classify substrates and habitats at various levels within the classification hierarchy tested. Extraction of meaningful and useful data on the spatial distribution of key habitats was achieved across a number of commonly encountered temperate marine benthic habitats.

The key findings of this thesis were that the SBES employed in this thesis was shown to be affected by changes in vessel speed, bottom depth, prevailing conditions and bottom slope. The magnitude of the error introduced by these factors was shown to be unlikely to be a major issue for a single factor at the substratum/ecotype level of the classification system, however if their effects are additive or at higher levels of classification then their effects are likely to severely limit the repeatability of classification of data from this system. For example if the errors combined to be greater than approximately 10 dB then the capacity to discriminate between the substrates investigated in this thesis would be compromised. The SBES used in this thesis was shown to have the capacity to detect differences in substrates at the substratum/ecotype and modifier levels of the hierarchical classification system. This included mapping of soft sediment habitats at the modifier level, the development of techniques for the classification of algal presence on reefs, and the development of techniques for the detection of large macroalgae in the water column. Classification techniques were then investigated for underwater video which is a common tool for sampling biota on the seafloor. Video was shown to be a useful tool for the classification of macroalgal communities, with the overall analysis generally not sensitive to the analysis method. Finally, a stereo video system was constructed and used to demonstrate that quantitative *in situ* measurements of sponge functional morphology are possible using a simple camera system, and that this can be used to make objective measurements of sponge functional diversity which are usually made through subjective interpretation of video observations.

Vessel speed, bottom depth, prevailing weather conditions, and bottom slope were all shown to have a measurable effect on SBES data based on extracted indices commonly used for substrate classification. The magnitude of these effects was shown to be at a level where individually these factors are unlikely to have a large effect on the overall classification accuracy at the substratum/ecotype level and above. However, if these effects are additive,

then where several are combined the capacity to classify substrates at any level is likely to be diminished. Previously these factors have been shown to impact on the classification accuracy of SBES surveys, although the magnitude of their effect on the raw acoustic data is rarely reported (Hamilton *et al.* 1999, Kloser *et al.* 2001b, von Szalay and McConnaughey 2002).

Changes in vessel speed have previously it has been reported to effect the E2 parameter of RoxAnn, but have show no significant effect on the E1 parameter of RoxAnn or the QTCView system (Hamilton *et al.* 1999, von Szalay and McConnaughey 2002). The E2 parameter of RoxAnn uses the second echo return, while both the E1 parameter of RoxAnn and the QTCView system use the first echo return (Hamilton *et al.* 1999, Freitas *et al.* 2005a). The second echo return must travel four times water depth compared to two times for the first echo return, the application of time varied gain will thus result in greater amplification of noise for the second echo than for the first at a given water depth. Further, pulses off the normal incident due to changes in vessel pitch will be compounded with the second echo. Within this study, both the E1 and E2 echo returns were found to be affected by changes in vessel speed. This was primarily attributed to large changes in vessel pitch with changing vessel speed, due to the vessel being a small planing hull vessel. It should be noted that this study was conducted from a small planing hull vessel (approximately 6.5 m long), the majority of published studies on this topic refer to larger displacement hull vessels ((Hamilton *et al.* 1999, von Szalay and McConnaughey 2002)).

Depth has frequently been shown to effect the acoustic return from the seabed, due to a combination of sperical spreading, absorption, and pulse effect (Hamilton *et al.* 1999, Kloser *et al.* 2001a, Freitas *et al.* 2003b). While improved processing methods and standardisation to a reference depth can reduce the depth dependence of SBES data, it is not possible to remove depth dependence completely from SBES data (Kloser *et al.* 2001a, Pouliquen 2004, Freitas *et al.* 2005b). This study supported the findings from previous studies, with depth dependence observed in SBES data; however found that the effect was not uniform across habitat types (reef, sand and silt). This may be due to the different scales of rugosity in these different habitats responding differently to changing acoustic footprint with increased depth, alternatively it may also reflect actual differences within the habitat across depth. This study aimed to sample identical substrates across a range of depths, however there may have been differences that were not apparent in either the video or sediment samples used to classify the substrates that may have affected the acoustic response.

Prevailing conditions were also shown to affect the acoustic return from the seabed, with measurable difference in the E1 and E2 indices between calm conditions and moderately rough conditions (> 15 kts and 1 m swell). The effect of prevailing conditions on SBES data are due to vessel pitch and roll resulting in acoustics being sampled off the normal incident, and aeration in the upper layers of the water column resulting in absorption of the acoustic signal (Kloser *et al.* 2001b). The effect of prevailing conditions is likely to be dependent on the vessel used in acoustic surveys. Larger more stable vessels with deeper transducer deployments are likely to be less affected by prevailing conditions than smaller vessels with shallow transducer deployments. Finally, the slope of the seafloor was also shown to affect the acoustic response, with steeper seafloor resulting in an increased in E1 and decreased in E2. This response is expected as a steep seafloor will increase the amount of energy reflected back from the edges of the acoustic footprint, while reflecting less of the energy from the central part of the acoustic beam back to the transducer. This study found that the E1 parameter was relatively stable to 10-15 degrees, while the E2 parameter showed small variation to 10 – 15 degrees, with significant decreases at angles greater than this. In previous work on the classification of SBES data using QTCView it has been reported that slopes exceeding 5 to 8 degrees caused complete breakdown in classification accuracy (von Szalay and McConnaughey 2002), while misclassification in areas with rocky outcrops on the seafloor has been reported for both QTCView and RoxAnn (Hamilton *et al.* 1999). It should be noted that in the study by von Szalay *et al.* (2002), classification accuracy was being assessed across a large number of substrate classes and across a large depth range, where as the current study was assessed the acoustic response from one substrate at a constant depth range. This may explain why the current study found the acoustic response of the seabed to be stable to a far greater slope angle.

The effect of vessel speed, bottom depth, prevailing weather conditions and bottom slope are likely to have a greater effect on classification accuracy at lower levels of classification, such as the modifier/eco-type level, where separation of acoustic data between different classes is potentially small.

At the modifier/eco-unit level of the hierarchy, methods were developed to classify SBES data including segmentation and classification of soft sediment communities, algal dominated and barren reef, and detection of sub-surface *Macrocystis pyrifera*. Extraction of information on habitats at the modifier/eco-unit level has previously been reported using commercial systems including QTCView, RoxAnn and BioSonics VBT (BioSonics 2001, Morrison *et al.*

2001a, Foster-Smith and Sotheran 2003). However, as these commercial systems are primarily targeted at physical substrate classification, the detection of biota is only possibly where the biota influence the parts of the echo return incorporated within the algorithms incorporated into these systems. The techniques developed within this thesis examined both standard integration techniques (roughness and hardness (Kloser *et al.* 2001b), and also developed algorithms to integrate parts of the echo return that would be expected to show differences due to the biota being detected. The capacity to remotely identify biota will have implications for marine ecosystem management through improve our understanding of seabed habitat distribution either through direct mapping or feeding into predictive modelling of habitat distribution (Holmes *et al.* 2008).

Methods to map the spatial distribution of soft sediment habitats within a scallop fishing zone were described in Chapter 3. Acoustic classes derived from standard acoustic indices (roughness and hardness) for soft sediment substrates were related to differences in surficial shell, sponge cover, and sediment particle size. Single beam systems operating at 120 to 150 kHz have been shown to be particularly good for classification of particle size (Hamilton *et al.* 1999, Freitas *et al.* 2005b, van Walree *et al.* 2005). SBES systems have also been shown to be sensitive to the presence of surficial shell (Williams *et al.* 2001, Stanton and Chu 2004), and the presence of biota on the substrate (Jordan *et al.* 2005b). However, despite the study site supporting a dense bed of scallops, which was heavily fished in the following fishing season, this area did not appear as a distinct acoustic class. Similarly, a dense scallop bed in the St Lawrence Estuary, Canada was unable to be segmented using SBES based on the QTCView system, however further processing and analysis of the raw S_v data was able to reveal the scallop bed in that instance (Hutin *et al.* 2005). Often multiple layers of information from a variety of tools can improve the capacity to map features at these hierarchical levels (Sutton and O'Keeffe 2007).

Maps of the distribution of soft sediment habitats derived from SBES data were related to the distribution of fishing effort derived from vessel monitoring system (VMS) data for the subsequent fishing season. Fishing effort was found to be concentrated along a narrow depth range on the transition between two of the acoustic classes, with little effort in the adjacent areas. Previous mapping studies of scallop habitat have used this type of information to improved the management of scallop fisheries, leading to including increased efficiency of fishers and decreased impact on the seafloor due to less time spent fishing (Pickrill and Todd 2003, Hutin *et al.* 2005). Information on seabed habitat spatial distribution can be used to gain

a better understanding on scallop distribution and the preferred scallop habitat, with flow on benefits to both management and habitat conservation (Kostylev *et al.* 2003).

At the modifier level/ecotype level of classification simple acoustic indices (such as roughness and hardness) were generally found to be less effective, especially in the segmentation of algae dominated reef from barren reef. Algorithms were developed to segment various reef habitat types including algal dominated reef, barren reef, and reef with giant string kelp, *Macrocystis pyrifera*, based on integration of regions above the sounder detected bottom. Acoustic systems have been shown to be useful for mapping of submerged aquatic vegetation, including seagrass and algae (Zabloudil *et al.* 1991, Foster *et al.* 2006). While BioSonics have produced a commercial system known as EcoSAV, which provides information on the presence/absence of aquatic vegetation, and also provides information on canopy height (BioSonics 2001). The EcoSAV system has been particularly applied to seagrass mapping (BioSonics 2001, Foster *et al.* 2006). The quality of the sounder detected bottom has been highlighted as of paramount importance for this system, with specialised algorithms developed to identify the seafloor in areas of dense vegetation. Similarly, within this thesis the quality of the sounder detected bottom was shown to influence the classification success of segmentation of algal dominated and barren reef, especially in areas of high relief or complex bottom structure.

The acoustic detection and mapping of giant string kelp, *Macrocystis pyrifera*, provided an example of using an acoustic system to map at the level of species. The acoustic system was shown to provide information that could complement traditional airborne remote sensing techniques, thus extending the mapping of *Macrocystis* to include sub-surface kelp. Sub-surface kelp has been identified as an important component of kelp beds, and in deeper water sub-surface kelp may provide refuge for this species in times of adverse environmental conditions (Ladah and Zertuche-González 2004). Acoustic systems have previously been applied to mapping *Macrocystis* (Zabloudil *et al.* 1991), however this previous work was done using paper charting sounders. The advance in digital echo sounder technology and acoustic processing software over the last two decades has presented the opportunity to revisit this topic and develop improved techniques for the identification and segmentation of *Macrocystis* from SBES data.

Whilst it was possible to develop techniques to identify *Macrocystis* from SBES data, this was largely due to this species having a unique and distinctive growth habit that lends itself to acoustic detection. For many algal species this is more difficult due to a combination of

similar growth habits, similar sizes and often highly mixed algal beds. For the mapping and assessment of algal communities video was examined. Video systems have often been used to characterise benthic flora and fauna (RosenKranz and Byersdorfer 2004, Kendall *et al.* 2005, Leach 2006, Carbines and Cole 2009). One of the major issues with the analysis of video for classification of benthic organisms is the large amount of processing time required. There are many approaches that have been adopted for the analysis of video data (Pitcher *et al.* 2001, Kohler and Gill 2006). This thesis examined several methods and found that for the characterisation of algal canopy species on temperate rocky reef, the final community structure identified was similar for most of the analysis techniques used. The processing time was generally the major difference between the different techniques. In a previous comparison of visual quadrats with photography it was found that the number of quadrats assessed was more important than the technique in the accuracy of classification (Foster *et al.* 1991). Based on this it could be expected that analysis methods that allow the largest number of video frames or sampling unites to be scored are potentially advantageous. Within this thesis Time based percent cover, frame based percent cover and frame based point intercept methods were all shown to have a similar performance in the classification of canopy algal species. Whilst point intercept methods are generally accepted as one of the best methods for quantitative video analysis (Kohler and Gill 2006), these methods were found to be the most time consuming. Hence methods such as the time based percent cover method may be just as useful, especially where time is limiting.

Single video camera systems are of limited use when underwater measurement is required. For quantitative measurement and 3 dimensional reconstruction multiple camera systems are preferred, with the most common of these a calibrated stereo camera system (Harvey *et al.* 2003). Chapter 7 examined the classification of sponge morphological diversity based on analysis of stereo video data. Calibrated stereo video systems have been applied to the measurement of numerous underwater organisms including fish (Harvey *et al.* 2002, Nicole *et al.* 2003, Watson *et al.* 2005), with the benefit of more robust estimates of fish size when compared to diver estimates, and better quantification of fish community structure as a result. Similarly measurement of hydrocorals using a stereo camera system provided a high level of measurement accuracy in the order of 1.2 mm accuracy 95% confidence interval and highlighted a high erosional rate in hydrocorals that had not previously been reported (Chong and Stratford 2002). Within this study a stereo video system was developed with a similar accuracy, enabling gross morphological metrics of sponges to be measured. These metrics were then used to classify sponges into morphological groups.

The methods developed within this thesis present a quantitative approach to the classification of sponge functional morphology, with high classification success for the majority of functional groups, but low classification success for morphologically similar groups. Sponge functional morphology has been shown to be a good surrogate for sponge species diversity (Bell and Barnes 2001), knowledge of which is important for conservation planning (Ward *et al.* 1999). For example, scallop dredging is known to have a large and detrimental impact on sponge beds (Kefalas *et al.* 2003). The capacity to make quantitative measures of sponge morphology will provide a means to monitor both that impact and subsequent recovery post fishing on sponge community structure and sponge size.

The methods developed within this thesis will help to improve our understanding of key temperate ecosystems, providing spatial data on habitat types including urchin barrens, sub-surface *Macrocystis* distribution, algal community structure, and sponge beds. Often there is difficulty linking fine scale ecological studies with broad scale biogeography (Connell and Irving 2008). Habitat mapping at the modifier/eco-type level will help provide this link.

The acoustic and video processing techniques developed within this thesis are also complementary, with the outputs from both systems able to be combined to obtain fine scale information on approaching that obtainable from dive surveys, but without the limitations of depth and bottom time. The use of underwater video and sediment sampling tools, when used in conjunction with acoustic survey tools (multibeam, seismic, sidescan, RoxAnn, QTCView, etc.), make possible the classification and mapping of marine benthic habitat and biological communities over large areas (Gordon 2000). Developments in underwater positioning technology, such as acoustic positioning, will also improve the links between video and acoustic systems, ultimately leading to the ability to easily relate ground truth data with acoustic data points in any depth of water.

The ability to accurately relate the ground truth information directly to the acoustic data was one of the major limitations of the method development in this thesis. Generally only areas were the seafloor was homogenous were used to develop methods, however determining homogeneity of the seafloor can be difficult, especially in deep water where the coverage of the ground truth data is generally small compared to the footprint of the acoustic system. In these cases there is a risk of inadvertently including multiple seafloor types which can affect classification accuracy.

In order to obtain complete coverage maps from SBES and video data interpolation is required. Interpolation of SBES data into coverage maps is commonly done to improve both

visual appearance and aid in the interpretation of these maps. A number of techniques have been employed for this interpolation, including hand digitising, inverse distance weighting and kriging (Guan *et al.* 1999, Valley *et al.* 2005, Foster *et al.* 2006). The choice of interpolation method employed has been shown to influence the accuracy of the final map product (Valley *et al.* 2005) however with any interpolation technique the quality of the data being used is paramount to the quality of the final map product. Data density, including transect spacing must reflect the scale of the features being mapped (Pinn and Robertson 2003). At the Biogeomorphic and Substrate/Ecotype levels of classification broader transects are generally applied as this reflects the overall distribution of these substrates, however at the modifier level fine transect spacing is generally required to reflect the patch size of habitats at this level. MBES and SSS provide swath coverage, and as such do not require interpolation. Whilst the development of classification techniques for these systems is an ongoing area of research (Ferrini and Flood 2006, Parnum *et al.* 2006, Blondel and Gómez Sichi 2008), the information they provide supports and adds to that obtainable from SBES, and as such they can be seen as complementary systems and not replacements.

The techniques developed for SBES processing in this these may also be used as a basis for the development of MBES processing techniques to enable full coverage maps of substrate at the modifier level of classification. Processing techniques for MBES are rapidly developing (Anderson *et al.* 2008, Kloser *et al.* 2010). The swath data from MBES includes both high resolution bathymetry and backscatter. MBES data can be used to characterize the seafloor based on the analysis of backscatter angular response, since this response is an intrinsic property of the seafloor (Fonseca *et al.* 2008), while the high resolution bathymetry from MBES is also used to classify the seafloor in terms of rugosity and seafloor features.

Maps of habitat at the modifier/eco-unit level of classification will improve our understanding of ecological processes at a scale above that obtainable from most ecological studies. For example spatial information at this level will greatly increase the understanding of temperate reef ecology, as quantitative observations of pattern provide the context and basis for studying mechanisms and processes (Underwood *et al.* 2000). Commonly within ecological studies habitat descriptors are used to define areas for sampling. Habitat descriptors commonly used within ecological on temperate rocky reef include kelp forest and urchin barren (Shears *et al.* 2004). Hence the capacity to develop broad scale spatial maps of these habitat descriptors will assist in the interpretation and extrapolation of results of such studies, and will allow ecological processes to be scaled by the area of habitat (Taylor 1998).

Maps of habitats can also be used to describe large scale patterns in communities (Solan *et al.* 2003, Parsons *et al.* 2004). Local environmental factors including wave exposure, nutrients, sea surface temperature, and underlying substrate are responsible for the patterns observed in ecology (Shears and Babcock 2002, Eriksson and Bergström 2005, Pepper and M.L. 2009). Combining maps of habitat with spatial data describing other environmental variables will provide a powerful tool for understanding these interactions. For example the use of tree classification methods has been applied to derived acoustic data on the physical substrate and video transect data to model the distribution of biota at lower hierarchical levels (Holmes *et al.* 2008). Using a combination of modelling and mapping data distribution of algal communities was able to be predicted with high success rates, clearly indicating the scope to improve our understanding of the marine environment.

Habitat descriptors based on the presence and composition of dominant algae have also been shown to be a useful predictor of fish and invertebrate communities (Levin and Hay 2002, Edgar *et al.* 2004, Ling 2008). Climate change is expected to cause changes to environmental conditions in many areas, including the east coast of Tasmania, causing changes in species distributions (Harris and Tyrrell 2001, Tegner *et al.* 2001, Edyvane 2003). It is important to be able to document the current ranges of species, not only for change detection, but also as a predictor of where change is most likely to occur. Thus the mapping techniques for rocky reef habitat developed within this thesis will provide valuable information required to improve our understanding on the function and patterns in temperate ecosystems in the light of changing environmental conditions.

The acoustic and video processing and analysis methods development within this thesis will improve the mapping and assessment of marine benthic habitats. These methods have been developed with relation to a hierarchical classification system, allowing the output from these methods to be integrated, and subsequently allowing maps of habitat to be produced which represent substrates at variety of classification levels. As no single tool can currently provide all the information required for the assessment and management of marine habitats, a combination of tools must be used to collect and collate this information. The SBES and underwater video systems and data analysis methods described in this thesis generally provide complimentary tools that can be used to build up layers of substrate and habitat distribution within the hierarchical classification system.

As technology advances the toolkit for inshore habitat mapping is constantly expanding, and can be expected to increasingly allow more of the substrates, habitats, and species within the

classification hierarchy to be spatially defined. Multibeam echo sounders and side scan sonar for example can provide full coverage maps of the seafloor (Anderson *et al.* 2008), and autonomous underwater vehicles provide a platform for both acoustic and video data to be collected across extensive areas with less effort and cost than traditional ship surveys (Fernandes *et al.* 2003). These types of developments will allow integration of habitat data at even lower levels of classification and across broader areas, with this information feeding into spatially explicit models for fisheries management, ecosystem management, conservation planning, and climate change monitoring.

The methods developed in this thesis contribute to comprehensive spatial representation of marine benthic habitats.

References

Abdel-Aziz, Y.I. 1974. Expected accuracy of convergent photos. *Photogrammetric Engineering & Remote Sensing*. **40:** (11) 1341-1346.

Acker, W.C., Burczynski, J., Dawson, J., Hedgepeth, J. and Wiggins, D. 1999. Digital Transducers: A New Sonar Technology. *Sea Technology*. **40:** (6) 31-38.

Ackers, R.G., Moss, D. and Picton, B.E. 1992. *Sponges of the British Isles (Sponge V).* Marine Conservation Society. Herefordshire, UK. 175.

Allee, R.J., Dethier, M., Brown, D., Deegan, L., Ford, R.G., Hourigan, T.F., Maragos, J., Schoch, C., Sealey, K., Twilley, R., Weinstein, M.P. and Yoklavich., M. 2000. Marine and Estuarine Ecosystem and Habitat Classification. *NOAA Technical Memorandum NMFS-F/SPO-4.* **3:** 43.

Anderson, J.T., Gregory, R.S. and Collins, W.T. 2002. Acoustic classification of marine habitats in coastal Newfoundland. *ICES Journal of Marine Science*. (59) 156-167.

Anderson, J.T., Van Holliday, D., Kloser, R., Reid, D.G. and Simard, Y. 2008. Acoustic seabed classification: current practice and future directions. *ICES Journal of Marine Science*. **65:** 1004-1011.

Andrew, N.L. 1993. Spatial heterogeneity, sea urchin grazing , and habitat structure on reefs in temperate Australia. *Ecology*. **74:** (2) 292-302.

Andrew, N.L. and O'Neill, A.L. 2000. Large-scale patterns in habitat structure on subtidal rocky reefs in New South Wales. *Marine and Freshwater Research*. **51:** 255-263.

Babcock, R.C., Kelly, S., Shears, N.T., Walker, J.W. and Willis, T.J. 1999. Changes in community structure in temperate marine reserves. *Marine Ecology Progress Series*. **189:** 125-134.

Barange, M. 1994. Acoustic identification, classification and structure of biological patchiness on the edge of the Agulhas Bank and its relation to frontal features. *South African Journal of Marine Science*. **14:** 333-347.

Barker, B., Helmond, I., Sherlock, M., Lewis, M., Williams, A., Bax, N. and Kloser, R. 2001. *Use of Towed Deepwater Video Systems at CSIRO Marine Research*. Proceedings of FRDC Workshop- Video Sensing of the Size and Abundance of Target and Non-target Fauna in Australian Fisheries - a National Workshop.

Barker, B.A.J., Helmond, I., Bax, N.J., Williams, A., Davenport, S. and Wadley, V.A. 1999. A vessel-towed camera platform for surveying seafloor habitats of the continental shelf. *Continental Shelf Research*. **19:** (9) 1161-1170.

Barrett, N., Sanderson, J.C., Lawler, M., Halley, V. and Jordan, A.R. 2001. *Mapping of inshore marine habitats in south-eastern Tasmania for marine protected area planning and marine management*. TAFI Technical Report Series. TAFI. Taroona. 74.

Barrett, N.S., Buxton, C.D. and Edgar, G.J. 2009. Changes in invertebrate and macroalgal populations in Tasmanian marine reserves in the decade following protection. *Journal of Experimental Marine Biology and Ecology*. **370:** 104-119.

Basu, A. and Saxena, N.K. 1999. A Review of Shallow-Water Mapping Systems. *Marine Geodesy*. (22) 249-257.

Bates, C.R. and Byham, P.W. 2001. Bathymetric sidescan techniques for near shore surveying. *Hydrographic Journal*. (100) 13-18.

Bates, C.R. and Whitehead, E.J. 2001. ECHOplus Measurements in Hopavaagen Bay, Norway. *Sea Technology*. **42:** (6) 34-43.

Bates, R. and Moore, C. 2002. Acoustical Methods for Marine Habitat Surveys. *Hydro International*. **6:** (1) 47-58.

Bax, N.J., Kloser, R., Williams, A., Gowlett-Holmes, K. and Ryan, T. 1999. Seafloor habitat definition for spatial management in fisheries: a case study on the continental shelf of southeast Australia. *Oceanologica Acta*. **22:** (6) 705-719.

Bell, J. 2008. The functional roles of marine sponges. *Estuarine, Coastal and Shelf Science*. **79:** 341-353.

Bell, J.J. and Barnes, D.K.A. 2000a. The distribution and prevalence of sponges in relation to environmental gradients within a temperate sea lough: Inclined cliff surfaces. *Diversity and Distributions*. **6:** (6) 305-323.

Bell, J.J. and Barnes, D.K.A. 2000b. The distribution and prevalence of sponges in relation to environmental gradients within a temperate sea lough: Vertical cliff surfaces. *Diversity and Distributions*. **6:** (6) 283-303.

Bell, J.J. and Barnes, D.K.A. 2000c. The influences of bathymetry and flow regime upon the morphology of sublittoral sponge communities. *Journal of the Marine Biological Association of the United Kingdom*. **80:** (4) 707-718.

Bell, J.J. and Barnes, D.K.A. 2001. Sponge morphological diversity: A qualitative predictor of species diversity? *Aquatic Conservation: Marine and Freshwater Ecosystems*. **11:** (2) 109-121.

Bell, J.J. and Barnes, D.K.A. 2002. Modelling sponge species diversity using a morphological predictor: A tropical test of a temperate model. *Journal for Nature Conservation*. **10:** (1) 41-50.

Bell, J.J., Barnes, D.K.A. and Shaw, C. 2002. Branching dynamics of two species of arborescent demosponge: The effect of flow regime and bathymetry. *Journal of the Marine Biological Association of the United Kingdom*. **82:** (2) 279-294.

Bergstedt, R.A. and Anderson, D.R. 1990. Evaluation of Line Transect Sampling Based on Remotely Sensed Data from Underwater Video. *Transactions of the American Fisheries Society*. **119:** 86-91.

Bernhardt, S.P. and Griffing, L.R. 2001. An evaluation of image analysis at benthic sites based on color segmentation. *Bulletin of Marine Science*. **69:** (2) 639-653.

Bertness, M.D., Leonard, G.H., Levine, J.M., Schmidt, P.R. and Ingraham, A.O. 1999. Testing the relative contribution of positive and negative interactions in rocky intertidal communities. *Ecology*. **80:** (8) 2711-2726.

BioSonics. 2001. *Assessment of Digital Sonar Technology to Map Eelgrass (Zostera marina) in the San Juan Islands*. BioSonics. Seattle. 10.

Blondel, P. and Gómez Sichi, O. 2008. Textural analyses of multibeam sonar imagery from Stanton Banks, Northern Ireland continental shelf. *Applies Acoustics*. **70:** (10) 1288-1297.

Blondel, P. and Murton, B.J. 1997. Handbook for Seafloor Sonar Imagery. John Wiley and Sons.

Bräger, S., Chong, A., Dawson, S., Slooten, E. and Würsig, B. 1999. A combined stereo-photogrammetry and underwater-video system to study group composition of dolphins. *Helgoland Marine Research*. **53:** 122-128.

Breen, P.A. and Mann, K.H. 1976. Changing lobster abundance and the destruction of kelp beds by sea urchins. *Marine Biology*. **34:** 137-142.

Brown, C., Mitchell, A., Limpenny, D.S., Robertson, M.R., Service, M. and Golding, N. 2005a. Mapping seabed habitats in the Firth of Lorn off the west coast of Scotland: evaluation and comparison of habitats maps produced using the acoustic ground-discrimination system, *RoxAnn*, and sidescan sonar. *ICES Journal of Marine Science*. **62:** 790-802.

Brown, C.J., Golding, N., Mitchell, A., Limpenny, D.S., Robertson, M.R. and Service, M. 2003. *Mapping seabed habitats in UK waters*. Practical Acoustic Ground Discrimination Workshop. 35.

Brown, C.J., Hewer, A.J., Meadows, W.J., Limpenny, D.S., Cooper, K.M., Rees, H.L. and Vivian, C.M.G. 2001. Mapping of gravel biotopes and an examination of the factors controlling the distribution, type and diversity of their biological communities. *Science series technical report. Centre for Environment, Fisheries and Aquaculture Science*. 114.

Brown, C.J., Mitchell, A., Limpenny, D.S., Robertson, M.R., Service, M. and Golding, N. 2005b. Mapping seabed habitats in the Firth of Lorn off the west coast of Scotland: evaluation and comparison of habitat maps produced using the acoustic ground-discrimination system, *RoxAnn*, and sidescan sonar. *ICES Journal of Marine Science*. **62:** 790-802.

Brown, M.T., Nyman, M.A., Keogh, J.A. and Chin, N.K.M. 1997. Seasonal growth of the giant kelp *Macrocystis pyrifera* in New Zealand. *Marine Biology*. **129:** 417-424.

Burczynski, J. 2001. *Bottom Classification*. BioSonics Inc. 14.

Butler, A.J., Althaus, F., Furlani, D. and Ridgway, K.R. 2002. *Assessment of the conservation values of the Bass Strait sponge bed areas*. Commonwealth Marine Conservation Assessment Program 2002 - 2004. Environment Australia. 64.

Byrne, R.H. 2002. Inorganic speciation of dissolved elements in seawater: the influence of pH on concentration ratios. *Geochemical Transactions*. **3:** (2) 11-16.

Caddell, S.E. 1998. Application of an acoustic sea floor classification system for benthic habitat assessment. *Journal of Shellfish Research*. **17:** (5) 1459-1461.

Carbines, G. and Cole, R.G. 2009. Using a remote drift underwater video (DUV) to examine dredge impacts on demersal fishes and benthic habitat complexity in Foveaux Strait, Southern New Zealand. *Fisheries Research*. **96:** 230-237.

Carleton, J.H. and Done, T.J. 1995. Quantitative video sampling of coral reef benthos: large-scale application. *Coral Reefs*. **14:** 35-46.

Carruthers, T.J.B. and Walker, D.I. 1999. Sensitivity of transects across a depth gradient for measuring changes in aerial coverage and abundance of *Ruppia megacarpa* Mason. *Aquatic Botany*. **65:** 281-292.

Chakraborty, B., Kodagali, V. and Baracho, J. 2003. Sea-floor classification using multibeam echo-sounding angular backscatter data: A real-time approach employing hybrid neural network architecture. *Ieee Journal of Oceanic Engineering*. **28:** (1) 121-128.

Chapman, A.R.O. 1981. Stability of sea urchin dominated barren grounds following destructive grazing of kelp in St. Margaret's Bay, Eastern Canada. *Marine Biology*. **62:** 307-311.

Chivers, R.C.E., N and Burns, D.R. 1990. New Acoustic Processing for Underway Surveying. *The Hydrographic Journal*. **56:** 9-17.

Choat, J.H. and Ayling, A.M. 1987. The relationship between habitat structure and fish faunas on New Zealand reefs. *Journal of Experimental Marine Biology and Ecology*. **110:** 257-284.

Cholwek, G., Bonde, J., Li, X., Richards, C. and Yin, K. 2000. Processing RoxAnn sonar data to improve its categorization of lake bed surficial substrates. *Marine Geophysical Researches*. **21:** (5) 409-421.

Chong, A.K. and Stratford, P. 2002. Underwater Digital Stereo-Observation Technique for Red Hydrocoral Study. *Photogrammetric Engineering & Remote Sensing*. **68:** (7) 745-751.

Cochrane, G.R. and Lafferty, K.D. 2002. Use of acoustic classification of sidescan sonar data for mapping benthic habitat in the Northern Channel Islands, California. *Continental Shelf Research*. **22:** (5) 683-690.

Cocito, S., Sgorbinio, S., Peirarno, A. and Valle, M. 2003. 3-D reconstruction of biological objects using underwater video technique and image processing. *Journal of Experimental Marine Biology and Ecology*. **297:** 57-70.

Coetzee, j. 2000. Use of a shoal analysis and patch estimation system (SHAPES) to characterise sardine schools. *Aquatic Living Resources*. **13:** (1) 1-10.

Collie, J.S., Escanero, G.A. and Valentine, P.C. 1997. Effects of bottom fishing on the benthic megafauna of Georges Bank. *Marine Ecology Progress Series*. **155:** 159-172.

Collie, J.S., Escanero, G.A. and Valentine, P.C. 2000. Photographic evaluation of the impacts of bottom fishing on benthic epifauna. *ICES Journal of Marine Science*. **57:** (4) 987-1001.

Collins, B. 1996. QTC View: A digital approach to seabed classification with applications in habitat assessment. *Sea Technology*.

Collins, M.B. and Voulgaris, G. 1993. Empirical field and laboratory evaluation of a real-time acoustic sea bed surveying system. *Proceedings of the Institute of Acoustics*. **15:** (2) 343-351.

Collins, W. and Galloway, J.L. 1998. Seabed classification and multibeam bathymetry: tools for multidisciplinary mapping. *Sea Technology*. **39:** 45 – 49.

Collins, W., Gregory, R. and Anderson, J. 1996. A digital approach to seabed classification. *Sea Technology*. **37:** (8) 83-87.

Committee of Ecosystem Effects of Fishing. 2002. *Effects of trawling and dredging on seafloor habitat*. Ocean Studies Board, Division of Earth and Life Studies, National Research Council. Washington, DC. 126.

Connell, S.D. and Irving, A.D. 2008. Integrating ecology with biogeography using landscape characteristics: a case study of subtidal habitat across continental Australia. *Journal of Biogeography*. **35:** 1608-1621.

Connell, S.D. and Lincoln-Smith, M.P. 1999. Depth and the structure of assemblages of demersal fish: experimental trawling along a temperate coast. *Estuarine, Coastal and Shelf Science*. **48:** 483-495.

Cresswell, G.R. 2000. Currents of the continental shelf and upper slope of Tasmania. *Papers and Proceedings of the Royal Society of Tasmania*. **133:** (3) 21-30.

Cutter-Jr., G.R., Rzhanov, Y. and Mayer, L.A. 2003. Automated segmentation of seafloor bathymetry from multibeam echosounder data using local Fourier histogram texture features. *Journal of Experimental Marine Biology and Ecology*. **285–286:** 355– 370.

Davies, C.E., Moss, D. and Hill, M.O. 2004. *EUNIS Habitat Classification Revised 2004*. European Environemnt Agency, European Topic Centre on Nature Protection and Biodiversity. 307.

de Kluijver, M.J. 1993. Sublittoral hard-substratum communities off Orkney and St Abbs (Scotland). *Journal of the Marine Biological Association of the United Kingdom*. **73:** 733-754.

De Robertis, A. and Higginbottom, I. 2007. A post-processing technique to estimate the signal-to-noise ratio and remove echosounder background noise. *ICES Journal of Marine Science*. **64:** 1282-1291.

de Voogd, N.J., Van Soest, R.W.M. and Hoeksema, B.W. 1999. Cross-shelf distribution of southwest Sulawesi reef sponges. *Memoirs of the Queensland Museum*. **44:** 147-154.

Deysher, L.E. 1993. Evaluation of remote sensing techniques for monitoring giant kelp populations. *Hydrobiologia*. **260-261:** (1) 307-312.

Dommisse, M., Urban, D., Finney, B. and Hills, S. 2005. Potential depth biasing using the Biosonics VBT Seabed classification software. *Marine Technology Society Journal*. **39:** (2) 90-93.

Doucette, J.S., Harvey, E.S. and Shortis, M.R. 2001. *Stereo-video observation of nearshore bedforms on a low energy beach*. Department of Geography , University of Western Australia, Australia. 35.

Drummond, S.P. and Connell, S.D. 2005. Quantifying percentage cover of subtidal organisms on rocky coasts: a comparison of the costs and benefits of standard methods. *Marine and Freshwater Research*. **56:** (6) 865–876.

Duarte, C.M. 1987. Use of echosounder tracings to estimate the above ground biomass of submerged plants in lakes. *Canadian Journal of Fisheries and Aquatic Sciences*. **44:** 732-735.

Duggins, D., Eckman, J.E., Siddon, C.E. and Klinger, T. 2001. Interactive roles of mesograzers and current flow in survival of kelps. *Marine Ecology Progress Series*. **223:** 143-155.

Edgar, G.J. 1983. The ecology of south-east tasmanian phytal animal communities. IV. Factors affecting the distribution of ampithoid amphipods among algae. *Journal of Experimental Marine Biology and Ecology*. **70:** 205-225.

Edgar, G.J. 1984. General features of the ecology and biogeography of Tasmanian rocky reef communities. *Papers and Proceedings of the Royal Society of Tasmania*. **118:** 173-186.

Edgar, G.J. 1997. Australian marine life : the plants and animals of temperate waters. Reed Books. Sydney. 544.

Edgar, G.J. and Barrett, N.S. 2002. Benthic macrofauna in Tasmanian estuaries:scales of distribution and relationships with environmental variables. *Journal of Experimental Marine Biology and Ecology*. **270:** 1 -24.

Edgar, G.J., Barrett, N.S., Morton, A.J. and Samson, C.R. 2004. Effects of algal canopy clearance on plant, fish and macroinvertebrate communities on eastern Tasmanian reefs. *Journal of Experimental Marine Biology and Ecology*. **312:** (1) Pages 67-87

Edgar, G.J., Moverley, J., Barrett, N.S., Peters, D. and Reed, C. 1997. The conservation related benefits of a systematic marine biological sampling programme: the Tasmanian reef bioregionalisation as a case study. *Biological Conservation*. **79:** 227-240.

Edwards, M.S. 2004. Estimating scale-dependency in disturbance impacts: El Ninos and giant kelp forests in the northern Pacific. *Oecologia*. **138:** 436-447.

Edyvane, K. 2003. *Conservation, Monitoring and Recovery of Threatened Giant Kelp (Macrocystis pyrifera) Beds in Tasmania – Final Report.* Report to Environment Australia (Marine Species Protection Program). 177.

Ellingsen, K., E., Gray, J., S. and Bjørnbom, E. 2002. Acoustic classification of seabed habitats using the QTC VIEW™ system. *ICES Journal of Marine Science*. **59:** 825-835.

Eos Systems Inc. 2000. PhotoModeler Pro. Vancouver.

Eriksson, B.K. and Bergström, L. 2005. Local distribution patterns of macroalgae in relation to environmental variables in the northern Baltic Proper. *Estuarine, Coastal and Shelf Science*. **62:** 109-117.

Fenstermacher, L.E., Crawford, G.B., Borgeld, J.C., Britt, T., George, D.A., Klein, M.A., Driscoll, N.W. and Mayer, L.A. 2001. Enhanced acoustic backscatter due to high abundance of sand dollars, *Dendraster excentricus*. *Marine Georesources & Geotechnology*. **19:** (2) 135-145.

Fernandes, P.G., Stevenson, P., Brierley, A.S., Armstrong, F. and Simmonds, E.J. 2003. Autonomous underwater vehicles: future platforms for fisheries acoustics. *ICES Journal of Marine Science*. **60:** 684-691.

Ferrini, V.L. and Flood, R.D. 2006. The effects of fine-scale surface roughness and grain size on 300 kHz multibeam backscatter intensity in sandy marine sedimentary environments. *Marine Geology*. **228:** 153-172.

Finkbeiner, M., Stevenson, B. and Seaman, R. 2001. *Guidance for benthic habitat mapping: an aerial photographic approach*. NOAA Coastal Services Center. 53.

Fonseca, l., Brown, C., Calder, B., Mayer, L. and Rzhanov, Y. 2008. Angular range analysis of acoustic themes from Stanton Banks Ireland: A link between visual interpretation and multibeam echosounder angular signatures. *Applies Acoustics*. **70:** (10) 1298-1304.

Foote, K.G., Knudsen, H.P., Vestnes, G., MacLennan, D.N. and Simmonds, E.J. 1987. *Calibration of acoustic instrumentation for fish density estimation: a practical guide*. Cooperative Research Report. ICES. Copenhagen. 69.

Foster-Smith, B., Brown, C., Meadows, B. and Rees, I. 2001. *Procedural Guidelines 1-3 Seabed mapping using acoustic ground discrimination interpreted with ground truthing*. Marine Monitoring Handbook March 2001. Joint Nature Conservation Committee. 183-197.

Foster-Smith, B., Brown, C., Meadows, B., White, W.H. and Limpenny, D.S. 2004a. Mapping seabed biotopes at two spatial scales in the eastern English Channel. Part 2. Comparison of two acoustic ground discrimination systems. *Journal of Marine Biology. UK*. **84:** 489-500.

Foster-Smith, R. and Sotheran, I.S. 2003. Mapping marine benthic biotypes using acoustic ground discrimination systems. *International Journal of Remote Sensing*. **24:** (13) 2761-2784.

Foster-Smith, R.L., Brown, C.J., Meadows, W.J., White, W.H. and Limpenny, D.S. 2004b. Mapping seabed biotopes at two spatial scales in the eastern English Channel. Part 2. Comparison of two acoustic ground discrimination systems. *Journal of Marine Biology. UK*. **84:** 489-500.

Foster, J.G., Riegl, B., Purkis, S.J. and Dodge, R.E. 2006. Mapping of Tropical Shallow Water Benthos (Algae, Seagrass, Corals) Using Three Single-Beam Acoustic Ground Discrimination Systems (QTCView, Echoplus, Biosonics). *2006 Ocean Sciences Meeting*. 87. Eos Trans. AGU.

Foster, M.S., Harrold, C. and Hardin, D.D. 1991. Point vs. photo quadrat estimates of the cover of sessile marine organisms. *Journal of Experimental Marine Biology and Ecology*. **146:** (2) 193-203.

Fowler-Walker, M.J. and Connell, S.D. 2002. Opposing states of subtidal habitat across temperate Australia: consistency and predictability in kelp canopy-benthic associations. *Marine Ecology Progress Series*. **240:** 49-56.

Francois, R.E. and Garrison, G.R. 1982. Sound absorption based on ocean measurements. Part II: Boric Acid contribution and equation for total absorption. *Journal of the Acoustical Society of America*. **72:** 1879-1890.

Freitas, R., Rodrigues, A.M. and Quintino, V. 2003a. Benthic biotopes remote sensing using acoustics. *Journal of Experimental Marine Biology and Ecology*. **285-286:** 339-353.

Freitas, R., Sampaio, L., Rodrigues, A.M. and Quintino, V. 2005a. Sea-bottom classification across a shallow-water bar channel and near-shore shelf, using single-beam acoustics. *Estuarine, Coastal and Shelf Science*. **65:** 625-632.

Freitas, R., Sampaio, L., Rodrigues, A.M. and Quintino, V. 2005b. Sea-bottom classification across a shallow-water bar channel and near-shore shelf, using single-beam acoustics. *Estuarine, Coastal and Shelf Science*. **65:** (4) 625-632.

Freitas, R., Silva, S., Quintino, V., Rodrigues, A.M., Rhynas, K. and Collins, W.T. 2003b. Acoustic seabed classification of marine habitats: studies in the western coastal-shelf area of Portugal. *ICES Journal of Marine Science*. **60:** 599-608.

Friedlander, A.M., Boehlert, G.W., Field, M.E., Mason, J.E., Gardner, J.V. and Dartnell, P. 1999. Sidescan-sonar mapping of benthic trawl marks on the shelf and slope off Eureka, California. *Fishery Bulletin*. **97:** (4) 786-801.

Fryer, J.G. 1983. A simple system for photogrammetric mapping in shallow water. *Photogrammetric Record*. **11:** (62) 203-208.

Fryer, J.G. and Done, T. 1982. An underwater trilateration. *The Australian Surveyor*. **31:** (1) 7-12.

Gagnon, P., Himmelman, J.H. and Johnson, L.E. 2004. Temporal variation in community interfaces: kelp-bed boundary dynamics adjacent to persistent urchin barrens. *Marine Biology*. **144:** 1191-1203.

Galloway, J.L. and Collins, W.T. 1998. *Dual frequency acoustic classification of seafloor habitat using the QTC VIEW*. Oceans 98 -- Engineering for sustainable use of the oceans. Nice (France). 1296-1300.

Gladstone, W. 2002. The potential value of indicator groups in the selection of marine reserves. *Biological Conservation*. **104:** (2) 211-220.

Goldberg, N.A. and Kendrick, G. 2004`. Effects of island groups, depth, and exposure to ocean waves on subtidal macroalgal assemblages in the Recherche Archipelago, Western Australia. *Journal of Phycology*. **40:** 631-641.

Gordon, D.J.K., ELR; Gilkinson, KD; McKeown, DL; Steeves, G; Chin-Yee, M; Vass, WP; Bentham, K; Boudreau, PR. 2000. Canadian imaging and sampling technology for studying marine benthic habitat and biological communities. *ICES, Copenhagen (Denmark). 11 pp. 2000.* 2000. ICES, Copenhagen (Denmark). 11 pp. 2000.

Green, J., Matthews, S. and Turanli, T. 2002. Underwater archaeological surveying using PhotoModeler, VirtualMapper: different applications for different problems. *The International Journal of Nautical Archaeology*. **31:** (2) 283-292.

Greene, H.G., Yoklavich, M.M., Starr, R.M., O'Connell, V.M., Wakefield, W.W., Sullivan, D.E., McRea, J.E. and Cailliet, G.M. 1999. A classification scheme for deep seafloor habitats. *Oceanologica Acta*. **22:** (6) 663-678.

Greenstreet, S.P.R., Tuck, I.D., Grewar, G.N., Armstrong, E., Reid, D.G. and Wright, P.J. 1997. An assessment of the acoustic survey technique, RoxAnn, as a means of mapping seabed habitat. *ICES Journal of Marine Science*. **54:** (5) 939-959.

Grove, R.S., Zabloudil, K., Norall, T. and Deysher, L.E. 2002. Effects of El Nino events on natural kelp beds and artificial reefs in southern California. *ICES Journal of Marine Science*. **59:** (s1) 330-337.

Guan, W., Chamberlain, R.H., Sabol, B.M. and Doering, P.H. 1999. Mapping submerged aquatic vegetation with GIS in the Caloosahatchee Estuary: Evaluation of different interpolation methods. *Marine Geodesy*. **22:** (2) 69-91.

Haddon, M., Harrington, J.J. and Semmens, J.M. 2005. *Bass Strait central zone scallop survey, March 2005*. AFMA Final Report, Australian Fisheries Management Authority.

Haddon, M., Harrington, J.J. and Semmens, J.M. 2006. *Juvenile scallop discard rates and bed dynamics: testing the management rules for scallops in Bass Strait*.

Haddon, M., Semmens, J.M. and Harrington, J.J. 2004. *Bass Strait central zone scallop survey, March 2004*. AFMA Final Report, Australian Fisheries Management Authority.

Hale, W.B. and Cook, C.E. 1962. Underwater microcontouring. *Photogrammetric Engineering*. **28:** (281) 96-98.

Hall-Spencer, J.M., Froglia, C., Atkinson, R.J.A. and Moore, P.G. 1999. The impact of Rapido trawling for scallops, *Pecten jacobaeus*(L.), on the benthos of the Gulf of Venice. *ICES Journal of Marine Science*. **56:** (1) 111-124.

Hall-Spencer, J.M. and Moore, P.G. 2000. Scallop dredging has profound, long-term impacts on maerl habitats. *ICES Journal of Marine Science*. **57:** (5) 1407-1415.

Hamilton, L.J., Mulhearn, P.J. and Poeckert, R. 1999. Comparison of RoxAnn and QTC-View acoustic bottom classification system performance for the Cairns area, Great Barrier Reef, Australia. *Continental Shelf Research*. **19:** 1577-1597.

Harold, C. and Reed, D.C. 1985. Food availability, sea urchin grazing, and kelp forest community structure. *Ecology*. **66:** (4) 1160-1169.

Harris, G., Nilsson, C., Clementson, L. and Thomas, D. 1987. The water masses of the east coast of Tasmania: seasonal and interannual variability and the influence on phytoplankton biomass and productivity. *Australian Journal of Marine and Freshwater Research*. **38:** (5) 569-590.

Harris, L.G. and Tyrrell, M.C. 2001. Changing community states in the Gulf of Maine: synergism between invaders, overfishing and climate change. *Biological Invasions*. **3:** 9-21.

Hart, M.W. and Scheibling, R.E. 1988. Heat waves, baby booms, and the destruction of kelp beds by sea urchins. *Marine Biology*. **99:** 167-176.

Harvey, E., Fletcher, D. and Shortis, M. 2001. Improving the statistical power of length estimates of reef fish: A comparison of estimates determined visually by divers with estimates produced by a stereo-video system. *Fishery Bulletin*. **99:** (1) 72-80.

Harvey, E.S., Fletcher, D. and Shortis, M.R. 2002. Estimation of reef fish length by divers and by stereo-video: a first comparison of the accuracy and precision in the field on living fish under operational conditions. *Fisheries Research*. **57:** (3) 255-265.

Harvey, E.S. and Shortis, M.R. 1998. Calibration stability of an underwater stereo-video system: Implications for measurement accuracy and precision. *Marine Technology Society Journal*. **32:** (2) 3-17.

Harvey, E.S., Shortis, M.R., Stadler, M. and Cappo, M. 2003. A comparison of the accuracy of measurements from single and stereo-video systems. *Marine Technology Society Journal*. **36:** (2) 38-49.

Heald, G.J. and Pace, N.G. 1996. *An analysis of the 1st and 2nd backscatter for seabed classification*. Proceedings of the 3rd European Conference on Underwater Acoustics. Crete. 649-654.

Heege, T., Hausknecht, P. and Kobryn, H. 2007. *Hyperspectral seafloor mapping and direct bathymetry calculation using HyMap data from the Ningaloo reef and Rottnest Island areas in Western Australia*. 5th EARSeL Workshop on Imaging Spectroscopy. Bruges, Belgium. 1-8.

Himmelman, J.H., Cardinal, A. and Bourget, E. 1983. Community development following removal of urchins, *Strongylocentrotus droebachiensis*, from the rocky subtidal zone of the St. Lawrence Estuary, Eastern Canada. *Oecologica*. **59:** 27-39.

Holmes, K.W., Van Niel, K.P., Radford, B., Kendrick, G.A. and Grove, S.L. 2008. Modelling distribution of marine benthos from hydroacoustics and underwater video. *Continental Shelf Research*. **28:** 1800-1810.

Hooge, P.N. and Eichenlaub, B. 2000. Animal movement extension to Arcview. ver. 2.0. Alaska Science Center - Biological Science Office, U.S. Geological Survey. Anchorage, AK, USA.

Hooper, J.N.A. and Kennedy, J.A. 2002. Small-scale patterns of sponge biodiversity (Porifera) on Sunshine Coast reefs, eastern Australia. *Invertebrate Systematics*. **16:** (4) 637-653.

Hopkins, R.E. and Edgerton, H.E. 1961. Lenses for underwater photography. *Deep-Sea Research*. **8:** (3/4) 312-317.

Humborstad, O.-B., Nottestad, L., Lokkeborg, S. and Rapp, H.T. 2004a. RoxAnn bottom classification system, sidescan sonar and video-sledge: spatial resolution and their use in assessing trawling impacts. *ICES Journal of Marine Science*. (61) 53-63.

Humborstad, O.-B., Nøttestad, L., Løkkeborg, S. and Rapp, H.T. 2004b. RoxAnn bottom classification system, sidescan sonar and video-sledge; spatial resolution and their use in assessing trawling impacts. *ICES Journal of Marine Science*. **61:** 53-63.

Hurd, C.L., Nelson, W.A., Falshaw, R. and Niell, K.F. 2004. History, current status and future of marine macroalgal research in New Zealand: Taxonomy, ecology, physiology and human uses. *Phycological Research*. **52:** 80-106.

Hutin, E., Simard, Y. and Archambault, P. 2005. Acoustic detection of a scallop bed from a single-beam echosounder in the St. Lawrence. *ICES Journal of Marine Science*. **62:** 966-983.

Irving, A.D. and Connell, S.D. 2006. Predicting understorey structure from the presence and composition of canopies: an assembly rule for marine algae. *Oecologia*. **148:** (3) 491-502.

Ivanoff, A. and Cherney, P. 1960. Correcting lenses for underwater use. *Journal of the Society of Motion Picture and Television Engineers*. **69:** 264-266.

Jeffrey, S.W., Rochford, D.J. and Cresswell, G.R. 1990. Oceanography of the Australasian region. *Biology of marine plants*. Longman Cheshire. Melbourne. 243 - 265.

Jensen, J.R., Estes, J.E. and Tinney, L. 1980. Remote sensing techniques for kelp surveys. *Photogrammetric Engineering & Remote Sensing*. **46:** (6) 743-755.

Jerlov, N.G. 1976. Marine Optics. *Elsevier Oceanographic Series*. 14. Elsevier Scientific Publishing Company. Amsterdam. 231.

Johnson, C.R., Ling, S., Ross, J., Shepherd, S.A. and Miller, K. 2004. *Range extension of the long-spined sea urchin (Centrostephanus rodgersii) in eastern Tasmania: Assessment of potential threats to fisheries*. FRDC Final Report. FRDC. 70.

Jordan, A., Lucieer, V.L. and Lawler, M. 2005a. *Linking habitat mapping with Fisheries Assessment in Key Commercial Fishing Grounds.* FRDC Final Report. Tasmanian Aquaculture and Fisheries Institute. Hobart. 85.

Jordan, A.R., Lawler, M., Halley, V. and Barrett, N. 2005b. Seabed habitat mapping in the Kent Group of Islands and its role in marine protected area planning. *Aquatic Conservation: Marine and Freshwater Ecosystems*. **15:** 51-70.

Kaiser, M.J., Armstrong, P.J., Dare, P.J. and Flatt, R.P. 1998. Benthic communities associated with a heavily fished scallop ground in the English Channel. *Journal of the Marine Biological Association of the United Kingdom*. **78:** (4) 1045-1059.

Kefalas, E., Castritsi-Catharios, J. and Miliou, H. 2003. The impacts of scallop dredging on sponge assemblages in the Gulf of Kalloni (Agean Sea, northeastern Mediterranean). *ICES Journal of Marine Science*. **60:** 402-410.

Kendall, M.S., Jensen, O.P., Alexander, C., Field, D., McFall, G., Bohne, R. and Monaco, M.E. 2005. Benthic mapping using sonar, video transects and an innovative approach to accuracy assessment: A characterization of bottom features in the Georgia Bights. *Journal of Coastal Research*. **21:** (6) 1154-1165.

Kendrick, G., Aylward, M., Crawley, K. and Hegge, B. 2001. *Use of towed video to accurately map seagrass assemblages in shallow water (<10 m) in Owen Anchorage and Cockburn Sound, Western Australia*. Proceedings of FRDC Workshop- Video Sensing of the Size and Abundance of Target and Non-target Fauna in Australian Fisheries - a National Workshop.

Kendrick, G., Eckersley, J. and Walker, D.I. 1999. Landscape-scale changes in seagrass distribution over time: a case study from Success Bank Western Australia. *Aquatic Botany*. **65:** 293-309.

Kendrick, G.A., Hegge, B.J., Wyllie, A., Davidson, A. and Lord, D.A. 2000. Changes in Seagrass Cover on Success and Parmelia Banks, Western Australia Between 1965 and 1995. *Estuarine, Coastal and Shelf Science*. **50:** 341-353.

Kennelly, S.J. 1995. Kelp Beds, In: . Edited by A.J. Underwood and M.G. Chapman. University of New South Wales Press. *Coastal Marine Ecology of Temperate Australia*. University of New South Wales Press. 106-120.

Kenny, A.J., Cato, I., Desprez, M., Fader, G., Schüttenhelm, R.T.E. and Side, J. 2003. An overview of seabed-mapping technologies in the context of marine habitat classification. *ICES Journal of Marine Science*. **60:** 411-418.

Kenyon, J.C., Brainard, R.E., Hoeke, R.K., Parrish, F.A. and Wilkinson, C.B. 2006. Towed-diver surveys, a method for mesoscale spatial assessment of benthic reef habitat: A case study at Midway Atoll in the Hawaiian Archipelago. *Coastal Management*. **34:** 339-349.

Kinlan, B.P. 2003. Linking environmental forcing, kelp forest habitat dynamics, and community structure in the northeast Pacific. *Journal of Phycology*. **39:** (S1) 29.

Klimley, A.P. and Brown, S.T. 1983. Stereophotography for the field biologist: measurement of lengths and three-dimensional positions of free swimming sharks. *Marine Biology*. **74:** 175-185.

Kloser, R.J., Bax, N.J., Ryan, T., Williams, A. and Barker, B.A. 2001a. Remote sensing of seabed types in the Australian South East Fishery: development and application of normal incident acoustic techniques and associated 'ground truthing'. *Marine and Freshwater Research*. **52:** (4) 475-489.

Kloser, R.J., Bax, N.J., Ryan, T., Williams, A. and Barker, B.A. 2001b. Remote sensing of seabed types in the Australian South East Fishery: development and application of normal incident acoustic techniques and associated 'ground truthing'. *Marine and Freshwater Research*. **52:** 475-489.

Kloser, R.J., Penrose, J.D. and Butler, A.J. 2010. Multi-beam backscatter measurements used to infer seabed habitats. *Continental Shelf Research*. **30:** (16) 1772-1782.

Kohler, K.E. and Gill, S.M. 2006. Coral Point Count with Excel extensions (CPCe): A Visual Basic program for the determination of coral and substrate coverage using random point count methodology. *Computers & Geosciences*. **32:** (9) 1259-1269.

Kostylev, V., E., Todd, B., J., Fader, G., B.J., Courtney, R.C., Cameron, G., D.M. and Pickrill, R., A. 2001. Benthic habitat mapping on the Scotian Shelf based on multibeam bathymetry, surficial geology and sea floor photographs. *Marine Ecology Progress Series*. **219:** 121-137.

Kostylev, V.E., Courtney, R.C., Robert, G. and Todd, B.J. 2003. Stock evaluation of giant scallop (*Placopecten magellanicus*) using high-resolution acoustics for seabed mapping. *Fisheries Research*. **60:** (2-3) 479-492.

Kvitek, R.G., Iampietro, P.J., Sandoval, E., Bretz, C.K., Derose, A. and Ventresca, D. 1999. Transducers, Cables and Kelp: Acoustic Mapping of Shallow Water Rockfish Habitat in California Kelp Forests. *Environmental Geosciences*. **6:** (3) 147-147.

Ladah, L.B. and Zertuche-González, J.A. 2004. Giant kelp (Macrocystis pyrifera) survival in deep water (25–40 m) during El Niño of 1997–1998 in Baja California, Mexico. *Botanica Marina*. **47:** (5) 367-372.

Lang, C. and Mann, K.H. 1976. Changes in sea urchin populations after the destruction of kelp beds. *Marine Biology*. **36:** 321-326.

Lauzon-Guay, J. and Scheibling, R.E. 2007. Seasonal variation in movement, aggregation and destructive grazing of the green sea urchin (*Strongylocentrotus droebachiensis*) in relation to wave action and sea temperature. *Marine Biology*. **151:** (6) 2109-2118.

Leach, J. 2006. The Korrong project- semi-submersible imaging for environmental mapping in shallow water. *Spatial science*. **51:** (1) 133-142.

Lee Long, W.J., Hundley, A.J., Roder, C.A. and McKenzie, L.J. 1998. *Preliminary Evaluation of an Acoustic Technique for Mapping Tropical Seagrass Habitats*. Great Barrier Reef Marine Park Authority. 29.

Levin, P. and Hay, M. 2002. Fish-seaweed association on temperate reefs: do small scale experiments predict large scale patterns? *Marine Ecology Progress Series*. **232:** 239-246.

Levitan, D.R. 1992. Community structure in time past: Influence of human fishing pressure on algal-urchin interactions. *Ecology*. **73:** (5) 1597-1605.

Lewis, R.J. and Neushul, M. 1994. Northern and Southern Hemisphere hybrids of *Macrocystis* (Phaeophyceae). *Journal of Phycology*. **30:** 246-353.

Ling, S.D. 2008. Range expansion of a habitat-modifying species leads to loss of taxonomic diversity: a new and impoverished reef state. *Oecologia*. **156:** (4) 883-894.

Lucieer, V., Lawler, M., Morffew, M. and Pender, A. 2007. *Mapping of inshore marine habitats from Schouten Island to Bicheno on the East Coast of Tasmania*. Final Report to NHT. Tasmanian Aquaculture and Fisheries Institute. Hobart. 109.

Lucieer, V., Lawler, M., Pender, A. and Morffew, M. 2009. *SeaMap Tasmania- Mapping the Gaps*. Final Report to NRM North. Tasmanian Aquaculture and Fisheries Institute. 188.

Mackenzie, K.V. 1981. Nine-term equation for sound speed in the oceans. *Journal of the Acoustical Society of America*. **70:** 807-812.

MacKinson, S., Freeman, S., Flatt, R. and Meadows, B. 2004. Improved acoustic surveys that save time and money: integrating fisheries and ground-discrimination acoustic technologies. *Journal of Experimental Marine Biology and Ecology*. **305:** 129-140.

MacLennan, D.N. 1986. Time-varied-gain functions for pulsed sonars. *Journal of Sound and Vibration*. **110:** 511-522.

MacLennan, D.N., Fernandes, P.G. and Dalen, J. 2002. A consistent approach to definitions and symbols in fisheries acoustics. *ICES Journal of Marine Science*. **59:** 365-369.

MacLennan, D.N. and Simmonds, J. 1992. Fisheries Acoustics. *Fish and Fisheries Series 5*. Chapman and Hall Co. New York. 325.

Magorrian, B.H., Service, M. and Clarke, W. 1995. An acoustic bottom classification of Strangford Lough, Northern Ireland. *Journal of the Marine Biological Association of the United Kingdom*. **75:** 982-987.

Mann, K.H. 1977. Destruction of kelp-beds by sea-urchins: A cyclical phenomenon or irreversible degradation? *Helgoländer wiss. Meeresunters*. **30:** 455-467.

Marsh, I. and Brown, C. 2008. Neural network classification of multibeam backscatter and bathymetry data from Stanton Bank (Area IV). *Applies Acoustics*. **70:** (10) 1269-1276.

Martin, C.J.M. and Martin, E.A. 2002. An underwater photomosaic technique using Adobe Photoshop (tm). *The International Journal of Nautical Archaeology*. **31:** (1) 137-147.

McConnaughey, R.A., Mier, K.L. and Dew, C.B. 2000. An examination of chronic trawling effects on soft-bottom benthos of the eastern Bering Sea. *ICES Journal of Marine Science*. **57:** (5) 1377-1388.

McNeil, G.T. 1968. Optical fundamentals of underwater photography. Photogrammetry, Inc. 115.

McRea, J.E., Greene, H.G., O'Connell, V.M. and Wakefield, W.W. 1999. Mapping marine habitats with high resolution sidescan sonar: Cartographie des habitats marins par sondage a balayage lateral de haute resolution. *Oceanologica Acta*. **22:** (6) 679-686.

Melville, A.J. and Connell, S.D. 2001. Experimental effects of kelp canopies on subtidal coralline algae. *Austral Ecology*. **26:** 102-108.

Miller, R.J. 1985. Succession in sea urchin and seaweed abundance in Nova Scotia, Canada. *Marine Biology*. **84:** 275-286.

Moore, E.J. 1976. Underwater Photogrammetry. *Photogrammetric Record*. **8:** (48) 748-763.

Morrison, M.A., Thrush, S.F. and Budd, R. 2001a. Detection of acoustic class boundaries in soft sediment systems using the seafloor acoustic discrimination system QTC VIEW. *Journal of Sea Research*. **46:** (3-4) 233-243.

Morrison, M.A., Thrush, S.F. and Budd, R. 2001b. Detection of acoustic class boundaries in soft sediment systems using the seafloor acoustic discrimination system QTC VIEW. *Journal of Sea Research*. **46:** 233-243.

Mount, R.E. 2005. Acquisition of through-water aerial survey images: surface effects and the prediction of sun glitter and subsurface illumination. *Photogrammetric Engineering & Remote Sensing*. **71:** (12) 14071415.

Mumby, P.J., Green, E.P., Edwards, A.J. and Clark, C.D. 1997. Measurement of seagrass standing crop using satellite and digital airborne remote sensing. *Marine Ecology Progress Series*. **159:** 51-60.

Negahdaripour, S., Madjidi, H. and Khamene, A. 2002. Stereovision imaging to map seafloor and benthic habitats. *Sea Technology*. **43:** (8) 35-39.

Nicole, H., Harvey, E.S. and Kendrick, G.A. 2003. Differences in fish assemblages from different reef habitats at Hamelin Bay, south-western Australia. *Marine and Freshwater Research*. **54:** 177-184.

Norris, J.G., Wyllie-Echeverria, S., Mumford, T., Bailey, A. and Turner, T. 1997. Estimating basal area coverage of subtidal seagrass beds using underwater videography. *Aquatic Botany*. **58:** (3-4) 269-287.

North, W.J., James, D.E. and Jones, L.G. 1993. History of kelp beds (*Macrocystis*) on Orange and San Diego Counties, California. *Hydrobiologia*. **260/261:** 277-283.

Orlowski, A. 1984. Application of multiple echo energy measurements for evaluation of sea bottom type. *Oceanologia*. **19:** 61-78.

Parnum, I.M., Gavrilov, A.N., Siwabessey, P.J.W. and Duncan, A. 2006. *Analysis of high-frequency multibeam backscatter statistics from different seafloor habitats.* 8th European Conference on Underwater Acoustics. Carvoeiro, Portugal. On line.

Parravicini, V., Morri, C., Ciribilli, G., Montefalcone, M., Albertelli, G. and Bianchi, C.N. 2009. Size matters more than method: Visual quadrats vs photography in measuring human impact on Mediterranean rocky reef communities. *Estuarine, Coastal and Shelf Science*. **81:** 359-367.

Parsons, D.M., Shears, N.T., Babcock, R.C. and Haggitt, T.R. 2004. Fine scale habitat change in a marine reserve, mapped using radio acoustically positioned video transects. *Marine and Freshwater Research*. **55:** 257-265.

Pasquilini, V., Pergent-Martin, C., Claubaut, P. and Pergent, G. 1998. Mapping of *Posidonia oceanis* using aerial photographs and side scan sonar: Application off the Island of Corsica (France). *Estuarine, Coastal and Shelf Science*. **47:** 359-367.

Patton, M.L., Valle, C.F. and Grove, R.S. 1994. Effects of bottom relief and fish grazing on the density of giant kelp, *Macrocystis*. *Bulletin of Marine Science*. **55:** (2-3) 631-644.

Peattie, M.E. and Hoare, R. 1981. The sublittoral ecology of the Menai Strait. II. The sponge *Halichondria panicea* (Pallus) and its associated fauna. *Estuarine, Coastal and Shelf Science*. **13:** 621-635.

Pederson, H.G. and Johnson, C.R. 2008. Growth and age structure of sea urchins (Heliocidaris erythrogramma) in complex barrens and native macroalgal beds in eastern Tasmania. *ICES Journal of Marine Science*. **65:** (1) 1-11.

Pepper, A. and M.L., P. 2009. *GREMO: A GIS-based generic model for estimating relative wave exposure*. 18th World IMACS Congress and MODSIM09 International Congress on Modelling and Simulation. Cairns, Australia. 1964-1970.

Pickrill, R.A. and Todd, B.J. 2003. The multiple roles of acoustic mapping in integrated ocean management, Canadian Atlantic continental margin. *Ocean & Coastal Management*. **46:** 601-614.

Pinn, E.H. and Robertson, M.R. 1998. The effect of bioturbation on RoxAnn, a remote acoustic seabed classification system. *Journal of the Marine Biological Association of the United Kingdom*. **78:** 707-715.

Pinn, E.H. and Robertson, M.R. 2003. Effect of track spacing and data interpolation on the interpretation of benthic community distributions derived from RoxAnn acoustic surveys. *ICES Journal of Marine Science*. **60:** (6) 1288-1297.

Pitcher, R., Smith, G., Wassenberg, T., Skewes, T., Gordon, S. and Cappo, M. 2001. *Quantitative Data from Underwater Video Sources (Tow-sled, Drop-camera, ROV) for Rapid Characterisation/Mapping of Shelf Seabed Habitats and for Measuring the Dynamics of Large Sessile Seabed Fauna*. Proceedings of FRDC Workshop- Video

Sensing of the Size and Abundance of Target and Non-target Fauna in Australian Fisheries - a National Workshop.

Populus, J. and Perrot, T. 2007. *Recommended operating guidelines (ROG) for single-beam echosounder surveying*. Mapping European Seabed Habitats- Recommended Operating Guidelines. Mapping European Seabed Habitats. 9.

Pouliquen, E. 2004. *Depth dependence correction for normal incidence echosounding*. Seventh European Conference on Underwater Acoustics. Delft, The Netherlands.

Preciado, I. and Maldonado, M. 2005. Reassessing the spatial relationship between sponges and macroalgae in sublittoral rocky bottoms: A descriptive approach. *Helgoland Marine Research*. **59:** (2) 141-150.

Preston, j. 2008. Automated acoustic seabed classification of multibeam images of Stanton Banks. *Applies Acoustics*. **70:** (10) 1277-1287.

Puente, A. and Juanes, J.A. 2008. Testing taxonomic resolution, data transformation and selection of species for monitoring macroalgae communities. *Estuarine, Coastal and Shelf Science*. **78:** 327-340.

Rebikoff, D. 1975. Underwater photogrammetry in 1975. *Colserange photogrammetric systems*. 270-279.

Reed, D.C. and Foster, M.S. 1984. The effects of canopy shadings on algal recruitment and growth in a giant kelp forest. *Ecology*. **65:** (3) 937-948.

Reid, D., Scalabrin, C., Petitgas, P., Masse, J., Aukland, R., Carrera, P. and Georgakarakos, S. 2000. Standard protocols for the analysis of schools based data from echo sounder surveys. *Fisheries Research*. **47:** 125-136.

Roberts, D.E. and Davis, A.R. 1996. Patterns in sponge (Porifera) assemblages on temperate coastal reefs off Sydney, Australia. *Marine and Freshwater Research*. **47:** 897-906.

Rochford, D.J. 1975. The physical setting. *Resource of the sea*. Royal Society of Tasmania

15-27.

RosenKranz, G.E. and Byersdorfer, S.C. 2004. Video scallop survey in the eastern Gulf of Alaska, USA. *Fisheries Research*. **69:** 131-140.

Ryan, T.E. and Kloser, R.J. 2004. *Improving the precision of ES60 and EK60 echosounder applications*. Report of the Working Group on Fisheries Acoustic Science and Technology. Gydnia, Poland.

Sabol, B.M. and Johnston, S. 2001. *Innovative techniques for improved hydroacoustic bottom tracking in dense aquatic vegetation*. US Army Corps of Engineers, Engineer Research and Development Centre. 16.

Sabol, B.M., Melton Jr, R.E., Chamberlain, R., Doering, P. and Haunert, K. 2002. Evaluation of a digital echo sounder system for detection of submersed aquatic vegetation. *Estuaries*. **25:** (1) 133-141.

Sánchez-Carnero, N., Bernárdez, C., Moszyński, M. and Freire, J. 2007. *Development of an open approach for acoustic marine benthic habitat classification*. 2nd International Conference & Exhibition on Underwater Acoustic Measurements: Techniques & Results. Crete. 1245-1252.

Schiagintweit, G.E.O. 1993. *Real-time acoustic bottom classification for hydrography a field evaluation of RoxAnn*. Oceans '93. Victoria, BC, Canada. 214-219.

Schiebener, P., Straub, J., Sengers, J. and Gallagher, J. 1990. Refractive index of water and steam as function of wavelength, temperature and density. *Journal of Physical and chemical reference data*. **19:** (3) 677-717.

Schiel, D.R. and Foster, M.S. 1986. The structure of subtidal algal stands in temperate waters. *Oceanography and Marine Biology: an Annual Review*. **24:** 265-307.

Schwinghamer, P., Guigne, J.Y. and Siu, W.C. 1996. Quantifying the impact of trawling on benthic habitat structure using high resolution acoustics and chaos theory. *Canadian Journal of Fisheries and Aquatic Sciences*. **53:** (2) 288-296.

Shears, N.T. and Babcock, R.C. 2002. Marine reserves demonstrate top-down control of community structure on temperate reefs. *Oecologia*. **132:** 131–142.

Shears, N.T., Babcock, R.C., Duffy, C.A.J. and Walker, J.W. 2004. Validation of qualitative habitat descriptors commonly used to classify subtidal reef assemblages in north-eastern New Zealand. *New Zealand Journal of Marine and Freshwater Research*. **38:** 743-752.

Shortis, M., Robson, S. and Harvey, E. 2001. *The design, calibration and stability of an underwater stereo-video system*. Proceedings of FRDC Workshop- Video Sensing of the Size and Abundance of Target and Non-target Fauna in Australian Fisheries - a National Workshop.

Siddon, C.E. and Witman, J.D. 2003. Influence of chronic, low-level hydrodynamic forces on subtidal community structure. *Marine Ecology Progress Series*. **261:** 99-110.

Simms, E.L. and Dubois, J.-M.M. 2001. Satellite remote sensing of submerged kelp beds on the Atlantic coast of Canada. *International Journal of Remote Sensing*. **22:** (11) 2083-2094.

Simons, D.G. and Snellen, M. 2008. A Bayesian approach to seafloor classification using multi-beam echo-sounder backscatter data *Applies Acoustics*. **70:** (10) 1258-1268.

Simrad. 2004. *Simrad ES60 Fisheries echo sounder: Instruction manual*. Horten, Norway. 213.

Siwabessy, J., Penrose, J., Kloser , R.J. and Fox, D.R. 1999. *Seabed habitat classification*. Shallow Survey 1999- International Conference on High Resolution Surveys in Shallow Water. Sydney, Australia. 1-9.

Siwabessy, P.J.W., Penrose, J.D., Fox, D.R. and Kloser, R.J. 2000. Bottom Classification in the Continental Shelf: A Case Study for the North-west and South-east Shelf of Australia. *Australian Acoustical Society Conference . Joondalup Australia 15-17November 2000*.

Siwabessy, P.J.W., Tseng, Y. and Gavrilov, A.N. 2004. *Seabed habitat mapping in coastal waters using a normal incident acoustic technique*. Acoustics 2004. Gold Coast, Australia.

Smith, G.F. and Greenhawk, K.N. 1998. Shellfish benthic habitat assessment in the Chesapeake Bay: Progress toward integrated technologies for mapping and analysis. *Journal of Shellfish Research*. **17:** (5) 1433-1437.

Solan, M., Germano, J.D., Rhoads, D.C., Smith, C., Michaud, E., Parry, D., Wenzhoefer, F., Kennedy, B., Henriques, C., Battle, E., Carey, D., Iocco, L., Valente, R., Watson, J. and Rosenberg, R. 2003. Towards a greater understanding of pattern, scale and process in marine benthic systems: a picture is worth a thousand worms. *Journal of Experimental Marine Biology and Ecology*. **285-286:** 313-338.

Sotheran, I.S., Foster-Smith, R.L. and Davies, J. 1997. Mapping of marine benthic habitats using image processing techniques within a raster-based geographic information system. *Estuarine, Coastal and Shelf Science*. **44:** (A) 25-31.

Stanic, S., Briggs, K.B., Fleischer, P., Sawyer, W.B. and Ray, R.I. 1989. High-frequency acoustic backscattering from a coarse shell ocean bottom. *Journal of the Acoustical Society of America*. **85:** (1) 125-136.

Stanley, E.M. 1971. The refractive index of seawater as a function of temperature, pressure and two wavelengths. *Deep-Sea Research*. **18:** 833-840.

Stanton, T.K. 1985. Volume scattering: Echo peak PDF. *Journal of the Acoustical Society of America*. **77:** 1358-1366.

Stanton, T.K. and Chu, D. 2004. On the acoustic diffraction by the edge of shells. *Journal of the Acoustical Society of America*. **116:** (1) 239-244.

Steneck, R.S., Graham, M.H., Bourque, B.J., Corbett, D., Erlandson, J.M., Estes, J.A. and Tegner, M.J. 2002. Kelp forest ecosystems: biodiversity, stability, resilience and future. *Environmental Conservation*. **29:** (4) 436-459.

Stevens, T. 2005. Scales of similarity in soft sediment epibenthic assemblages: implications for marine protected area design. *Marine Biology*. **146:** 345-354.

Stevens, T. and Connolly, R.M. 2005. Local-scale mapping of benthic habitats to assess representation in a marine protected area. *Marine and Freshwater Research*. **56:** 111-123.

Stokesbury, K.D.E. 2002. Estimation of sea scallop abundance in closed areas of Georges Bank, USA. *Transactions of the American Fisheries Society*. **131:** (6) 1081-1092.

Sutton, G. and O'Keeffe, E. 2007. *Annex II: Seabed mapping: Multibeam bathymetry, backscatter and video imaging of the seabed in the south east coast scallop grounds*. Final Report of Project 01.SM.T1.07. Galway. 20.

Tao, C.V. and Hu, Y. 2002. 3D Reconstruction Methods Based on the Rational Function Model. *Photogrammetric Engineering & Remote Sensing*. **68:** (7) 705-714.

Taylor, R.B. 1998. Density, biomass and productivity of animals in four subtidal rocky reef habitats: the importance of small mobile invertebrates. *Marine Ecology Progress Series*. **172:** 37-51.

Tegner, M.J. and Dayton, P.K. 1987. El Nino effects on southern Californian kelp forest communities. *Advances in Ecological Research*. **17:** 243-279.

Tegner, M.J. and Dayton, P.K. 1991. Sea urchins, El Ninos, and the long term stability of Southern California kelp forest communities. *Marine Ecology Progress Series*. **77:** 49-63.

Tegner, M.J. and Dayton, P.K. 2000. Ecosystem effects of fishing in kelp forest communities. *ICES Journal of Marine Science*. **57:** 579-589.

Tegner, M.J., Haaker, P.L., Riser, K.L. and Vilchis, L.I. 2001. Climate variability, kelp forests, and the southern California red abalone fishery. *Journal of Shellfish Research*. **20:** (2) 755-763.

Thomas, G.L., Thiesfeld, S.L., Bonar, S.A., Crittenden, R.N. and Pauley, G.B. 1990. Estimation of submergent plant biovolume using acoustic range information. *Canadian Journal of Fisheries and Aquatic Sciences*. **47:** 805-812.

Thorndike, E.M. 1950. A wide-angle, underwater camera lens. *Journal of the Optical Society of America*. **40:** (12) 823-824.

Thorndike, E.M. 1967. 2. Physics of underwater photography. *Johns Hopkins Oceanographic Studies*. **3:** 43-45.

Thorne, R.E. 1998. Review: Experiences with shallow water acoustics. *Fisheries Research*. **35:** (1-2) 137-141.

Thrush, S.F., Schultz, D., Hewitt, J.E. and Talley, D. 2002. Habitat structure in soft-sediment environments and abundance of juvenile snapper *Pagrus auratus*. *Marine Ecology Progress Series*. **245:** 273-280.

Torlegard, A.K.I. 1974. Under-water analytical systems. *Photogrammetric Engineering*. **40:** (3) 287-293.

Tuya, F., Wernberg, T. and Thomsen, M.S. 2008. The spatial arrangement of reefs alter the ecological patterns of fauna between interspersed algal habitats. *Estuarine, Coastal and Shelf Science*. **78:** 774-782.

Underwood, A.J., Chapman, M.G. and Connell, S.D. 2000. Observations in ecology: you can't make progress on processes without understanding the patterns. *Journal of Experimental Marine Biology and Ecology*. **250:** (1-2) 97-115.

Underwood, A.J., Kingsford, M.J. and Andrew, N.L. 1991. Patterns in shallow subtidal marine assemblages along the coast of New South Wales. *Australian Journal of Ecology*. **6:** 231-249.

Urick, R.J. 1983. Principles of Underwater Sound. Peninsula Publishing. 100.

Valentine, J.P. and Johnson, C.R. 2003. Establishment of the introduced kelp *Undaria pinnatifida* in Tasmania depends on disturbance to native algal assemblages. *Journal of Experimental Marine Biology and Ecology*. **295:** (1) 63-90.

Valentine, J.P. and Johnson, C.R. 2005. Persistence of sea urchin (*Heliocidaris erythrogramma*) barrens on the east coast of Tasmania: inhibition of macroalgal recovery in the absence of high densities of sea urchins. *Botanica Marina*. **48:** 106-115.

Valentine, P.C., Todd, B.J. and Kostylev, V.E. 2004. Classification of marine sublittoral habitats with application to the northeastern North America region. *Benthic habitats and the effects of fishing*. American Fisheries Society Symposium. Maryland.

Valley, R.D., Drake, M.T. and Anderson, C.S. 2005. Evaluation of alternative interpolation techniques for the mapping of remotely-sensed submersed vegetation abundance. *Aquatic Botany*. **81:** 13-25.

van Walree, P.A., Tegowski, J., Laban, C. and Simons, D.G. 2005. Acoustic seafloor discrimination with echo shape parameters: A comparison with the ground truth. *Continental Shelf Research*. **25:** (18) 2273-2293.

von Szalay, P. and McConnaughey, R. 2002. The effect of slope and vessel speed on the performance of a single beam acoustic seabed classification system. *Fisheries Research (Amsterdam)*. **56:** (1) 99-112.

Wakimoto, Z. 1967. On designing underwater camera lenses. *Photogrammetric Engineering*. 925-936.

Ward, T.J., Vanderklift, M.A., Nichols, A.O. and Kenchington, R.A. 1999. Selecting marine reserves using habitats and species assemblages as surrogates for biological diversity. *Ecological Applications*. **9:** 691-698.

Watson, D.L., Harvey, E.S., Anderson, M.J. and Kendrick, G.A. 2005. A comparison of temperate reef fish assemblages recorded by three underwater stereo-video techniques. *Marine Biology*. **148:** 415-425.

Wentworth, C.K. 1922. A scale of grade and class terms for clastic sediments. *Journal of Geology*. **30:** 377-392.

Wilding, T.A., Sayer, M.D.J. and Provost, P.G. 2003. Factors affecting the performance of the acoustic ground discrimination system RoxAnn^{TM}. *ICES Journal of Marine Science*. **60:** 1373-1380.

Williams, I. and Leach, J. 2001. Video Remote Sensing for Seafloor Mapping. *Mers, Department of Geomatics*.

Williams, K.L., Richardson, M.D., Briggs, K.B. and Jackson, B.L. 2001. Scattering of high-frequency energy from discrete scatterers on the seafloor: Glass spheres and shells. *Proceedings of the Institute of Acoustics*. **23:** 369-374.

Willis, T.J. and Babcock, R.C. 2000. A baited underwater video system for the determination of relative density of carnivorous reef fish. *Marine and Freshwater Research*. **51:** 755-763.

Ysebaert, T. and Herman, P.M.J. 2002. Spatial and temporal variation in benthic macrofauna and relationships with environmental variables in an estuarine, intertidal soft sediment environment. *Marine Ecology Progress Series*. **244:** 105-124.

Yunus, W.M.M. 1992. Temperature dependence of refractive index and absorption of Nal, MgCl2, and Na2SO4 solutions as major components in natural seawater. *Applied Optics*. **31:** (16) 2963-2964.

Zabloudil, K., Reitzel, J., Schroeter, S., Dixon, J., Dean, T.A. and Norall, T. 1991. *Sonar mapping of giant kelp density and distribution*. Coastal Zone '91- Proceedings of the Seventh Symposium on Coastal and Ocean Management. 391-406.

Zimmerman, R.C. and Robertson, D.L. 1985. Effects of El Nino on local hydrography and growth of the giant kelp, *Macrocystis pyrifera*, at Santa Catalina Island, California. *Limnology & Oceanography*. **30:** (6) 1298-1302.